Application of Reliability in Breakwater Design

Christiani, Erik

Publication date:
1997

Document Version
Publisher's PDF, also known as Version of record

SERIES PAPER 14

ISSN 0909-4296

Erik Christiani

Application of Reliability in Breakwater Design

Hydraulics & Coastal Engineering Laboratory
Department of Civil Engineering
Aalborg University

Hydraulics & Coastal Engineering Laboratory
Department of Civil Engineering
Aalborg University
Sohngaardsholmsvej 57
DK–9000 Aalborg, Denmark

ISSN 0909–4296
SERIES PAPER No. 14

Application of Reliability in Breakwater Design

by

Erik Christiani

Published 1997 by
Hydraulics & Coastal Engineering Laboratory
Aalborg University

Printed in Denmark by
Centertrykkeriet, Aalborg University

ISSN 0909–4296
SERIES PAPER No. 14

Preface

This thesis *Application of Reliability in Breakwater Design* is submitted as a partial fulfillment for the Danish Ph.D. degree according to notice no. 989 of the 11th December 1992 from the Danish Ministry of Education and Research.

The study was financed by the Danish Technical Research Council (STVF) and the support is greatly acknowledged. The work was carried out at the Hydraulics & Coastal Engineering Laboratory, Aalborg University, Denmark in the period from the 1st October 1993 to the 31st January 1997 under supervision of Professor, dr. techn. H.F. Burcharth.

Especially, I would like to thank Associate Professor Ph.D. John Dalsgaard Sørensen for many fruitful and inspiring discussions on the reliability based calculations. Special thanks to Professor A. Lamberti, Bologna University, Italy, on technical discussions of the main armour and toe berm interaction laboratory tests performed by Bologna University, during my stay at Bologna University spring 1996.

The author wishes to thank everybody in the department for their support and assistance during the study.

Special thanks to Ian Young of L.S.C. Brunette and Partners, Blantyre, Malawi for proof reading the manuscript, and my fiancée and children for patience and support throughout the study.

Aalborg, September 1997

Erik Christiani

Contents

List of symbols

The main list of symbols are presented in the following. Due to a large number of symbols which stem from breakwater engineering, foundation engineering and structural reliability; their will be some symbols which overlap. It should be easy to distinguish between the same symbols in the text.

A	Effective foundation area in the general bearing capacity equation, area or a parameter.
A_c	Crest height of the rubble mound breakwater from the sea water level to the armoured crest.
B, b	Width of the crown wall, vertical breakwater or a parameter.
B_m	Berm width of the rubble mound foundation in front of caisson breakwater.
B_{mr}	Berm width of the rubble mound foundation on the rear side of the caisson breakwater.
B_z	Initial rupture zone width.
c	Cohesion of the soil kN/m^2 or shape parameter.
c_u	Undrained shear strength of clay kN/m^2.
C_n	Constant in the toe berm and armour layer equation, $n = 1....$
C_{F_1}	Cost of failure of the vertical breakwater before construction.
C_{F_2}	Cost of the vertical breakwater after construction.
C_I	Initial cost of the vertical breakwater
C_T	Total cost of the breakwater.
D^a_{n50}	Nominal armour rock diameter calculated from the median particle mass M_{50}.
D^t_{n50}	Nominal toe berm rock diameter calculated from the median particle mass M_{50}.
D^*_T	Damage level corresponding to increased movement of the armour layer.
D^{cr}_T	Accepted toe berm damage level for design.
$f(x)$	Joint probability density function.
f_c	Vertical distance from armour crest to top of crown wall face (unprotected part of the crown wall face).

f_R	Factor for the wave transmission.
F_G	Reduced weight of a caisson breakwater due to buoyancy.
F_{Goda}	Goda wave induced load, either F_H or F_U.
F_H	Horizontal wave induced force .
$F_{H'}$	Horizontal hydrostatic force for the crown wall .
F_H^p	Horizontal wave induced force including pore pressure along the slip line.
F_{H_s}	Uncertainty of the wave elevations in terms of the measuring device.
F_R	Resultant force acting on the base of a vertical breakwater.
F_{rubble}	Horizontal active rubble pressure.
F_{SLICE}	Safety factor for the BISHOPS method of slices.
F_U	Wave induced uplift force.
F^*	Non dimensional overtopping coefficient.
F_w	Weight of the rubble on the seaward side.
F_H^{3D}	Horizontal wave load in a short crested sea.
F_U^{3D}	Wave induced uplift force in a short crested sea.
$F(\varphi')$	Empirical function to calculate N_γ.
g	Gravitational acceleration.
g_γ	Rear slope factor of the self weight of the soil.
$g(x)$	Limit state function.
G	Upper berm width of a rubble mound breakwater .
G_L	Frequency dependent directionally averaged spectral multiplication factor
G_n	Limit state equations for the failure modes $i = 1...n$.
h	height.
h_b	Waterdepth $5H_s$ from the foot of the vertical breakwater.
h_c	Crest height of a vertical breakwater.
h_{prot}	Height of the stone protected section of the crown wall face.
h_{II}	Height of the rubble mound (vertical breakwaters).
h_r	Reduced run up height.

h_s	Water depth at the toe of the structure.
h_t	Water depth from the top of the toeberm to the surface.
h_{tot}	Total design water depth $h_{tot} = h_s + \eta_s + \zeta$.
h'	Water depth at which the armour units are placed or submerged water height in a caisson.
h_w	Height of the concrete crown wall or vertical breakwater caisson.
H	Wave height from trough to crest.
H_b	Wave breaking height in the surf zone.
H_{design}	Design wave height in Goda's formula corresponding to $1.8H_s$.
H_I	Incident wave height.
H_R	Reflected wave height.
H_s	Significant wave height, average of highest one third of wave heights.
$H_{1/3}$	Significant wave height, average of highest one third of wave heights.
H_{so}	Deepwater significant wave height, average of highest one third of wave heights.
H_T	Transmitted wave height .
H_s^{50}	Deepwater significant wave height with a return period of 50 years.
$H_{1/250}$	Mean of the wave heights of the waves included in 1/250 of the total number of waves.
H_s^T	Central estimate of the significant wave height which is exceeded in T years .
H_s^{TL}	Central estimate of the significant wave height which is exceeded in T years .
$H.W.L.$	High water level.
i_c	Inclination factor for the cohesion.
i_c^o	Inclination factor of the undrained shear strength of clay.
i_q	Inclination factor for the overlying weight.
i_γ	Inclination factor for the self weight of the soil.
k	Wave number= $2\pi/L$ or a probability distribution parameter .
K_s	Shoaling coefficient.
K_R	Reflection coefficient H_R/H_I.

K_{To}	Transmission coefficient through the structure.
K_{Ts}	Transmission coefficient due to overtopping.
l	Geometrical length parameter.
l_s	Length of the structure.
L	Wave length in the direction of propagation, corresponding to water depth h.
L_c	Effective length of the foundation.
L_m	Local wave length corresponding to the wave period T_m.
L_o	Deepwater wave length in the direction of propagation.
$L_{1/3}$	Significant wave length.
M	Mass of armour unit.
M_G	Reduced moment of a caisson breakwater due to buoyancy.
M_H	Horizontal wave induced moment .
M_U	Wave induced uplift moment (from Goda's formula).
$M_o(F_H)$	Moment of the wave induced horizontal force.
$M(\theta)$	Factor the bishops method of slices.
$M.W.L.$	Mean water level.
N	Number of waves.
N_{od}	Number of stones displaced within a strip width D_{n50}.
N_s	$= (K_D\, cot\alpha)^{1/3}$ damage number.
N_c	Bearing capacity factor, considering cohesion.
N_c^o	Bearing capacity factor of the undrained shear strength of clay.
N_q	Bearing capacity factor of the overlying soil.
N_γ	Bearing capacity factor for the self weight.
p_m	Stagnation pressure at the crown wall face.
p_n	Wave pressure on a caisson $n = 1, 2, 3, 4$.
p_u	Wave induced uplift pressure at the front edge of the caisson.
P	Permeability factor for the stability of the armour layer or force.
$P(F)$	Probability of the wave load F.
P_f	Probability of failure.

P_{fi}	Probability of failure, where i=1,2... .
P_f^{Ls}	Lower bound probability of failure for a series system.
P_f^s	Probability of failure for a series system.
P_f^{Lp}	Lower bound probability of failure for a parallel system.
P_f^p	Probability of failure for a parallel system.
P_f^{Us}	Upper bound probability of failure for a series system.
P_f^{Up}	Upper bound probability of failure for a parallel system.
P_p	Vertical induced pore force.
$\overline{Q}_m$	Average overtopping in $m^3/m/s$.
q	External load applied to the foundation from the caisson.
q_n	Bearing load values, for n=1,2... .
Q	Bearing capacity or overtopping in $m^3/m/s$.
r	Geometrical radius of the rotational fans or factor.
R_u	Run up level on the rubble mound breakwater.
$R_{u,x}$	Run up level exceeded by x percent waves.
s_m	Local wave steepness based on T_m.
s_q	Form factor for the overlying soil on the rear end of the foundation.
s_c	Form factor for the cohesion.
s_c^o	Form factor for the undrained shear strength of clay.
s_q	Form factor for the overlying soil on the rear end of the foundation.
s_γ	Form factor for the self weight of the soil.
s_{op}	Local wave steepness based on T_s.
S	Damage value equal to erosion of the armour layer divided by the nominal rock diameter squared.
T_m	Mean wave period.
T_s	Significant or peak wave period.
$S.W.L.$	Sea water level
U	Uplift due to the buoyancy of the structure.
$\mathbf{V}$	Reduction factor for the wave impact.

V_1, V_2	Volumes.
W	Weight of each slice for bishops method of slices.
W_E	External work done in the failure mechanism.
W_I	Total internal work done in failure mechanism.
W_n	The individual work contributions in the soil, n=1,2.... etc.
$W_{caisson}$	Weight of the caisson.
W_{rubble}	Weight of the rubble mound.
X_i	Stochastic parameter where, n=1,2... etc
y	Vertical run up wedge thickness.
y_{eff}	Effective wave pressure impact zone height.
Z_{F_H}	Uncertainty of wave induced horizontal force.
Z_{F_U}	Uncertainty of wave induced uplift force.
Z_{M_H}	Uncertainty of wave induced horizontal moment.
Z_{M_U}	Uncertainty of wave induced uplift moment.
Z_{toe}	Uncertainty of the toe berm equation.
Z^1_{toe}	Uncertainty of the modified toe berm equation.
Z^2_{toe}	Uncertainty of the modified toe berm equation.
α	Slope angle.
α^2_n	Sensitivity values from the reliability evaluation, where n=1,2,3... .
α_n	Empirical coefficients from Goda's equations, where n=1,2,3... .
α^*	Empirical coefficients (impulsive wave action).
α_{Io}	Empirical coefficients (impulsive wave action).
α_{I1}	Empirical coefficients (impulsive wave action).
α_I	Empirical coefficients (impulsive wave action).
β	Reliability index.
β_{HL}	Hasofer and Lind Reliability index, the same as β.
β_o, β^*_o	Coefficients for the incident wave height in the surf zone.
β_1, β^*_1	Coefficients for the incident wave height in the surf zone.
$\beta_{max}, \beta^*_{max}$	Coefficients for the incident wave height in the surf zone.

β^J	Joint reliability index.
β_i^c	Reliability index of the individual components.
β^P	System reliability index for a parallel system.
β^S	System reliability index for a series system.
β^l	Lower bound reliability index.
β^u	Upper bound reliability index.
Δ	$\rho/\rho_w - 1$, Where ρ and ρ_w are mass density of armour and sea water.
δ_n	Empirical coefficients (impulsive wave action) n=1,2, 1 1, 2 2 .
η^*	Elevation to which the wave pressure is exerted (Goda formula).
η_s	Storm surge elevation.
ρ_c	Average density of the caisson or crown wall.
ρ_s	Average density of the rock material.
ρ_{sea}	Average mass density of the sea water.
ρ_w	Average density of water.
γ_w	Specific mass density of water.
γ_s	Specific mass density of the rubble mound.
γ_{θ_I}	Coefficient for the incident wave angle (overtopping short crested seas).
γ_σ	Coefficient for the directional energy spreading (overtopping short crested seas).
$\gamma_{geometry}$	Coefficient for the geometry of the vertical breakwater (overtopping short crested seas).
ψ_1	Angle of dilation of the rubble mound (material property).
ψ_2	Angle of dilation of the subsoil (material property).
φ'	Effective friction angle.
φ_1'	Effective friction angle of the rubble mound.
φ_2'	Effective friction angle of the subsoil.
φ_d	Reduced effective friction angle.
φ_{d_1}	Reduced effective friction angle for the rubble mound.
φ_{d_2}	Reduced effective friction angle for the subsoil.

θ	Geometrical angle in degrees or radians.
θ_I	Angle of the incidence waves (angle between wave crest and front of structure).
μ_{X_i}	Mean value of the stochastic parameter X_i.
μ	Takayama's friction coefficient.
σ	Stress or directional spreading in a short crested sea.
σ_{X_i}	Standard deviation of the stochastic parameter X_i.
ω_n	Displacement vector of stiff zones of soil , n=1,2,3..
ω_{nH}	Horizontal displacement vector of stiff zones of soil , n=1,2,3.. .
ω_{nV}	Vertical displacement vector of stiff zones of soil , n=1,2,3.. .
ζ	Tidal elevation.
ξ_m	The surf similarity parameter based on the deepwater wave length.
ξ_{mc}	Average surf similarity parameter.

Abstract

Breakwater design methods have been improved over the past years, especially the mathematical formulations of the failure mechanisms. In the case of rubble mound breakwaters, and vertical breakwaters, the last decade has been used to develop methods to evaluate e.g. the wave loads and hydraulic response, but in one area information has been lacking; bearing capacity has not been treated in depth in a probabilistic manner for breakwaters.

Reliability analysis of conventional rubble mound breakwaters and conventional vertical breakwaters is exemplified for the purpose of establishing new ways of approaching design problems in an early stage of breakwater design.

The deterministic design of *rubble mound breakwaters* with emphasis on the armour layer, toe berm and crown wall, and conventional vertical breakwaters is reviewed. Breakwater failure modes are reviewed with emphasis on establishing new methods to design certain types of breakwaters.

Reliability analyses of the main armour and toe berm interaction is exemplified to show the effect of a multiple set of failure mechanisms. First the limit state equations of the main armour and toe interaction are derived from laboratory tests performed by Bologna University. Thereafter a multiple system of failure for the interaction is established. Relevant stochastic parameters are characterized prior to the reliability evaluation.

Application of reliability in crown wall design is illustrated by deriving relevant single foundation failure modes in the rubble mound only. A crown wall with a plane base and with an extended leg on the seaward side is analysed. Relevant stochastic parameters are characterized prior to a reliability evaluation. The reliability is performed with real sea states to measure the influence of the chosen deterministic design.

Reliability based design of *conventional vertical breakwaters* is considered. Probabilistic models of important failure modes such as sliding and rupture failure in the rubble mound and the sand or clay subsoil are described. Characterization of the relevant stochastic parameters are presented, and relevant design variables are identified. The long-term goal is to be able to determine an optimal based design of vertical breakwaters where all relevant failure modes are modelled as components in a series system.

Dansk Resumé

Der er sket fremskridt på det vandbygningstekniske område inden for den fysiske formulering af de brudmåder, der indgår ved kystkonstruktioner. Inden for det sidste årti er der videreudviklet metoder til at bestemme f.eks. bølgelaster og hydraulisk respons for stenkastings- og vertikalmoler. Endnu mangler der informationer om, hvorledes bæreevnestabilitet skal behandles på probabilistisk vis i design af kystkonstruktioner.

Pålidelighedsanalyse af konventionelle stenkastningsmoler og vertikalmoler er eksemplificeret med henblik på at etablere nye måder at behandle design problemer på et tidligt planlægningsstadium.

Det deterministiske design af stenkastningsmoler med henblik på dæklag, tå og bølgeskærmstabilitet samt konventionelle vertikalmoler er gennemgået. Bølgebrydernes svigtformer er gennemgået med henblik på at etablere nye metoder til design af bestemte typer bølgebrydere.

Pålidelighedsanalyse af dæklag og tå interaktion er eksemplificeret for at vise den kombinerede effekt af svigtformerne. Først ved at udlede de fysiske ligninger fra laboratorieforsøg udført af Bologna Universitet. Derefter ved etablering af et kombineret svigtsystem for interaktionen. Karakterisering af relevante stokastiske parametre førend pålidelighedsevaluering.

Anvendelse af pålidelighed i bølgeskærmsdesign, baseret på udledelse af bæreevnebrudformer i stenkastningsmolen. En bølgeskærm med en plan bund og med en fod på søsiden er blevet analyseret. Karakterisering af relevante stokastiske parametre for at etablere en pålidelighedsevaluering er gennemført. Pålideligheden er udført med virkelige søtilstande, for at måle indflydelsen af de valgte deterministiske design.

Pålidelighedsbaseret design af konventionelle vertikalmoler er behandlet. Probabilistiske modeller af forskellige svigtformer, såsom glidning og bæreevnesvigt i stenkastningsvolden samt sand- og lerundergrund er beskrevet. Karakterisering af relevante stokastiske parametre er præsenteret og relevante design variabler er identificeret. Det langsigtede mål er at specificere optimal design af vertikalmoler i et serielt system af svigtformer bestående af bæreevnebrud.

1

Introduction

A number of breakwater failures has been reported during the last 20 years for rubble mound breakwaters as well as for vertical breakwaters, e.g. Bilbao (Spain), Tripoli (Libya), and Mutsu-Ogawara Port (Japan). This has resulted in new ways of approaching the design problems related to breakwaters. Probabilistic methods are being brought forward as an alternative to deterministic methods to solving breakwater design problems in the early stage of planning.

Conventional deterministic design of breakwaters is based on the design load philosophy which cannot exceed the resisting load (carrying capacity) of the breakwater. The design load is usually based on the typical probabilistic mean value for the 50 year return period, often without taking the uncertainties of the applied design load into consideration. The resistance is exemplified as the reaction of the design load in terms impact and damage to the breakwater, but not the ultimate deformation of the structure. Most design formulae are based on wave characteristic and structural and hydraulic response of the breakwater, e.g. sliding of acaisson/crown wall, static stability, overtopping, overturning etc.An example is static stability of the armour layer (rubble mound breakwater). Almost all such design formulae are semi-empirical and centrally fitted to small scale model test results. The test results include a considerable amountof scatter and the uncertainty of the scatter related to the expected value is not considered in conventional (deterministic) design of the breakwater.

Probabilistic modelling of structures improves feasible decision making, but at the same time requires improved knowledge of the statistical properties of design and resistance loads. This is clearly an important step towards obtaining a rational assessment of the reliability of breakwaters.

Regardless of the amount of information available the uncertainties cannot be completely eliminated. The uncertainties originate from inherent random fluctuations, incomplete statistical information, model idealization and lastly human errors.

1.1 Rubble mound breakwaters

Rubble mound breakwaters are normally divided into conventionally designed structures with a stable armour layer and structures where the armour layer is allowed to reshape.

Reshaped breakwaters are usually defined as berm breakwaters, which are designed so that the armour layer on the seaward side can be rearranged by the wave load to a state of equilibrium. Berm breakwaters are not constructed with a crown wall.

Conventional rubble mound breakwaters are constructed so that little or no movement of the armour layer is accepted on the seaward side. Conventional rubble mound breakwaters are often constructed with a crown wall compared to berm breakwaters. In the following the term rubble mound breakwater will be used instead of conventional rubble mound breakwater

Rubble mound breakwaters are built up of different materials. Especially the outer layer of a rubble mound breakwater can consist of Rocks, Cubes, Dolosses, Tetrapods, Accropod, Cob, see Burcharth (1993). The inclination of the seaward slope often determines the type of armour to be used. Inclination of rubble mound breakwaters are usually in the range of 1:1.5 to 1:3.5. The core usually consists of fine material, and a filter layer and a underlayer are placed under the armour layer to prevent wash out of the finer material. Typical cross sections of a rubble mound with a crown wall and without a crown wall are presented figure 1.1

Rubble mound breakwaters in recent years have been constructed in deep water as vessels grew in size. The increase in water depth has simultaneously increased the vulnerability of wave impact on breakwaters in comparison to breakwaters in shallow waters. This has resulted in increased research of rubble mound breakwater design and other types of breakwater designs.

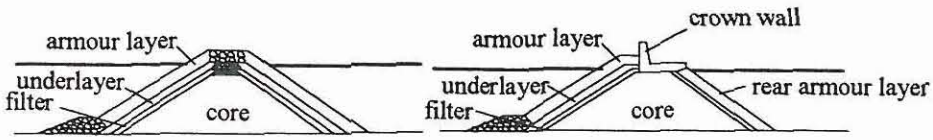

Figure 1.1: *Examples of typical rubble mound breakwater cross sections, with out a crown wall and with a crown wall*

1.1.1 Rubble mound breakwater failure modes

Parts of a rubble mound breakwater or the whole structure may fail during its lifetime. The various failure types can be regarded as failure modes. Figure 1.2 illustrates the various failure modes, which can occur during the life time of a rubble mound breakwater.

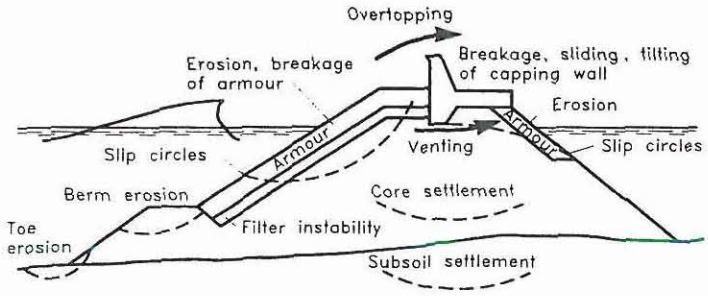

Figure 1.2: *Failure modes for conventional rubble mound breakwater, Burcharth (1991)*

Some modes of damage can be accepted, such as limited overtopping because little activity is expected on the rear side of the breakwater during severe storms, but each failure mode should be analysed and taken into consideration in the design phase. Primary failure modes are designated as the most vulnerable parts of a rubble mound breakwater, i.e. armour layer, toe berm, toe erosion and crown wall.

Research cooperation between Universities and consulting engineers has increased the knowledge in rubble mound breakwater design. One of these projects namely 'Rubble Mound Breakwater Failure Modes', MAST II (Marine Science and Technology) (1993 -1995) sponsored by the European Union investigated rubble mound failure modes and there interaction.

Application of reliability was mainly focussed on the failure mechanisms armour layer, toe berm and crown wall foundation stability.

1.2 Vertical breakwaters

The main concept of vertical breakwaters is to reflect waves, while rubble mound breakwaters are mainly used to reduce the reflection and increase the amount of wave dissipation on the structure. Vertical wall breakwaters can be constructed in a number of different ways. The most common types are shown in Figure 1.3.

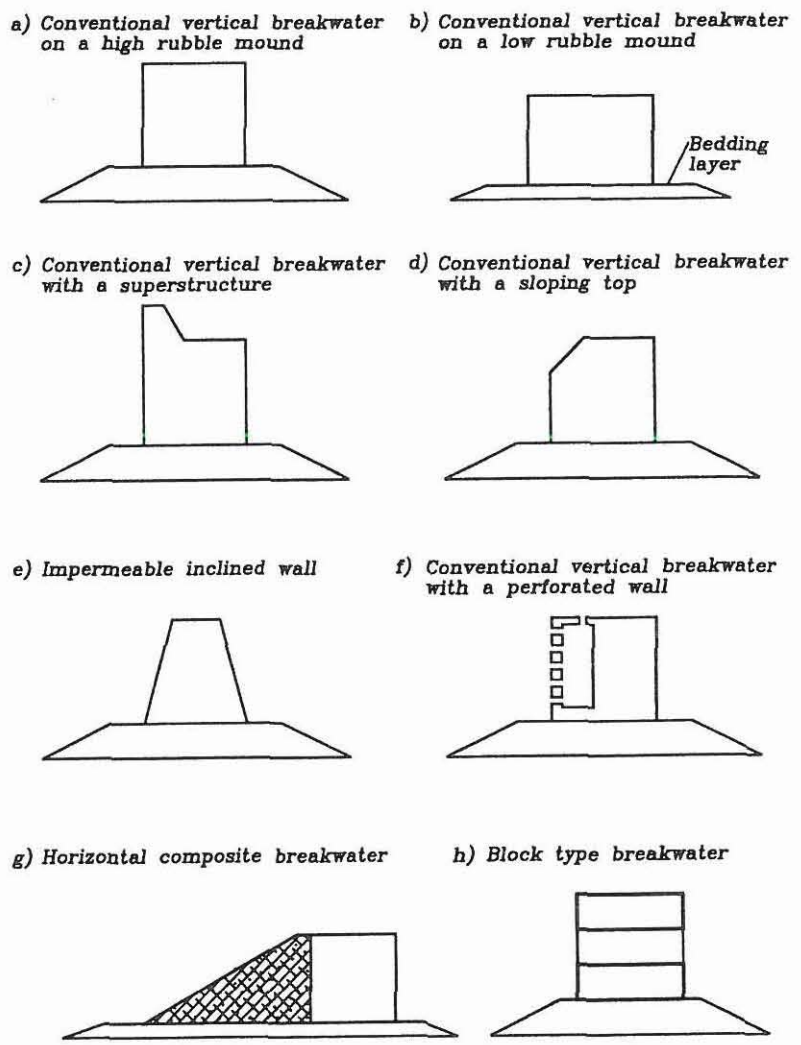

Figure 1.3: *Illustration of typical types of vertical breakwaters in use today.*

The most common types of vertical breakwaters are the conventional type on a high rubble mound, thin bedding layer, and a conventional vertical breakwater with a superstructure cf. 1.3 (a,b,c). To reduce wave reflection and the breaking force, alternative structures are used, i.e. conventional vertical breakwater with a sloping top, figure 1.3 (d), impermeable inclined wall 1.3 (e), caisson with a perforated wall on the seaward side 1.3 (f) and horizontal composite breakwater with wave dissipating blocks, which has similar response to wave loads as rubble mound breakwaters 1.3 (g). The block type breakwater 1.3 (h) consists of massive concrete blocks placed on each other to form a vertical breakwater.

In the following chapters conventional vertical breakwaters on high and low rubble mound cf. Figure 1.3 (a,b) will be considered in depth for alternative design procedures.

1.2.1 Vertical breakwater failure modes

The important failure modes for these types of breakwaters are sliding and failure of the foundation. However, a large number of foundation failure modes exists and must all be considered in a design procedure. Important examples are shown in Figure 1.4.

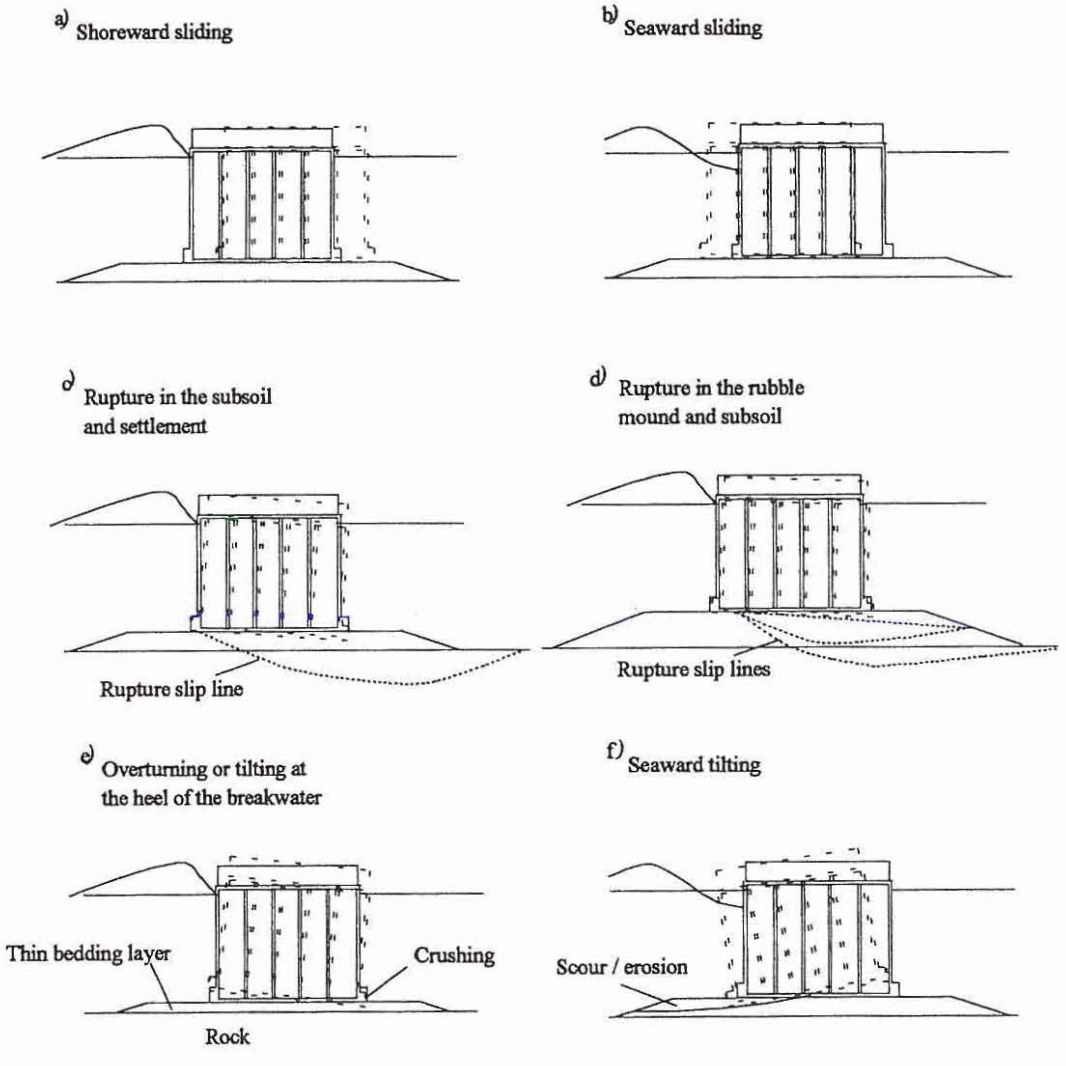

Figure 1.4: *The main failure modes for conventional vertical breakwaters*

The primary vertical breakwater failure modes in Figure 1.4, consist of shoreward sliding cf. Figure 1.4 (a), where the horizontal wave induced load exceeds the weight of structure reduced for wave induced uplift multiplied by the friction coefficient between the structure base and rubble mound. In the case of seaward sliding Figure 1.4 (b), a deep wave trough in front of the structure lies lower than the mean water level on the harbour side, thus causing an increase in the hydrostatic force in the seaward direction compared to the stabilizing force. A slight rupture in the rubble or subsoil will often result in settlement of the caisson thus reducing the effective weight of the caisson and allowing more overtopping than expected cf. Figure 1.4 (c). Rupture in the rubble mound and subsoil due to limiting bearing capacity of the foundation will cause instantaneous instability of the caisson, and increased overtopping levels cf. Figure 1.4 (d). When a vertical breakwater is relatively higher than the width, and the caisson is simultaneously placed on a thin bedding layer with a hard and compact subsoil, an increase possibility of overturning can be expected, see Figure 1.4 (e). An increase in scour or erosion of the rubble mound on the seaward side and a situation of a wave trough will increase the possibility of seaward tilting which is shown in Figure 1.4 (f).

Other local failure modes exist e.g scour at the toe (subsoil and/or rubble mound), stability of the rubble mound, wave transmission under the foot blocks at the foot of the caisson on the seaward side, structural failure of the caisson (cracks, sea water infiltration, wash out, corrosion causing reduced strength of the reinforced concrete walls). These local failure modes can initiate the main failure modes, thus causing instability of the vertical breakwater itself.

1.3 Improvement in the state of knowledge

Breakwaters are usually evaluated from the primary Failure modes cf. Figure 1.4 and 1.2. Working across international borders in MAST I, II and III (sponsored by the directorate General XII of the Commission of the European Community), and PIANC (Permanent International Association of Navigation Congresses), (working group 12, rubble mound breakwaters) and (working group 28, vertical breakwaters) enables comparison of related breakwater design procedures of structures. This exchange of knowledge and research has improved the basis for applying probabilistic based design methods as statistical information has been available for the design procedures.

1.3.1 Traditional design procedures

Civil Engineers generally refer to an idealized approach to design based on long term practice. These approaches involve safety margins, usually semi-empirically based on past experience, to account for all uncertainties. Breakwater design is mainly based on design related national recommendations from different regions in the world i.e. OCDI (1991), Technical standards for port and harbour facilities in Japan. Other recommendation are produced by international organisations like PIANC.

Traditional design is based on a deterministic approach. As an example sliding, overturning, and bearing pressure at the heel of a vertical breakwater are commonly used as design criterias for vertical breakwaters in Japan. The maximum design wave height is used as the only probabilistic parameter giving the desired wave height for a 50 year return period. In the case of sliding and overturning a safety factor of 1.2 (Japan) is applied so that the resistive load is 20 % greater than the design load. The acceptable bearing pressure at the heel is in the range 400 kN/m^2 to 600 kN/m^2

1.3.2 Reliability based design

Before a reliability analysis can be performed a clearly defined deterministic method has to be presented for the significant failure modes in question. It is the main scope of the upcoming work to show the relevance of incorporating foundation failure of vertical breakwaters and crown walls on rubble mound breakwaters, and main armour and toe berm interaction for rubble mound breakwaters. Numerous number of failure modes exists for breakwaters and it is beyond the scope of this thesis to include all failure modes in the following. Reference is given to Burcharth (1991), van der Meer (1993), and Goda (1985), for rubble mound breakwaters and vertical breakwaters. Reliability based calculations are not common practice in breakwater engineering. Therefore, it is also the scope of the thesis to show the applicability of reliability based design of breakwater structures.

Probabilistic calculations of breakwater reliability require that the failure modes are identified and expressed as analytical functions. Uncertain parameters are modelled as stochastic variables. These variables have to be given by their expected(mean) value, and their standard deviation, preferably also their distribution functions and correlations should be known.

Prior to a probabilistic evaluation of breakwaters, a series of preliminary investigations have to be done to clearly identify relevant stochastic parameters i.e. the the wave climate, the uncertainty of the analytic design function.

This thesis presents a probabilistic formulation of geotechnical stability assessment of vertical breakwaters and crown walls (rubble mound breakwaters), based on kinematical admissible rupture mechanisms of the foundation (rubble mound and subsoil). When evaluating plastic collapse of the foundation, no amount of site exploration can identify sufficient information of the soil parameters for a detailed description of the bearing capacity as local soil strength variations may influence the stability of the foundation. However, probabilistic models can capture a number of the uncertain features with a minimum number of additional soil parameters.

Single failure modes presented in Figure 1.2 and 1.4 (a) - (f), seldom occur in reality. A combination of the failure modes usually occurs thus presenting a multiple set of breakwater failures which cause a system to be evaluated. The following failure modes are analysed:

- Interaction of primary failure modes for rubble mound breakwaters,i.e. armour and toe berm failure based from laboratory work.
- System evaluation of vertical breakwater failure modes sliding, rupture failure, and overturning.

Application of reliability in a system evaluation of failure modes is presented for design of a conventional vertical breakwater, main armour and toe berm interaction.

Optimal based design of a breakwater is important in terms of monetary aspects, as a cost benefit analysis will usually decide the final design. Here optimal reliability based design of a conventional vertical breakwater using the system of foundation failure modes including overturning will be evaluated from a cost optimization principle based on the weight of the material used to construct the breakwater, i.e. the rubble foundation and caisson.

2

Vertical breakwaters

The present chapter is devoted to the summary of the design tools for vertical breakwaters based on long crested and short crested seas. Failure modes like sliding, overturning and rupture failure of the rubble mound and sand or clay subsoil for vertical breakwaters are presented.

2.1 Design of vertical breakwaters

A typical cross section of a conventional vertical breakwater is shown in Figure 2.1. The caisson is often divided into a number of chambers which are supported by reinforced concrete walls. The chambers are filled with sand, capped by concrete.

Foot protection blocks are placed on the seaward side to prevent erosion of the bedding layer subsoil. The armour protection blocks are installed to prevent damage to the rubble mound. For scour protection, additional gravel can be placed to form a gravel mat. A geotextile sheet can also be used to prevent scouring of the subsoil under the rubble mound.

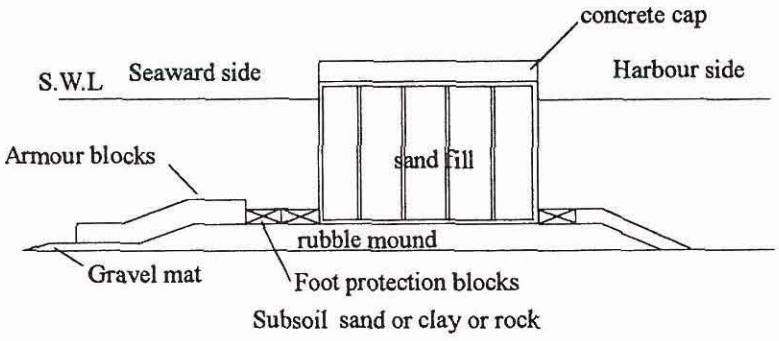

Figure 2.1: *Typical cross section of a conventional vertical breakwater.*

2.2 Introduction to wave loads on vertical breakwaters

The horizontal wave loads have traditionally been determined until the early 1980s from Hiroi (1919) and Sainflou (1928) design equations. Hiroi's wave load equation was based on vertical breakwaters in shallow waters, where extensive wave breaking took place. Sainflou's design equations was based on standing waves of the non breaking type, and the vertical breakwater was placed in deeper waters. To some extent Hiroi's design equations were on the conservative side while Sainflou's design equations had a tendency to underestimate the actual wave loads. Both Hiroi (1919) and Sainflou (1928) design equations were based on regular waves and no overtopping. This gave rise to implement irregular waves and limited wave breaking for the design of vertical breakwaters by Goda (1973).

Today it is accepted to apply Goda's wave load equations for long crested waves which are based on laboratory and prototype work, for the design of vertical breakwaters in Japan.

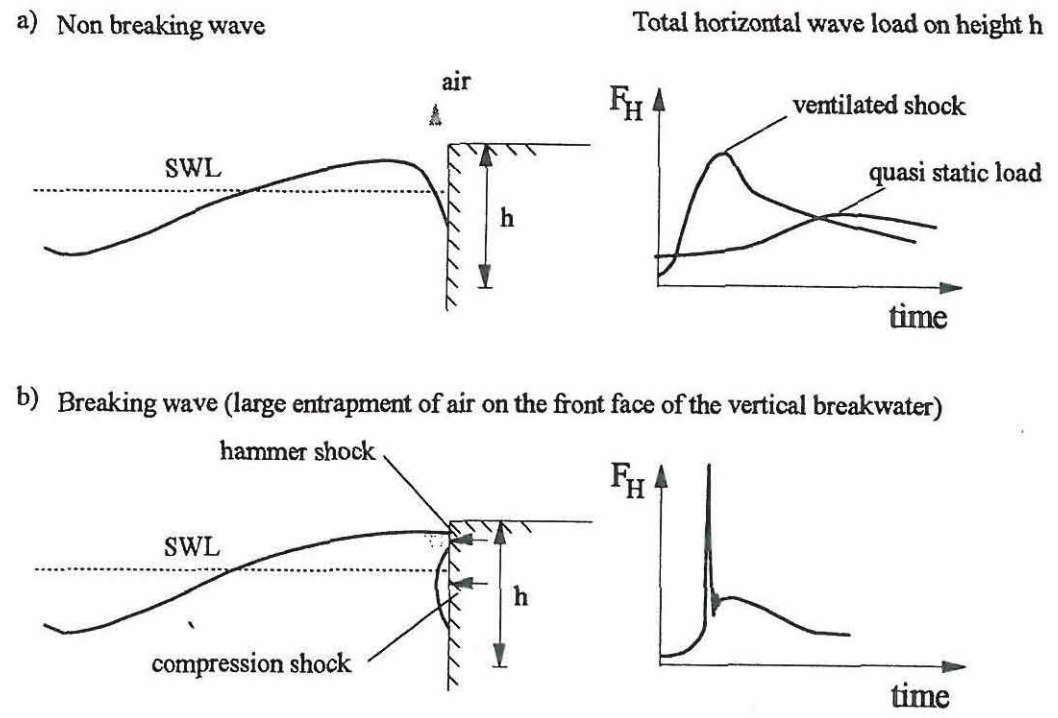

Figure 2.2: *Typical horizontal load histories induced by non breaking waves and breaking waves.*

It is accepted today that the wave pressures from non-breaking waves and breaking waves should be treated separately. The horizontal wave induced loads for non breaking waves are much less than the case of breaking waves; this is illustrated in Figure 2.2 a,b. The differentiation between non breaking waves and breaking waves was first realized by Bagnold (1939), and confirmation of the phenomenon was done by a series of laboratory experiments. Lundgren (1969) adapted the three wave shock types from Bagnold (1939), ventilated shock (no entrapped air), and hammer and compression shock (entrapped air), cf. Figure 2.2 a,b.

When a non-breaking wave approaches the front face of a vertical wall; the air between the wave and wall can escape in an upward direction. In the case of a slowly varying wave period, entrapment of air will not occur; thus resulting in gentle pressures variations in time, which can be termed as *quasi static wave loads*, see the illustration of the horizontal wave load in Fig. 2.2 a. As the wave period is about 10 to a 50 times larger than the natural period of the vertical breakwater.

In some cases of irregular seas the ventilated shock involves a fast rise in pressure (within tenths of a second), according to Lundgren (1969).

When a plunging breaker wave hits the wall at very high but short duration pressures will occur. The pressure rise time will be in the order of hundreths of a second, cf. Fig. 2.2 b. When an air pocket is entrapped to loading is in principal seperated in a socalled hammer shock caused by the impinging wave crest, and in a socalled compression shock caused by compressed air. The compressed air usually vibrates thus giving a high frequency load. An increase in the air pocket volume will decrease the load due to the buffer effect. Breaking waves at the front face of a vertical breakwater are usually termed as implusive wave loads.

In this thesis the *quasi static wave loads*, and implementation of impulsive wave coefficient in Goda's design equations from Takahshi et al. (1994) are treated as static loads. This is a simplification, and it should be noted that if impulsive wave action is dominant in design; the dynamic response of the vertical breakwater should be investigated. This has been done by Goda (1994b), Oumeraci et al. (1994) and Klammer et al. (1996).

In the following, a review of the wave heights in the surf zone as presented by, Goda (1994a), and the Goda wave load formulae for long crested waves will be presented. A method will be shown to determine wave loads in a short crested sea (non-breaking waves) based on laboratory work, Franco (1996). For a general description of the wave loads in non-breaking short crested sea on a vertical wall, reference is given to Battjes (1982) theory based on linear waves. Franco's design equation will give a rough approximation of the actual wave loads in a real irregular sea (non-breaking waves).

2.2.1 Design wave heights in the surf zone

The design wave height, i.e with a 50 year return period, is usually determined from an extreme statistical distribution, i.e. Weibull, Gumbel and Exponential distribution in deep water. Breakwaters are often situated close to land so in many cases part of the structures will be placed in both deep and shallow waters. Therefore the design wave will often be limited by the water depth causing waves to break in the surf zone. Goda (1975) proposed a set of equations to calculate the design wave height in shallow waters.

$$H_s = \begin{cases} K_s H_{so} & : \; h/L_o \geq 0.2 \\ min\{(\beta_o H_{so} + \beta_1 h), \beta_{max} H_{so}, K_s H_{so}\} & : \; h/L_o < 0.2 \end{cases} \tag{2.1}$$

where K_s is the shoaling coefficient of the finite amplitude waves cf. Figure 2.3, H_{so} is the equivalent deepwater significant wave height, h the water depth, L_o is the deepwater wavelength. The function $min\{a, b, c\}$ takes the minimum value among a, b and c. The coefficients β subscript are listed in the set of equations (2.2)

Coefficients for the significant wave height H_s in the surf zone

$$\begin{aligned} \beta_o &= 0.028(H_{so}/L_o)^{-0.38} \exp(20 \tan^{\frac{3}{2}} \theta) \\ \beta_1 &= 0.52 \exp(4.2 \tan \theta) \\ \beta_{max} &= max\{0.92, 0.32(H_{so}/L_o)^{-0.29} \exp(2.4 \tan \theta)\} \end{aligned} \tag{2.2}$$

$$H_{design} = \begin{cases} 1.8 K_s H_{so} & : \; h/L_o \geq 0.2 \\ min\{(\beta_o^* H_{so} + \beta_1^* h), \beta_{max}^* H_{so}, 1.8 K_s H_{so}\} & : \; h/L_o < 0.2 \end{cases} \tag{2.3}$$

Coefficients for the corresponding design wave height $H_{design} = H_{1/250}$ in the surf zone

$$\begin{aligned} \beta_o^* &= 0.052(H_{so}/L_o)^{-0.38} \exp(20 \tan^{\frac{3}{2}} \theta) \\ \beta_1^* &= 0.63 \exp(4.2 \tan \theta) \\ \beta_{max}^* &= max\{1.65, 0.53(H_{so}/L_o)^{-0.29} \exp(2.4 \tan \theta)\} \end{aligned} \tag{2.4}$$

In case of a surf zone in front of the structure the breaker height is taken as (Goda, 1994 b)

$$H_b = L_0 \, 0.17 \left(1 - exp\left(-1.5 \frac{\pi h_b}{L_0} \left(1 + 15 tan^{4/3} \theta\right)\right)\right) \tag{2.5}$$

where h_b is the water depth at a distance $5H_s$ seaward of the structure.

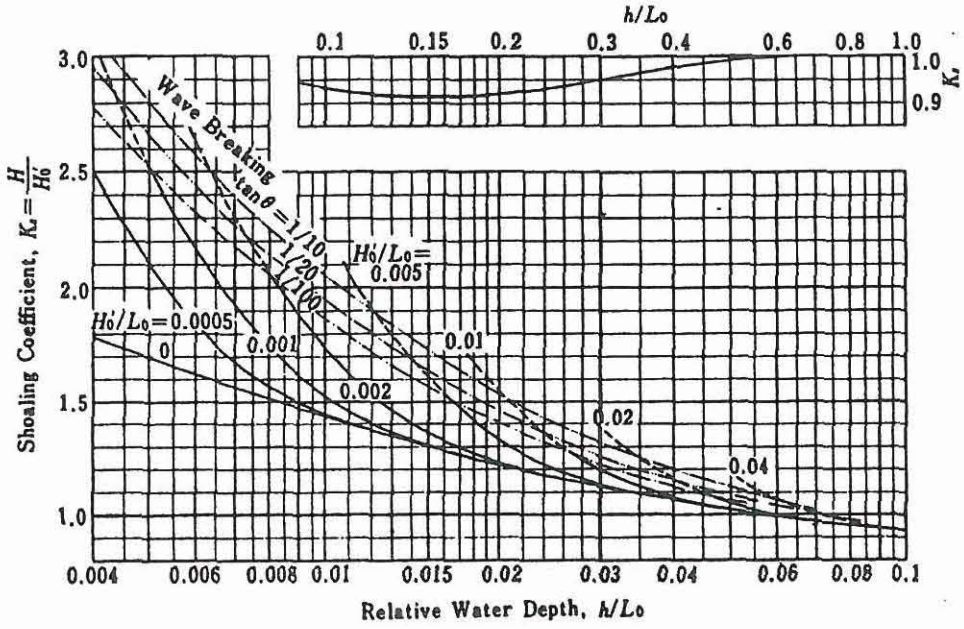

Figure 2.3: *Shoaling coefficient K_s as a function of h/L_o (redrawn from Goda (1992)).*

2.2.2 Wave loads in long crested seas

Wave pressure formulae have been developed by Goda et al. (1972) and Goda (1974) for the case of a conventional vertical front where wave breaking on the wall is not enhanced by a steep sea bed or structural configurations. The formulae are based on model tests in head-on waves but were modified to cover also oblique waves on the basis of work by Tanimoto et al. (1976). The formulae include the effect of breaking waves to the extent of normal accidental (non-provoked) wave breaking. The formulae are currently used in the Japanese standards. Figure 2.4 shows the related definition sketch for the wave induced pressure under a wave crest.

$$\eta^* = 0.75(1 + cos\theta_I)\, H_{design} \tag{2.6}$$

$$p_1 = 0.5(1 + cos\theta_I)(\alpha_1 + \alpha_2 cos^2\theta_I)\, \rho_w\, g\, H_{design} \tag{2.7}$$

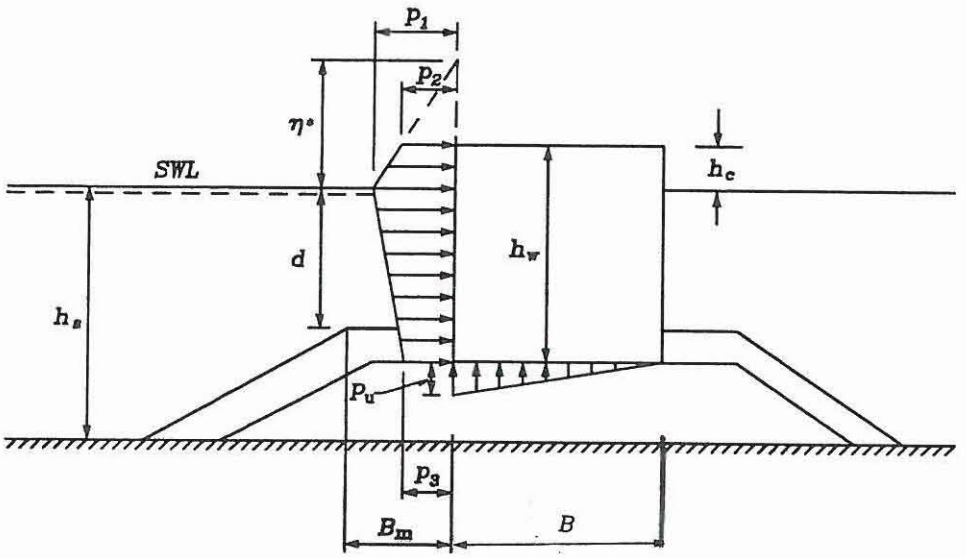

Figure 2.4: *Definition sketch for the Goda formula for wave induced pressure under a wave crest.*

$$p_2 = \begin{cases} \left(1 - \frac{h_c}{\eta^*}\right) p_1 & \text{for } \eta^* > h_c \\ 0 & \text{for } \eta^* \leq h_c \end{cases} \tag{2.8}$$

$$p_3 = \alpha_3 \, p_1 \tag{2.9}$$

where

θ_I angle of incidence of waves (angle between wave crest and front of structure)

H_{design} design wave height defined as the highest wave in the design sea state at a location just in front of the breakwater. If seaward of a surf zone a value of 1.8 H_s might be used corresponding to the 0.1% exceedence value for Rayleigh distributed wave heights. If within a surf zone H_{design} is taken as the highest of the random breaking waves at a distance $5H_s$ seaward of the structure.

L wave length corresponding to that of the significant wave $T_s \simeq 1.1T_m$, where T_m is the average period.

$$\alpha_1 = 0.6 + \frac{1}{2}\left[\frac{4\pi\, h_s/L}{sinh\ (4\pi\, h_s/L)}\right]^2 \tag{2.10}$$

$$\alpha_2 = \text{the smallest of } \frac{h_b - d}{3\, h_b}\left(\frac{H_{design}}{d}\right)^2 \text{ and } \frac{2d}{H_{design}} \tag{2.11}$$

$$\alpha_3 = 1 - \frac{h_w - h_c}{h_s}\left[1 - \frac{1}{cosh\ (2\pi\, h_s/L)}\right] \tag{2.12}$$

h_b water depth at a distance of $5H_s$ seaward of the breakwater front wall.

Although the wave induced uplift pressure, p_u, at the front edge of the base plate is equal to p_3 it is suggested by Goda to use a somewhat reduced value

$$p_u = \frac{1}{2}\,(1 + cos\theta_I)\ \alpha_1\, \alpha_3\, \rho_w\, g\, H_{design} \tag{2.13}$$

This is because analyses of the behaviour of Japanese breakwaters revealed that the use of $p_u = p_3$ together with an assumed triangular distribution of the uplift pressure gave too conservative results.

Modification of Goda's horizontal wave pressure, considering impulsive breaking wave forces

Goda's horizontal wave pressure formulae do not consider frequent wave breaking close to and at the vertical breakwater. Therefore the extra effect of larger impulsive forces from breaking waves has been investigated and incorporated in Goda's formulae by Takahashi et al. (1994). The modification of Goda's formula concerns the formula for the pressure p_1 at the water surface, equation (2.7) and is a replacement of α_2 coefficient with a impulsive pressure coefficient α_*. The impulsive pressure coefficient α_* is determined from regular wave tests and is assumed to be a good approximation until further research has confirmed the validity of the impulsive wave coefficient based on irregular waves.

$$p_1 = 0.5(1 + cos\theta_I)(\alpha_1 + \alpha_* cos^2\theta_I)\, \rho_w\, g\, H_{design} \tag{2.14}$$

where α_* can be expressed as follows

$$\alpha_* = max\{\alpha_2, \alpha_I\} \tag{2.15}$$

where α_2 is derived from Goda's formula, equation 2.11, and α_I is a non-dimensional impulsive pressure coefficient being the product of α_{I0} and α_{I1}, where α_{I0} represents the effect on the design wave heigth and α_{I1} represents the shape of the rubble mound.

$$\alpha_{I0} = \begin{cases} H_{design}/d & H_{design}/d \leq 2 \\ 2.0 & H_{design}/d > 2 \end{cases} \tag{2.16}$$

where d is the water depth at the crest of the rubble mound berm in front of the caisson.

$$\alpha_{I1} = \begin{cases} \frac{\cos \delta_2}{\cosh \delta_1} & \delta_2 \leq 0 \\ \frac{1}{\cosh \delta_1 \cdot (\cosh \delta_2)^{\frac{1}{2}}} & \delta_2 > 0 \end{cases} \tag{2.17}$$

where δ_1 and δ_2 are coefficients which depend on the structural dimensions of the rubble mound in front of the caisson , cf. Figure 2.4, on the incident wave.

$$\delta_1 = \begin{cases} 20 \cdot \delta_{1\,1} & \delta_{1\,1} \leq 0 \\ 15 \cdot \delta_{1\,1} & \delta_{1\,1} > 0 \end{cases} \tag{2.18}$$

$$\delta_{1\,1} = 0.93 \left(\frac{B_m}{L} - 0.12 \right) + 0.36 \left(\frac{h_s - d}{h_s} - 0.6 \right) \tag{2.19}$$

$$\delta_2 = \begin{cases} 4.9 \cdot \delta_{2\,2} & \delta_{2\,2} \leq 0 \\ 3 \cdot \delta_{2\,2} & \delta_{2\,2} > 0 \end{cases} \tag{2.20}$$

$$\delta_{2\,2} = -0.36 \left(\frac{B_m}{L} - 0.12 \right) + 0.93 \left(\frac{h_s - d}{h_s} - 0.6 \right) \tag{2.21}$$

where B_m berm width of the rubble mound foundation in front of the caisson breakwater, cf. Figure 2.4

L wave length corresponding to that of the significant wave period $T_s \simeq 1.1T_m$, where T_m is the average period.

The term α_I reaches a maximum value of 2, when $B_m/L = 0.12$, $d/h_s = 0.4$ and $H_{design}/d \geq 2$. When the term $d/h_s > 0.7$, then impulsive pressures rarely occur and α_I is close to zero and smaller than α_2.

The wave induced horizontal force, F_H, uplift force F_U and the reduced weight of the vertical structure due to buoyancy F_G can be calculated from equations by Goda and Takahashi.

$$F_H = \frac{1}{2}(p_1 + p_2)h_c + \frac{1}{2}(p_1 + p_3)(h_w - h_c) \quad kN/m \tag{2.22}$$

$$F_U = \frac{1}{2}p_u B \quad kN/m \tag{2.23}$$

$$F_G = \rho_c\, gBh_w - \rho_w gB(h_w - h_c) \quad kN/m \tag{2.24}$$

where B is the caisson width, ρ_c density of the caisson and ρ_w is the density of the sea water.

The moment about the heel M_H, moment of the wave induced uplift force M_U and moment of the weight M_G of the caisson breakwater can be calculated by applying Goda's and Takahashi's formulae to the above given parameters:

$$M_H = \frac{1}{6}(2p_1 + p_3)(h_w - h_c)^2 + \frac{1}{2}(p_1 + p_2)(h_w - h_c)h_c + \frac{1}{6}(p_1 + 2p_2)h_c^2 \quad kN \tag{2.25}$$

$$M_U = \frac{1}{3}p_u B^2 \quad kN \tag{2.26}$$

$$M_G = \frac{1}{2}(\rho_c gBh_w - \rho_w gB(h_w - h_c))B \quad kN \tag{2.27}$$

2.2.3 Wave loads in a short crested sea

Improvements in prefabrication of large conventional breakwaters from the traditional (20 - 40 m) up to 100 m have given thought to alternative design considerations for evaluating the extreme wave loads encountered along the structure on the seaward side. Correct assessment of the wave induced load in 3 - dimensional directional sea state may allow for substantial savings in construction.

The breakwater designer is always interested in reducing the overall wave loads and at the same time ensuring sufficient stability of the structure. Therefore introducing directional spreading in the sea state will effectively reduce the wave load along the structure length compared to a fictive 2 dimensional sea state.

Battjes (1982) derived a theoretical approach using linear wave theory for **non breaking short crested waves**. The outcome was expressed as a frequency dependent directionally averaged spectral multiplication factor, G_L, for the load relative to the case of normally incident long crested waves. $G_L^{0.5}$ expresses the ratio of the actual load to the load from head on long–crested waves. The load is the integrated wave generated pressure over the length of the structure, ℓ_s.The uneven load distribution over ℓ_s, which might cause horizontal turning of the structure, is not given.

Figure 2.5 shows for a cos^2 type directional distribution the load reduction factor $G_L^{0.5}$ as a function of the angle of incidence θ_I for the mean direction of wave propagation, and of ℓ_s/L where L is the wave length corresponding to the spectral peak frequency.

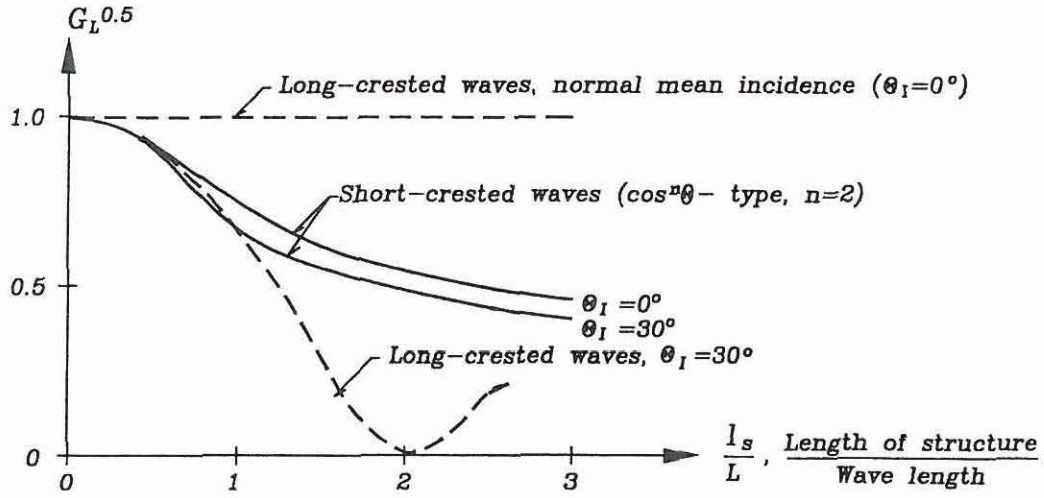

Figure 2.5: Examples of load reduction factors for non–breaking short–crested seas. (Based on diagrams given in Battjes, 1982.)

Wave loads in a short crested sea, based on laboratory tests (non-breaking waves)

A series of laboratory experiments were performed by Delft Hydraulics, Politecnico di Milano and Aalborg University within the combined MAST II-LIP project, to describe the wave loads in a non breaking short crested sea. From the extensive data set, which included different types of vertical breakwaters, different sea states and measured wave pressures on the test caisson, it is possible to describe the horizontal and vertical induced loads in a short-crested sea by means of a statistical distribution, notably a 2-parameter Weibull distribution eq. (2.28), Franco (1996).

$$P(F) = \exp\left[-\left(2.547\frac{F}{rF_{Goda}}\right)^{b}\right] \tag{2.28}$$

where the factor r is the bias of the measured wave load divided by the calculated wave load by the Goda in an assumed long crested sea state. The shape parameter b is given in Table 2.1 for the horizontal wave load and wave induced uplift for conventional vertical breakwater. The coefficient 2.547 is determined by substituting the probability of exceedence $P(F_{0.152\%}) = 0.00152$, corresponding to Goda's definition of $F_{1/250}$ (average of the highest 1/250 waves) into a Rayleigh distribution $P(F) = exp\left[-(F/a)^2\right]$, $1/a = 2.547$. F_{Goda} is the horizontal wave load and wave induced uplift given by Goda for long crested seas.

Wave load type	s_p	r		b	
		μ	σ/μ	μ	σ/μ
Horizontal wave load F_H^{3D}	0.04	0.84	0.12	2.13	0.24
	0.02	0.83	0.14	2.26	0.23
Wave induced uplift F_U^{3D}	0.04	1.04	0.06	2.37	0.29
	0.02	0.93	0.14	2.18	0.10

Table 2.1: Mean values and coefficient of variation for factor r , and shape parameter b for two wave steepness s_p, taken from Franco (1996).

The factor r and the shape parameter b have little dependency on the main wave direction, and the directional spreading which was calculated from the two sea states 23° and 28°. Therefore equation (2.28) should only be regarded as a rough estimation of the actual wave induced loads in a non-breaking short crested sea state.

2.3 Failure modes for vertical breakwaters

The following section is devoted to relevant failure modes for vertical breakwaters: Sliding, foundation failure of the rubble and sand or clay subsoil, overturning and bearing pressure at the heel. Hydraulic responses (overtopping, reflection and wave transmission) of the breakwater is reviewed to give the reader an illustration of other important design factors, but they will not be investigated in detail.

2.3.1 Sliding

Stability against sliding exists when the ratio of the resultant horizontal force, F_H, to the resultant vertical force is equal to or less than the coefficient of friction, μ, between the base plate and the underlayer, i.e.

$$F_H \leq (F_G - F_U)\ \mu \tag{2.29}$$

where F_G is the weight of the caisson reduced for buoyancy and F_U is the wave induced uplift force on the concrete base plate of caisson. F_H is calculated by using the Goda's wave pressure formula.

The friction coefficient is according to Takayama, 1992, assumed normal distributed with mean value $\mu = 0.636$ and a coefficient of variation of 15%.

The following table is taken from Japanese design guide lines OCDI (1991) and gives friction coefficient values for different kinds of materials.

Concrete against concrete	0.5
Concrete against bed rock	0.5
Concrete in water against bed rock	0.7 (bedrock cracks) - 0.8
Concrete in water against rubble	0.6
Rubble against rubble	0.8
Timber against timber	0.5 (dry) - 0.2 (wet)

Table 2.2: Coefficients of static friction. OCDI (1991)

2.3.2 Overturning

Stability against overturning exists when the moment of horizontal forces M_H is equal to or less than the resultant moment of vertical forces about the heel:

$$M_H \leq (M_G - M_U) \tag{2.30}$$

where M_G is the moment around the heel induced by the weight of the caisson, reduced for buoyancy and M_U is the moment around the heel and calculated from the wave induced uplift forces.

2.3.3 Foundation stability

The foundation of vertical breakwaters is important to fully evaluate the stability of the breakwater. The bearing capacity of the rubble mound and subsoil should be analysed while subjected to inclined and eccentric loads from the wave loads and weight of the breakwater. To evaluate the stability of the rubble mound foundation, sand subsoil and clay subsoil, a method of limit state analysis is formulated, which also can be applied in a probabilistic design procedure.

Bearing capacity of vertical breakwaters are traditionally designed on the basis of stability of slopes, i.e Bishops simple method of slices, or the general bearing capacity equation from DS 415 (1984). The rupture slip line in Bishop's methods of slices is predetermined by a circular slip surface which is not applicable to rubble mound or a sand subsoil, except in the case of cohesion based soil. The rupture slip line in the rubble mound and subsoil usually follows a rupture slip line different from a circular slip failure.

Plasticity theorems can assist the designer to define the bounds of plastic collapse loads of structures. Investigation into more refined soil models can also clarify certain aspects of the stability of the foundation. The upper bound theorem of plasticity is one of the methods, which is applicable to foundation stability and at the same time ideal for a probabilistic evaluation. Upper bound theorem is based on equating the external work to rate of internal energy dissipation in an assumed velocity field. The velocity field should satisfy the velocity boundary conditions, and the strain and velocity compatability conditions are not less than the actual collapse load. This is termed as a kinematical admissible velocity field. So the upper bound theorem states that if a kinematical velocity field can be established, unchangeable plastic flow must have taken place previously. The upper bound theorem contains velocity modes (displacement vectors) and energy dissipations, and the stress distribution need not be in equilibrium, see Chen et al. (1990).

In reality the difficulty lies in the discrepancy of plastic deformation of ideal material and real material, as the real material will exhibit some degree of work softening and may not follow the associated flow rule.

The normality condition (assumed associated flow rule) is a simplification which enables the derivation of the bearing capacity of the foundation, as the angle of dilation is taken equal to the effective friction angle $\psi=\varphi'$, which results in a bearing capacity to be on the unsafe side, see Chen et al. (1990).

Application of the upper bound theorem from general plasticity theory requires that the normality condition is fulfilled. Experience shows that good estimates of the bearing capacity can be obtained using a reduced effective friction angle, φ_d from the effective friction angle, φ', and the angle of dilation, ψ, see Hansen (1979).

$$\tan\varphi_d = \frac{\sin\varphi'\cos\psi}{1-\sin\varphi'\sin\psi} \tag{2.31}$$

Bearing pressure at the heel of a conventional breakwater

The following procedure to determine the maximum heel pressure is traditionally applied in the design of conventional breakwaters in Japan OCDI (1991). It is assumed that the bearing pressure distribution under gravity structures are either trapezoidal or triangular cf. Figure 2.6

The bearing pressure q_1 and q_2 can be calculated using

$$t_e > \frac{B}{3} \quad q_1 = 2(F_G - F_U)/B(2-3t_e/B) \tag{2.32}$$

$$q_2 = 3(F_G - F_U)/B(2t_e/B-1) \tag{2.33}$$

$$t_e \leq \frac{B}{3} \quad q_1 = 2(F_G - F_U)/3te \tag{2.34}$$

$$q_2 = 0 \tag{2.35}$$

$$t_e = (M_G - M_U - M_H)/(F_G - F_U) \tag{2.36}$$

The maximum allowable heel pressure according to Japanese design guidelines is taken as 400 kN/m^2 to 600 kN/m^2 or greater, especially for deepwater breakwaters.

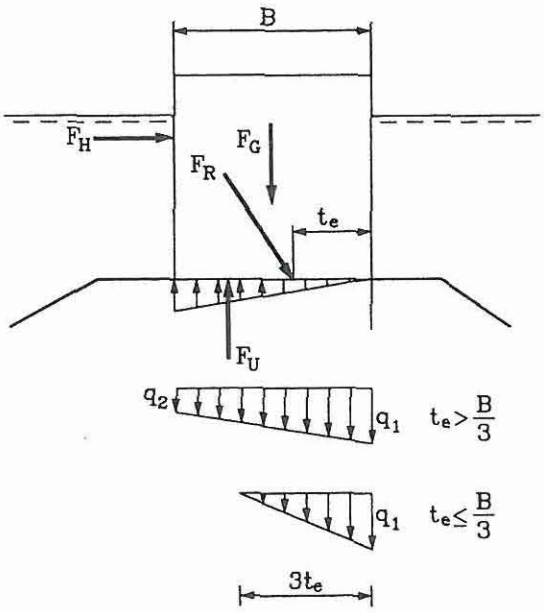

Figure 2.6: *Definition sketch for the bearing pressure under gravity structures .*

Circular slip failure in the rubble foundation and subsoil

The circular slip failure of the rubble mound is determined by the simplified Bishops method. The simplified Bishop method is based on the method of slices. Kobayashi (1987) proposed a load distribution along the rubble mound as q cf. Figure 2.7. This external load is implemented in the simplified Bishop method.

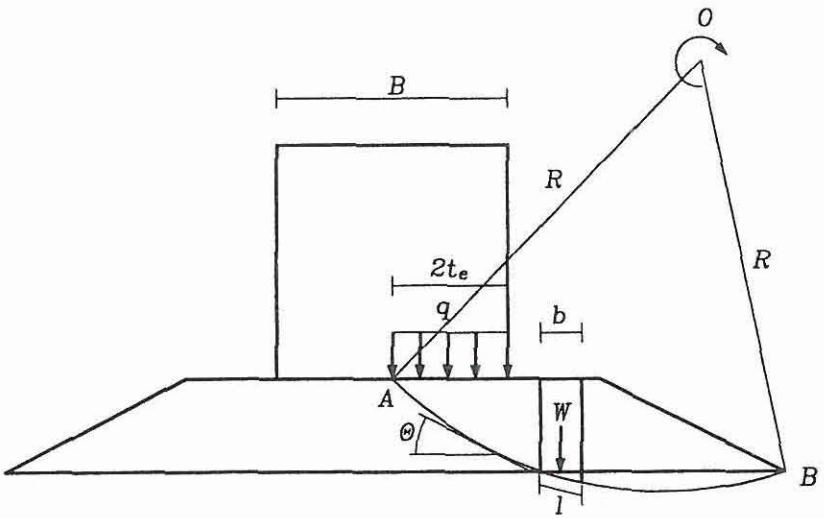

Figure 2.7: *Definition sketch for the circular slip failure of the rubble mound subsoil.*

$$q = \frac{B}{4t_e}(q_1 + q_2) \quad t_e > \frac{B}{3} \tag{2.37}$$

$$q = \frac{3}{4}q_1 \qquad t_e \leq \frac{B}{3} \tag{2.38}$$

where q_1 and q_2 are given by equation (2.32) and (2.33) and t_e is given by equation (2.36)

The simplified Bishop method of slices is applied to determine the safety factor of the slope on the rear side of the vertical breakwater. This method is traditionally used by Japanese design guide lines OCDI (1991).

$$F_{slice} = \frac{\sum [c'b + (W - U + q)\tan\varphi'] \frac{1}{M(\theta)}}{\sum (W - U + q)\sin\theta + \frac{1}{R}\sum M_o(F_H)} \tag{2.39}$$

where c' is the cohesion, W is the weight of each slice, U is the uplift due to the buoyancy of the rubble, b is the width of each slice , θ is the slope of each slice cf. Figure 2.7 , $Mo(F_H)$ is the moment of the horizontal wave induced load about point O and $M(\theta)$ is factor shown below:

$$M(\theta) = \cos(\theta) \cdot \left(1 + \frac{\tan\theta \tan\varphi'}{F_{slice}}\right) \tag{2.40}$$

The equation (2.39) is solved by dividing the slope into a number of slices and through a trial procedure the safety factor F_{slice} is calculated. A first value of F_{slice} i.e. 1 is introduced to compute $M(\theta)$ into equation (2.39) which gives a new value to iterate, until small difference in the safety factor is obtained.

General bearing capacity formula

The general bearing formula is based on applying plasticity theory to a rupture field which is statically and kinematical admissible. For traditional single-, continuous-, footing foundation with horizontal terrain/rear slope and a horizontal base can the soils bearing capacity be determined by the general bearing capacity equation.

$$\frac{Q}{A} = \frac{1}{2}\gamma B_z N_\gamma s_\gamma i_\gamma g_\gamma + q N_q s_q i_q g_q + c N_c s_c i_c g_c \tag{2.41}$$

where A is the effective area of the foundation, B_z is the effective width of the foundation, Q is the bearing capacity, γ is the specific weight of the underlying soil, N_γ is the bearing capacity factor for the self weight, i subscript is the inclination factor, s subscript is the form factor, q is the vertical load from the overlying soil, g subscript is the rear slope factor, c is the cohesion, N_c is the bearing capacity factor, considering cohesion, N_q is the bearing capacity factor considering overlying soil or extra weight on the rear side of the foundation. All the factors and the bearing capacity equation are described in detail in DS 415 (1984).

Bearing capacity equation for sand and gravel on a horizontal terrain with a slope on the rear side, when $c = 0$ and $q = 0$ is given by:

$$\frac{Q}{A} = \frac{1}{2}\gamma B_z N_\gamma s_\gamma i_\gamma g_\gamma \tag{2.42}$$

where N_γ is given by:

$$N_\gamma = F(\varphi')\left(\frac{1+\sin\varphi'}{1-\sin\varphi'} e^{\left(\frac{3\pi}{2}\tan\varphi'\right)} - 1\right) \tag{2.43}$$

$$F(\varphi') \approx 0.08705 + 0.3210\sin 2\varphi' - 0.04836\sin^2 2\varphi' \tag{2.44}$$

where φ' is the effective friction angle of the rubble or sand.

The form factor s_γ is given by:

$$s_\gamma = 1 - 0.4\frac{B_z}{L_c} \tag{2.45}$$

where L_c is the effective length of the foundation (caisson breakwater).

The dimensionless inclination factor i_γ is given by:

$$i_\gamma = \left(1 - \frac{F_H}{(F_G - F_U) + B_z c \cot\varphi'}\right)^4 \tag{2.46}$$

where F_H is the horizontal wave induced load, F_G is the weight of the caisson reduced for buoyancy, F_U is the wave induced uplift force on the base plate, and c is the cohesion of the rubble or sand.

The dimensionless slope factor g_γ is given by:

$$g_\gamma = 1 - \sin 2\theta_g \tag{2.47}$$

where $\theta_g = \arctan(s)$, s is the slope at the rear side $(1 : s)$.

Bearing capacity equation for horizontal terrain (short period bearing capacity of the clay subsoil), where $\varphi' = 0$ and $q = 0$ can be written as:

$$\frac{Q}{A} = c_u N_c^o s_c^o i_c^o \tag{2.48}$$

The bearing capacity factor for the undrained shear strength of the clay is:

$$N_c^o = \pi + 2 = 5.14 \tag{2.49}$$

The form factor s_c^o is given by:

$$s_c^o = 1 - 0.2\frac{B_z}{L_c} \tag{2.50}$$

where L_c is the effective length of the foundation (caisson breakwater).

The dimensionless inclination factor i_c^o is given by:

$$i_c^o = 0.5 + 0.5\sqrt{1 - \frac{F_H}{Ac_u}} \tag{2.51}$$

where F_H is the horizontal wave induced load, and c_u is the undrained shear strength of the clay.

In the case of a continuous footing: A should be replaced with B_z and $s = s_c^o = s_\gamma = 1$ per definition.

Foundation failure modes

The following 10 kinematically admissible rupture figures have been identified see Figure 2.8 a - 2.8 b. The 10 rupture figures are used to derive the bearing capacity by applying the upper theorem of plasticity, corresponding to static load cases only. Derivation of the bearing capacities is explained in depth in Appendix A.

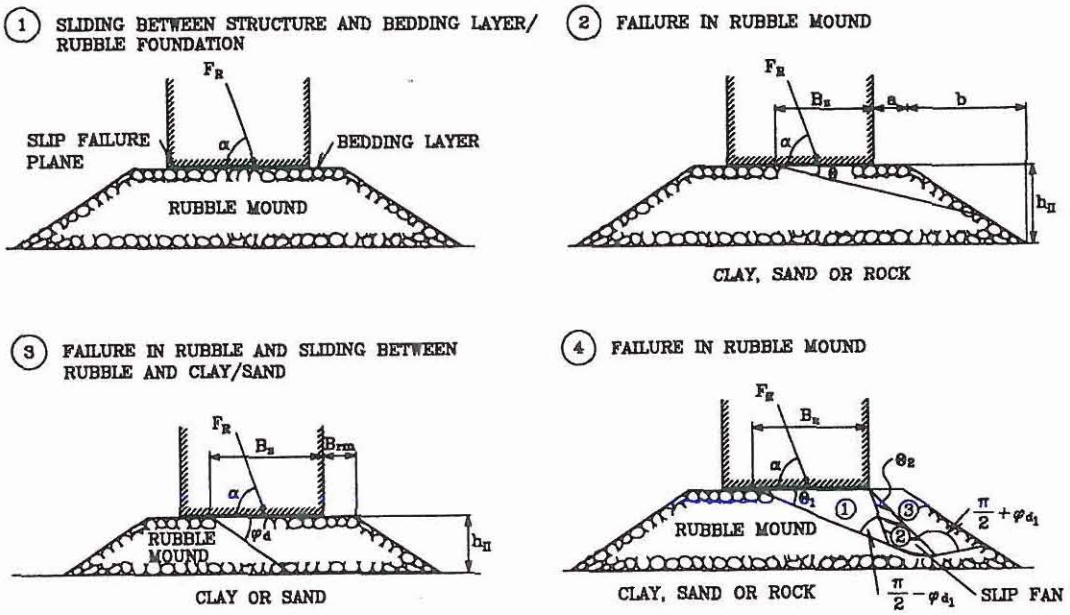

Figure 2.8: a: *Various kinematically admissible foundation failure modes.*

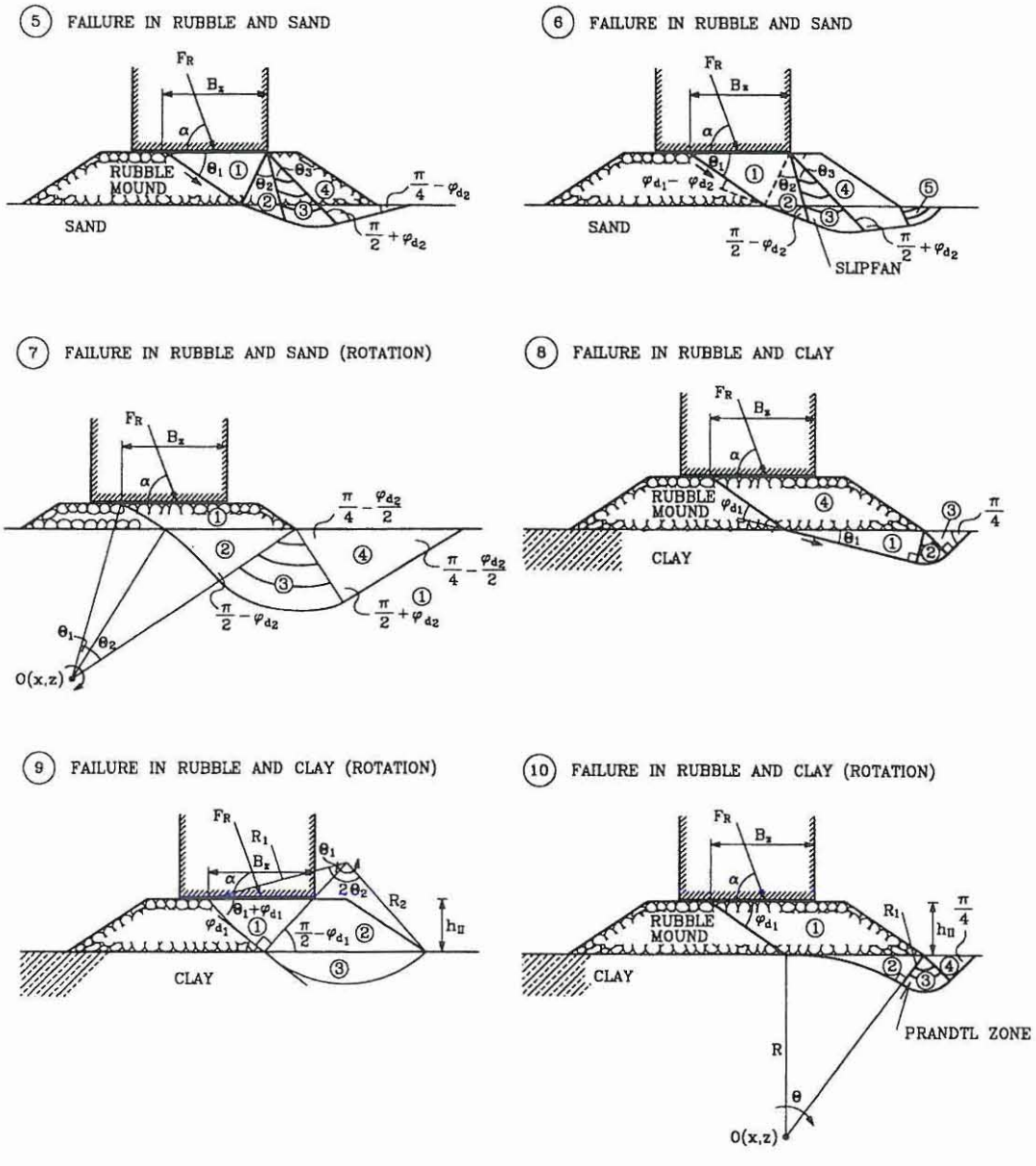

Figure 2.8 b: *Various kinematically admissible foundation failure modes.*

2.3.4 Hydraulic responses

The hydraulic response is described as the response of the breakwater structure induced by the propagating waves. Hydraulic response is signified as overtopping, wave transmission (disrupting harbour activity) and wave reflection on the seaward side of the structure. These three 'failure modes' are determining the breakwater type in terms of preliminary structural dimensions and permeability of the structure.

Overtopping

Overtopping is defined as a wave on the seaward side of a caisson breakwater which splits over the crest of the structure, and settles on the structure and on the rear side. Mild overtopping in the form of spray can be of inconvenience, if there is a road or concentrated traffic on the rear side of the breakwater. A great deal of laboratory work has been performed by Franco (1996), which has given basis to a formulation of overtopping in an environment of 2D and 3D waves. The equation is fitted within the 95 % confidence band by regression analysis and the rate of overtopping is formulated by Franco (1996) as:

$$Q = 0.192 \exp\left(\frac{bh_c}{H_s \gamma_{\theta_I} \gamma_\sigma \gamma_{geometry}}\right) \tag{2.52}$$

in which Q is the rate of overtopping in $m^3/m/s$, h_c crest height of the vertical breakwater from sea water level, γ_{θ_I} is the coefficient which signifies the angle of the incident wave eq. (2.53) - (2.54), where b is the coefficient corresponding the type of breakwater cf. Table 2.3, γ_σ is the directional energy spreading coefficient (3D effects) cf. Table 2.4 and $\gamma_{geometry}$ is the geometrical coefficient cf. Table 2.3.

For long crested waves γ_{θ_I}:

$$\gamma_{\theta_I} = 1.02 \cos^{1/3}(\theta_I) \tag{2.53}$$

For short crested waves γ_{θ_I}:

$$\gamma_{\theta_I} = 0.92 \cos^{2/3}(10^o - \theta_I) \tag{2.54}$$

A Froude scaling 1:30 is considered as a reasonable scaling ratio to prototype Franco (1996).

The following Tables cf. 2.3 - 2.4 correspond to a series of laboratory results with different types of vertical breakwaters.

Geometrical shape	*Type*	b	$\gamma_{geometry}$
Plain wall	A	-4.209	1.000
Wall with a nose	B	-4.526	0.930
1:3 smooth slope	C	-3.613	1.165
1:3 smooth slope with a berm	D	-5.719	0.736
Circular perforation	E	-4.794	0.878
Rectangular perforation	F	-4.950	0.850
Rectangular perforation (open deck)	G	-5.502	0.765

Table 2.3: Geometrical coefficients for the overtopping eq. (2.52)

Wave conditions			**Vertical breakwater type**						
θ_I	σ	s_{op}	**A**	**B**	**C**	**D**	**E**	**F**	**G**
			γ_σ	γ_σ	γ_σ	γ_σ	γ_σ	γ_σ	γ_σ
0	0	0.02	1.23						
0	0	0.04	1.05	0.93	1.18	0.93	0.88	0.72	0.64
0	15	0.04	0.89						
0	15	0.02	0.89						
0	30	0.04	0.88	0.82	1.05	0.80	0.79	0.68	0.64
10	15	0.04	0.93						
20	15	0.04	0.93	0.81	1.02	0.74	0.82	0.71	0.67
20	15	0.02	0.88	0.76	1.12	0.85	0.82	0.75	0.74
20	0	0.04	1.04	0.95	1.08	0.86	0.82	0.73	0.66
20	30	0.04	0.88	0.88	1.00	0.76	0.76	0.68	0.68
30	15	0.04	0.94						
40	0	0.04	0.89						
40	15	0.04	0.84	0.74					
40	15	0.02	0.89	0.80					
40	30	0.04	0.79	0.79	1.02	0.72	0.70		0.59
50	15	0.04	0.79						
60	15	0.04	0.73			0.65	0.59		
60	0	0.04	0.88	0.72					
60	15	0.02	0.68	0.65	0.82	0.57	0.55		0.53

Table 2.4: Overtopping coefficients and reduction factors for different degrees of wave energy spreading, considering wave steepness and incident wave angle, where σ is the directional spreading in degrees. (taken from Franco (1996)).

The uncertainty of the overtopping eq.(2.52) can be characterized as having a normal distribution with a standard deviation 0.27.

Wave transmission

The reduction of wave transmission is an important factor when a certain breakwater design has to be considered, as the disruption of harbour activity should be kept at a minimum. Wave transmission occurs through the structure, i.e. under the foot blocks or through the caisson, and as overtopping. The wave transmission coefficient can be expressed as K_T:

$$K_T = \left(K_{Ts}^2 + K_{To}^2\right)^{\frac{1}{2}} \tag{2.55}$$

where K_{Ts} is the transmitted wave height divided by the incident wave height (wave transmission through the structure), K_{To} is the transmitted wave height divided by the incident wave height (wave transmission due to overtopping).

In the case of vertical breakwaters, wave transmission is mainly dominated by overtopping; therefore the term K_{Ts} can be neglected. The principle variables are the crest height h_c and the incident wave height H_I. This was observed through a series of test by Goda (1969) and he proposed a set of wave transmission coefficients for vertical breakwaters, which are shown below:

$$K_T = \left(0.25\left(1 - \sin((\frac{\pi}{2\alpha})(\frac{h_c}{H_I} + f_R))\right)^2 + 0.01(1 - \frac{(h_w - h_c)}{h})^2\right)^{\frac{1}{2}}$$

$$; \quad f_R - \alpha < \frac{h_c}{H_I} < \alpha - f_R \tag{2.56}$$

$$K_T = 0.1\left(1 - \frac{(h_w - h_c)}{h}\right); \quad \frac{h_c}{H_I} \geq \alpha - f_R \tag{2.57}$$

where $\alpha = 2.2$ and factor f_R can be found from Figure 2.9 for a conventional vertical breakwater:

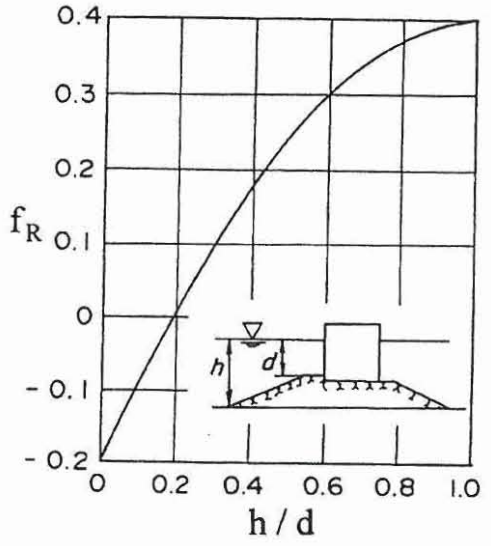

Figure 2.9: *Nomograph for determining f_R, taken from Goda (1969)*

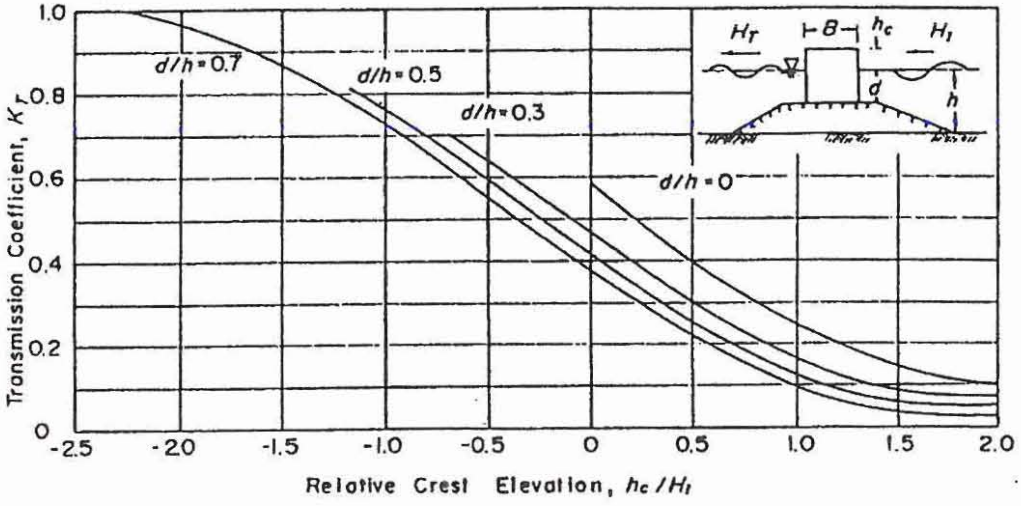

Figure 2.10: *Transmission coefficients for vertical breakwaters , taken from Goda (1969)*

The wave transmission coefficient equations (2.56) - (2.57) are derived from regular wave tests and are applicable for irregular waves with a significant wave height. The majority of vertical breakwaters in Japan today are designed with a relative crest height divided by the significant wave height, $h_c/H_{1/3} = 0.6$ and water level in the caisson divided by the waterdepth at the foot of the rubble mound $h_w - h/h = 0.7$. This gives a wave transmission coefficient equal to 0.2 based on equations (2.56) - (2.57).

The wave transmission coefficients are also illustrated in Figure 2.10 for different relative water depth at the foot of the caisson divided by the water depth at the foot of the rubble mound.

Wave reflection

All vertical breakwaters reflect incoming waves, and reflections can have a significant impact on neighbouring coastal area and maneuverability in the vicinity of harbour entrances. The building of a conventional vertical breakwater will result in a completely reflected wave equal in height to the incident wave. Supposition of waves occur when the incident and reflected waves coincide, resulting in a wave twice as high. A strong reflection can also undermine the stability of the structure by increased scour / sediment transport at the foot of the vertical breakwater. Analysis of the wave field close to the structure will enable a clear description of the reflection characteristics. The amount of wave reflection is usually measured by the reflection coefficient K_R given by:

$$K_R = H_R/H_I \tag{2.58}$$

where H_R is the reflected wave height, H_I is the incident wave height, and are usually characterized as the significant wave height.

In general, a conventional vertical breakwater placed on a rubble mound will result in a reflection coefficient less than one. This is due to the effect of the rubble mound foundation causing wave breaking, and overtopping. A large increase in wave breaking close to the structure will result in a lower reflection coefficient as shown in Figure 2.11, from Tanimoto et al., (1987). The influence of the rubble mound is important as increased wave breaking at the structure will result in larger wave loads. Therefore in many instances a high reflection coefficient must be accepted.

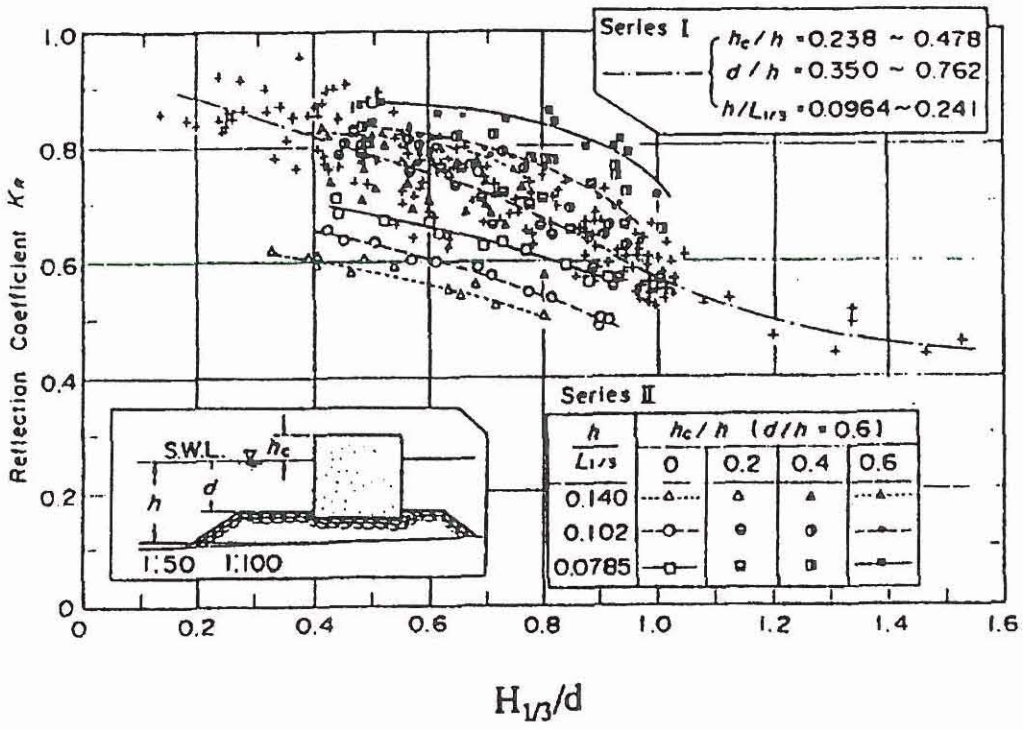

Figure 2.11: *Reflection coefficients of conventional vertical breakwaters, taken from Tanimoto et al., (1987)*

If wave reflection is a problem, a different type of structure can be used, cf. Figure 1.3 d, f and g, to reduce wave reflection. Advanced methods in reflection analysis for long crested and short crested waves based on vertical breakwaters has been investigated in depth by Helm-Petersen (1997), and will therefore not be pursued further.

2.4 Deterministic design of a conventional vertical breakwater on a high and low rubble mound

Vertical breakwaters are usually constructed in shallow and deep water and this often results in vertical breakwaters placed on a low and high rubble mound. A low rubble mound in this thesis is defined as a vertical breakwater where the ratio between the height of the rubble mound divided by the water depth is less than $h_{II}/h_s \leq 3.5/15$, and for the high rubble the ratio is $h_{II}/h_s > 3.5/15$. This definition does not correspond to the guide lines given by PIANC, but rather to the sensitivity of two different vertical breakwater geometries to foundation failure modes. An example will be presented in the following where a vertical breakwater is placed on a low and high rubble mound, using the same wave loading, geotechnical parameters and density of the caisson including a concrete cap.

The example of a caisson on a low rubble mound and high rubble mound is shown in Figure 2.12 a,b.

a) Vertical breakwater on a low rubble mound

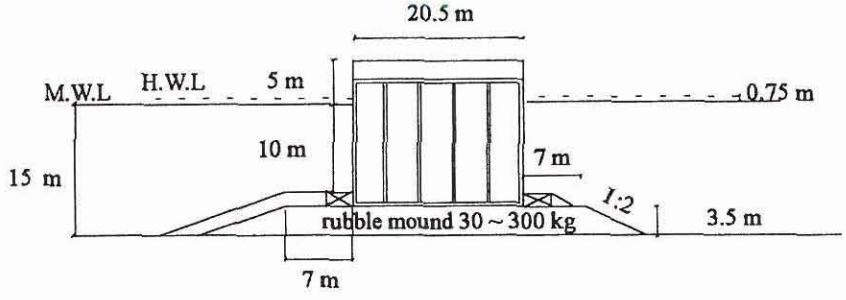

b) Vertical breakwater on a high rubble mound

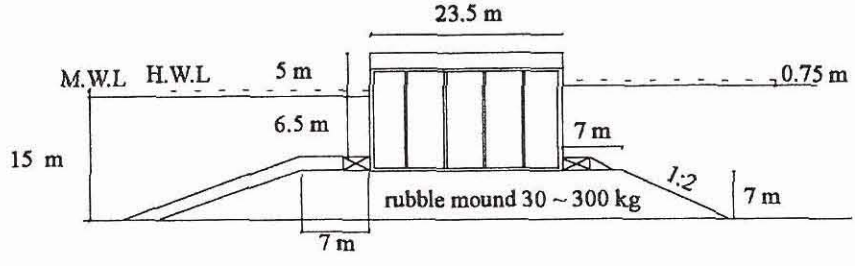

Figure 2.12: *Example of a vertical breakwater on a low and high rubble mound.*

The main deterministic parameters used in the following are: The effective friction angle of the rubble mound is $\varphi_1' = 0.61\ rad\ (35^o)$ and sand subsoil is $\varphi_2' = 0.57\ rad\ (32.7^o)$. The average mass density of the caisson in the air including a concrete cap is $\rho_c = 2.2\ t/m^3$, the sea bottom slope on the seaward side is 1/50 and the mass density of the sea is taken as $\rho_{sea} = 1.03\ t/m^3$. The significant wave height in deep water is $H_{so}^{50} = 6.5\ m$ (with a return period of 50 years), significant wave period $T_s = 13\ s$ and the wave direction is head on to the structure, i.e. $\theta_I = 0\ rad$. The breaker heights in the surf zone are calculated by using the simplified formula for shoaling and wave breaking Goda (1975, 1985), and the wave induced loads are determined from Goda et al. (1972) and Takahashi (1994) for impulsive wave loads. Design water level is taken as 0.75 m above M.W.L. The design wave height $H_{design} = H_{1/250} = 11.2\ m$. In the deterministic design sliding, overturning, bearing pressure at the heel and rupture in the rubble mound and subsoil are considered.

The vertical breakwater on low and high rubble mound are designed according to Japanese design guide lines using a safety factor of 1.2 for sliding, overturning, and bearing pressure in the range 400 KN/m^2 - 600 KN/m^2. For rupture failure the limit state $g > 0$ (assumed safety factor is greater than 1). Results from the stability calculations are presented in Table 2.5

Failure modes	high rubble mound	low rubble mound
Sliding	1.20	1.43
Overturning	3.40	2.75
Sliding on rubble φ_{d_1}'	1.36	1.62
Rupture failure rubble **2**	> 1	$\gg 1$
Rupture failure rubble **3**	$\gg 1$	$\gg 1$
Rupture failure rubble **4**	$\gg 1$	$\gg 1$
Rupture failure subsoil **5**	$\gg 1$	> 1
Rupture failure subsoil **6**	$\gg 1$	> 1
Rupture failure subsoil **7**	$\gg 1$	$\gg 1$
Bearing pressure at the heel	322 kN/m^2	431 kN/m^2

Table 2.5: Deterministic design of a vertical breakwater on a low and high rubble mound

Sliding, overturning and sliding on rubble are denoted as safety factors, according to national codes. Rupture in the rubble mound and subsoil are denoted as limit states, such that the $g(B, h_{II}) > 0$, where B is the width of the caisson, and h_{II} is the height of the rubble mound. This means that the value shown in the table is greater than 1, thus giving a design on the safe side.

It is seen from Table 2.5 that in the case of a high rubble mound sliding is the dominant failure mode deciding design. In the case of a low rubble mound, failure in the sand subsoil governs design.

3

Crown wall on rubble mound breakwaters

In this chapter the wave loading, and the overtopping for crown walls with a plane base and a crown wall with an extended leg on rubble mounds are reviewed including the derivation of the rubble mound foundation failure modes.

3.1 Foundation failure of a crown wall with a plane base and an extended leg on the seaward side

A crown wall is usually placed on a rubble mound to reduce the overall costs of the rubble mound, by reducing the amount of stone material needed to construct the rubble mound. In the design of the concrete crown wall, the construction and the underlaying soil have to sustain the wave forces, active soil pressure on the seaward side as well as weight of the crown wall during the design lifetime.

The principle failure modes for the crown wall are shown in Figure 3.1 (a) - (e). The failure modes in Figure 3.1 (a) and (b) are related to the structural failure of the crown wall and 1(e) considers the erosion of the upper armour layer, which results in instability on the seaward side. The failure modes in Figure 3.1 (a), (b) and (e) will not be considered in depth in this thesis.

Acceptable overtopping levels are first considered as this will give the preliminary dimensions of a crown wall. The main geometrical parameters of the crown wall is described by the G the berm width, A_c is the water level from sea water level to berm crest, and R is the freeboard height.

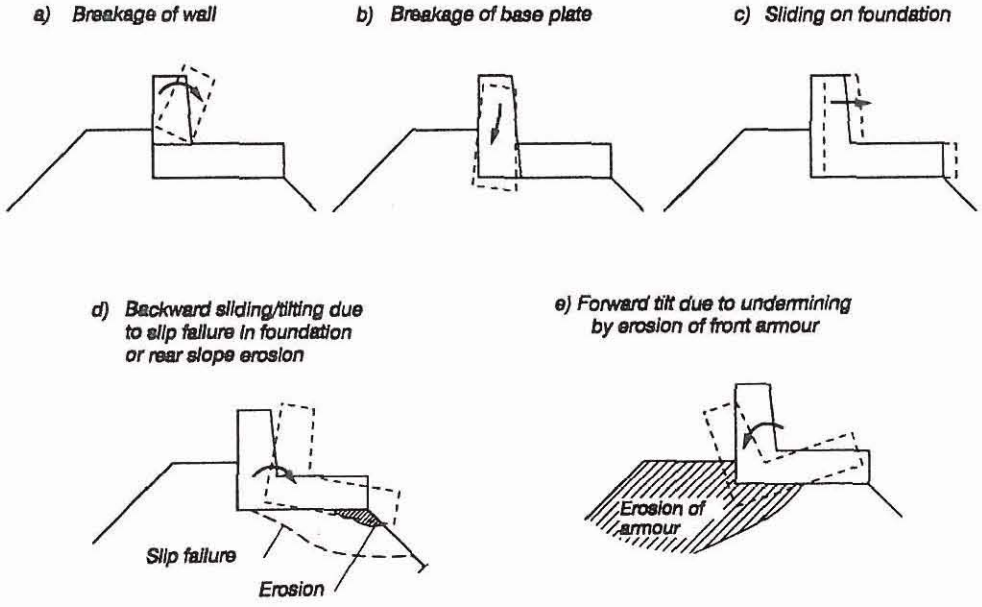

Figure 3.1: *Common failure modes for concrete crown walls (taken from Burcharth (1993)).*

Formulation of the soil rupture mechanisms will be derived on the basis of two principle crown wall designs. A crown wall with a plane base and an extended leg (foot) on the seaward side cf. Figure 3.2.

Wave loads are calculated by Pedersen's wave force formula for a conventional crown wall, Pedersen (1996).

Failure modes involving foundation failures must be evaluated in any design. Slip failure modes represent failure states and any related calculation can only give information related to the safety against failures, i.e no information related to in-service conditions can be extracted. The evaluation of safety against foundation slip failures is based on the force balance and the work balance equations and is in this chapter related to kinematically correct slip surface and failure zones (stiff zones and slip fans in friction based soil). The ratio between stabilizing and driving forces/moments are taken as a measure of the safety level. Foundation stability calculations based on kinematically correct slip failures provides in principle results on the unsafe side.

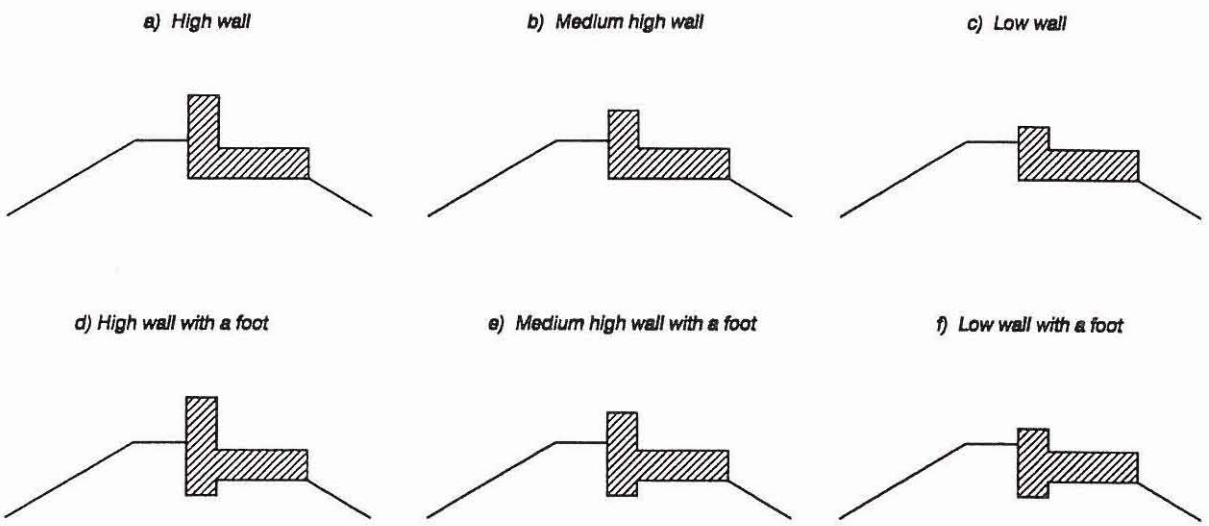

Figure 3.2: *Six different types of crown wall design.*

3.1.1 Formulae for wave loads on the crown wall

Pedersen's wave pressure formula (1996)

A method of estimating the wave load on a crown wall is to consider the hypothetical run-up, R_u, on an imaginary elongation of the slope and assume part of a related hydrostatic pressure distribution to act on the wall, cf. Figure 3.3 a,b.

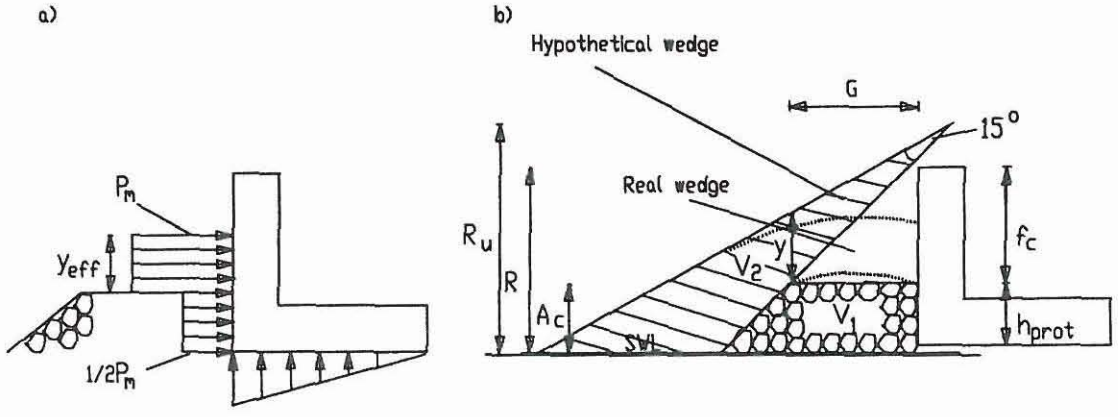

Figure 3.3: *a) Assumed pressure distribution on the face of the crown wall (taken from Pedersen (1996)).*
b) Design parameters associated to determination of the horizontal and uplift force (taken from Pedersen (1996)).

The wave loading is determined by first calculating the run-up level $R_{u,0.1\%}$ from the design wave in deepwater.

The run-up R_u can be modelled by introducing a two parameter Weibull distribution, as suggested by van der Meer et al. (1991).

$$F(R_u) = 1 - exp\left(-\left(\frac{R_u}{b}\right)^c\right) \tag{3.1}$$

where R_u is the run-up level exceeded by $1 - F(R_u)$ of the run-up levels, b is a scale parameter, and c is a shape parameter, defining the shape of the curve.

The scale parameter b is defined as:

$$\frac{b}{H_s} = 0.4 s_m^{-0.25} cot\alpha^{-0.2} \tag{3.2}$$

where H_s is the significant wave height, $s_m = \frac{H_s 2\pi}{g T_m^2}$ is the wave steepness, and α is the slope of the armour layer. T_m is the mean wave period.

The shape parameter is described by:

for plunging waves:

$$c = 3.0 \xi_m^{-0.75} \tag{3.3}$$

for surging waves:

$$c = 0.52 P^{-0.3} \xi_m^P \sqrt{cot\alpha} \tag{3.4}$$

where $\xi_m = \tan\alpha / \sqrt{H_s / L_m}$ is the surf similarity parameter based on the mean wave length L_m in deepwater, significant wave height H_s and the slope of the armour layer α. A threshold value of ξ_{mc} is defined as:

$$\xi_{mc} = \left[5.77 P^{0.3} \sqrt{\tan\alpha} \right]^{\left(\frac{1}{P+0.75}\right)} \tag{3.5}$$

where P is the permeability of the structure under the armour layer and lies in the range of $P = 0.4 - 0.6$, van der Meer (1988). For $\xi_m < \xi_{mc}$, equation (3.3) should be applied, and to $\xi_m > \xi_{mc}$, equation (3.4) should be applied.

The reliability of the distribution of the run-up levels is modelled by considering the fitted scale factor b as a stochastic variable. For a permeable core the variation coefficient of the scale factor b is 6% and for an impermeable core it is 9%.

The wave loading can now be estimated from Pedersen's (1996) experimental work. He assumes a run-up wedge to have an angle of $\theta = 15°$, cf. Figure 3.3 b. The height of the wedge (y) from the armour crest can be calculated as:

$$y = \frac{R_{u,0.1\%} - A_c}{\sin\alpha} \cdot \frac{\sin 15°}{\cos(\alpha - 15°)} \tag{3.6}$$

where A_c, R_u and y are defined in Figure 3.3 b.

The impact height, known as the effective height is given by y_{eff}:

$$y_{eff} = \mathbf{min}\left[\frac{y}{2}; f_c\right] \tag{3.7}$$

where f_c is the height of the unprotected wall face cf. Figure 3.3 b. For negative values of $\frac{y}{2}(R_{u,0.1\%} - A_c)$ a value of $y_{eff} = 0$ is used.

Thereafter it is possible to calculate the stagnation pressure p_m from the impounding run-up on the wall, cf. Figure 3.3 a:

$$p_m = \rho_w g(R_{u,0.1\%} - A_c) \tag{3.8}$$

For low run-up levels the two volumes V_1 (volume of the armour layer on the front crown face) and V_2 (volume of the hypothetical wedge) must be determined. The design equations for the wave loading, corresponding to central estimates of the horizontal force:

$$F_{H,0.1\%} = 0.21\sqrt{\frac{L_m}{G}}\left(1.6p_m \cdot y_{eff} + \mathbf{V}\frac{p_m}{2}h_{prot}\right) \tag{3.9}$$

where y_{eff}, G, and h_{prot} are given in Figure 3.3 a,b. The constant 0.21 and 1.6 can be modelled as normal distributed variables with standard deviations corresponding to $\sigma = 0.02$ and $\sigma = 0.01$. Including the effective volume at low run-up levels is given by $\mathbf{V}$:

$$\mathbf{V} = \begin{cases} < \frac{V_1}{V_2} & \text{for } V_2 < V_1 \\ = 1 & \text{for } V_2 \geq V_1 \end{cases} \tag{3.10}$$

The wave induced uplift pressure at the front edge of the crown wall is equal to the horizontal pressure at the foot of the crown wall and is approximated to vary linearly to the heel of the crown wall. So the wave induced uplift load is given by:

$$F_{U,0.1\%} = 1 \cdot \mathbf{V}p_m\frac{1}{2}B \tag{3.11}$$

where B is the width of the crown wall, 1 in the equation is assumed normal distributed with a standard deviation equal to 0.3.

The horizontal wave load and uplift force based on run-up is valid in the bounds of the experimental work performed by Pedersen (1996) and is given below in Table 3.1

Parameter	Range
ξ_m	1.1 - 4.2
H_s/A_c	0.5 - 1.5
R/A_c	1 -2.6
A_c/G	0.3 -1.1
$\cot\alpha$	1.5 - 3.5

Table 3.1: Parameter range for the design equations (3.9) - (3.11), (taken from Pedersen (1996))

where the parameter R in Table 3.1 is the height from the sea water level to the crest of the crown wall.

Overtopping rates over a crown wall according to Bradbury et al. (1988 a,b)

Overtopping of *breakwaters with crown walls* were studied by Bradbury et al. (1988a and b). In order to obtain a better fit to model test data they introduced the dimensionless freeboard:

$$F^* = \left(\frac{R}{H_s}\right)^2 \left(\frac{s_m}{2\pi}\right)^{0.5} \tag{3.12}$$

and obtained the empirical formula for the average overtopping discharge, $\overline{Q}$,

$$\overline{Q}_m / \left(g\, H_s\, T_m\right) = a\ (F^*)^{-b} \tag{3.13}$$

where a and b are empirical coefficients dependent on the cross sectional geometry.

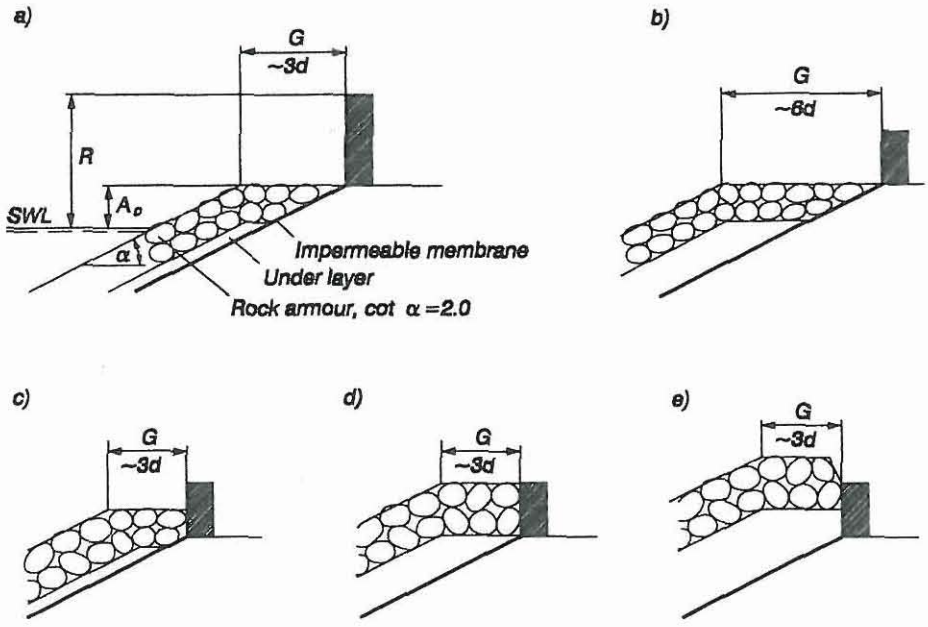

Section	G/H_s	G/R	A_c/R	$a\ 10^0$	b
a	0.79-1.7	0.75	0.28	6.7	3.5
		0.58	0.21	3.6	4.4
		1.07	0.39	5.3	3.5
		0.88	0.32	1.8	3.6
b	1.6-3.3	2.14	0.39	1.0	2.8
c	0.79-1.7	1.07	0.71	1.6	3.2
d	0.79-1.7	1.07	1.00	0.37	2.9
e	0.79-1.7	0.83	1.00	1.30	3.8

Figure 3.4: *Coefficients for overtopping discharges. Non-depth limited wave conditions, (taken from Burcharth (1993)). d is the stone diameter.*

Values are presented in Figure 3.4 for a rock armoured slope ($cot\alpha = 2.0$) on an impermeable core with various configurations of crown walls and front berms. The coefficients given in Figures 3.4 are based on model tests with waves in relatively deep water (water depth larger than $2\,H_s$). For shallower conditions including depth limited waves reference is made to Ahrens et al. (1986) who tested an armoured sea wall with different crown wall details including recurved fronts.

Wave induced uplift pressure in the soil, under a crown wall base

The wave induced hydrostatic pressure at the front edge of the crown wall is equal to the wave induced uplift pressure at the seaward base edge. The uplift pore pressure is assumed to have a triangular distribution from the foot to the heel, as presented in Figure 3.5. Figure 3.5 shows the related definition sketch for the uplift pressure.

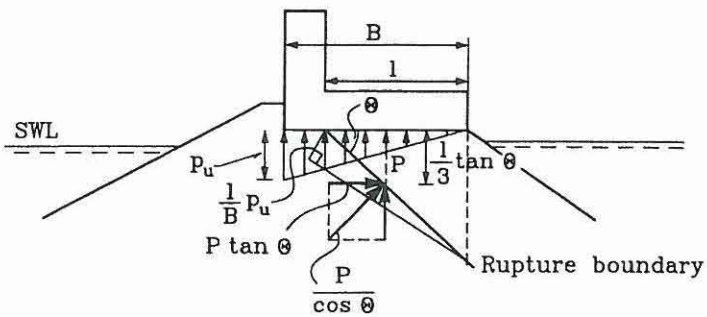

Figure 3.5: *Definition sketch for the wave induced uplift pressure along the slip line.*

The wave induced uplift pressure, p_u is calculated along the base plate of the crown wall and only gives the vertical component of the pressure cf. Figure 3.5. θ is the angle between the crown wall base and the rupture slip line.

The pore pressure resultant along the rim of the rupture zone in the soil is $P/\cos\theta$, where P is the vertical force component along the length l. The horizontal component of the force is:

$$P\tan\theta = \frac{1}{2}\frac{l^2}{B}p_u\tan\theta \tag{3.14}$$

The horizontal wave induced pressure arises along the pore pressure build up in the rubble mound due to the impermeable concrete plane base. In the following derivation of the foundation failure modes an extra contribution is added on the horizontal load component along the rupture boundary. This decreases the safety of a given design of a crown wall.

3.1.2 Active rubble force on the seaward side of the crown wall

The rupture zone is characterized by the rupture Figure ABC cf. Figure 3.6. applying the upper bound method gives a fairly accurate value for the rubble force acting in the direction of the wave induced horizontal force.

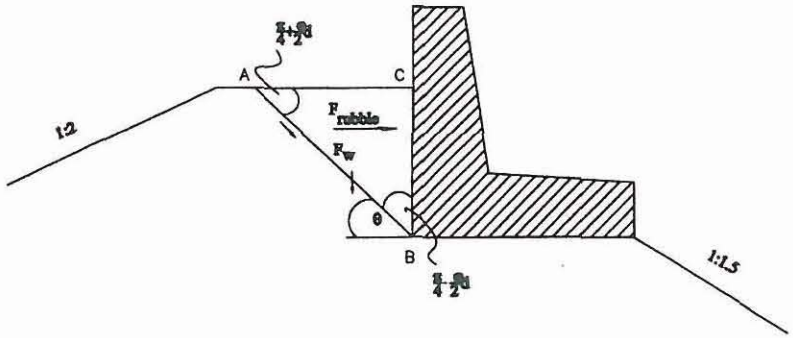

Figure 3.6: *Rupture zone on the seaward side of a crown wall structure.*

A unit displacement in the direction AB, causes a kinematical admissible movement of the stiff zone ABC in the horizontal direction. The displacement vectors of the stiff zone ABC are shown in Figure 3.7

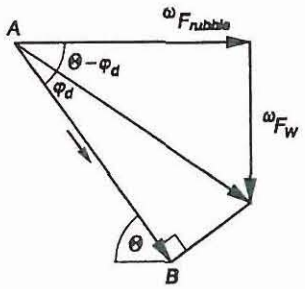

Figure 3.7: *Displacement Figure for the rupture zone ABC.*

The horizontal force F_{rubble} is derived from the displacement of the stiff zone ABC along the slip line AB in the extreme case.

$$F_{rubble} = F_w \tan(\frac{\pi}{4} - \frac{\varphi_d}{2}) \tag{3.15}$$

where the F_w= is the weight of the rubble material in the rupture zone ABC.

3.1.3 Rupture failure under a crown wall with a plane base and an extended leg on the seaward side

A correct solution for the bearing capacity of a crown wall has to be statically and kinematically admissible. It is difficult to find solutions that fulfil both conditions. In general a solution is kinematical admissible if the displacement field satisfies the boundary conditions for the displacement and the flow rule (normality condition). In the following the upper bound method will be applied to determine the bearing capacity of crown walls with a plane base and an extended leg on the seaward side. Rupture failure is not an isolated phenomenon so therefore a series of assumptions prior to the derivation are taken into account

- The effective friction angle and angle of dilation will be based on the core material as it is the dominant material in a rubble mound structure
- The normality condition has to be fulfilled, so that the soils angle of dilation and the effective friction angle are the same.
- The reduced effective friction angle is calculated from the effective friction angle and the angle of dilation as proposed by Hansen (1979).

$$\varphi_d = \tan^{-1}\left(\frac{\sin\varphi' \cos\psi}{1 - \sin\varphi' \sin\psi}\right) \tag{3.16}$$

  Both φ' and ψ are dependent on the stress level for which reason either reasonable mean values must be used, or calculations must be performed on increments.

- The porosity of the consolidated sand material is regarded as constant.
- Rupture failure is considered. Investigations into consolidation of the foundation is not taken into consideration
- The rubble mound is regarded as friction based material.

Sliding between crown wall and rubble underlayer (1)

Sliding is the result of slippage on the sand/rubble material along the slip line from the edge of the foot to the rear end of the crown wall. The crown wall sliding plane is shown in Figure 3.8.

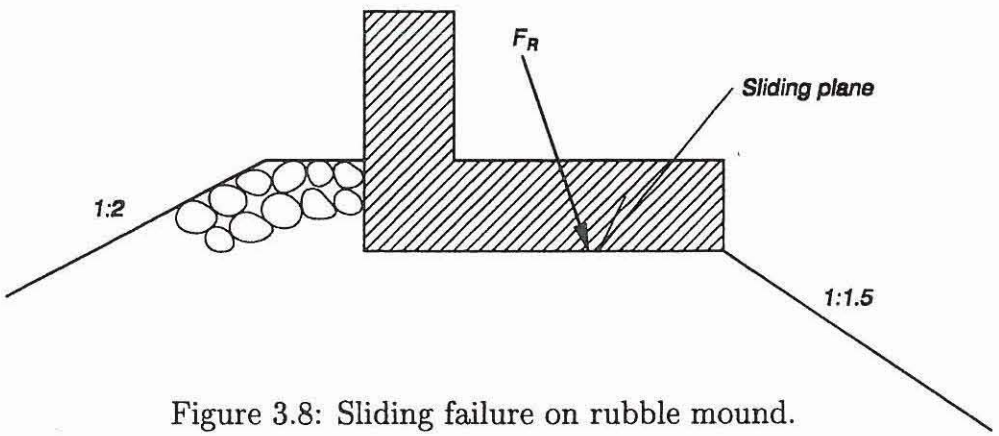

Figure 3.8: Sliding failure on rubble mound.

Sliding of the crown wall is defined as a displacement, unit increment $\delta = 1$ along the rubble bed. F_R is the resultant force derived from the weight of the crown wall reduced for uplift and the horizontal wave load.

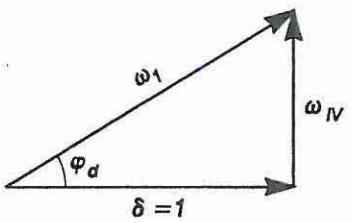

Figure 3.9: Displacement field for sliding along a rubble underlayer.

The displacement field is shown in Figure 3.9, where ω_{1V} is the displacement vector of the vertical load $\omega_{1V} = \omega_1 \sin\varphi_d$, $\omega_1 = \frac{1}{cos\varphi_d}$ and φ_d is the reduced effective friction angle.

$$F_H + F_{rubble} = (F_G - F_U) \cdot \tan\varphi_d \tag{3.17}$$

where F_H is the horizontal force from the wave forces, F_{rubble} is the horizontal active rubble force from the seaward side of the crown wall, F_G is the weight of the crown wall and F_U is the wave induced uplift force.

It must be mentioned that sliding between the concrete base plate and the rubble material is an important failure mode in which the angle of friction between concrete and rubble is the key factor.

Foundation failure along the slip line AB (2)

The kinematical admissible rupture slip zone is shown in Figure 3.10. This rupture failure mode is applicable when the optimization angle θ is less than the reduced effective friction angle φ_d.

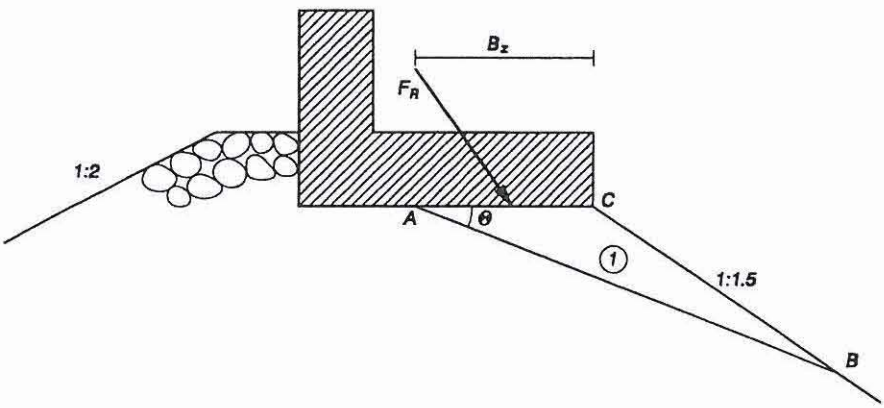

Figure 3.10: *Rupture failure in the rubble mound.*

The rupture failure is characterized by a slip line along AB. The corresponding translation of the stiff mass takes place in the direction forming an angle of φ_d with the slip plane A to B. This is due to the dilation of the soil. The displacement field is shown in Figure 3.11 for the slip line along the line AB.

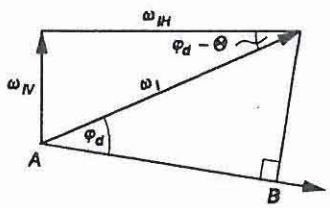

Figure 3.11: *Displacement field for the stiff rupture zone.*

The displacement vectors for the horizontal load ω_{1H} and vertical load ω_{1V} are shown below:

$$\omega_1 = \frac{1}{\cos\varphi_d} \tag{3.18}$$

$$\omega_{1H} = \frac{\cos(\varphi_d - \theta)}{\cos\varphi_d} \tag{3.19}$$

$$\omega_{1V} = \frac{\sin(\varphi_d - \theta)}{\cos\varphi_d} \tag{3.20}$$

The weight of zone 1 as a function of θ is

$$F_{G_1} = \frac{1}{2}(\gamma_s - \gamma_w)B_z^2 \frac{\tan\theta}{1 - 1.5\tan\theta} \tag{3.21}$$

where $(\gamma_s - \gamma_w)$ is the reduced specific weight of the rubble.

The final work equation as a function of θ, by equating the external work and internal work for an infinitesimal deformation ω_1:

$$\begin{aligned} 0 = {} & F_{G_1}\frac{\sin(\varphi_d - \theta)}{\cos\varphi_d} - (F_H^p + F_{rubble})\frac{\cos(\varphi_d - \theta)}{\cos\varphi_d} \\ & + (F_G - F_U)\frac{\sin(\varphi_d - \theta)}{\cos\varphi_d} \end{aligned} \tag{3.22}$$

where F_H^p is derived from the wave pressure, and pore pressure along the rupture boundary, F_{rubble} is the active earth pressure on the front side of the crown wall, $F_G - F_U$ is the buoyancy reduced weight of the crown wall minus the wave induced uplift, φ_d is the angle of dilation of the rubble mound material and B_z is the rupture width of the crown wall. The angle θ cf. Figure 3.10 is the unknown angle to be determined by minimizing the ratio between the stabilizing work and the driving work.

Foundation failure in the rubble mound (3)

The considered failure mode is shown in Figure 3.12.

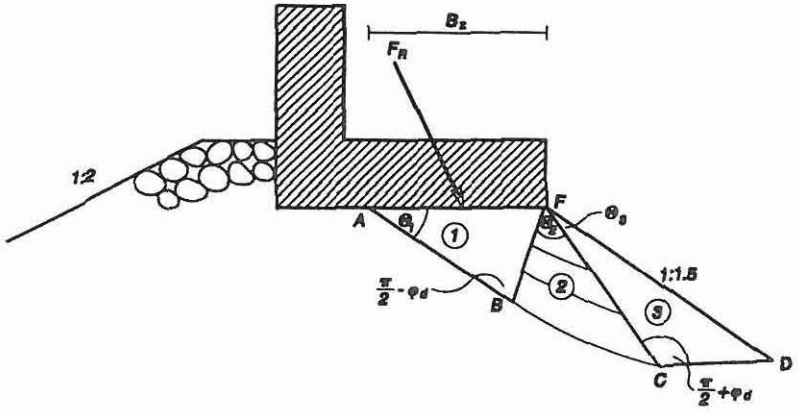

Figure 3.12: *Failure in rubble mound in friction based soil.*

Rupture failure is characterized by forcing a displacement, unit increment $\delta = 1$ along the first slip line AB in the mound.

Zone 1 is characterized as a stiff zone which exhibits no internal energy dissipation as is the case for zones 1 - 3 along the rim of the rupture boundary as the normality condition is fulfilled. This zone slides down the rupture line AB causing an instantaneous shift of zone 1. Zone 2 is a set of rotating logarithmic slip fans which exhibit displacement in the same direction as zone 1 until a resultant displacement reverses and causes the soil to exhibit a holding capacity. Zone 3 moves as a stiff zone holding part of zone 2, zone 1 and the external forces, when equilibrium is present.

The geometric lengths of the rupture zones are presented as r (radius) and l (length) subscript. These geometrical lengths are determined to calculate the area of each individual rupture zone.

The initial radius of the rupture fan, close to the first stiff zone.

$$r_{BF} = B_z \frac{\sin\theta_1}{\sin(\frac{\pi}{2} - \varphi_d)} \tag{3.23}$$

The radius of the logarithmic spiral, zone 2 along CF.

$$r_{CF} = r_{BF} e^{\theta_2 \tan\varphi_d} \tag{3.24}$$

The following length parameters are derived to determine the area of zone 3.

$$l_{EF} = \frac{r_{FC}\sin(\frac{\pi}{2} + \varphi_d)}{\sin\theta_7} \tag{3.25}$$

where l_{EF} is defined in Figure 3.13.

$$l_{CE} = \frac{r_{FC}\sin(\theta_3 + \frac{\pi}{2} - \arctan(1.5))}{\sin\theta_7} \tag{3.26}$$

where $\theta_7 = \frac{\pi}{4} - \frac{\varphi_d}{2}$

$$l_{DE} = \frac{l_{EF}\sin(\frac{\pi}{2} - \arctan(1.5))}{\sin\theta_6} \tag{3.27}$$

where $\theta_6 = \frac{\varphi_d}{2} + \frac{\pi}{4} + \arctan(1.5)$.

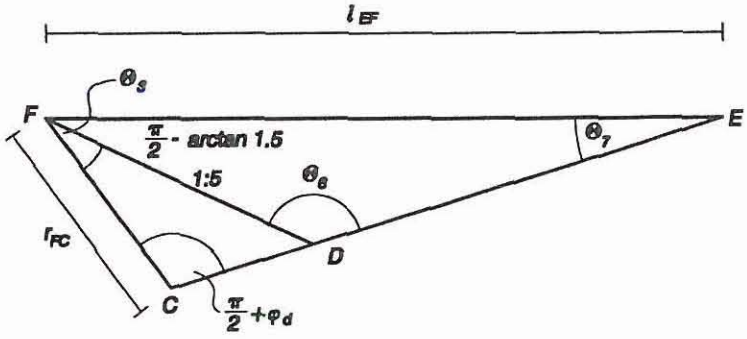

Figure 3.13: *Geometrical figure of zone 3.*

Displacement field corresponding to the three rupture zones

$$\omega_1 = \frac{1}{\cos\varphi_d} \tag{3.28}$$

$$\omega_{1H} = \omega_1\cos(\theta_1 - \varphi_d) \tag{3.29}$$

$$\omega_{1V} = \omega_1\sin(\theta_1 - \varphi_d) \tag{3.30}$$

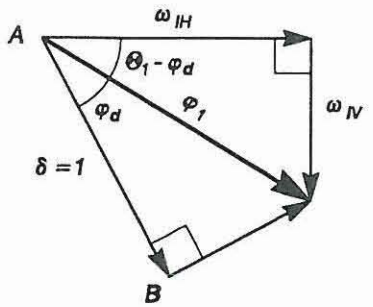

Figure 3.14: *Displacement field of the first stiff zone .*

The vertical displacement vector ω_{2V} in zone 2 as a function of θ

$$\omega_{2V}(\theta) = \omega_1 e^{\theta \tan \varphi_d} \sin(\varphi_d - \theta_1 + \theta);\ \theta \in [0; \theta_2] \tag{3.31}$$

where ω_1 is the displacement of the slip fan along the rupture boundary line BF.

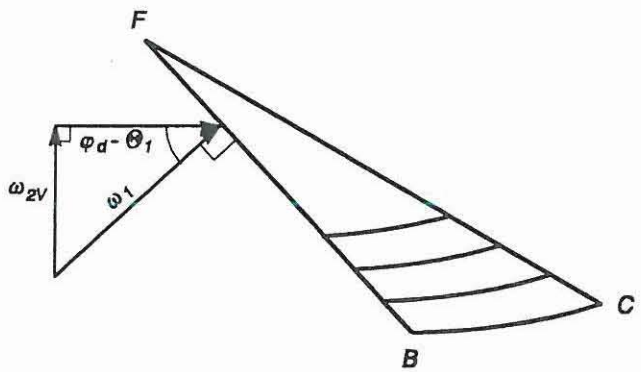

Figure 3.15: *Displacement field of the slip fans along BF.*

The displacement field for zone 3, see Figure 3.16.

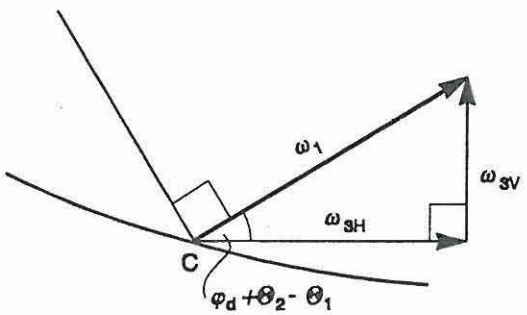

Figure 3.16: *Displacement field of zone 3.*

$$\omega_3 = \omega_1 e^{\theta_2 \tan \varphi_d} \tag{3.32}$$

$$\omega_{3V} = \omega_3 \sin(\varphi_d + \theta_2 - \theta_1) \tag{3.33}$$

Self weight of the soil in the rupture zones 1 - 3

Work done by the self weight of the soil in zone 1, W_1.

$$W_1 = (\gamma_s - \gamma_w)\omega_{1V}\Omega_1 \tag{3.34}$$

where Ω_1 is the area of rupture zone 1

$$\Omega_1 = \frac{1}{2} B_z l_{AB} \sin\theta_1 \tag{3.35}$$

Work done by the self weight of the slip fan in zone 2, W_2.

$$W_2 = (\gamma_s - \gamma_w) \int_0^{r_{CF}} \int_0^{\theta_2} \omega_{2V}(\theta) r \, dr \, d\theta \tag{3.36}$$

where the analytic solution of W_2 is

$$\begin{aligned} W_2 = \frac{(\gamma_s - \gamma_w) r_{CF}^2}{2\tan^2\varphi_d + 2} \left[e^{\theta_2 \tan\varphi_d} \left[\tan\varphi_d \sin(\varphi_d - \theta_1 + \theta_2) \right.\right. \\ \left.\left. - \cos(\varphi_d - \theta_1 + \theta_2) \right] - \tan\varphi_d \sin(\varphi_d - \theta_1) - \cos(\varphi_d - \theta_1) \right] \end{aligned} \tag{3.37}$$

Work done by the self weight of the soil in zone 3, W_3.

$$W_3 = (\gamma_s - \gamma_w)\omega_{3V}\Omega_3 \tag{3.38}$$

where Ω_3 is the area of rupture zone 3

$$\Omega_3 = \frac{1}{2} l_{EF} l_{CE} \sin\theta_7 - \frac{1}{2} l_{EF} l_{DE} \sin\theta_7 \tag{3.39}$$

To establish the work done in equilibrium, the work from the external forces and self weight in each individual zone are computed giving the following bearing capacity:

$$0 = -(F_H^p + F_{rubble})\omega_{1H} - (F_G - F_U)\omega_{1V} - W_1 + W_2 + W_3 \tag{3.40}$$

where θ_1 is the unknown angle to be determined by minimizing the ratio between the stabilizing work and driving work and F_{rubble} is the active rubble pressure on the seaward side.

Sliding failure of the crown wall with an extended leg on the seaward side (4)

Sliding is the result of slippage on the sand/rubble material along the slip line from the edge of the foot to the rear end of the crown wall. The crown wall sliding plane is shown in Figure 3.17.

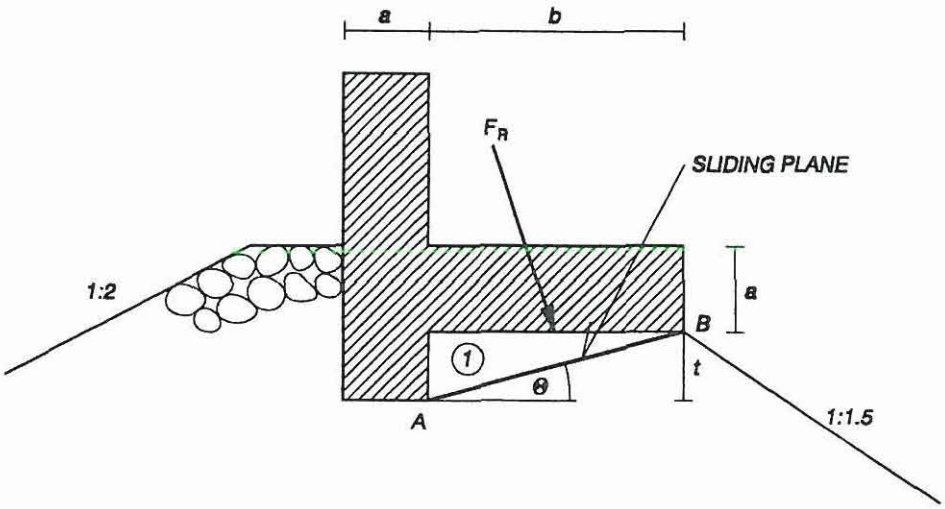

Figure 3.17: *Sliding failure on rubble mound.*

Sliding of the crown wall is defined as a displacement, unit increment $\delta = 1$ along the rubble bed. F_R is the resultant force derived from the weight of the crown wall reduced for uplift and the wave horizontal load.

The resulting displacements are shown in Figure 3.18, where ω_{1V} is the displacement of the vertical force $\omega_{1V} = \omega_1 \sin\varphi_d$, where $\omega_1 = \frac{1}{cos\varphi_d}$ and φ_d is the effective friction angle, assuming that the normality condition is fulfilled.

The weight of zone 1 F_{G_1} is equal to

$$F_{G_1} = \frac{1}{2}(\gamma_s - \gamma_w)bt \tag{3.41}$$

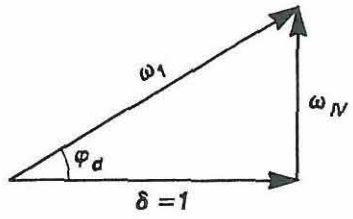

Figure 3.18: *Displacement field for sliding along a rubble underlayer.*

The final work equation for limited bearing capacity is

$$\frac{F_H + F_{rubble}}{\cos\theta} = (F_G - F_U + F_{G_1}) \cdot (\sin\theta + \frac{\sin\varphi_d}{\cos\varphi_d}\cos\theta) \tag{3.42}$$

where F_H is the horizontal force from the wave forces, F_{rubble} is the horizontal active rubble force from the seaward side of the crown wall, F_G is the weight of the crown wall, F_U is the wave induced uplift force, F_{G_1} is the weight of rubble in zone 1 cf. Figure 3.17 and θ is the angle between the horizontal and the slip line AB.

Foundation failure in the rubble mound with an extended leg on the seaward side (5)

The kinematical admissible rupture slip zone as shown in Figure 3.19 is applicable when the optimization angle, θ is less than the reduced effective friction angle φ_d.

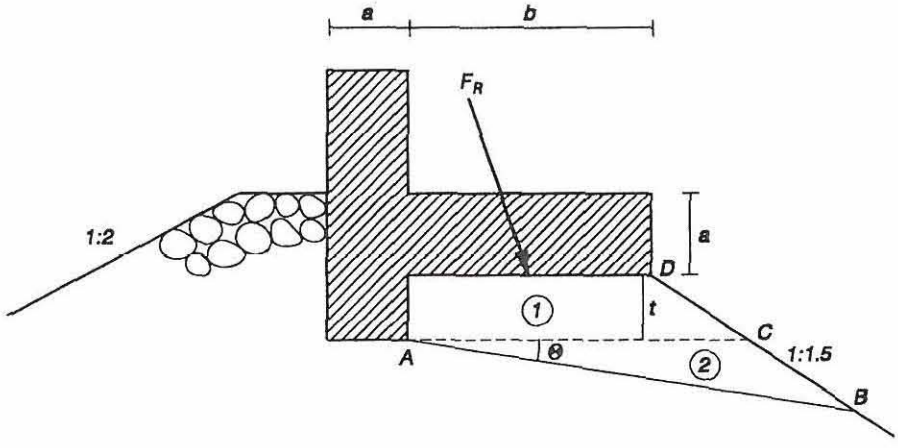

Figure 3.19: *Rupture failure in the rubble mound.*

The rupture failure is characterized by a slip line along AB. The corresponding translation of the stiff mass takes place in the direction forming an angle of φ_d with the slip plane A to B. This is due to the dilation of the soil. The displacement field is shown in Figure 3.20 for the slip line along the line

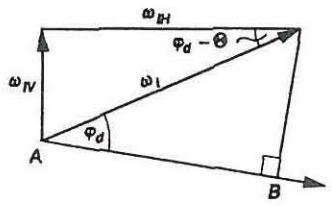

Figure 3.20: *Displacement field for the stiff rupture zone.*

The displacement vectors for the horizontal load ω_{1H} and vertical load ω_{1V} are shown below:

$$\omega_1 = \frac{1}{\cos\varphi_d} \tag{3.43}$$

$$\omega_{1H} = \frac{\cos(\varphi_d - \theta)}{\cos\varphi_d} \tag{3.44}$$

$$\omega_{1V} = \frac{\sin(\varphi_d - \theta)}{\cos\varphi_d} \tag{3.45}$$

The weight of zone 1 and 2 as a function of θ is

$$\begin{aligned} F_{G_{1,2}} &= \frac{1}{2}(\gamma_s - \gamma_w)\left[t(b + \frac{3}{4}t) + (b + \frac{3}{2}t)^2\right. \\ &\quad \left.\left(\cos\theta\sin\theta + \sin^2\theta\tan(\frac{\pi}{2} + \theta - \arctan(1/1.5))\right)\right] \end{aligned} \tag{3.46}$$

where $(\gamma_s - \gamma_w)$ is the reduced specific weight of the rubble.

The final work equation as a function of θ, by equating the external work and internal work for a infinitesimal deformation ω_1:

$$\begin{aligned} 0 &= F_{G_{1,2}}\frac{\sin(\varphi_d - \theta)}{\cos\varphi_d} - (F_H^p + F_{rubble})\frac{\cos(\varphi_d - \theta)}{\cos\varphi_d} \\ &\quad + (F_G - F_U)\frac{\sin(\varphi_d - \theta)}{\cos\varphi_d} \end{aligned} \tag{3.47}$$

where F_H^p is derived from the wave pressure, and pore pressure along the rupture boundary, F_{rubble} is the active earth pressure on the front side of the crown wall, $F_{G_{1,2}} + F_G - F_U$ is the weight of the rubble material in zone 1 plus the buoyancy reduced weight of the crown wall and minus the wave induced uplift, φ_d is the angle of dilation of the rubble mound material and B_z is the rupture width of the crown wall. The angle θ cf. Figure 3.19 is the unknown angle to be determined by minimizing the ratio between the stabilizing work and the driving work.

Foundation failure in the rubble mound on the seaward side (6)

The considered failure mode is shown in Figure 3.21.

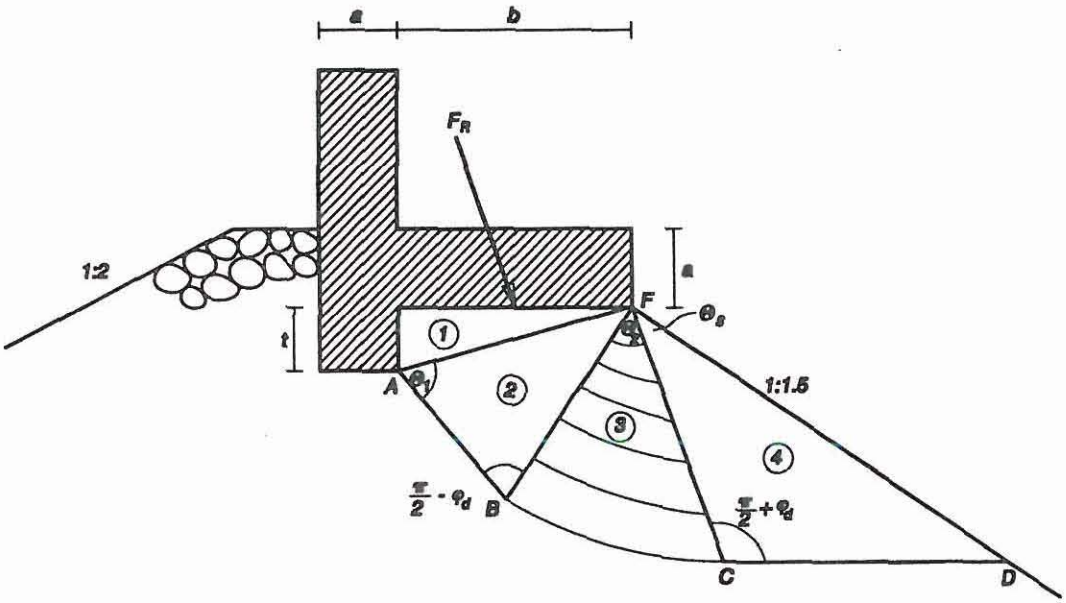

Figure 3.21: *Failure in rubble mound in friction based soil.*

Considering that the soil exhibits plastic behaviour, the work equation can be formulated as shown in the following, when the foundation is forced to move a unit increment $\delta = 1$ along the first slip line AB.

Zone 1 and 2 are characterized as a stiff zone which exhibits no internal energy dissipation as is the case for zones 2 - 4 along the rim of the rupture boundary as the normality condition is fulfilled. These zones slide down the rupture line AB causing a instantaneous shift of zone 3. Zone 3 is a set of rotating logarithmic fans which exhibit displacement in the same direction as zone 2 until a resultant displacement reverses and causes the soil to exhibit a holding capacity. Zone 4 moves as a stiff zone holding part of zone 3, zone 1, 2 and the external forces, when equilibrium is present.

The geometric lengths of the rupture zones are presented as r (radius) and l (length) subscript. These geometrical lengths are determined to calculate the area of each individual rupture zone.

The initial radius of the rupture fan, close to the first stiff zone.

$$r_{BF} = \sqrt{b^2 + t^2} \frac{\sin\theta_1}{\sin(\frac{\pi}{2} - \varphi_d)} \tag{3.48}$$

The radius of the logarithmic spiral, zone 2 along CF.

$$r_{CF} = r_{BF} e^{\theta_2 \tan\varphi_d} \tag{3.49}$$

The following length parameters are derived to determine the area of zone 3.

$$l_{EF} = \frac{r_{FC} \sin(\frac{\pi}{2} + \varphi_d)}{\sin\theta_7} \tag{3.50}$$

where l_{EF} is the berm width on the rear side of the crown wall cf. Figure 3.22.

$$l_{CE} = \frac{r_{FC} \sin(\theta_3 + \frac{\pi}{2} - \arctan(1.5))}{\sin\theta_7} \tag{3.51}$$

where $\theta_7 = \frac{\pi}{4} - \frac{\varphi_d}{2}$

$$l_{DE} = \frac{l_{EF} \sin(\frac{\pi}{2} - \arctan(1.5))}{\sin\theta_6} \tag{3.52}$$

where $\theta_6 = \frac{\varphi_d}{2} + \frac{\pi}{4} + \arctan(1.5)$.

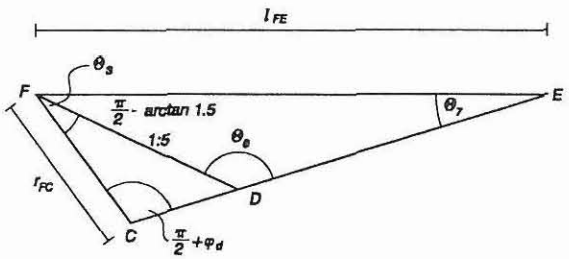

Figure 3.22: *Geometrical figure of zone 4.*

Displacement field corresponding to the three rupture zones

$$\omega_1 = \frac{1}{\cos\varphi_d} \tag{3.53}$$

$$\omega_{1H} = \omega_1 \cos(\theta_1 - \varphi_d) \tag{3.54}$$

$$\omega_{1V} = \omega_1 \sin(\theta_1 - \varphi_d) \tag{3.55}$$

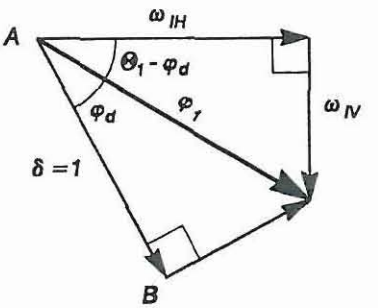

Figure 3.23: *Displacement field of the second zone .*

The vertical displacement vector ω_{2V} in zone 2 as a function of θ

$$\omega_{2V}(\theta) = \omega_1 e^{\theta \tan\varphi_d} \sin(\varphi_d - \theta_1 + \theta);\ \theta \in [0; \theta_2] \tag{3.56}$$

where ω_1 is the displacement of the slip fan along the rupture boundary line BF.

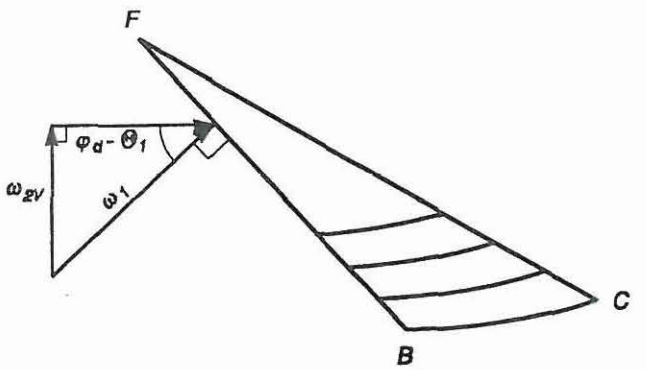

Figure 3.24: *Displacement field of the slip fans along BF.*

The displacement field for zone 4, see Figure 3.25.

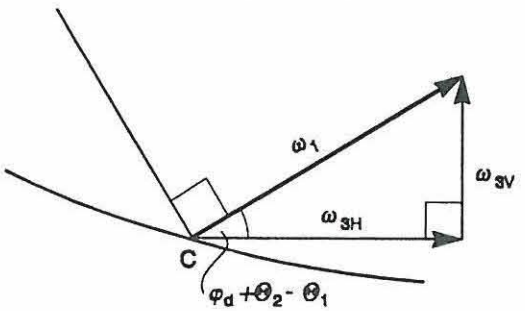

Figure 3.25: *Displacement field of zone 4.*

$$\omega_3 = \omega_1 e^{\theta_2 \tan \varphi_d} \tag{3.57}$$

$$\omega_{3V} = \omega_3 \sin(\varphi_d + \theta_2 - \theta_1) \tag{3.58}$$

Self weight of the soil in the rupture zones 1 - 4

Work done by the self weight of the soil in zone 1, W_1.

$$W_1 = (\gamma_s - \gamma_w)\omega_{1V}\Omega_1 \tag{3.59}$$

where Ω_1 is the area of rupture zone 1

$$\Omega_1 = \frac{1}{2}bt \tag{3.60}$$

Work done by the self weight of the soil in zone 2, W_2.

$$W_2 = (\gamma_s - \gamma_w)\omega_{1V}\Omega_2 \tag{3.61}$$

where Ω_2 is the area of rupture zone 2

$$\Omega_2 = \frac{1}{2}r_{BF}\sqrt{b^2 + t^2}\sin(\frac{\pi}{2} + \theta_1 + \varphi) \tag{3.62}$$

Work done by the self weight of the slip fan in zone 3, W_3.

$$W_3 = (\gamma_s - \gamma_w) \int_0^{r_{CF}} \int_0^{\theta_2} \omega_{2V}(\theta) r dr d\theta \tag{3.63}$$

where the analytic solution of W_3 is

$$\begin{aligned} W_3 = & \frac{(\gamma_s - \gamma_w) r_{CF}^2}{2\tan^2\varphi_d + 2} \left[e^{\theta_2 \tan\varphi_d} [\tan\varphi_d \sin(\varphi_d - \theta_1 + \theta_2) \right. \\ & \left. - \cos(\varphi_d - \theta_1 + \theta_2)] - \tan\varphi_d \sin(\varphi_d - \theta_1) - \cos(\varphi_d - \theta_1) \right] \end{aligned} \tag{3.64}$$

Work done by the self weight of the soil in zone 4, W_4.

$$W_4 = (\gamma_s - \gamma_w) \omega_{3V} \Omega_4 \tag{3.65}$$

where Ω_4 is the area of rupture zone 4

$$\Omega_4 = \frac{1}{2} l_{EF} l_{CE} \sin\theta_7 - \frac{1}{2} l_{EF} l_{DE} \sin\theta_7 \tag{3.66}$$

To establish the work done in equilibrium, the work from the external forces and self weight in each individual zone are computed giving the following bearing capacity:

$$0 = -(F_H^p + F_{rubble})\omega_{1H} - (F_G - F_U)\omega_{1V} - W_1 - W_2 + W_3 + W_4 \tag{3.67}$$

where θ_1 is the unknown angle to be determined by minimizing the ratio between the stabilizing work and driving work and F_{rubble} is the active rubble pressure on the seaward side.

3.2 Deterministic design of 12 crown walls with a plane base, and with an extended leg on the seaward side

The principle crown wall geometries used in this example set are based on the Figure 3.2 a – f in the beginning of this chapter.

In Table 3.2 a series of synthetic crown wall examples are listed, considering two different types of real sea waves (locations Bilbao and Fallornica).

The soil parameters are based on the lower 5 % fractile of the angle of dilation and the effective friction angle to determine the reduced effective friction angle. The angle of dilation is modelled by a log normal distribution with a mean value 0.29 *rad* and a standard deviation equal to 0.035 *rad*. In the case of the effective friction angle the mean value is 0.73 *rad* and the standard deviation is 0.09 *rad*.

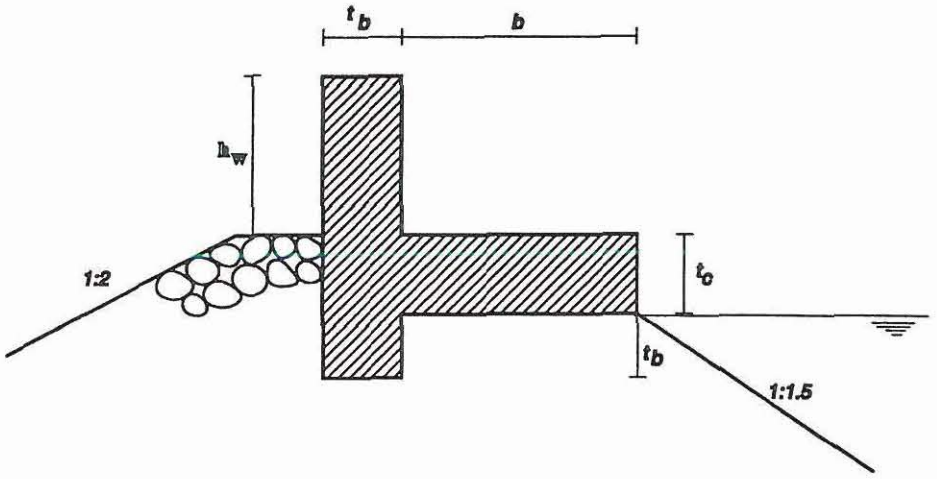

Figure 3.26: *Geometry of the crown wall*

The weight of the two crown wall geometries is given by the following two equations:

Plane crown wall

$$F_G = (h_w t_c + (b - t_c)t_b)\rho_c g \quad kN/m \tag{3.68}$$

Crown wall with a leg

$$F_G = (h_w t_c + (b - t_c)t_b)\rho_c g + t_b^2(\rho_c - \rho_{sea})g \quad kN/m \tag{3.69}$$

where F_G is the weight of the crown wall with out including buoyancy, t_b is the thickness of the crown wall base, t_c is the thickness of the crown wall crest, b is the width of the crown wall (not including the width of the crest section of the crown wall), h_w is the height of the crown wall. The selected parameters are illustrated in Figure 3.26.

In the following Table 3.2, the optimal crown wall width is determined based on the above mentioned parameters and the parameters listed in the table.

The parameters in Table 3.2 from left to right are, $\overline{Q}$ overtopping rates, R (freeboard height), A_c (height from sea water level to the berm crest), G (Berm width), $\overline{Q}^{T_L}$ actual overtopping rate, T_L return period in years for the overtopping rate, thickness of the crown wall base t_b and thickness of crown wall crest is t_c.

In Table 3.2 the deterministic design of 12 crown walls design are based on sliding failure and rupture failure in the rubble mound. For the plane crown wall the width decreases as the crown wall height increases. This is due to the resultant force acting on the base of the crown wall is shifted towards the seaward edge of the crown wall; thus decreasing the bearing capacity of the crown wall. The large weight of the crown wall on the seaward side is more dominant than on the rear side of the breakwater even though the height of the crown wall decreases. Rupture failure mechanism 2 (crown wall failure) was the failure mode which decided the design in the first three cases in Table 3.2.

The weight of the leg on the seaward side and the upper wall are dominant compared to the plane crown wall case. This is the reason the crown wall width decreases with decreasing crest height. Rupture failure mechanism 6 (crown wall failure) was the failure mode which decided the design in the last three cases in Table 3.2.

Design No.	Water depth (m)	$\overline{Q}$ Design	R m	A_c m	G m	H_{so}^{50} m	$\overline{Q}^{T_L}$ m^3/sm	T_L return Years	Width b plane (m)	Width b leg (m)	t_b (m)	t_c (m)
1	26	L	16	9.0	8.2	8.44	$0.39 \cdot 10^{-3}$	6.2	23.87	23.03	3.00	6.00
2	26	M	15	9.0	8.2	8.44	$0.62 \cdot 10^{-3}$	6.1	23.58	22.43	3.00	6.00
3	26	H	14	9.0	8.2	8.44	$0.11 \cdot 10^{-2}$	6.1	24.25	21.82	3.00	6.00
4	12	L	11	8	7.5	5.36	$0.9 \cdot 10^{-4}$	5.7	12.32	13.52	2.00	3.00
5	12	M	10	8	7.5	5.36	$0.2 \cdot 10^{-3}$	3.87	13.48	13.06	2.00	3.00
6	12	H	9	8	7.5	5.36	$0.5 \cdot 10^{-3}$	1.75	15.64	12.56	2.00	3.00

Table 3.2: Deterministic design of 12 crown wall designs, corresponding to 2 wave states (Bilbao and Fallornica) and 3 overtopping levels, for a plane crown wall with an extended leg and without an extended leg. T_L corresponds to the return period in years for a given wave height $H_{so}^{T_L}$.

4

Main armour and toe in rubble mound breakwaters

Failure of various sections of a rubble mound breakwater can be crucial for the stability of the rubble mound breakwater as a whole. This is illustrated in Figure 4.1, showing a series of failure modes for a rubble mound structure. Ensuring static stability of the armour layer and toe berm and crown, enables stability of the primary sections of a rubble mound breakwater. The combined static stability of the armour layer and toe berm will be investigated.

The main function of the toe berm, is to keep the main armour layer in place so that movement is restricted to a minimum. As the water depth is lowered at the breakwater, the stability of the toe will usually decrease, although still depending on the water depth at foot of the breakwater. The armour layer is also more susceptible to damage close to the toe, when the water level decreases towards the toe berm, due to possible increase in the effect of run down which simultaneously affects the stability of the toe berm.

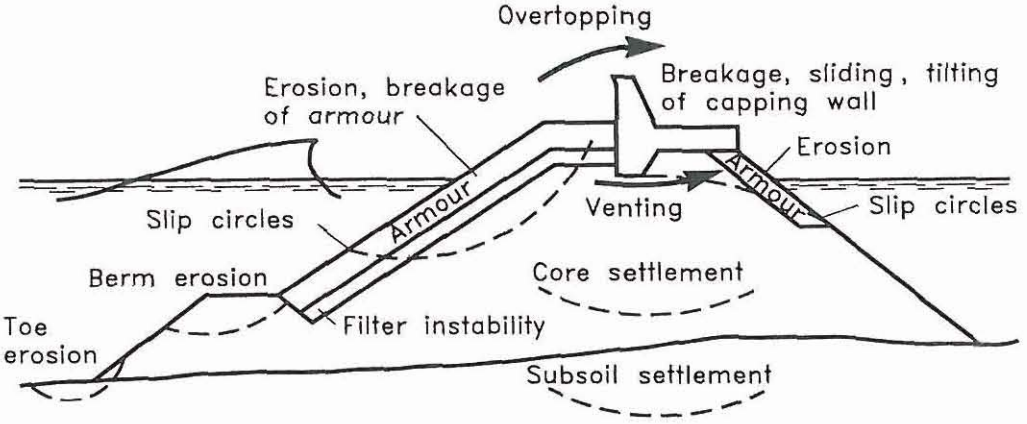

Figure 4.1: *Failure modes for a conventional rubble mound breakwater, Burcharth (1991)*

Stability of the armour layer and armour layer will be determined, using van der Meer's static stability formula (1988) and Gerding's (1993) toe berm stability formula. Further experimental data from Lamberti (1994) will be used to model the interaction between the armour layer and toe berm interaction.

4.1 Stability of the toe (rock)

The toe keeps the armour in place, to ensure that the armour layer does not slide down towards the sea bed. The toe is usually designed using smaller rock material than the armour layer, due to the reduced effect of run down.

The stability of the toe berm has been derived from laboratory tests performed by Gerding (1993). The parameters of significance from his data analyses was found to be:

significant wave height	:	H_s
nominal stone diameter of the toe	:	D^t_{n50}
stone mass density	:	ρ_s
water depth at the foot of the toe	:	h_s
water depth at the foot of the armour layer	:	h_t
relative mass density	:	$\Delta = (\rho_s - \rho_w)/\rho_w$

The stability of the toe was based on a complete stable armour layer. Gerding (1993) did not find a clear correlation between the damage of the toe and the wave steepness, and the berm width. The damage level is classified as N_{od} (number of stones displaced within a strip width D^t_{n50}):

N_{od}=0.5	hardly any damage
N_{od}=2	acceptable damage, design criterion
N_{od}=4	unacceptable damage

The toe stability is shown graphically in Figure 4.2 based on Gerdings (1993) results:

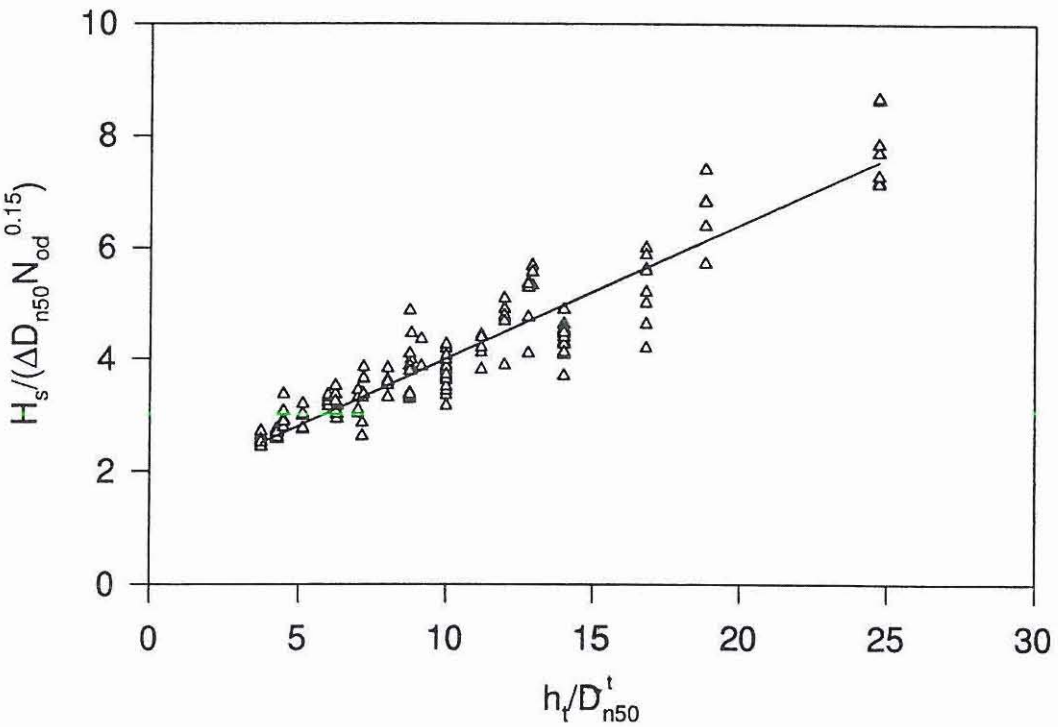

Figure 4.2: *Design line for toe berm stability, reproduced from Gerdings experimental data.*

$$\frac{H_s}{\Delta D^t_{n50}} = (0.24 \cdot \frac{h_t}{D^t_{n50}} + 1.6) \cdot N_{od}^{0.15} \tag{4.1}$$

Equation (4.1) are valid within the following boundaries, equation (4.2) - (4.2), set by the laboratory tests.

$$0.4 < \frac{h_t}{h_s} < 0.9 \tag{4.2}$$

$$0.93 < \frac{h_t}{D^t_{n50}} < 25 \tag{4.3}$$

It should be noted that the toe berm equation is valid for rock with a density of approximately 2680 kg/m^3. The uncertainty of the toe berm stability equation (4.1) can be modelled as having a mean value of 0.96 and standard deviation 0.1 based on Gerdings laboratory results.

4.2 Stability of the armour layer rock

The armour layer in the rubble mound is the outermost rock layer susceptible to wave attack. Therefore the stability of the armour layer is of vital importance as the safety of the rubble mound breakwater depends strongly on this layer.

Static stability of the armour layer is dependent of the gravitational forces. The rough classification $H_s/\Delta D^a_{n50}$ (where D^a_{n50} is the nominal stone diameter of armour rock) indicates that the stability coefficient for stable breakwaters lies in the region 1 - 4 , where little damage is allowed under severe design conditions. The relationships between the governing variables can be given by two stability equation, one for plunging waves and for surging waves, taken from van der Meer (1988).

For plunging waves $\xi_m \geq 1.5$:

$$\frac{H_s}{\Delta D^a_{n50}} \cdot \sqrt{\xi_m} = 6.2P^{0.18}\left(\frac{S}{\sqrt{N}}\right)^{0.2} \tag{4.4}$$

For surging waves $\xi_m \geq 5$:

$$\frac{H_s}{\Delta D^a_{n50}} = 1.0P^{-0.13}\left(\frac{S}{\sqrt{N}}\right)^{0.2} \cdot \sqrt{\cot\alpha}\,{\xi_m}^p \tag{4.5}$$

where S is the damage parameter equal to eroded area of the armour layer over the nominal armour diameter squared, i.e. $S = A_e/{D^a_{n50}}^2$, P is the permeability, N is the number of waves, α is the slope of the rubble mound and the surf similarity parameter $\xi_m = \tan\alpha/\sqrt{H_s/L_m}$, where L_m is the mean wave length based on the mean wave period.

The transition from plunging to surging waves is described by interpolation between the two equations (4.4) and (4.5):

$$\xi_m = \left(6.2P^{0.31}\sqrt{\tan\alpha}\right)^{\frac{1}{P+0.5}} \tag{4.6}$$

Depending on the slope angle and permeability the transition lies between $\xi_m =$ 2.5 and 4. This is usually the region where the incident wave collapses on the rubble mound.

The limits of the governing variables is given by:

$$\begin{array}{ccccc} 0.1 & \leq & P & \leq & 0.6 \\ 0.005 & \leq & s_m & \leq & 0.06 \\ 2.0\ t/m^3 & \leq & \rho_s & \leq & 3.1\ t/m^3 \\ N & \leq & 7500 & & \end{array}$$

The permeability coefficient P can be related to the volume of water dissipated in the core of the structure. Equations (4.4) and (4.5) have been confirmed in conjunction with large scale tests. In a stochastic model the uncertainty of the equations (4.4) and (4.5) can be modelled by considering the constants 6.2 and 1.0 as stochastic variables. The two constants can be assumed to be normal distributed with a standard deviation of 0.4 for the constant 6.2 and 0.08 for 1.0, see van der Meer (1993). These values can be used in evaluating the uncertainty of the design equations for the design of the armour layer.

4.3 Evaluation of the failure mode interaction between main armour and toe berm

A combined analysis of the multiple failure modes of armour layer and toe berm will result in an alternative evaluation of the existing single failure modes as the separate failure modes of the armour layer and toe berm may not sufficiently establish design of the structure. In reality the armour layer and toe berm will interact under certain design wave conditions and result in a combined failure mode of a system. The following interaction schemes have been established from video recordings of the tests performed by Bologna University:

- Failure of the toe berm can be affected by partial failure of the main armour (positive effect) cf. Figure 4.3. The run down will cause partial failure of the armour layer and will move rocks from the armour layer to the toe berm, thus improving the stability of the toe berm. However, the run down can also be of a magnitude where rock from the armour layer will force movement of the existing rock material in the toe berm and hereby reduce the stability of the toe berm.

- Failure of the armour is affected partly by the failure of the toe berm (negative effect) cf. Figure 4.4 Partial damage of the toe berm will cause instability of the armour layer when the width of the toe berm is reduced to an extent where the toe berm is not able to hold the armour layer back from sliding. The magnitude of the run down can affect the overall stability of the armour layer by forcing armour rocks to move the smaller rocks in the toe berm.

The most important factors describing the damage levels are N_{od} (damage level considering displacements in a strip of D_{n50}), and S (damage level related to gravel or rock of smaller size, eroded from the rubble mound).

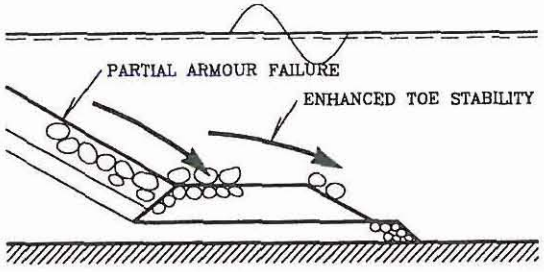

Figure 4.3: *Stability of the toe berm affected by partial failure of the armour layer (positive effect)*

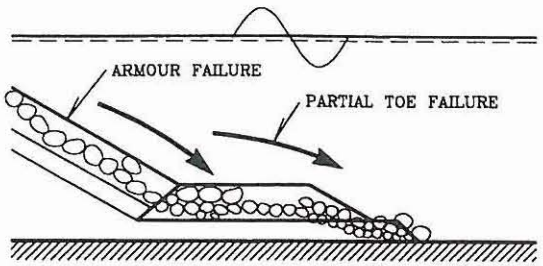

Figure 4.4: *Failure of armour layer affected by partial failure of the toe berm (negative effect)*

4.4 Definition of the damage level between armour layer and toe to interpret armour layer and toe berm interaction

A series of definitions of the damage levels are done to interpret the interaction between the armour layer and toe berm. The damage levels are quantified in such a way that the interaction can be resolved and the new design equations can be calibrated. The test series used by Lamberti et al.(1994) consist of small rock size, for the armour layer $D^a_{n50} = 2.4\ cm\ -\ 1.5\ cm$ and for the toe $D^t_{n50} = 2.04\ cm\ -\ 0.68\ cm$. The damage level S and N_{od} will be used to quantify the stability of the armour layer and toe berm.

- The damage level in the armour layer is denoted as S_A
- The damage level in the toe layer is denoted as D_T
- The critical damage level in the armour layer is S^{cr}_A and this is regarded as the accepted damage level regarding a specific design.
- The critical damage level in the toe berm is D^{cr}_T and this is regarded as the accepted damage level regarding a specific design.

Armour failure alone

Failure occurs when $S_A > S^{cr}_A$. This is usually the case, unless erosion takes place locally in the armour layer, thus resulting in little or few stones reaching the toe berm.

Toe berm failure alone

Failure occurs when $D_T > D_T^{cr}$. The damage level D_T is often influenced by movement of stone material from the armour layer to the toe berm.

Armour failure with a negative effect from the toe berm (interaction)

Failure occurs when $D_T \geq D_T^*$ and $S_A^1 > S_A^{cr}$

D_T^* corresponds to the critical level of damage of the toe berm causing instability of the armour layer ($D_T^* \leq D_T^{cr}$, stable toe) and S_A^1 corresponds to the damage level of the armour layer caused by the instability of the toe when ($D_T \geq D_T^*$).

Armour failure with a positive effect on the toe berm (interaction)

Failure occurs when $S_A \geq S_A^*$ and $D_T^1 > D_T^{cr}$

S_A^* corresponds to the critical level of damage of the armour layer causing an increase in the stability of the toe berm as long as ($S_A^* \leq S_A^{cr}$) and D_T^1 corresponds to the revised damage level of the toe berm from the deposition of the armoured stones on the toe berm.

4.4.1 Derivation of the modified design equations for armour layer and toe berm

A series of laboratory tests of different main armour and toe berm cross sections were performed at The University of Bologna, to establish a measurable effect of main armour and toe berm interaction. The test setup and laboratory test results of the main armour and toe berm interaction are documented in Lamberti et al. (1994).

The armour layer stability equation cf. section 4.1 and toe berm stability equation cf. section 4.2, are used as a basis to derive the interaction between the main armour and toe berm from the experimental data provided by University of Bologna. The accepted damage level and critical damage level have been evaluated for the toe berm and armour layer in section 4.4. These damage levels give the range in which each design equation is valid in the following. It should be noted that the damage parameters in section 4.4 are calculated on the basis of the significant design parameters for each design equation, i.e. the damage level criterion cannot be evaluated as a isolated phenomenon.

The following design equation (4.7) for the toe berm Gerding's equation (4.1). It is valid in the interval $0 < h_t/D^t_{n50} < 4$, where little effect on the stable toe berm is expected from the movement in the armour layer cf. Figure 4.5.

$$\frac{H_s}{\Delta D^t_{n50}} = Z_{toe}(0.24 \cdot \frac{h_t}{D^t_{n50}} + 1.60) \cdot N_{od}^{0.15} \tag{4.7}$$

Z_{toe} is the uncertainty of the equation and is assumed to be normally distributed with an expected value equal to 0.96 and a coefficient of variation equal to 0.1.

The design equation for the main armour *plunging waves* is expressed as:

$$\frac{H_s}{\Delta D^a_{n50}} = 6.2P^{0.18}\left(\frac{S}{\sqrt{N}}\right)^{0.2}\frac{1}{\sqrt{\xi_m}} \tag{4.8}$$

where the equation (4.8) covers breaking and non-breaking wave conditions, with the limits given by van der Meer (1988), the equation is the same as equation (4.4).

The stabilizing effect on the toe berm from the rock material in the armour layer can be derived from Figure 4.5 and is modelled by equation (4.9), with new calibration constants C_1 and C_2. It should be noted that the derivation does not include the points for $h_t/D^t_{n50} > 13$ as the toe berm is wide here. Also the data points included in Figure 4.5 only include the positive effect of deposition of the armour layer on the toe berm. This has been confirmed from the video recordings of the tests series.

$$\frac{H_s}{\Delta D^t_{n50}} = Z^1_{toe}(C_1 \cdot \frac{h_t}{D^t_{n50}} + C_2) \cdot N_{od}^{0.15} \tag{4.9}$$

$C_1 = 0.26$ and $C_2 = 1.52$, Z^1_{toe} is the uncertainty of the modified toe berm equation which is assumed to follow a normal distribution with a coefficient of variation equal to 18%. The equation (4.9) is expected to be valid for:

$$0.6 < \frac{h_t}{h_s} < 0.9 \tag{4.10}$$

$$4 < \frac{h_t}{D^t_{n50}} < 13 \tag{4.11}$$

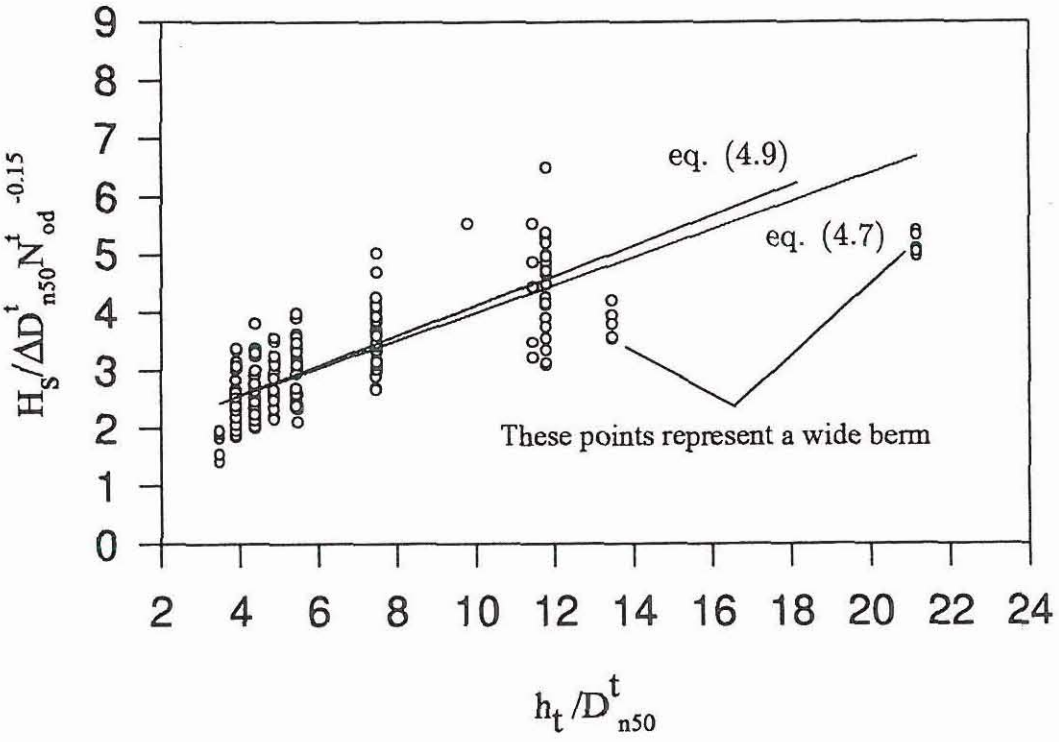

Figure 4.5: *Toe berm data from University of Bologna compared with Gerdings modified equation (showing a positive effect).*

The corresponding damage level of the armour at the intersection point is defined as S_A^*, cf. Figure 4.6. This is the point where van der Meers equation (4.4) intersects with the new modified van der Meer equation(4.12).

$$\frac{H_s}{\Delta D^a_{n50}} = C_3 P^{0.18} \left(\frac{S}{\sqrt{N}}\right)^{C_4} \frac{1}{\sqrt{\xi_m}} \tag{4.12}$$

where $C_3 = 8.44$ and $C_4 = 0.32$, C_3 is modelled as the uncertainty of the modified armour equation and assumed to follow a normal distribution with a coefficient of variation equal to 30%. The equation (4.12) is valid in the boundaries given by:

$$\begin{array}{lcccl} P & \approx & 0.4 & & \\ 0.02 & \leq & s_m & \leq & 0.05 \\ \rho_s & = & 2650\ kg/m^3 & & \\ N & \leq & 7500 & & \end{array}$$

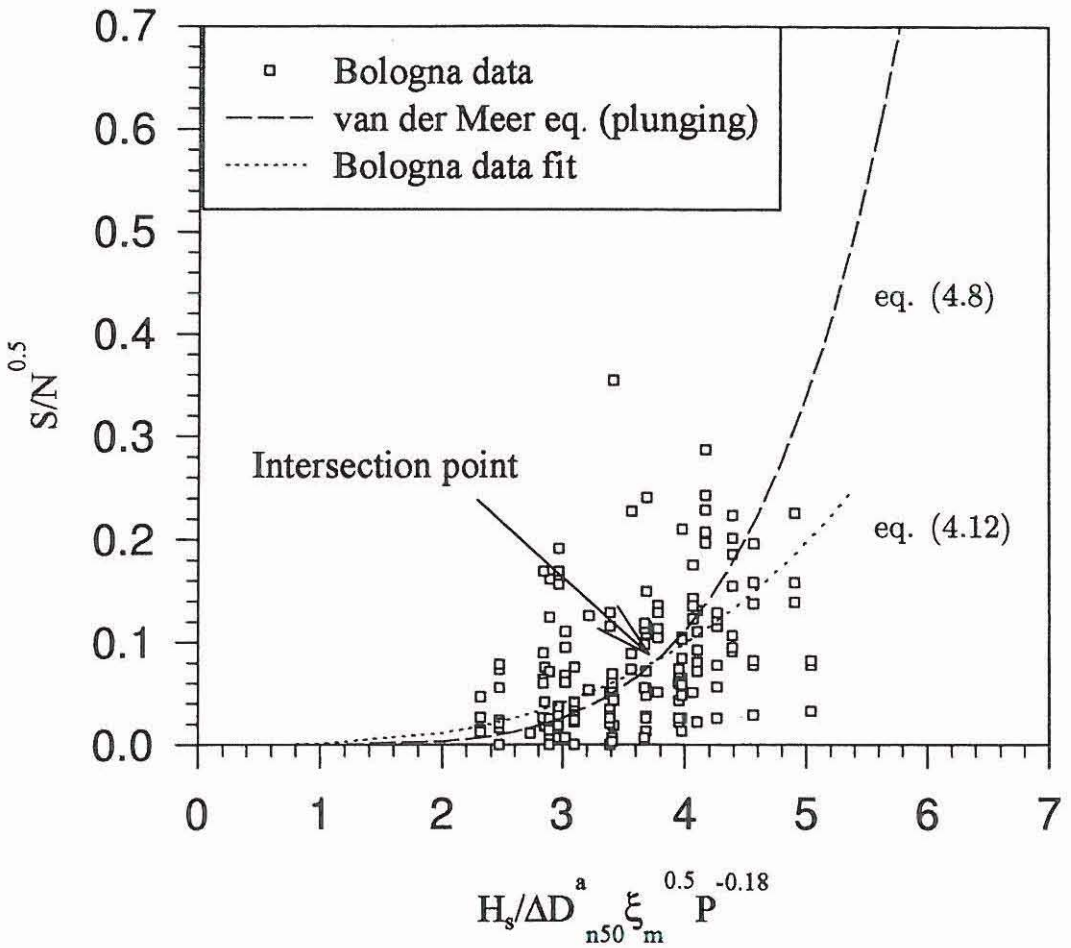

Figure 4.6: *Design equations based on armour layer damage to determinate* S_A^* *(positive effect).*

The stability of the toe is reduced when the toe berm width is simultaneously reduced, thus altering the present static stability of the armour layer. This is shown graphically in Figure 4.7, where equation (4.1) has been fitted to the data set from Bologna University. The data set only includes the negative effect of the toe berm on the armour layer. This has been confirmed from video recordings of the tests.

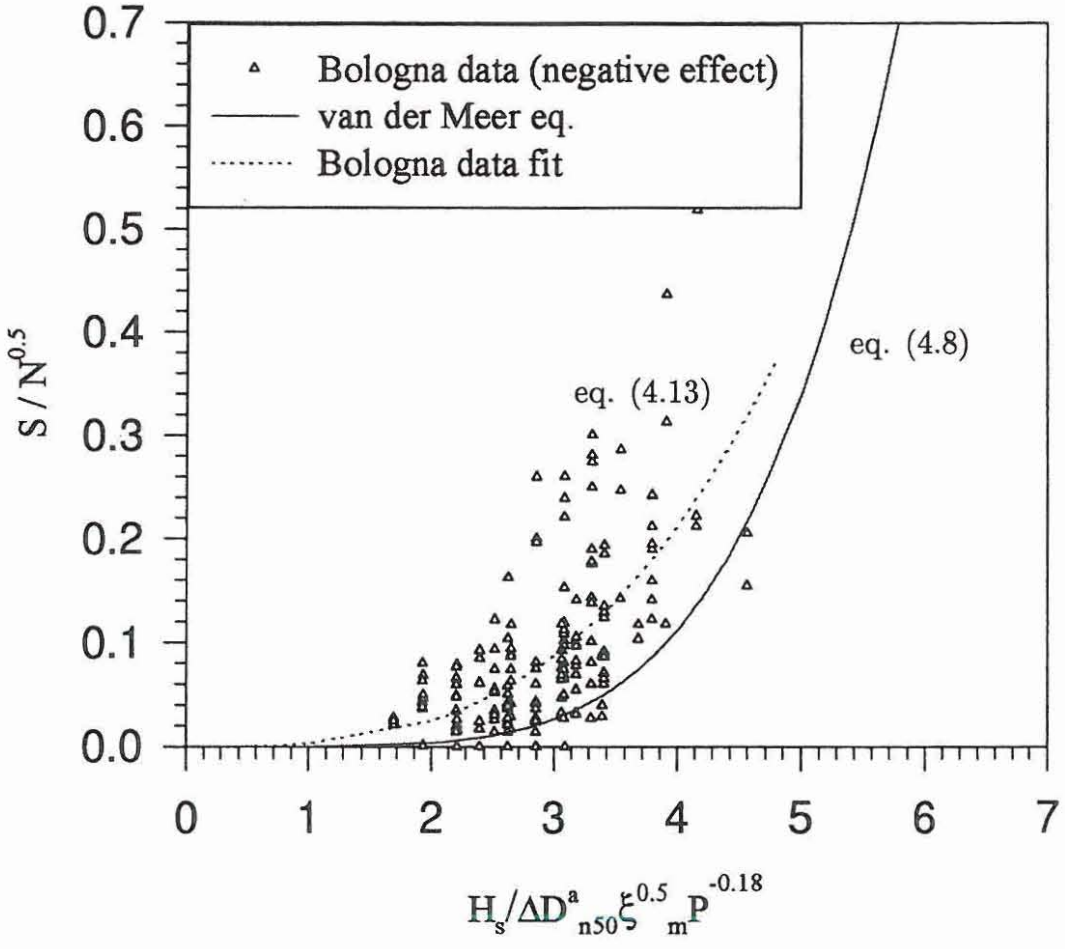

Figure 4.7: *Armour layer data from University of Bologna compared with van der Meers formula (1988) (negative effect)*

The design equation for the main armour after partial damage from the toe berm is expressed by adjusting the constant C_5 and C_6 in equation (4.13).

$$\frac{H_s}{\Delta D^a_{n50}} = C_5 P^{0.18} \left(\frac{S}{\sqrt{N}}\right)^{C_6} \frac{1}{\sqrt{\xi_m}} \tag{4.13}$$

where $C_5 = 6.6$, $C_6 = 0.32$, $C_5 = 6.6$ is assumed to have a variation coefficient corresponding to 29%. Equation (4.13) is expected to be valid in the boundaries:

$$\begin{array}{ccccc} P & \approx & 0.4 & & \\ 0.02 & \leq & s_m & \leq & 0.05 \\ \rho_s & = & 2650\ kg/m^3 & & \\ N & \leq & 7500 & & \end{array}$$

The negative effect is expected to commence when $N_{od} \geq D_T^*$, at the intersection point cf. Figure 4.8.

$$\frac{H_s}{\Delta D_{n50}^t} = Z_{toe}^2 \left(C_7 \cdot \frac{h_t}{D_{n50}^t} + C_8 \right) \cdot N_{od}^{0.15} \tag{4.14}$$

where $C_7 = 0.13$ and $C_8 = 2.58$, Z_{toe}^2 is the uncertainty of the modified toe berm equation assumed to follow a normal distribution with a coefficient of variation equal to 26%.

The equation (4.14) is expected to be valid for:

$$0.6 < \frac{h_t}{h_s} < 0.9 \tag{4.15}$$

$$4 < \frac{h_t}{D_{n50}^t} < 25 \tag{4.16}$$

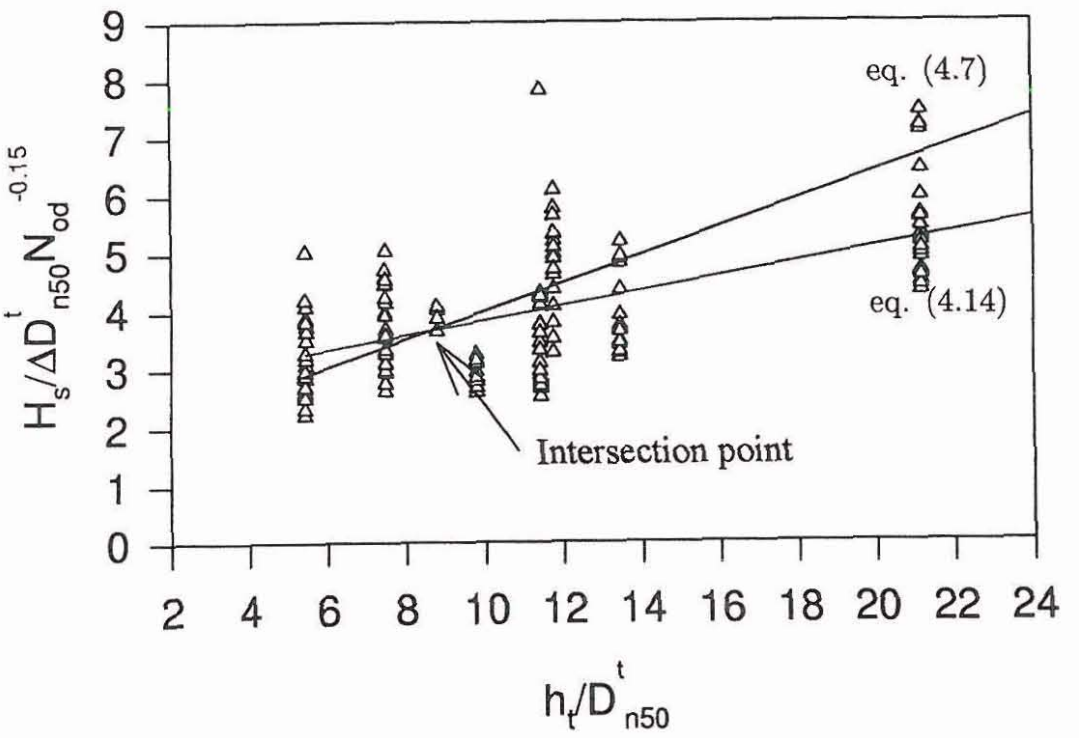

Figure 4.8: *Design equations based on toe berm damage to determinate D_T^* (negative effect).*

The design equations derived from data provided by Lamberti (1994), do not give a clear indication of the armour layer and toe berm interaction cf. Figure 4.5 - 4.8. The large deviation in the measured damage levels N_{od} and S compared to experimental data from Gerding (1993) and van der Meer (1988) indicate a combined effect of the armour layer and toe berm. Interpretation of the damage level in the toe berm is of high importance when evaluation of the interaction takes place. The damage level in the toe berm could be derived in terms of $N^t_{od}(D^t_{n50}, D^a_{n50})$ or $S^t(D^t_{n50}, D^a_{n50})$. The effect of wave steepness and berm width should also have been implemented in the toe berm equations. This would at present drastically increase the uncertainty of the toe berm stability equations, so this is left aside till further investigation.

It should be noted that D^*_T and S^*_A are based on the laboratory tests performed by Bologna University and cannot be regarded as global constants covering all cases of design of rubble mound breakwaters. Also D^*_T and S^*_A should not be evaluated as a strict criterion as some fluctuation at the intersection points is expected.

5

Reliability methods

This chapter is devoted to description of reliability methods. A general discussion of reliability methods can be found in Sørensen (1994a), Burcharth (1992), Madsen et al. (1986) and Thoft-Christensen et al.(1982). The necessary tools to solve non-linear problems, system reliability and reliability based optimization will be presented in the following.

5.1 Reliability modelling

Physical, statistical and model uncertainty of uncertain parameters are modelled by a set of n stochastic basic variables $\mathbf{X} = (X_1, X_2..., X_n)$ defined by the joint probability density function $f_{\mathbf{x}}(\mathbf{x})$.

The failure state is modelled as a limit state function $g(\mathbf{x})$ which describes the boundary between failure state, limit state and safe states. For an outcome $\mathbf{x}$ of $\mathbf{X}$, $g(\mathbf{x})$ is defined by:

$$g(\mathbf{x}) \begin{cases} < 0 & \text{failure} \\ = 0 & \text{limit state} \\ > & \text{safe state} \end{cases} \tag{5.1}$$

The reliability is measured by the probability of survival R

$$R = 1 - P_f \tag{5.2}$$

where the probability of failure is defined as

$$P_f = P\left(g(\mathbf{X}) \leq 0\right) = \int_{g(\mathbf{X} \leq 0)} f_{\mathbf{X}}(\mathbf{x}) d\mathbf{x} \tag{5.3}$$

This multi dimensional integral can generally not be solved analytically and numerical integration is not possible when dimensions are greater than two. Feasible techniques are level II reliability methods First Order Reliability Method (FORM) where linearization of the failure surface is performed around the design point and Second Order Reliability Method (SORM) where a quadratic approximation to the failure surface is performed around the design point. Simulation methods can also be efficient in a number of cases.

5.2 Levels of reliability methods

Structural reliability can be subdivided into levels, depending on the amount of information available in a problem formulation. This can lead to different types of classifications of reliability levels. The ones used here are from Burcharth(1992) and Madsen et al. (1986) and consist of four major levels.

- Level I reliability methods are characterized by a single value for each uncertain quantity i.e. partial safety factors.
- Level II reliability methods are characterized as having two values of each uncertainty quantity, this could be the mean value and the standard deviation.
- Level III reliability methods are characterized by the joint distribution of uncertainty quantities.
- Level IV reliability methods which are based on the total expected utility of the structures to be designed and employ the knowledge of costs and benefits of construction, inspection, maintenance, experiments, consequences of failure etc.

In this thesis no clear differentiation between level II and level III will be made as information will often exceed a level II reliability evaluation, but not completely satisfying a joint distribution necessary for a level III reliability evaluation. Level IV will not be investigated in detail in this thesis, but is a step towards realization of a structure to be constructed and evaluated on a probabilistic basis.

5.3 First and second order reliability

Limit state equations are often of a non-linear type and therefore, a linearization of the failure function is performed using a Taylor expansion series resulting in the method First Order Reliability Methods, FORM and Second Order Reliability Methods, SORM, where a quadratic approximation is assumed. In order to determine the probability of failure by use of FORM/SORM the following procedure is adopted.

The basic variables $\mathbf{X}$ must be transformed into a set of independent standard normally distributed variables $\mathbf{U}$ by the transformation $\mathbf{T}$, $\mathbf{T}(\mathbf{X}) = \mathbf{U}$. The limit state function for an outcome $\mathbf{x}$ of $\mathbf{X}$ becomes

$$g(\mathbf{x}) = g(\mathbf{T}^{-1}(\mathbf{u})) = g_u(\mathbf{u}) \tag{5.4}$$

Stochastic variables can be non-normal distributed resulting in a necessary transformation of non-normal dependent stochastic distributed parameters so that the reliability index can be determined, Nataf (1962). For dependent stochastic variables X_i, $i = 1, ...n$ the Rosenblatt Transformation can be used to define a transformation to the u-space of uncorrelated and normalized normally distributed variables u_i, $i = 1, ...n$. Two different transformations are often used in the transformation of dependent, non normal distributed variables, Rosenblatt Transformation, Madsen et al. (1986) and the approximate Nataf Transformation The choice of transformation depends on the available statistical information.

The Hasofer & Lind reliability index β is defined as the smallest distance from the origin O in the u-space after the transformation from the x space, cf. 5.1, to the failure surface $g_u(\mathbf{u})$ =0. β is commonly known as the first order reliability index cf. Figure 5.2.

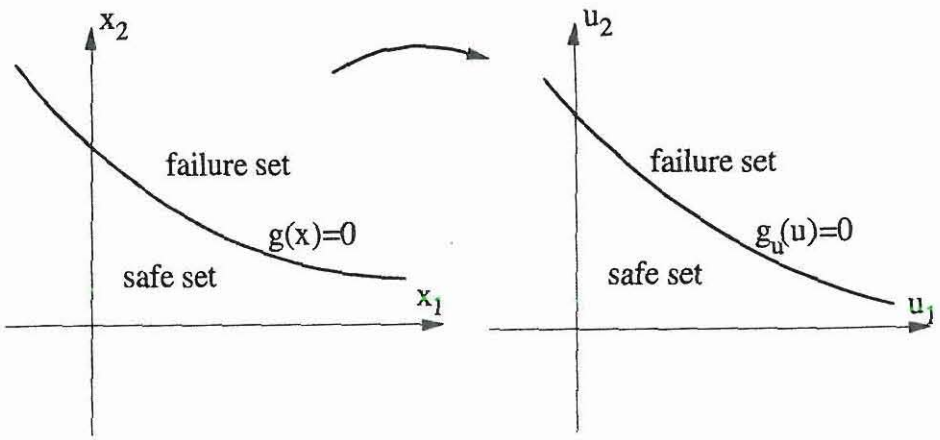

Figure 5.1: *Definition of the transformation from x-space to u-space .*

The minimum distance from a point on the failure surface to the origin in the standard normal space must be found. This design point $\mathbf{u}^*$ is called the β point and can be formulated by the optimization problem

$$\min_{\mathbf{u}} \quad \sqrt{\mathbf{u}^T\mathbf{u}} \tag{5.5}$$

$$s.t. \quad g(\mathbf{T}^{-1}(\mathbf{u})) = 0 \tag{5.6}$$

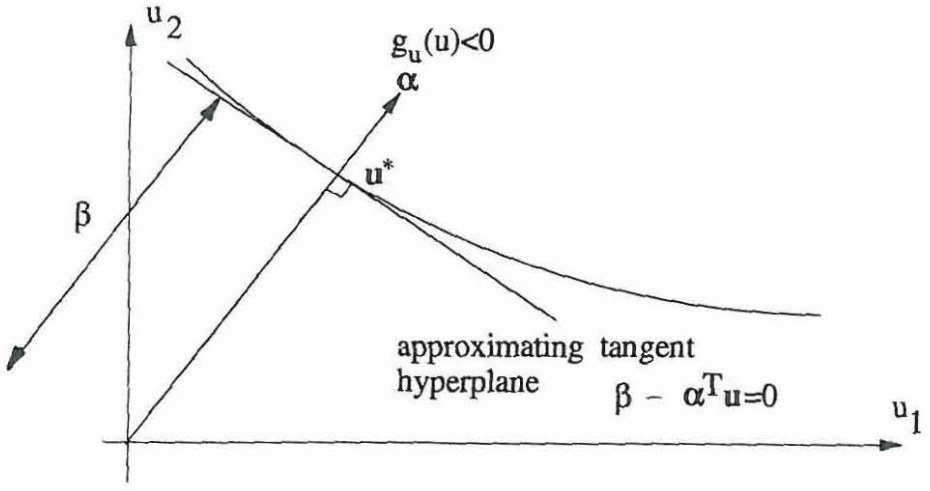

Figure 5.2: *Definition of β in the u-space .*

and the minimum distance is $\beta = \sqrt{\mathbf{u}^{*T}\mathbf{u}^{*}}$. The design point is shown in u-space in figure 5.2

The probability of failure corresponding to the linearization of the failure surface at the design point, cf Figure 5.3. can be approximated by

$$P_f = \Phi(-\beta) \tag{5.7}$$

where Φ is the standard normal distribution function.

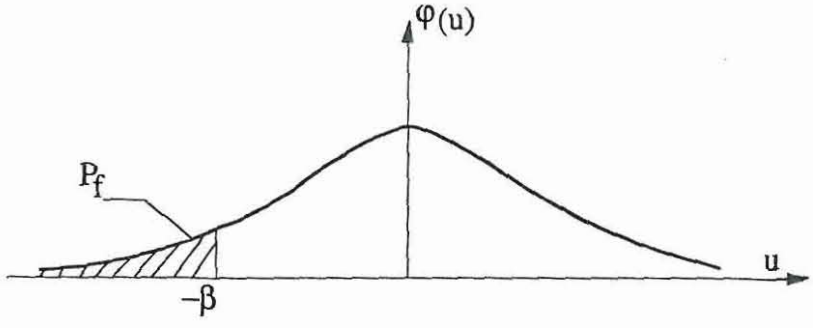

Figure 5.3: *Illustration of the reliability index and probability failure.*

The unit normal vector α to the linearized tangent hyperplane is:

$$\alpha = \frac{-\nabla_u g(\mathbf{T}^{-1}(\mathbf{u}))}{|\ \nabla_u g(\mathbf{T}^{-1}(\mathbf{u}))\ |} \tag{5.8}$$

where $\nabla_u g(\mathbf{T}^{-1}(\mathbf{u}))$ is the gradient vector g with respect to $\mathbf{u}$

When the failure surface is strongly non-linear a better approximation of the probability of failure can be obtained by applying SORM which uses a quadratic approximation to the failure surface at the β point.

5.4 Systems reliability

Failure of a structure is seldom signified by one failure mode, i.e a set of single failure modes of a structure may introduce a multiple set of failure modes, resulting in a system of failure which are referred to as series and/or parallel system. Illustration of failure components in a series system and parallel system can be seen in Figure 5.4

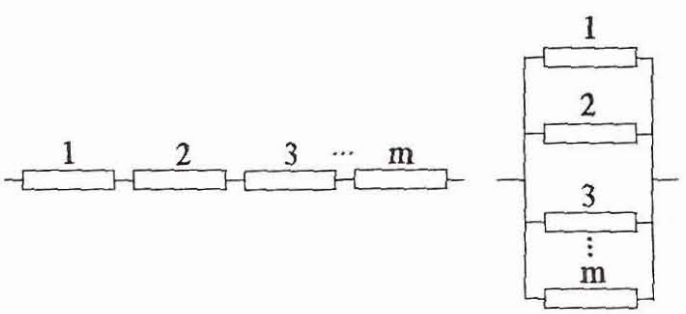

Figure 5.4: *Illustration of a series and parallel system of failure components.*

where 1...m denote the single failure components modelled in a series system and parallel system.

5.4.1 Series system

When one of the failure components fail then the systems fail, i.e the breakwater has no load carrying capacity after one component fails. The probability of system failure P_f^s can be written as a probability of unions:

$$P_f^s = P\left(\bigcup_{i=1}^{m} g_i(\mathbf{X}) \leq 0\right) = \int_{\bigcup_{i=1}^{m} g_i(\mathbf{X}) \leq 0} f_{\mathbf{X}}(\mathbf{x}) d\mathbf{x} \tag{5.9}$$

where $g_i(\mathbf{X})$ is the failure function corresponding to $i = 1, 2..m$ and the FORM approximation of the generalized serie systems reliability index β^s can be estimated as:

$$\beta^s = -\Phi^{-1}(1 - \Phi_m(\boldsymbol{\beta}^c, \boldsymbol{\rho})), \quad \text{or} \quad P_f^s = 1 - \Phi_m(\boldsymbol{\beta}^c, \boldsymbol{\rho}) \tag{5.10}$$

where Φ_m is the m-dimensional standardized normal distribution function, $\boldsymbol{\beta}^c$ is the vector of the reliability indices of the individual failure modes $\boldsymbol{\beta}^c = (\beta_1^c, \beta_2^c ... \beta_m^c)^T$ and $\boldsymbol{\rho}$ the corresponding matrix of the correlation coefficient's determined as

$$\rho_{ij} = \boldsymbol{\alpha}_i{}^T \boldsymbol{\alpha}_j \tag{5.11}$$

where $\boldsymbol{\alpha}_i$ is the normalized $\alpha-$vector component i given by eq. (5.8) for further information see Madsen et al. (1986).

Simple upper and lower bound techniques can also be applied to estimate the probability of failure of a series system. The simple upper and lower bounds for the probability of failure for a series system is:

$$\text{Upper bound} \quad P_f^{Us} = 1 - (1 - P_{f1})(1 - P_{f2})...(1 - P_{fm}) \tag{5.12}$$

$$\text{Lower bound} \quad P_f^{Ls} = \max_{i=1}^{m} P_{fi} \tag{5.13}$$

where P_{fi} corresponds to probability of failure of the components $i = 1...m$, the upper bound corresponds to no correlation between the failure components and the lower bound corresponds to full correlation. When failure of one component is not dominating compared to the other failure components in the series system the simple bounds offer too wide a range and therefore are of minor interest and practical use. An improved upper and lower bound can be determined by the narrow bounds developed by Ditlevsen (1979).

5.4.2 Parallel system

A parallel system fails when all the components fails, i.e. the parallel system is defined as intersections of failure events. The probability of failure of a parallel system consisting of m components can be written as

$$P_f^p = P\left(\bigcap_{i=1}^{m} g_i(\mathbf{X}) \leq 0\right) = \int_{\bigcap_{i=1}^{m} g_i(\mathbf{X})\leq 0} f_{\mathbf{X}}(\mathbf{x})dx \tag{5.14}$$

where $g_i(\mathbf{X})$ is the failure function corresponding to $i = 1, 2..m$ and the FORM approximation of the generalized parallel systems reliability index β^p can be estimated as:

$$\beta^p = -\Phi^{-1}(\Phi_m(-\boldsymbol{\beta}^{\mathbf{c}}, \boldsymbol{\rho})), \quad \text{or} \quad P_f^p = \Phi_m(-\boldsymbol{\beta}^{\mathbf{c}}, \boldsymbol{\rho}) \tag{5.15}$$

where Φ_m is the m-dimensional standardized normal distribution function, $\boldsymbol{\beta}^{\mathbf{c}}$ is the vector of indices at component level $\boldsymbol{\beta}^{\mathbf{c}} = (\beta_1^c, \beta_2^c ... \beta_m^c)$ and $\boldsymbol{\rho}$ the corresponding matrix of the correlation coefficients.

In a parallel system where the failure surface is non-linear, equation (5.15) will result in an unrefined approximation, see Hohenbichler (1987). An improved approximation of the reliability index for a parallel failure set can be obtained by by use of a joint β^J point and not the individual β points obtained from the component reliability analyses.

The joint β^J point can be obtained from the following optimization problem.

$$\min_{\mathbf{u}} \qquad \sqrt{\mathbf{u}^T\mathbf{u}} \tag{5.16}$$

$$s.t. \quad g_i(\mathbf{T}^{-1}(\mathbf{u})) \leq 0 \quad , i = 1, 2..., m \tag{5.17}$$

At the joint β point in the standard normal $u-$ space generally $m_A \leq m$ failure functions intersect. The corresponding estimate of the probability of failure and reliability index is

$$\beta^p = -\Phi^{-1}(\Phi_{m_A}(-\boldsymbol{\beta}^J, \boldsymbol{\rho}^J)), \quad \text{or} \quad P_f^p = \Phi_{m_A}(-\boldsymbol{\beta}^J, \boldsymbol{\rho}^J) \tag{5.18}$$

where $\boldsymbol{\beta}^J$ and $\boldsymbol{\rho}^J$ correspond to linearization made at the joint β point.

A better approximation of parallel system probability of failure can be obtained by including the inactive constraints, see Hohenbichler et al. (1987).

Simple upper and lower bound techniques can also be applied to estimate the probability of failure of a parallel system. The simple upper and lower bounds for the probability of failure for a parallel system is:

$$\text{Upper bound} \quad P_f^{Up} = \min_{i=1}^{m} P_{fi} \tag{5.19}$$

$$\text{Lower bound} \quad P_f^{Lp} = P_{f1} P_{f2} ... P_{fm} \tag{5.20}$$

where P_{fi} corresponds to probability of failure of the components $i = 1...m$, the upper bound corresponds to full correlation between the failure components and the lower bound corresponds to independence.

5.4.3 Series system of parallel systems

Failure of a structure is seldom signified by a single failure component but a set of failure modes in a multiple system consisting of a series system of parallel systems. Illustration of failure components in a series system of parallel systems can be seen in Figure 5.5

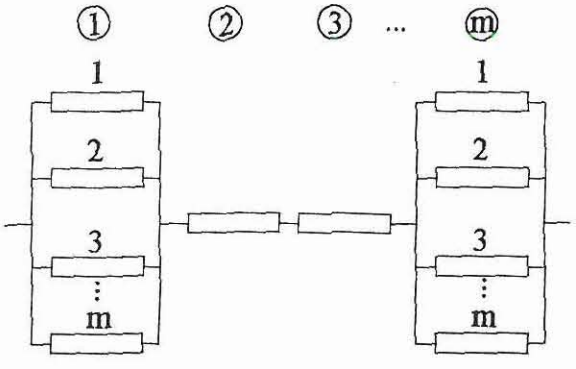

Figure 5.5: *Illustration of failure components in a series system of parallel systems.*

where $1...m$ denotes the single failure components modelled in a parallel system, and the encircled numbers signify the series system consisting of single failure components and parallel systems. The reliability of the multiple system is analysed by solving the parallel system as described in section 5.4.2, and thereafter treating the system as a series system as described in section 5.4.1. For a more detailed explanation of serie system of parallel systems , see Sørensen (1994a)

5.5 Sensitivity evaluation

Sensitivity of a reliability evaluation can be divided up into sensitivity of the reliability index to a deterministic parameter or a stochastic parameter. The sensitivity of the stochastic parameters to a given reliability index can also be evaluated, to show the significance of the individual stochastic parameters in design. Sensitivity of the stochastic parameters can be characterized as elements in the α vector, defined in equation (5.8) The α vector is a unit normal vector of the tangent hyperplane cf. figure 5.2, i.e. $|\boldsymbol{\alpha}| = 1$. Therefore for independent stochastic variables α_i^2 must give the percentage of the total uncertainty associated with U_i and X_i. A more thorough application of α_i^2 as a sensitivity measure can be seen in Madsen et al. (1986).

Parameterization of the sensitivity parameters are defined as derivatives with respect to the deterministic parameters b_i. The sensitivity parameter can be derived from the limit state equation in transformed form $g(\mathbf{T}^{-1}\mathbf{U}, \mathbf{b})$ or as a stochastic related variable $\mathbf{X}$ with a given probability distribution, where $\mathbf{X}$ is related the standardized variable $\mathbf{U}$ by $\mathbf{U} = \mathbf{T}(\mathbf{X}, \mathbf{b})$.

For a given deterministic parameter in terms of a limit state formulation, the sensitivity of the first order reliability index is:

$$\frac{\partial \beta}{\partial b_i} = \frac{1}{|\nabla_u g(\mathbf{T}^{-1}(\mathbf{u}^*), \mathbf{b})|} \frac{\partial g(\mathbf{T}^{-1}(\mathbf{u}^*), \mathbf{b})}{\partial b_i} \tag{5.21}$$

For a distribution parameter the sensitivity of the first order reliability index β is:

$$\frac{\partial \beta}{\partial b_i} = \frac{1}{\beta} \mathbf{u}^{*T} \frac{\partial \mathbf{T}(\mathbf{x}^*, \mathbf{b})}{\partial b_i} \tag{5.22}$$

where $\mathbf{u}^*$ and $\mathbf{x}^*$ are the β point in $\mathbf{u}$-space and $\mathbf{x}$-space.

For the corresponding first order estimate of the probability of failure the sensitivity is:

$$\frac{\partial P_f}{\partial b_i} = -\varphi(-\beta)\frac{\partial \beta}{\partial b_i} \tag{5.23}$$

where φ is the standard normal density function.

5.6 Non-linear optimization

The failure surface presented in figure 5.2 can be very non-linear, so in terms of accuracy and time, an efficient non-linear algorithm is sought to determine the minimum distance to the failure surface from origo in the standard normal space, see section 5.3. A general optimization problem can be formulated in the continuity space as

$$\min_{\mathbf{z}} \quad F(\mathbf{z}) \tag{5.24}$$

$$s.t. \quad f_i(\mathbf{z}) = 0 \quad ,i = 1,\ldots,m_e \tag{5.25}$$

$$f_i(\mathbf{z}) \geq 0 \quad ,i = m_e+1,\ldots,m \tag{5.26}$$

$$z_i^l \leq z_i \leq z_i^u, i = 1,\ldots,N \tag{5.27}$$

where $z = (z_1 ... z_N)^T$ are the optimization variables, $F(\mathbf{z})$ is the objective function, f_i, $i = 1...m_e$ is the equality constraints and f_i, $i = 1 + m_e...m$ are the inequality constraints and $z_i^l \leq z_i \leq z_i^u, i = 1,\ldots,N$ is the lower and upper bound to z_i in the continuous solution space.

The solution to an optimization problem is denoted as z^*. Equations (5.24) to (5.27) and the constraints for which $f_i(z^*) = 0$, $i = 1,...m$ are denoted as the active constraints. Usually the optimization problem equations (5.24) to (5.27) is non-linear and non convex.

The formulated continuous non-linear formulation in this thesis is solved using the first order algorithm NLPQL by Schittkowski (1985). The NLPQL algorithm is based on the sequential quadratic optimization method by Han, Powell and Wilson, see Schittkowski (1985), which approximates the Hessian matrix from gradients by BFGS method, see Gill, Murray & Wright (1981).

5.7 Reliability based optimization

Optimal design of a breakwater for construction or rehabilitation is always of interest to a design engineer, so that the monetary aspects (cost benefit analysis) of the structure is kept at a minimum without compromising the project. Optimal reliability based design of a structure is way of devising an ideal structure for the client based on a fixed reliability index. An example is presented in the following where the reliability index is fixed and the decision variables could be the geometrical values from a cross section of a vertical breakwater including the rubble mound.

The design (decision) variables are denoted $\mathbf{b} = (b_i, \ldots, b_N)$, for $i = 1..N$, i.e. the number of design variables N.

If the objective function is chosen as the total expected costs C_T of the structure during the lifetime, the optimal design can be found as the solution to the optimization problem

$$\min_{\mathbf{b}} \quad C_T(\mathbf{b}) = C_I(\mathbf{b}) + C_F P_f(\mathbf{b}) \tag{5.28}$$

$$s.t. \quad B_i(\mathbf{b}) \geq 0 \qquad , i = 1, \ldots, M \tag{5.29}$$

$$b_i^l \leq b_i \leq b_i^u \qquad , \; i = 1, \ldots, N \tag{5.30}$$

where b_i^l and b_i^u are lower and upper bounds to b_i, B_i is the deterministic constraint associated with the design variables b_i , C_I is the initial/construction costs, C_F is the costs of failure, andP_f is the probability of failure during the expected lifetime of the breakwater.

Alternatively an element reliability-index based optimization problem can be formulated

$$\min_{\mathbf{b}} \quad C_I(\mathbf{b}) \tag{5.31}$$

$$s.t. \quad \beta_i(\mathbf{b}) \geq \beta_i^{min} \qquad , i = 1, \ldots, m \tag{5.32}$$

$$B_i(\mathbf{b}) \geq 0 \qquad , i = 1, \ldots, M \tag{5.33}$$

$$b_i^l \leq b_i \leq b_i^u \qquad , i = 1, \ldots, N \tag{5.34}$$

where β_i is the reliability index for failure mode i and β_i^{min} is the corresponding lower bound on the reliability index. Equivalent solutions from (5.28)-(5.30) and (5.31)-(5.32) can be obtained by suitable choices of $\beta_i^{min} \;\; i = 1, ...m$ The above optimization problems are usually non-linear and non-convex. The optimization

problems can be solved effectively using non-linear optimization algorithms and FORM.

The reliability indices in (5.32) are determined on the basis of limit state functions written as $g_i(\mathbf{x}(\mathbf{b}), \mathbf{b}) = 0,\ i = 1, ..., m$. In a traditional deterministic design the design (optimization) problem the constraint (5.32) is exchanged by the deterministic constraint

$$B_i(\mathbf{b}) = g_i(\mathbf{x}^{\mathbf{D}}(\mathbf{b}, \gamma), \mathbf{b}) \geq 0 \quad , i = 1, \ldots, m \tag{5.35}$$

where $\mathbf{x}^{\mathbf{D}}$ are design values calculated using the statistical parameters for the stochastic variables, $\mathbf{X}$, and γ are the partial safety factors.

6

Reliability based design of vertical breakwaters

The following chapter is devoted to characterizing the stochastic variables used in formulating the limit state equations for design of vertical breakwater foundation failure modes so that a reliability evaluation can be performed. Application of reliability analysis on existing vertical breakwaters based on the rupture failure of the foundation, sliding and overturning will be shown to give a qualitative evaluation of the failure modes. Further more an example of a vertical breakwater on a high and low rubble mound, under similar wave conditions will be evaluated to determine the sensitivity of the foundation failure modes. This chapter is an based on the preceeding chapters. The principle design algorithm for a reliability evaluation is presented in Figure 6.1

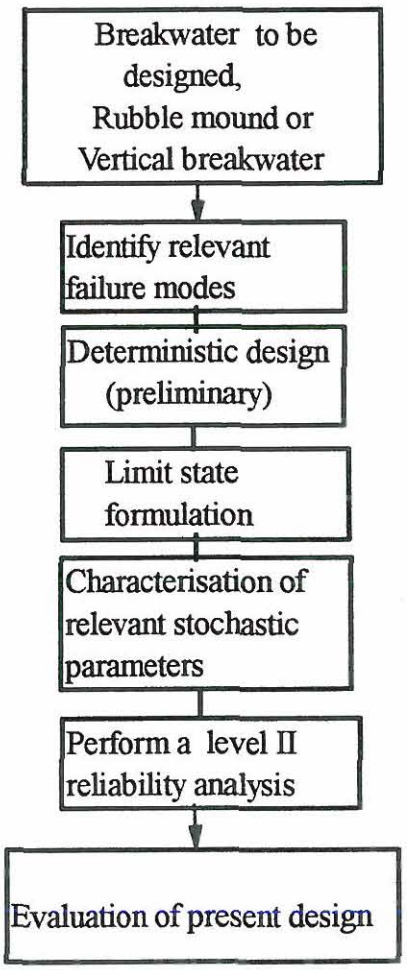

Figure 6.1: *Design flow diagram for a reliability evaluation of breakwaters.*

6.1 Characterization of stochastic variables for vertical breakwaters

All variables are in principle stochastic parameters in a limit state formulation. In a level II reliability evaluation the parameters should be defined by a normal distribution with a mean value and standard deviation, if no other distribution can clarify the statistically uncertainty of the parameter in question. Some parameters e.g. the geometrical parameters have small coefficients of variation and can be regarded as deterministic variables. The parameters which have some degree of uncertainty in breakwater design will be discussed in the following. It is regarded that all characterized stochastic parameters are independent, unless stated otherwise in the text.

6.1.1 Modelling uncertainty of the Goda's wave load model

Statistical uncertainty of physical-mathematical models will always have relevance, as the mathematical model of physical processes are often calibrated by means of small scale experiments or prototype observations. The limited number of experiments or observations and imperfection of the model will result in differences which will exist between predicted and observed outcomes.

The model uncertainty of *Goda's wave load formulation* is assumed to be modelled by normal distributed stochastic variables. This has been clarified by van der Meer (1992) and Bruining (1994) whom performed a number of laboratory tests to evaluate the uncertainty related to the horizontal wave load, wave induced uplift force, horizontal moment and wave induced uplift moment. In Table 6.1 the uncertainty of Goda's wave load formulation compared to recorded wave loads from the laboratory are presented.

X_i	μ_{X_i}	σ_{X_i}	$\frac{\sigma_{X_i}}{\mu_{X_i}}\%$	Reference
Z_{F_H}	1.20	0.25	0.20	van der Meer et al. (1992)
Z_{F_U}	1.40	0.25	0.18	Bruining (1994)
Z_{M_H}	1.49	0.37	0.25	Bruining (1994)
Z_{M_U}	1.34	0.40	0.30	Bruining (1994)

Table 6.1: Uncertainty of the horizontal wave induced force, uplift force, horizontal moment and uplift moment (vertical composite type).

It is clear from Table 6.1 that the coefficient of variation are very high for the wave induced uplift moment and the horizontal wave load moment. The horizontal wave load is clearly dependent on the horizontal moment through the formulation of Goda's wave loads, so therefore the correlation must be taken into consideration when the reliability analysis is performed. The same applies for the wave induced uplift force and wave induced uplift moment.

Incorporation of the model uncertainty in Goda's wave load formulation is presented in the following. The wave induced horizontal force, uplift force and the reduced weight of the vertical structure due to buoyancy can be calculated from equations by Goda and Takahashi. The geometrical parameters are shown in Figure 2.4

$$F_H = Z_{F_H}\left[\frac{1}{2}(p_1+p_2)h_c + \frac{1}{2}(p_1+p_3)h'\right] \quad kN/m \tag{6.1}$$

$$F_U = Z_{F_U} \cdot \frac{1}{2} p_u \cdot B \quad kN/m \tag{6.2}$$

$$F_G = \rho_c \, B \cdot h_w \cdot 9.81 - B \cdot \rho_{sea}(h' + \zeta) \cdot 9.81 \quad kN/m \tag{6.3}$$

Z_{F_H} is the stochastic variable signifying the uncertainty of the horizontal force and Z_{F_U} is the stochastic variable signifying the uncertainty of the uplift force.

The moment about the heel of the caisson breakwater can be calculated by applying Goda's and Takahashi's formulae to the above given parameter values as:

$$M_H = Z_{M_H} \left[\frac{1}{6}(2p_1 + p_3)h'^2 + \frac{1}{2}(p_1 + p_2 h' h_c + \frac{1}{6}(p_1 + 2p_2)h_c^2 \right] \quad kN \tag{6.4}$$

$$M_U = Z_{M_U} \cdot \frac{1}{3} p_u \cdot B^2 \quad kN \tag{6.5}$$

$$M_G = \frac{1}{2}(\rho_c \, B \cdot h_w \cdot 9.81 - B\rho_{sea} \cdot (h' + \zeta) \cdot 9.81)B \quad kN \tag{6.6}$$

Z_{M_H} is the stochastic variable signifying the uncertainty of the horizontal moment and Z_{M_U} is the stochastic variable signifying the uncertainty of the uplift moment.

6.1.2 Modelling uncertainty of the design wave parameters

Statistically variability of wave parameters i.e. significant wave height H_s and peak wave period T_s are the most significant parameters in breakwater design. For design purposes the 50 year return wave heights are of interest and signified as H_s^{50}. Analysis of extreme wave height is quite diverse, but the method often used is the peak value method which employs the peak wave heights of individual storm events, see Burcharth and Liu (1994) for further explanation of fitting methods. The extreme wave data height are usually modelled by extreme distributions which are explained in depth in the next section.

The wave period can be modelled in a joint distribution with the significant wave height, but this is often based on semi-empirical relations which do not clearly model the situation.

A possible way to formulate the joint distribution of the extreme wave heights and corresponding periods is to e.g. apply a conditional three parameter Weibull distribution of the period, conditioned by the significant wave height in deep water.

$$F_{H_{so}^T}(H_{so}) = \left[1 - exp\left(-\left(\frac{H_{so} - B_{H_{so}}}{A_{H_{so}}}\right)^{k_{H_{so}}}\right)\right]^{\lambda T} \qquad H_{so} \gg B_{H_{so}} \quad (6.7)$$

$$F_{T_s}(T_s \mid H_{so}) = 1 - exp\left(-\left(\frac{T_s - B_{T_s|H_{so}}}{A_{T_s|H_{so}}}\right)^{k_{T_s|H_{so}}}\right) \qquad T_s \gg B_{T_s|H_{so}} (6.8)$$

where the parameters A, B, k subscript are the Weibull parameters and λ is the average number of H_{so} data values per year.

As wave data is usually lacking with respect to extreme events H_{so} and T_s, using a joint distribution may not unambiguously clarify the wave period in a conditional distribution as uncertainty of the parameters $A_{T_s|H_{so}}, B_{T_s|H_{so}}, k_{T_s|H_{so}}$ in for example determining H_{so}^{100} and corresponding T_s may lie outside the bounds of available wave data. Therefore it does not seem applicable at present to incorporate the wave period into a joint distribution, and implementation into design. Presently the wave period for design is taken from an interval which corresponds to the extreme wave heights for design.

6.1.3 Modelling uncertainty of the design wave height in deep water

The *deep water wave climate* characterized by H_{so} usually follow a extreme wave height distribution i.e. Weibull, Gumbel or Exponential distribution. The maximum significant wave height within T years for a Weibull distribution is then given by as:

$$F_{H_{so}^T}(H_{so}) = \left[1 - exp\left(-\left(\frac{H_{so} - B}{A}\right)^{k}\right)\right]^{\lambda T} \quad (6.9)$$

where λ is the average number of H_{so} data values per year and the equation is the same as eq. (6.7). B is usually regarded as a deterministic parameter.

The stochastic uncertainty of the A and k values are taken as normal distributed stochastic variables with a variance based on the maximum likelihood estimates. The expected value and standard deviation of A and k are presented in Table 6.2.

	mean	standard deviation, σ
k	μ_k	$\simeq \sqrt{\frac{1}{N}}$ (approximation)
A	μ_A	$\left[\frac{{\mu_A}^2}{N}\left(\frac{\Gamma(1+2/\mu_k)}{\Gamma^2(1+1/\mu_k)}-1\right)\right]^{0.5} \simeq \mu_A\left(\frac{0.3}{N}\right)^{0.5}$

Table 6.2: *Mean and standard deviation of A and k values in a Weibull distribution, (taken from Burcharth (1992b)).*

where N is the number of available H_{s0}-values and Γ is the gamma function.

6.1.4 Modelling the uncertainty of the short varaibility of the measured wave height

The extreme wave heights are measured by means of different technics e.g. accelerometer buoy, hindcast etc. and this may influence the chosen distribution. The parameter F_{H_s} models the measurement errors and the short term variability of the significant wave height H_s. This parameter has a mean value equal 1 and a standard deviation $\sigma_{F_{H_s}}$ which lies in the range $0.05 - 0.35$ depending on different measurement technics.

In this thesis F_{H_s} is expected to be normal distributed with a mean value equal 1 and a standard deviation equal to 0.05. Reference is given to PIANC Working Group 12, Subgroup 12, Burcharth (1992a) for further information.

6.1.5 Modelling the uncertainty of wave heights in the surf zone

As the waterdepth decreases from deep water to shallow water, wave transformation will result in refraction (when waves are not head on), shoaling and finally wave breaking. When structures are placed in shallow water the breaker heights have to be considered to determine the true wave induced loads.

Uncertainty of the wave heights in deep water will diminish, when the breaker wave heights come into effect. Therefore the uncertainty of the breaker heights should be considered in design in depth limited cases.

The *design wave height* $H_{design} = H_{1/250}$ to be applied in the Goda formula is in the case of no surf zone in front of the structure taken as $1.8 \cdot H_{so}$.

Goda (1994a) concluded that the uncertainties related to *shoaling wave heights* are low. He applied laboratory data from Tanimoto (1984) and concluded that the coefficient of variation of the design wave height H_{design} in the surf zone is estimated to be be 9% in the range $h_b/H_{so} < 0.2$. This variation coefficient can be applied prior to wave breaking and without any addition of variability from deep water

In case of a surf zone in front of the structure the breaker height is taken as (Goda, 1994a)

$$H_b = L_0\, 0.17 \left(1 - exp\left(-1.5\frac{\pi h_b}{L_0}\left(1 + 15tan^{4/3}\theta\right)\right)\right) \tag{6.10}$$

where h_b is the water depth at a distance $5H_s$ seaward of the structure and L_0 is the deep water wavelength. Consequently, $H_{design} = min[1.8H_{so}, H_b]$.

Wave breaking fluctuates at fixed locations even under controlled laboratory conditions. This was observed from numerous laboratory tests which were analysed by Goda (1994a) to determine the coefficient of variation for the breaker height ratio H_b/h_b, where $h_b = h_s + 5H_{so}\tan\theta$ and $\tan\theta$ is the slope of the foreshore. The variation coefficient for different foreshore slopes are summarized in Table 6.3.

Foreshore slope $\tan\theta$	$\frac{1}{100}$	$\frac{1}{50}$	$\frac{1}{30}$	$\frac{1}{20}$	$\frac{1}{10}$
$\frac{\mu_{H_b/h_b}}{\sigma_{H_b/h_b}}$	0.05	0.06	0.08	0.10	0.13

Table 6.3: *Coefficient of variation of the breaker height ratio* H_b/h_b.

6.1.6 Modelling the uncertainty of the waterdepth at the structure

The waterlevel at sea in a design condition often includes extreme conditions of wind setup resulting in storm surge, high water level or low water level. Real tides usually fluctuate over a long time duration and the tidal wave length is long compared to the tidal elevation, so for simplicity the *tidal elevation* ζ is assumed to follow a cosine distribution function (6.11), from Takayama (1992).

$$F_\zeta(\zeta) = -\frac{1}{\pi} arc\,cos\left(\frac{\zeta}{\zeta_a} - 1\right) - 1 \tag{6.11}$$

where ζ varies between $\pm\zeta_a$ in m is the amplitude of the variation of the tidal level.

The probability density equation (6.11) explicitly shows the occurrence probability is large at the low and high tidal level.

The *storm surge* η_s should be considered when the structure is in shallow water, due to possible change in breaker wave heights and buoyancy of the structure.

The total water depth cf. Figure 2.4 in front the structure is $h_{tot} = h_s + \eta_s + \zeta$, where h_s is the mean sea water level at the foot of the structure, without influence from the storm surge or tidal level.

6.1.7 Modelling the weight of vertical breakwaters

The *average mass density of a conventional vertical breakwater* including sand ballast, reinforced walls and concrete cap is assumed to be normal distributed with mean value in the range $\rho_c = 2.15 - 2.3\ t/m^3$ and a coefficient of variation of 5%.

6.1.8 Modelling the uncertainty of soil properties

Variability of soil properties such as the the effective friction angle, undrained shear strength of the clay, cohesion, and angle of dilation are relevant parameters in determining the bearing capacity of the foundation. The stress history of the soil is seldom known and samples extracted from sites may not be homogeneous and isotrop. This is the reason that authors Nadim et al. (1994) and Cherubini (1992) have encountered variability in the soil parameters such as the effective friction angle, undrained shear strength of the clay and cohesion.

Three major sources of uncertainty can be found in soil.

- The natural heterogeneity or in-situ variability of the soil
- Natural soils have variation in the mineral composition and stress history
- Fluctuation in moisture content and density

It is generally accepted that the spatial variability of the *effective friction angle* of a well known sample is small, but authors such as Nadim et al. (1994) and Cherubini (1992) have encountered variation coefficients in the range 3% to 15%. The high degree of variability observed by authors may be due to non linear increase of the effective friction angle, which is illustrated in Figure 6.2, as authors Nadim et al. (1994) and Cherubini (1992) have fitted a straight line to the failure envelope.

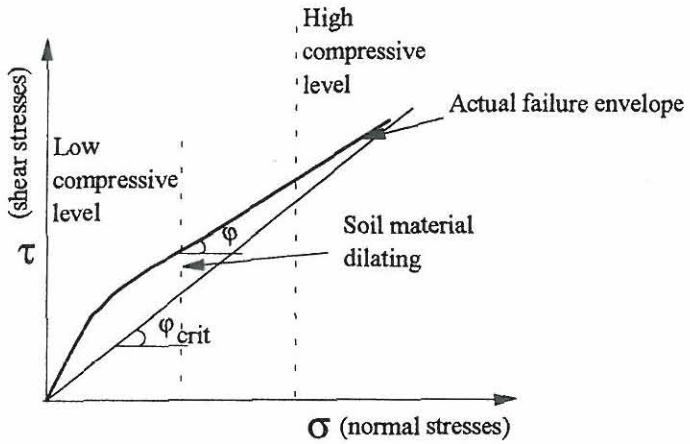

Figure 6.2: *Illustration of the effective friction angle in a shear stress and normal stress diagram.*

At low compressive levels the influence of the angle of dilation of the material increases the real failure envelope and at high compressive level the angle of dilation has little or no effect, where the critical friction angle φ_{crit} is close to the local effective friction angle φ i.e. the failure envelope falls in line with a tangent corresponding to φ_{crit} at a high compressive level:

The *friction coefficient* between the base plate and rubble is assumed normal distributed with a mean value $\tan\mu = 0.636$ and a coefficient of variation of 15 %, Takayama (1992).

Even homogeneous soil layers exhibit change in strength from point to point. The *undrained shear strength of clay* is an example where spatial variability exist, which can be modelled by a log-Gaussian stochastic field $\{c_u(x,z)\}$where x is the horizontal coordinate and z the vertical coordinate. The mean value function and covariance function are in this thesis assumed to be:

$$E[c_u(x,z)] = \mu_{c_u} + az \tag{6.12}$$

$$Cov[c_u(x_1,z_1), c_u(x_2,z_2)] = \tag{6.13}$$

$$\sigma^2_{c_u} \exp\Big(-|\frac{z_1 - z_2}{3.0}|\Big) \exp\Big(-(\frac{x_1 - x_2}{30.0})^2\Big)$$

where c_u is in kPa and x, z are taken in meters, (origo $(x,z) = (0,0)$ is at the point where the rupture slip line enters the clay subsoil), μ_{c_u} is the expected value of the undrained shear strength, σ_{c_u} is the standard deviation of the undrained shear strength and a is a constant signifying the linear increase of the undrained shear strength of the clay subsoil. The correlation lengths 3.0 and 30 are taken as typical values for clay, taken from Keaveny et al. (1989).

The uncertainty of the derived bearing capacity of the foundation, based on the upper bound theorem is assumed to be normal distributed with a coefficient of variation equal to 10 %. This has been accepted as a reasonable assumption based on the work by Sørensen et al. (1993).

6.2 System of vertical breakwater failure modes

It is clear from Figure 1.4 that failure of a vertical breakwater can be modelled as a system of components. As interaction between components may impose failure on other components and result in failure of the vertical breakwater. A fault tree is often used to clarify the modes of failure of a structure.

A fault tree describes the relationship between the failures of a system. This is illustrated in Figure 6.3 for vertical breakwaters. The excessive wave transmission can cause damage to the harbour side thus disrupting harbour activity.

Each number encircled in the right corner of each failure mode identified cf. Figure 6.3 can be subdivided into a number of principle failure modes which can be modelled in a system, i.e. rupture failure of the rubble mound, sand subsoil, clay subsoil and overturning. Sliding and rupture failure is often denoted as the most significant failure modes for conventional vertical breakwaters. An example of 4 from the simplified flow diagram is shown in Figure 6.4. As a simplification settlement and scouring is not included.

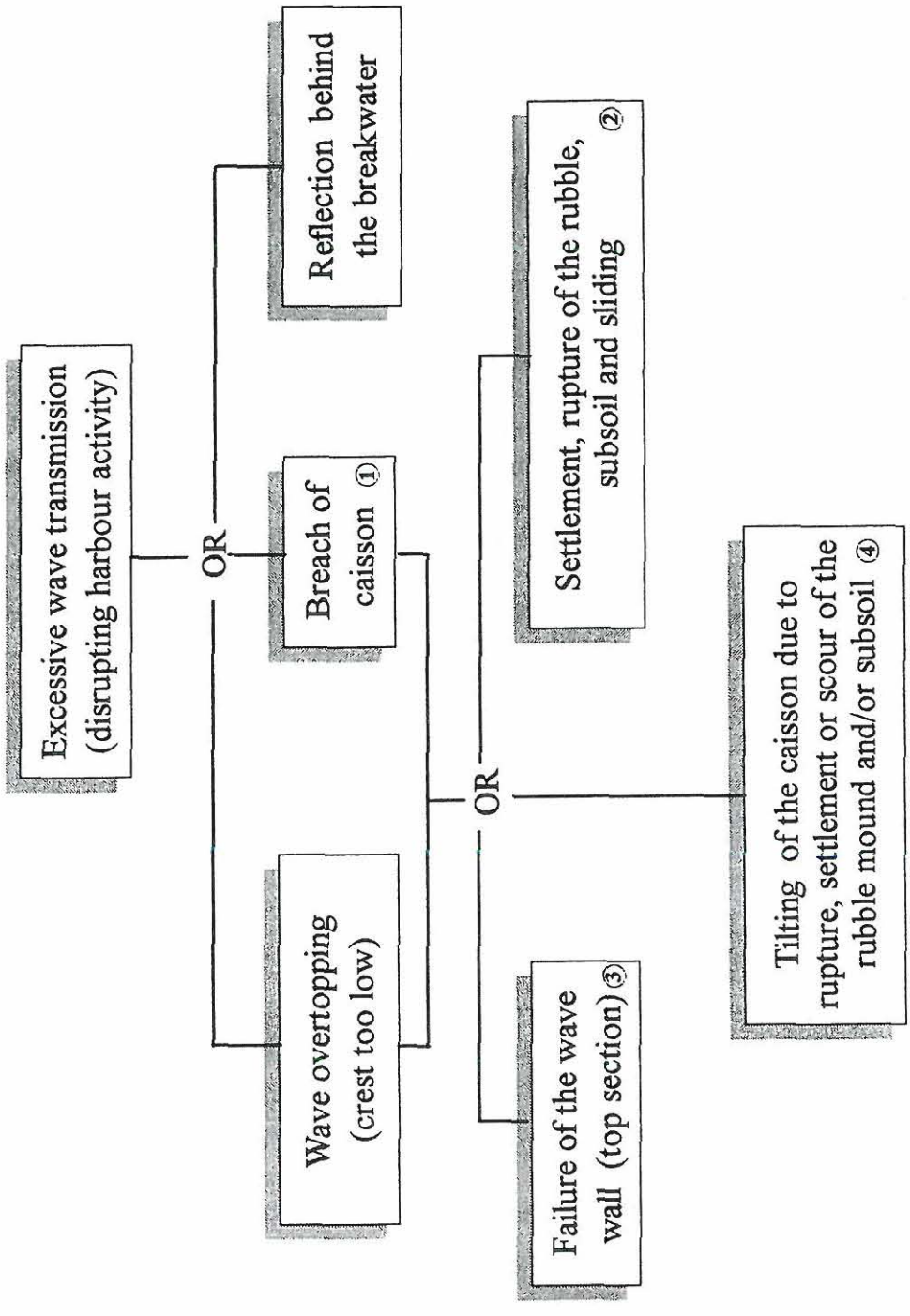

Figure 6.3: *Simplified fault tree for a conventional vertical breakwater.*

a) Rubble mound and sand subsoil

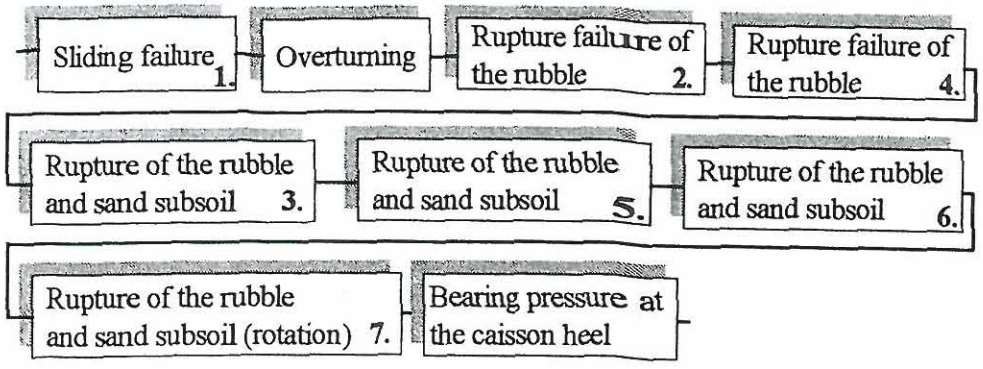

b) Rubble mound and clay subsoil

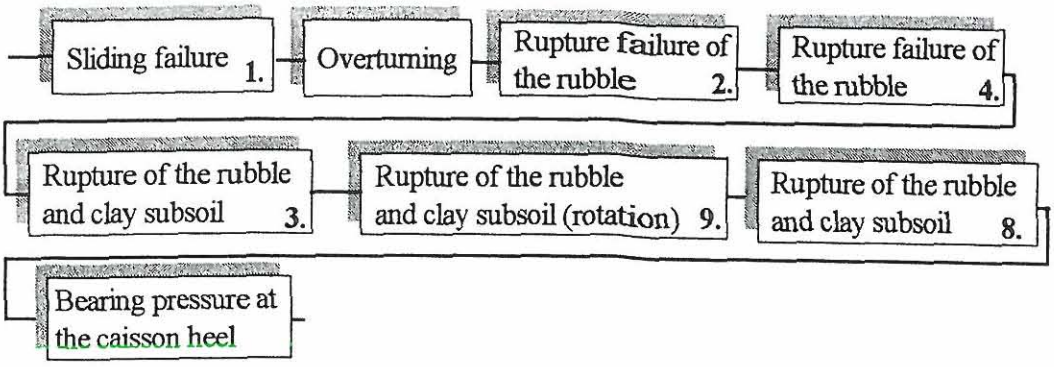

Figure 6.4: *Series system of failure modes for rupture failure of the sand and clay subsoil.*

The numbers denoted in the right hand corner of each flow box refers to the rupture failure modes cf. Figure 2.8 a and b. In design of vertical breakwaters, the main concern is sliding, rupture failure of the rubble mound, subsoil, overturning and bearing pressure. These sets of failure modes implies a series system of failure modes to be evaluated.

6.3 Limit state equations for vertical breakwaters

Failure modes of importance are sliding, rupture failure of the rubble mound, sand or clay subsoil and overturning. Overturning is often only relevant in the case of a vertical breakwater on a thin bedding layer and rock underlayer. The following rupture equations for the rubble mound and subsoil are derived and explained in depth in Appendix A. Only a simplified expression will be presented in the following to illustrate the limit state equations for design of vertical breakwaters.

The stochastic variables are explained in depth in section 6.1 and should be implemented in the limit state equations prior to a reliability evaluation.

In the following F_H is the horizontal wave force, F_H^p is the horizontal load (derived from wave pressure and pore pressure along the rupture boundary in the rubble mound), $F_G - F_U$ is the weight of the caisson considering buoyancy and wave induced uplift, φ_{d_1} is the modified friction angle of the rubble mound material, φ_{d_2} is the modified friction angle of the sand subsoil, ω_{iH} is the horizontal displacement vector for zones $i = 1...5$ in the kinematical admissible rupture mechanism, ω_{iV} is the vertical displacement vector for zones $i = 1...5$ in the kinematical admissible rupture mechanism, $(\gamma_s - \gamma_w)$ is the reduced specific weight of the rubble and B_z is the rupture width in the caisson or rubble mound.

The undrained shear strength of the clay subsoil is modelled as a log-Gaussian stochastic field $\{c_u(x,z)\}$ (cases 8, 9 and 10), see e.g. Keaveny et al. (1989) and Andersen et al. (1992). If only uncertainty related to c_u is considered and the correlation lengths for $\{c_u(x,z)\}$ are small compared to the integration intervals it follows from the central limit theorem that the total internal work can be approximated by a normal distributed stochastic variable W_I with a mean value μ_{W_I} and standard deviation σ_{W_I}, where W_I is the sum of internal energy dissipation in the clay subsoil.

6.3.1 Overturning

Stability against overturning exist when the horizontal moment M_H is equal to or less than the resultant vertical moment about the heel:

$$G_{over} = (M_G - M_U) - M_H \tag{6.14}$$

where M_G is the moment around the heel induced by the weight of the caisson, reduced for buoyancy and M_U is the moment around the heel and calculated from the uplift forces.

6.3.2 Sliding failure

Case 1

Sliding between the caisson base and rubble is described by the following limit state equation:

$$G_{1_b} = (F_G - F_U)\tan\mu - F_H \tag{6.15}$$

Rupture along the top of rubble mound is described by the following limit state equation:

$$G_{1_r} = (F_G - F_U)\tan\varphi_{d_1} - F_H \tag{6.16}$$

6.3.3 Rupture failure in the rubble mound

Case 2

Rupture takes place in the rubble mound, and is described by the following limit state equation:

$$\begin{aligned} G_2 &= F_{G_1}\frac{\sin(\varphi_{d_1} - \theta)}{\cos\varphi_{d_1}} - F_H^p\frac{\cos(\varphi_{d_1} - \theta)}{\cos\varphi_{d_1}} \\ &\quad +(F_G - F_U)\frac{\sin(\varphi_{d_1} - \theta)}{\cos\varphi_{d_1}} \end{aligned} \tag{6.17}$$

where F_{G_1} is the weight of the rupture zone in the rubble mound.

6.3.4 Rupture failure in the rubble mound and rupture between the rubble mound and clay or sand subsoil

Case 3

Rupture takes place in the rubble mound and along the base of the rubble mound. This failure mechanism is described by the following limit state equation for *clay* subsoil:

$$G_{3_c} = c_u(B_z + a + b - \frac{h_{II}}{\tan\varphi_{d_1}}) - F_H^p \tag{6.18}$$

where a is the width of the berm on the rear side and b is the width of the rubble slope mound on the rear side.

Rupture takes place in the rubble mound and along the base of the rubble mound. This failure mechanism is described by the following limit state equation for *sand* subsoil:

$$G_{3_s} = (F_G - F_U)\tan\varphi_{d_2} + F_{G_1}\tan\varphi_{d_2} - F_H^p \tag{6.19}$$

where F_{G_1} the weight of the rupture zone in the rubble mound.

6.3.5 Rupture in the rubble mound

Case 4

Rupture takes place in the rubble mound, and is described by the following limit state equation:

$$G_4 = -F_H^p\omega_{1H} - (F_G - F_U)\omega_{1V} - W_1 + W_2 + W_3 \tag{6.20}$$

where W_1,W_2,W_3 is the self weight of the rupture zones 1, 2 and 3 multiplied by the the corresponding displacement vector.

6.3.6 Rupture in the rubble mound and sand subsoil

Case 5

Rupture takes place in the rubble mound and in the sand subsoil. This failure mechanism is described by the following limit state equation:

$$G_5 = -F_H^p \omega_{1V} - (F_G - F_U)\omega_{1H} - W_1 - W_2 + W_3 + W_4 \quad (6.21)$$

where W_1,W_2,W_3, W_4 is the self weight of the rupture zones $1, 2, 3$ and 4 multiplied by the the corresponding displacement vector.

6.3.7 Rupture in the rubble mound and sand subsoil

Case 6

Rupture takes place in the rubble mound and in the sand subsoil. This failure mechanism is described by the following limit state equation:

$$G_6 = -F_H^p \omega_{1V} - (F_G - F_U)\omega_{1H} - W_1 - W_2 + W_3 + W_4 + W_5 \quad (6.22)$$

where W_1,W_2,W_3, W_4, W_5 is the self weight of rupture zones $1, 2, 3, 4$ and 5 multiplied by the the corresponding displacement vector.

6.3.8 Rupture in the rubble mound and sand subsoil-rotation mechanism

Case 7

Rupture takes place in the rubble mound and in the sand subsoil. This failure mechanism is described by the following limit state equation:

$$G_7 = W_3 + W_4 - W_1 - W_2 - W_E \quad (6.23)$$

where the external work W_E is the moment of the wave induced loads including horizontal pore pressure in the rubble mound and weight of the structure relative to the point of rotation, W_1,W_2,W_3, W_4 is the self weight of rupture zones $1, 2, 4$ and 4 multiplied by the the corresponding rotational displacement vector.

6.3.9 Rupture in the rubble mound and clay subsoil

Case 8 Rupture takes place in the rubble mound and in the clay subsoil. This failure mechanism is described by the following limit state equation:

$$G_8 = \mu_{W_I} + u_W \sigma_{W_I} - W_E = \sum_{i=1}^{7} E[W_{Ri}] + u_W \cdot \left(\sum_{i=1}^{7} \sum_{j=1}^{7} Cov[W_{Ri}, W_{Rj}] \right)^{\frac{1}{2}} - W_E \tag{6.24}$$

where u_W is a realization of a normal distributed stochastic variable U_W with a mean value 0 and a unit standard deviation, W_E is the external work from the wave induced loads including horizontal pore pressure in the rubble mound and weight of the structure and W_I is the sum of internal work along the rupture boundary and self weight of each rupture zone.

Further, as an exemplification of the rupture elements in equation (6.24), the mean value of W_4 is

$$E[W_4] = \delta R_1 \int_0^{R_1} \int_0^{\theta_1 + \frac{\pi}{4}} E[c_u(a, \theta_{1\,1})] d\theta_{1\,1} da \tag{6.25}$$

where $E[c_u(a, \theta_{1\,1})]$ is the expected value of the undrained shear strength of the clay c_u at positions described by a and $\theta_{1\,1}$. Both positions a and $\theta_{1\,1}$ can be described according to c_u at positions x (horizontal coordinate) and z (vertical coordinate). The variance of W_4 is given by:

$$Var[W_4] = \delta^2 R_1^2 \int_0^{R_1} \int_0^{\theta_1 + \frac{\pi}{4}} \int_0^{\theta_1 + \frac{\pi}{4}} \int_0^{R_1} Cov[c_u(a_1, \theta_{1\,1}), c_u(a_2, \theta_{1\,2})] d\theta_{1\,1}\, da_1\, d\theta_{1\,2}\, da_2 \tag{6.26}$$

where $Cov[c_u(a_1, \theta_{1\,1}), c_u(a_2, \theta_{1\,2})]$ is the covariance function of c_u at the positions corresponding to $(a_1, \theta_{1\,1})$ and $(a_2, \theta_{1\,2})$.

6.3.10 Rupture in the rubble mound and clay subsoil - rotation mechanism

Case 9

Rupture takes place in the rubble mound and in the clay subsoil. This failure mechanism is described by the following limit state equation:

$$\begin{aligned} G_{clay} &= \mu_{W_I} + u_W \sigma_{W_I} - W_{1,2} - W_E \\ &= E[W_3] + u_W \sigma_{W_3} - W_{1,2} - W_E \end{aligned} \tag{6.27}$$

where u_W is a realization of a normal distributed stochastic variable U_W with a mean value 0 and unit standard deviation, the external work W_E is the moment of the wave induced loads including horizontal pore pressure in the rubble mound and weight of the structure relative to the point of rotation, $W_{1,2}$ is the self weight of rupture zones 1 and 2 multiplied by the the corresponding rotational displacement vector.

Further, as exemplification of the elements in eq. (6.27), the mean value of W_3 is given by:

$$E[W_3] = \delta R_2^2 \int_0^{2\theta_2} E[c_u(a,\theta)] d\theta \; da \tag{6.28}$$

where $E[c_u(a,\theta)]$ is the expected value of the undrained shear strength of the clay c_u at positions described by a and θ. Both positions a and θ can be described according to c_u at positions x (horizontal coordinate) and z (vertical coordinate). The variance of W_3 is given by:

$$\begin{aligned} Var[W_3] \;\; &= \;\; \sigma_{W_3}^2 = \delta^2 R_2^4 \int_0^{2\theta_2} \\ &\int_0^{2\theta_2} Cov[c_u(a,\theta), c_u(a_1,\theta_1)] d\theta_1 \; da_1 \; d\theta \; da \end{aligned} \tag{6.29}$$

where $Cov[c_u(a,\theta), c_u(a_1,\theta_1)]$ is the covariance function of c_u at the positions corresponding to (a,θ) and (a_1,θ_1).

6.3.11 Rupture in the rubble mound and clay subsoil - rotation mechanism

Case 10

Rupture takes place in the rubble mound and in the clay subsoil. This failure mechanism is described by the following limit state equation:

$$G_{10} = \sum_{i=1}^{5} E[W_{Ri}] + \mu_W \cdot \left(\sum_{i=1}^{5} \sum_{j=1}^{5} Cov[W_{Ri}, W_{Rj}] \right)^{\frac{1}{2}} - M_o \qquad (6.30)$$

where u_W is a realization of a normal distributed stochastic variable U_W with a mean value 0 and a unit standard deviation, M_o is the moment of the wave induced loads including horizontal pore pressure in the rubble mound, weight of the structure and weight of the rubble in zone 1 relative to the point of rotation.

As an example the mean value W_5 is shown below:

$$E[W_5] = \delta \int_0^{R_1} \int_0^{R-a} E[c_u(a,l)] da \; dl \qquad (6.31)$$

where $E[c_u(a,l)]$ is the expected value of c_u at the position described by (a,l) and the variance of W_5 is given by:

$$V[W_5] = \delta \int_0^{R_1} \int_0^{R_1-a} \int_0^{R_1} \int_0^{R_1-a} Cov[c_u(a_1,l_1), c_u(a_2,l_2)] da_1 \; da_2 \; dl_1 \; dl_2 \qquad (6.32)$$

where $Cov[c_u(a_1,l_1), c_u(a_2,l_2)]$ is the covariance function of c_u at the positions corresponding to (a_1,l_1) and (a_2,l_2).

6.4 Vertical breakwater case studies

In this section the deterministic and probabilistic modelling of existing vertical breakwaters will be studied. The case studies are taken from PIANC PTC working group report 28 (1996). The case studies are implemented to illustrate reliability evaluation of existing vertical breakwaters.

6.4.1 East breakwater at Mutsu-Ogawara v- section

Deterministic safety analysis of the design cross section and the partly completed Mutsu-Ogawara v-section

Mutsu-Ogawara Port is situated at the North Eastern part of Japan. The v-section conventional vertical breakwater is part of a protective barrier outside the main port entrance. Sliding of 0.5 - 1 m occurred to the almost completed v-section on February 16 th - 17 th 1991. The concrete cap on top of the caisson was not yet cast leaving the crest 1.25 m below design crest level. The v-section is part of the North wing wave barrier and the cross section is shown in Figure 6.5. The significant wave height in deep water during the storm exceeded the actual design wave height, $H_{so} = 9.94\ m$ (storm of February 16 th - 17 th 1991), significant wave period $T_s = 13.4\ s$ and corresponding wave direction $\theta_I = 0.122\ rad.$

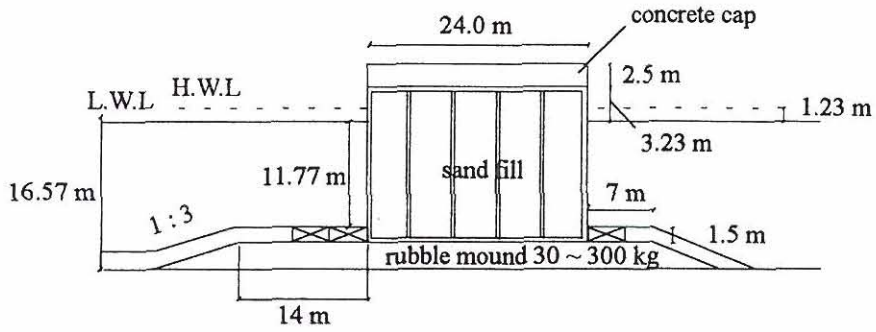

Figure 6.5: *Original cross section of v-section breakwater, Mutsu-Ogawara Port.*

For the deterministic design the following data are used: The effective friction angle of the rubble mound and subsoil are $\varphi_1' = 0.61\ rad$, $\varphi_2' = 0.52\ rad$ respectively. The average mass density in air of the caisson including concrete cap is $\rho_c = 2.2\ t/m^3$, sea bottom slope on the seaward side is $1/50\ -\ 1/60$, and the mass density of the seawater is taken as $\rho_{sea} = 1.03\ t/m^3$.

The significant wave height in deep water is $H_{so} = 8.0\ m$, the significant wave period is $T_s = 13\ s$, and the wave direction is head onto the structure, i.e. $\theta_I = 0\ rad$. The breaker heights in the surf zone are calculated by using the simplified formula for shoaling and wave breaking Goda (1975, 1985), and the wave induced loads are determined from Goda et al. (1972) and Takahashi (1994) for impulsive wave loads. The design water level is 1.23 m above L.W.L. (low water level). The design wave height $H_{design} = 13.2\ m$. In the deterministic design the following failure modes are considered: sliding, overturning, bearing pressure at the heel, and rupture in the rubble mound and subsoil are considered.

The stability factors and heel pressure for the completed and partly completed cross section is shown in Table 6.4

Failure modes	Completed Design cross section	Partly completed cross section
Sliding	1.40	1.17
Overturning	2.70	2.35
Sliding on rubble φ'_{d_1}	1.58	1.33
Rupture failure subsoil **5**	< 1	< 1
Rupture failure subsoil **6**	< 1	< 1
Bearing pressure	498 KN/m^2	472 KN/m^2

Table 6.4: Stability factors and heel pressure of Mutsu-Ogawara v-section

Sliding, overturning and sliding on rubble are denoted as safety factors, according to national codes. Rupture in the rubble mound and subsoil are denoted as limit states, such that the $g(B, h_{II}) > 0$, where B is the width of the caisson, and h_{II} is the height of the rubble mound. This means that when the value shown in the table is greater than 1, then the design is on the safe side.

Rupture in the rubble mound and subsoil is expected from foundation failure mode **5** and **6**. Rupture failure modes **1,2,4,7** are on the safe side, see Appendix A for the foundation failure modes. The Japanese design guide lines use a safety factor of 1.2 for sliding and overturning and bearing pressure in the range 400 KN/m^2 - 600 KN/m^2. It is clear from the deterministic evaluation that sliding will not occur independently for the completed design cross section or the partly completed cross section. The sliding failure observed by Hatachi (1994) may have been caused by rupture of the sand subsoil.

Reliability evaluation of the completed and partly completed Mutsu-Ogawara v-section

Characterization of the stochastic parameters have to be established prior to a reliability evaluation. The stochastic parameters used in this reliability evaluation are shown in Table 6.5. The deep water significant wave heights are calculated from the significant wave heights (breaker height considered) corresponding to the 10 and 50 years return period from Hitachi (1994): $H_{so}^{10} = 6.55\ m$ and $H_{so}^{50} = 8.0\ m$.

The significant wave heights in deep water are assumed to follow a Weibull distribution, see section 6.1.3 for further details of the Weibull distribution.The parameter values $\lambda = 1$, $k = 0.9$, $A = 0.71$ and $B = 4.75$ are found to fit the two given wave heights. It is assumed that the number of data per year is $N = 30$. The standard deviation of A and k can be estimated from Table 6.2. The observed significant wave height in deep water which caused the damage to the partly completed v-section is $H_{so} = 9.94\ m$ and will be regarded as a deterministic parameter in the reliability evaluation. The uncertainty of the soil parameters, angle of dilation, effective friction angle of the rubble mound and subsoil is assumed to have a coefficient of variation equal to 10%.

Results from the reliability evaluation are presented in Table 6.6 in terms of the reliability index β and the probability of failure P_f within an expected lifetime of 50 years.

The reliability levels are seen to be rather low compared with conventional civil engineering structures. But compared with observed failure rates for breakwaters the reliability levels are realistic. Also shown in Table 6.6 are sensitivities of β with respect to changes in ζ (tidal elevation) and B (width of the caisson). The deep water wave height for the completed and partly completed cross section is reduced by the breaker heights in the surf zone. This is the reason why the difference in probability of failure is small between the same failure mechanism.

It is clear from the reliability analysis of Mutsu-Ogawara v-section that the rupture failure in the rubble mound and sand subsoil (failure modes **5** and **6**) are dominant. In this case the sand subsoil is weak and the rubble mound is low ($h_{II} = 3m$), and this results in the rupture failure mechanisms in the sand subsoil are dominant. However, sliding was observed in the prototype. This indicates that rupture failure in the subsoil will probably cause sliding.

i	X_i	Definition	Mean μ_{X_i}	Standard deviation σ_{X_i}	$\frac{\sigma_{X_i}}{\mu_{X_i}}$	Distribution	Reference
1	H_{so}	Deep water significant wave height (m)				weibull	
2	k	Weibull parameter	0.90	0.18	0.20	normal	Burcharth (1994)
3	A	Weibull parameter	0.71	0.07	0.10	normal	Burcharth (1994)
4	ζ	Tidal elevation (m)				cosine	Takayama (1992)
5	U_{F_H}	Goda horizontal wave load	0.90	0.25	0.28	normal	Bruining (1994)
6	U_{F_U}	Goda wave induced uplift	0.77	0.25	0.32	normal	Bruining (1994)
7	U_{M_H}	Moment of horizontal force about the heel	0.81	0.41	0.51	normal	Bruining (1994)
8	U_{M_U}	Moment of uplift about the heel	0.72	0.37	0.51	normal	Bruining (1994)
9	ρ_c	Average density of caisson (t/m^3)	2.2	0.11	0.05	normal	Burcharth (1994)
10	ψ_1	Angle of dilation rubble mound (rad)	0.40	0.04	0.10	normal	
11	ψ_2	Angle of dilation sand subsoil (rad)	0.30	0.03	0.10	normal	
12	φ_1'	Effective friction angle of rubble mound (rad)	0.61	0.06	0.10	normal	
13	φ_2'	Effective friction angle of sand subsoil (rad)	0.52	0.05	0.10	normal	
14	Z	Uncertainty of the the rupture equations	1	0.10	0.10	normal	Sørensen C.S. (1993)
15	f	Friction factor	0.636	0.0954	0.15	normal	Takayama (1992)
16	H_B/h_b	Wave breaking/water depth	1.00	0.06	0.06	normal	Goda (1994a)

Table 6.5: Characterization of the stochastic parameters for the Mutsu-Ogawara v-section

Failure mode	Completed cross section				Partly completed cross section			
	β	P_f	$d\beta/dB$	$d\beta/d\zeta$	β	P_f	$d\beta/dB$	$d\beta/d\zeta$
Sliding (friction coeff.)	1.948	0.026	0.139	-0.060	1.795	0.036	0.130	-0.103
Sliding on rubble φ'_{d_1} **1**	2.567	0.005	0.160	-0.155	2.154	0.016	0.149	-0.140
Overturning	3.905	0.00005	0.272	-0.225	3.611	0.0002	0.228	-0.216
Rupture failure rubble **2**	1.594	0.055	0.181	-0.058	1.430	0.076	0.169	-0.095
Rupture failure rubble **3**	2.910	0.018	0.186	-0.170	2.675	0.004	0.169	-0.154
Rupture failure rubble **4**	1.342	0.090	0.207	-0.015	1.347	0.089	0.204	-0.047
Rupture failure subsoil **5**	0.662	0.254	0.230	-0.015	0.565	0.286	0.220	-0.018
Rupture failure subsoil **6**	0.638	0.262	0.228	-0.014	0.540	0.295	0.218	-0.017
Rupture failure subsoil **7**	1.86	0.031	0.197	-0.002	1.567	0.059	0.232	-0.002

Table 6.6: Reliability index and probability of failure for the completed and partly completed Mutsu-Ogawara v-section,

Completed cross section	failure mode 4 rubble mound	failure mode 5 rubble & subsoil	failure mode 6 rubble & subsoil
reliability index β	1.342	0.662	0.638
failure probability P_f	0.090	0.254	0.262
$\alpha^2_{H_{s_o}}$	0.022	0.008	0.008
α^2_k	0.006	0.002	0.002
α^2_A	0.014	0.005	0.005
α^2_ζ	0.028	0.038	0.037
$\alpha^2_{\rho_c}$	0.016	0.014	0.013
$\alpha^2_{U_{F_H}}$	0.446	0.538	0.542
$\alpha^2_{U_{F_U}}$	0.037	0.042	0.041
$\alpha^2_{U_{M_H}}$	0.036	0.045	0.044
$\alpha^2_{U_{M_U}}$	0.021	0.026	0.025
$\alpha^2_{\psi'_1}$	0.002	0.000	0.000
$\alpha^2_{\varphi'_1}$	0.336	0.038	0.037
$\alpha^2_{\psi'_2}$		0.001	0.001
$\alpha^2_{\varphi'_2}$		0.203	0.203
$\alpha^2_{Z_{rup}}$	0.001	0.001	0.001
$\alpha^2_{H_B/h_b}$	0.033	0.039	0.040
Σ	1.00	1.00	1.00

Table 6.7: Failure probabilities and relative influence of the stochastic parameters for rupture failure in the rubble mound alone, and rubble mound and sand subsoil(failure modes **4**, **5** and **6** designed v-section)

The α^2-sensitivity values related to the horizontal induced wave load, reduced friction angle of the rubble mound and subsoil are dominating, cf. Table 6.7 where examples of rupture in the rubble alone, and rubble and subsoil are presented for the designed v-section. The deep water wave height is reduced due to breaking in the surf zone, therefore the sensitivity of the design wave height is low even when considering the uncertainty of the wave breaking equation.

6.4.2 West Breakwater at Niigata East Port (I2 - section)

Deterministic safety analysis of the design cross section and the partly completed Niigata East Port (I2 - section)

Niigata port is situated in central Japan facing the sea of Japan where the West Breakwater is the main breakwater protecting the outer harbour. Damage occurred at the head of the West Breakwater during construction in 1976, where the design wave height was exceeded by an extreme wave causing extensive sliding of a large number of composite breakwater sections. Three main composite cross sections were identified, from the severe storm, (I2, J1, and J2) which have similar cross sections, therefore only the I2 cross section will be investigated in detail and reference is given to PIANC PTC working group report 28 (1996), for the rest of the cross sections. The I2 cross section is presented below in Figure 6.6

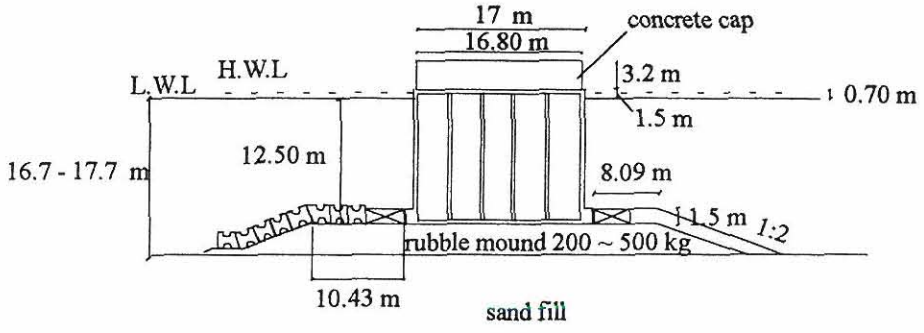

Figure 6.6: *Original cross section of west breakwater, Niigata East Port (I2).*

For the deterministic design the following data are used: The effective friction angle of the rubble mound is assumed to be $\varphi_1' = 0.61\ rad$ and the sand subsoil to be $\varphi_2' = 0.52\ rad$, the average density of the caisson including concrete cap is $\rho_c = 2.175\ t/m^3$, sea bottom slope on the seaward side is 1/50, density of the sea is taken as $\rho_{sea} = 1.03\ t/m^3$. The significant wave height for the I2 - section is $H_s = 7.0\ m$, significant wave period is $T_s = 13\ s$ and incident waves are at an angle of $\theta_I = 0.38\ rad$. Design water level is taken as $0.70\ m$ above L.W.L.

The damaging waves in 1976 that hit the structure were measured to be $H_{so} = 7.68\ m$ after considering refraction, the peak period was 13.55 seconds, tidal elevation was $\zeta = 0.7\ m$, and the waves were head on, i.e. $\theta_I = 0$.

The breaker heights in the surf zone are calculated by using the simplified formula for shoaling and wave breaking Goda (1975, 1985), and the wave induced loads are determined from Goda et al. (1972) and Takahashi (1994) for impulsive wave loads.

In the deterministic design sliding, overturning, bearing pressure at the heel, and rupture failure rubble mound and sand subsoil is considered. The results are presented in Figure 6.8.

Failure modes	Design wave conditions	Damaging wave conditions
Sliding	1.03	0.90
Overturning	1.55	1.35
Sliding on rubble φ'_{d_1}	1.16	1.02
Rupture failure subsoil **2**	$\ll 1$	$\ll 1$
Rupture failure subsoil **3**	> 1	> 1
Rupture failure subsoil **4**	$\ll 1$	$\ll 1$
Rupture failure subsoil **5**	$\ll 1$	$\ll 1$
Rupture failure subsoil **6**	$\ll 1$	$\ll 1$
Rupture failure subsoil **7**	$\gg 1$	$\gg 1$
Bearing pressure	777 KN/m^2	974 KN/m^2

Table 6.8: Stability factors and heel pressure of West Breakwater Niigata East Port, I2 - section

It is clear that sliding is the most probable cause of failure when the storm damaged the structure in 1976. This was also observed after the storm. It should be noted that the heel pressure has been exceeded for both design and damaging wave conditions as the maximum allowable pressure is 600 KN/m^2. It is also interesting to note that all rupture failures cause instability except sliding on rubble, and rupture failure in the subsoil, failure modes **3** and **7**.

Reliability evaluation of West Breakwater Niigata East Port (I2)

Characterization of the stochastic parameters have to be established prior to a reliability evaluation. The stochastic parameters used in this reliability evaluation are shown in Table 6.9. It is assumed that the significant wave height in deep water is modelled by a a Weibull distribution. The deep water significant wave height is calculated from the significant wave height for design (breaker height considered including shoaling). The significant wave height in deep water $H_s^{50} = 7.5\ m$ is modelled by a Weibull distribution, and assumed to have parameter values $\lambda = 1$, $k = 1.5$, $A = 2.0$ and $B = 2.54$, see section 6.1.3. It is assumed that the number of data per year is $N = 30$, to calculate the standard deviations of A and k. The observed significant wave height in deep water which caused the damage to the partly completed structure is $H_{so} = 7.68\ m$, and will be regarded as a deterministic value in the reliability evaluation.

The uncertainty of the soil parameters, angle of dilation, effective friction angle of the rubble mound, and sand subsoil are assumed to have a coefficient of variation equal to 10%.

Results from the reliability evaluation are presented in Table 6.10 in terms of the reliability index β and the probability of failure P_f within an expected lifetime of 50 years.

The reliability levels are seen to be rather low compared with conventional civil engineering structures. But compared with observed failure rates for breakwaters the reliability levels are realistic. Also shown in Table 6.10 are sensitivities of β with respect to changes in ζ (tidal elevation) and B (width of the caisson). The deep water wave height for the completed and partly completed cross section is reduced by the breaker heights in the surf zone. This is the reason why the difference in probability of failure is small between the same failure mechanisms.

It is clear from the reliability analysis of I2 section that the rupture failure in the rubble mound and subsoil (failure modes **5** and **6**) are dominant. However, sliding was observed in prototype. This indicates that rupture failure in the subsoil will probably cause sliding.

The α^2-sensitivity values related to the horizontal wave induced load, and friction coefficient, Takayama (1992) are dominant in the case of sliding, cf. Table 6.11. For the failure in the rubble mound alone (failure mode **4**) the sensitivity values of the design wave height, horizontal wave induced load and the effective friction angle of the rubble mound are more pronounced. In the case of failure mode **6** the sensitivity parameters for the wave height and wave induced horizontal load are dominant. It should be noted that the design wave height in deep water has little influence on the reliability of the breakwater for sliding and failure mode **4**, due to wave breaking in the surf zone, except for failure in the sand subsoil (failure mode **6**), where the wave height parameters have a large influence on the calculated reliability index.

i	X_i	Definition	Mean μ_{X_i}	Standard deviation σ_{X_i}	$\frac{\sigma_{X_i}}{\mu_{X_i}}$	Distribution	Reference
1	H_{so}	Deep water significant wave height (m)				weibull	Burcharth (1992)
2	k	Weibull parameter	1.50	0.33	0.22	normal	Burcharth (1994)
3	A	Weibull parameter	2.0	0.20	0.10	normal	Burcharth (1994)
4	ζ	Tidal elevation (m)				cosine	Takayama (1992)
5	ρ_c	Average density of caisson (t/m^3)	2.23	0.11	0.05	normal	Burcharth (1994)
6	F_{H_s}	Uncertainty of the measured wave data	1.00	0.05	0.05	normal	Burcharth (1992a)
7	U_{F_H}	Goda horizontal wave load	0.90	0.25	0.28	normal	Bruining (1994)
8	U_{F_U}	Goda wave induced uplift	0.77	0.25	0.32	normal	Bruining (1994)
9	U_{M_H}	Moment of horizontal force about the heel	0.81	0.41	0.51	normal	Bruining (1994)
10	U_{M_U}	Moment of uplift about the heel	0.72	0.37	0.51	normal	Bruining (1994)
11	ψ_1	Angle of dilation rubble mound (rad)	0.40	0.04	0.10	normal	
12	φ_1'	Effective friction angle of rubble mound (rad)	0.61	0.06	0.10	normal	
13	ψ_2	Angle of dilation sand subsoil (rad)	0.30	0.03	0.10	normal	
14	φ_2'	Effective friction angle of the sand subsoil (rad)	0.52	0.05	0.10	normal	
15	Z	Uncertainty of the rupture equations	1	0.10	0.10	normal	Sørensen C.S. (1993)
16	f	Friction factor	0.636	0.0954	0.15	normal	Takayama (1992)
17	H_B/h_b	Wave breaking/water depth	1.00	0.06	0.06	normal	Goda (1994a)

Table 6.9: Characterization of the stochastic parameters for the West Breakwater Niigata East Port -section I(2)

Failure mode	Design				Partly completed cross section			
	β	P_f	$d\beta/dB$	$d\beta/d\zeta$	β	P_f	$d\beta/dB$	$d\beta/d\zeta$
Sliding (friction coeff.)	1.855	0.032	0.140	-0.027	1.91	0.028	0.141	-0.003
Sliding on rubble φ'_{d_1} **1**	2.141	0.016	0.167	-0.046	2.36	0.009	0.170	-0.004
Overturning	3.57	0.0002	0.284	-0.129	4.11	0.00002	0.250	-0.010
Rupture failure rubble **2**	1.486	0.069	0.139	0.003	1.46	0.072	0.190	-0.005
Rupture failure rubble **3**	2.83	0.002	0.194	-0.0165	3.22	0.0001	0.203	-0.014
Rupture failure rubble **4**	1.631	0.051	0.175	0.006	1.58	0.057	0.223	-0.011
Rupture failure subsoil **5**	0.871	0.192	0.171	-0.005	0.47	0.318	0.223	-0.005
Rupture failure subsoil **6**	0.865	0.194	0.169	-0.005	0.46	0.321	0.221	-0.004
Rupture failure subsoil **7**	2.21	0.014	0.164	0.0003	2.25	0.012	0.163	0.0002

Table 6.10: Probability of failure for the West Breakwater Niigata East Port -section I(2), design wave conditions and for damaging wave conditions during the storm of 1976

Designed cross section	Sliding	failure mode **4** rubble mound	failure mode **6** rubble & subsoil
reliability index β	1.855	1.631	0.875
failure probability P_f	0.032	0.051	0.194
$\alpha^2_{H_{s0}}$	0.047	0.136	0.276
α^2_k	0.012	0.032	0.070
α^2_A	0.012	0.038	0.073
α^2_ζ	0.015	0.001	0.004
$\alpha^2_{\rho_c}$	0.101	0.018	0.009
$\alpha^2_{F_{H_s}}$	0.005	0.014	0.028
$\alpha^2_{U_{F_H}}$	0.390	0.360	0.354
$\alpha^2_{U_{F_U}}$	0.031	0.046	0.029
$\alpha^2_{U_{M_H}}$		0.030	0.023
$\alpha^2_{U_{M_U}}$		0.024	0.018
$\alpha^2_{\psi'_1}$		0.001	0.001
$\alpha^2_{\varphi'_1}$		0.290	0.030
$\alpha^2_{\psi'_2}$			0.001
$\alpha^2_{\varphi'_2}$			0.086
$\alpha^2_{Z_{rup}}$		0.000	0.000
α^2_f	0.349		
$\alpha^2_{H_B/h_b}$	0.034	0.008	0.000
Σ	1.00	1.00	1.00

Table 6.11: Failure probabilities and relative influence of the stochastic parameters for sliding, rupture failure in the rubble mound, and rubble mound and sand subsoil (failure modes sliding, **4** and **6** for designed wave conditions)

6.4.3 Second West Breakwater at Niigata West Port

Deterministic safety analysis of the design cross section and the partly completed Second West Breakwater at Niigata West Port

Niigata West Port is situated in central Japan facing the sea of Japan. The construction of the Second West Breakwater was initiated in 1973 and partly completed in 1976 when high waves damaged numerous number of caissons. After the storm in 1976, settlement, sliding and scouring which caused seaward tilting was observed. The weak subsoil was the main reason for settlement reducing the dry weight of the caisson causing an increase possibility of sliding.

The concrete cap on top of the caisson was not yet cast leaving the crest 1.00 m below design crest level at the time of damage. The significant wave height in deep water during the storm exceeded design wave height, $H_{so} = 7.685\ m$, significant wave period $T_s = 13.60\ s$ and corresponding wave direction $\theta_I = 0\ rad$ i.e head on waves. The main geometrical parameters for the standard B - type is shown in figure6.7

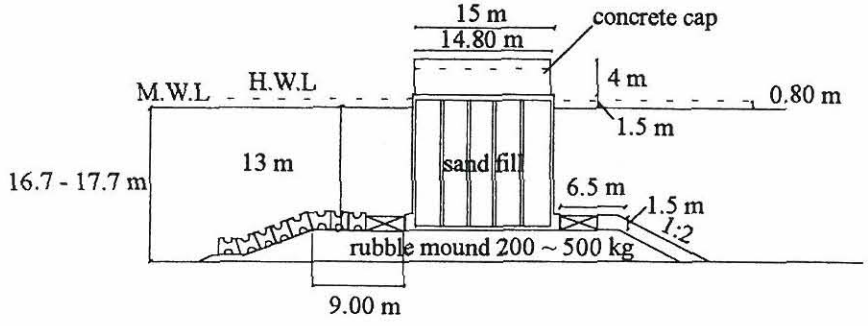

Figure 6.7: *Original cross section of Second West Breakwater (B-type cross section), Niigata West Port.*

For the deterministic design the following data are used: The effective friction angle of the rubble mound and subsoil are assumed to be $\varphi_1' = 0.61\ rad$, $\varphi_2' = 0.52\ rad$ respectively. The average mass density in air of the caisson including concrete cap is $\rho_c = 2.23\ t/m^3$, sea bottom slope on the seaward side is 1/100, and the mass density of the seawater is taken as $\rho_{sea} = 1.03\ t/m^3$. The significant wave height in deep water is $H_{so} = 7.63\ m$, the significant wave period is $T_s = 13.05\ s$, and the incident wave direction is $\theta_I = 0.54\ rad$ and $\theta_I = 0\ rad$. The breaker heights in the surf zone are calculated by using the simplified formula for shoaling and wave breaking Goda (1975, 1985), and the wave induced loads are determined from Goda et al. (1972) and Takahashi (1994) for impulsive wave loads. The design water level is 0.80 m above M.W.L. The design wave height $H_{design} = 12.59\ m$.

In the deterministic design the following failure modes are considered: sliding, overturning, bearing pressure at the heel, and rupture in the rubble mound and subsoil. The stability factors and heel pressure for the completed and partly completed cross section is shown in Table 6.4.3

The stability of the B-type cross section at the two different water levels are unstable as sliding is expected, bearing pressure at the heel exceeds the upper limit of 600 KM/m^3 and rupture failure is expected in the rubble mound and subsoil. The following vertical breakwater is not expected to withhold the design wave load or the damaging wave load.

		Design (crest height is 5.5 m above mean water level)									
Wave direction *rad*	Water Depth (m)	Sliding	Over-turning	Sliding on rubble φ'_{d_1}	Rupture failure rubble **2**	Rupture failure rubble **3**	Rupture failure rubble **4**	Rupture failure subsoil **5**	Rupture failure subsoil **6**	Rupture failure subsoil **7**	Bearing pressure KN/m^2
0	16.7	0.94	1.17	1.06	$\ll 1$	>1	$\ll 1$	$\ll 1$	$\ll 1$	$\gg 1$	2122
	17.7	0.94	1.18	1.06	$\ll 1$	>1	$\ll 1$	$\ll 1$	$\ll 1$	$\gg 1$	2117
0.54	16.7	1.06	1.30	1.20	$\ll 1$	>1	$\ll 1$	$\ll 1$	$\ll 1$	$\gg 1$	1259
	17.7	1.06	1.34	1.20	$\ll 1$	>1	$\ll 1$	$\ll 1$	$\ll 1$	$\gg 1$	1246
		Partly completed cross section (*crest height is 4.5 m above M.W.L.*									
0	16.7	0.89	1.16	1.01	$\ll 1$	>1	$\ll 1$	$\ll 1$	$\ll 1$	$\gg 1$	2089
	17.7	0.88	1.14	0.99	$\ll 1$	>1	$\ll 1$	$\ll 1$	$\ll 1$	$\gg 1$	2318
0.54	16.7	1.01	1.32	1.14	$\ll 1$	>1	$\ll 1$	$\ll 1$	$\ll 1$	$\gg 1$	1189
	17.7	1.00	1.31	1.13	$\ll 1$	>1	$\ll 1$	$\ll 1$	$\ll 1$	$\gg 1$	1234

Table 6.4.3 Overall safety factors for the Second West Breakwater Niigata West Port, for a completed and partly completed structure

i	X_i	Definition	Mean μ_{X_i}	Standard deviation σ_{X_i}	$\frac{\sigma_{X_i}}{\mu_{X_i}}$	Distribution	Reference
1	H_{so}	Deep water significant wave height (m)				weibull	Burcharth (1992)
2	k	Weibull parameter	1.50	0.33	0.22	normal	Burcharth (1994)
3	A	Weibull parameter	2.0	0.20	0.10	normal	Burcharth (1994)
4	ζ	Tidal elevation (m)				cosine	Takayama (1992)
5	ρ_c	Average density of caisson (t/m^3)	2.23	0.11	0.05	normal	Burcharth (1994)
6	F_{H_s}	Uncertainty of the measured wave data	1.00	0.05	0.05	normal	Burcharth (1992a)
7	U_{F_H}	Goda horizontal wave load	0.90	0.25	0.28	normal	Bruining (1994)
8	U_{F_U}	Goda wave induced uplift	0.77	0.25	0.32	normal	Bruining (1994)
9	U_{M_H}	Moment of horizontal force about the heel	0.81	0.41	0.51	normal	Bruining (1994)
10	U_{M_U}	Moment of uplift about the heel	0.72	0.37	0.51	normal	Bruining (1994)
11	ψ_1	Angle of dilation rubble mound (rad)	0.40	0.04	0.10	normal	
12	φ_1'	Effective friction angle of rubble mound (rad)	0.61	0.06	0.10	normal	
13	ψ_2	Angle of dilation sand subsoil (rad)	0.30	0.03	0.10	normal	
14	φ_2'	Effective friction angle of the sand subsoil (rad)	0.52	0.05	0.10	normal	
15	Z	Uncertainty of the rupture equations	1	0.10	0.10	normal	Sørensen C.S. (1993)
16	f	Friction factor	0.636	0.0954	0.15	normal	Takayama (1992)

Table 6.12: Characterization of the stochastic parameters for the Second West Breakwater Niigata West Port

Reliability evaluation of the completed and partly completed Second West Breakwater - B type section

Characterization of the stochastic parameters have to be established prior to a reliability evaluation. The stochastic parameters used in this reliability evaluation are shown in Table 6.12. It is assumed that the significant wave height in deep water is modelled by a a Weibull distribution. The deep water significant wave height is calculated from the significant wave height for design (breaker height considered including shoaling). The significant wave height in deep water is modelled by a Weibull distribution and is assumed to have parameter values $\lambda = 1$, $k = 1.5$, $A = 2.0$ and $B = 2.665$ (based on the design wave height with a 50 year return period). It is assumed that the number of data per year is $N = 30$, to calculate the standard deviation of A and k. The observed significant wave height in deep water which caused the damage to the partly completed structure is $H_{so} = 7.685\ m$, and the tidal elevation $\zeta = 0.7\ m$ is assumed to follow a cosine distribution Takayama (1992). The incident wave angle is taken as $\theta_I = 0\ (rad)$ (head on waves). The uncertainty of the soil parameters, angle of dilation, effective friction angle of the rubble mound and sand subsoil are assumed to have a coefficient of variation equal to 10%.

Results from the reliability evaluation are presented in Table 6.13 in terms of reliability index β and the probability of failure P_f within a 50 year return period. Also the sensitivity of β with respect to changes in B (width of the caisson) are shown in Table 6.13.

	Completed cross section			Partly completed cross section		
Failure mode	β	P_f	$d\beta/dB$	β	P_f	$d\beta/dB$
Sliding (friction coeff.)	0.229	0.410	0.204	-0.424	0.664	0.186
Sliding on rubble φ'_{d_1} **1**	1.074	0.141	0.242	0.311	0.378	0.221
Overturning	1.375	0.085	0.386	0.869	0.192	0.344
Rupture failure rubble **2**	-0.160	0.563	0.386	-0.688	0.754	0.200
Rupture failure rubble **3**	1.443	0.068	0.290	0.762	0.223	0.204
Rupture failure rubble **4**	-0.421	0.663	0.237	-0.762	0.760	0.208
Rupture failure subsoil **5**	-0.678	0.751	0.183	-0.947	0.828	0.152
Rupture failure subsoil **6**	-0.678	0.751	0.183	-0.947	0.828	0.152
Rupture failure subsoil **7**	-0.079	0.531	0.230	0.306	0.380	0.225

Table 6.13: Probability of failure for the Second West Breakwater, Niigata West Port B-type section, design wave conditions, and damaging wave conditions during the storm of 1976

The reliability indices are very low, so therefore the B -type breakwater is expected to fail under the design wave loads and the damaging wave loads.

It is clear from the reliability analysis of the B type section that the rupture failure in the rubble mound and sand subsoil (failure modes **5**and **6**) are dominant. However, sliding was observed in prototype. This indicates that rupture failure in the subsoil will probably cause sliding.

The α^2-sensitivity values related to the horizontal wave induced load and friction coefficient Takayama (1992) are dominant in the case of sliding, cf. Table 6.14. For the failure in the rubble mound alone (failure mode **4**) and rupture failure of the rubble mound and sand subsoil, failure mode **6** the sensitivity parameter related to the wave induced horizontal load is very dominant.

Designed cross section	Sliding	failure mode **4** rubble mound	failure mode **6** rubble & subsoil
reliability index β	1.074	-0.424	-0.080
failure probability P_f	0.141	0.664	0.752
$\alpha^2_{H_{s_o}}$	0.000	0.000	0.000
α^2_k	0.000	0.000	0.000
α^2_A	0.000	0.000	0.000
α^2_ζ	0.040	0.000	0.000
$\alpha^2_{\rho_c}$	0.068	0.010	0.000
$\alpha^2_{F_{H_s}}$	0.000	0.000	0.000
$\alpha^2_{U_{F_H}}$	0.656	0.758	0.863
$\alpha^2_{U_{F_U}}$	0.018	0.018	0.010
$\alpha^2_{U_{M_H}}$		0.085	0.054
$\alpha^2_{U_{M_U}}$		0.009	0.006
$\alpha^2_{\psi'_1}$		0.001	0.000
$\alpha^2_{\varphi'_1}$		0.120	0.033
$\alpha^2_{\psi'_2}$			0.000
$\alpha^2_{\varphi'_2}$			0.031
$\alpha^2_{Z_{rup}}$			
α^2_f	0.218		
$\alpha^2_{H_B/h_b}$	0.034	0.008	0.000
Σ	1.00	1.00	1.00

Table 6.14: Failure probabilities and relative influence of the stochastic parameters for sliding and rupture failure in the rubble mound, and rubble mound and sand subsoil (failure modes **4** and **6**) for the designed B type section, and design wave conditions)

6.5 Reliability evaluation of a vertical breakwater on a low and high rubble mound

Vertical breakwaters are usually constructed in shallow and deep water and this often results in vertical breakwaters placed on a low and high rubble mound. An example will be presented in the following where a vertical breakwater is placed on a low and high rubble mound, using the same wave loading, geotechnical parameters and density of the caisson including a concrete cap. Thereafter the probability of failure as a function of the caisson width B will be presented to evaluate the sensitivity of sliding and rupture failure of the rubble mound and sand subsoil.

The example of a caisson on a low rubble mound and high rubble mound is shown in Figure 6.8 a,b.

a) Vertical breakwater on a low rubble mound

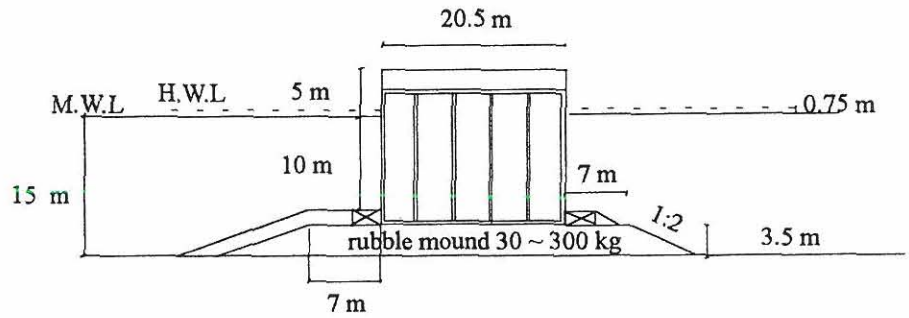

b) Vertical breakwater on a high rubble mound

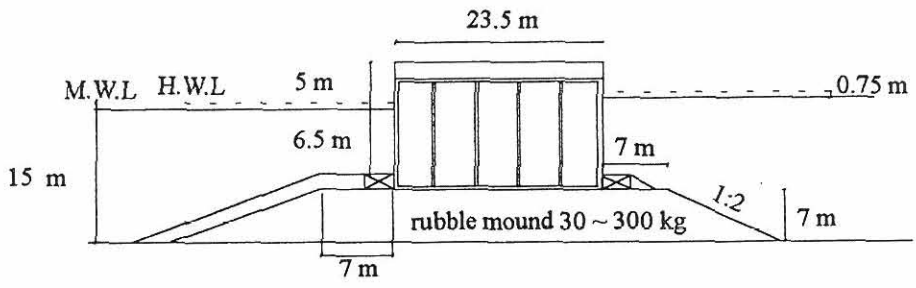

Figure 6.8: *Example of a vertical breakwater on a low and high rubble mound.*

i	X_i	Definition	Mean μ_{X_i}	Standard deviation σ_{X_i}	$\frac{\sigma_{X_i}}{\mu_{X_i}}$	Distribution	Reference
1	H_{so}	Deep water significant wave height (m)				weibull	
2	k	Weibull parameter	2.00	0.18	0.09	normal	Burcharth (1994)
3	A	Weibull parameter	2.50	0.25	0.10	normal	Burcharth (1994)
4	ζ	Tidal elevation wave height (m)				cosine	Takayama (1992)
5	U_{F_H}	Goda horizontal wave load	0.90	0.25	0.28	normal	Bruining (1994)
6	U_{F_U}	Goda wave induced uplift	0.77	0.25	0.32	normal	Bruining (1994)
7	U_{M_H}	Moment of horizontal force about the heel	0.81	0.41	0.51	normal	Bruining (1994)
8	U_{M_U}	Moment of uplift about the heel	0.72	0.37	0.51	normal	Bruining (1994)
9	ρ_c	Average density of caisson (t/m^3)	2.2	0.11	0.05	normal	Burcharth (1994)
10	ψ_1	Angle of dilation rubble mound (rad)	0.40	0.04	0.10	normal	
11	ψ_2	Angle of dilation sand subsoil (rad)	0.30	0.03	0.10	normal	
12	φ_1'	Effective friction angle of rubble mound (rad)	0.61	0.061	0.10	normal	
13	φ_2'	Effective friction angle of sand subsoil (rad)	0.57	0.057	0.10	normal	
14	Z	Uncertainty of the the rupture equations	1	0.10	0.10	normal	Sørensen C.S. (1993)
15	f	Friction factor	0.636	0.0954	0.15	normal	Takayama (1992)
16	H_B/h_b	Wave breaking/water depth	1.00	0.06	0.06	normal	Goda (1994a)

Table 6.15: Characterization of the stochastic parameters for a vertical breakwater on a high and low rubble mound

Characterization of the stochastic parameters for the reliability evaluation of a vertical breakwater on a low and high rubble mound

Characterization of the stochastic parameters have to be established prior to a reliability evaluation. The stochastic parameters used in this reliability evaluation are shown in Table 6.15. The deep water significant wave height is modelled by a a Weibull distribution. The deepwater water significant wave height $H_{so}^{50} = 6.5\ m$ and $\lambda = 1$, the exponent $k = 2.0$, $A = 2.5$ and $B = 1.55$ in the Weibull distribution. The number of data available for analysis is assumed to be $N = 30$. This is used to calculate the standard deviation of A and k. The uncertainty of the soil parameters, angle of dilation, effective friction angle of the rubble mound and subsoil is assumed to have a variation coefficient of 10%. The rest of the deterministic parameters are given section 2.4 for this example. Results from the reliability evaluation are presented in Figure 6.9

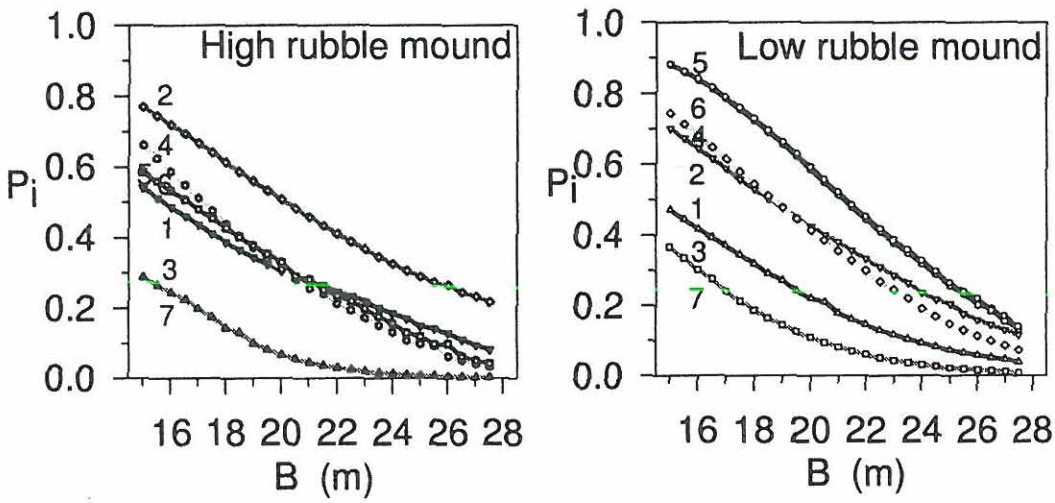

Figure 6.9: *Effect of the width B of the caisson on the probability of failure P_i within a return period of 50 years, considering a low and high rubble mound on a sand subsoil.*

Numbers in the graphs refer to type of foundation failure mechanisms. Rupture failure in the high rubble mound is more pronounced than in the sand subsoil. Here rupture failure mechanisms 2 and 4 in the rubble mound are dominant. In the case of the low rubble mound, rupture failure in the sand subsoil is dominant (rupture mechanism in the rubble mound and sand subsoil 5 and 6), but this is when the sand subsoil is comparatively weaker than the rubble mound. An increase in the caisson width indicates that the low rubble mound will be favored in design as this structure has a lower probability of failure during the expected lifetime of the structure.

7

Reliability based design of crown walls

The following chapter is devoted to characterization of the stochastic parameters for crown walls, limit state formulation of the bearing capacity including sliding, and an illustrative example is given.

7.1 Characterization of the stochastic parameters variables for the foundation stability crown walls

Typical parameters of importance are described in the following and should be used in the reliability evaluation of the crown wall geotechnical failure modes. The parameters should at least be defined by a mean value and a standard deviation (normal distributed) if the actual distribution is unknown. Some of the parameters have very small variational coefficients and can be regarded as deterministic parameters. This holds for all the geometrical parameters applied in the forthcoming reliability evaluation.

7.1.1 Modelling uncertainty of the design equations (run up and wave loads based on run up)

The uncertainty of the run up equation is given in section 3.1, and based on the work by van der Meer et al.(1991).

The uncertainty of the wave loading based on run up is given in section 3.1, and based on the work by Pedersen (1996).

7.1.2 Modelling uncertainty of the design wave parameters

Statistically variability of wave parameters i.e. significant wave height H_s and peak wave period T_p are the most significant parameters in breakwater design. For design purposes the 50 year return wave heights are used to design the breakwater. Modelling the wave height in deepwater is presented in subsection 6.1.3.

The extreme wave heights to be used in design of the crown walls is shown in Table 7.1.

	k	A	B	λ	H_{so}^{50}
BILBAO	1.39	1.06	4.90	4.17	8.44
FALLORNICA	1.14	0.58	2.69	5.94	5.36

Table 7.1: *Original wave data modelled by a Weibull distribution*

The *significant wave height* H_s to be applied in the run-up formulae, equation (3.2), are in case of no surf zone in front of the structure taken as H_{so} (deep water value corresponding to the 0.1% exceedence value for Rayleigh distributed wave heights, i.e. the highest of 1000 waves).

7.1.3 Modelling the uncertainty of the waterdepth at the structure

The waterlevel at sea in a design condition often include tidal elevation , and extreme conditions of wind setup resulting in storm surge. Reference is given to subsection 6.1.6.

7.1.4 Modelling the average mass density of rock, and crown wall

The *average mass density of the crown wall* is assumed normal distributed with mean value $\rho_c = 2.3\ t/m^3$ and a coefficient of variation of 5%, which is accepted by authors Burcharth (1992) and van der Meer (1993)..

7.1.5 Modelling the uncertainty of soil properties

Variability of soil properties such as the the effective friction angle, , and angle of dilation are relevant parameters in determining the bearing capacity of crown walls. Reference is given to subsection 6.1.8

The uncertainty of the derived bearing capacity of the foundation, based on the upper bound theorem is assumed to be normal distributed with an coefficient of variation equal to 10 %. This has been accepted as a reasonable assumption based on the work by Sørensen et al. (1993).

7.2 Limit state equations for crown wall foundation failure

Failure modes of importance for crown walls is sliding and rupture failure of the rubble mound. The following rupture equations have been derived and explained in depth in section 3.1.3. Only a simplified expression will be presented in the following to illustrate the limit state equations for design of crown walls.

The stochastic variables are explained in depth in section 7.1 and should be implemented prior to a reliability evaluation.

In the following F_H^p is the horizontal force (derived from induced pressure and pore pressure along the rupture boundary in the rubble mound), $F_G - F_U$ is the weight of the caisson considering buoyancy and wave induced uplift, F_{rubble} is the horizontal active rubble force from the seaward side of the crown wall, φ_d is the modified friction angle of the rubble mound material, ω_{iH} is the horizontal displacement vector for zones $i = 1...3$ in the kinematical admissible rupture mechanism, ω_{iV} is the vertical displacement vector for zones $i = 1...3$ in the kinematical admissible rupture mechanism, W_i is the self weight of zones $i = 1...4$ multiplied by the corresponding displacement vector, $(\gamma_s - \gamma_w)$ is the reduced specific weight of the rubble, and B_z is the rupture width in the caisson or rubble mound.

Case (1)

Sliding between the caisson base and rubble (plain crown wall) is described in the following limit state equation:

$$G_{c1} = -F_H - F_{rubble} + (F_G - F_U) \cdot \frac{\sin \varphi_d}{\cos \varphi_d} \tag{7.1}$$

where F_H is the horizontal force from the wave forces.

Case (2)

Foundation failure in the rubble mound (plain crown wall) is described in the following limit state equation:

$$\begin{aligned} G_{c2} &= F_{G_1} \frac{\sin(\varphi_d - \theta)}{\cos \varphi_d} - (F_H^p + F_{rubble}) \frac{\cos(\varphi_d - \theta)}{\cos \varphi_d} \\ &\quad + (F_G - F_U) \frac{\sin(\varphi_d - \theta)}{\cos \varphi_d} \end{aligned} \tag{7.2}$$

where F_{G_1} is the reduced weight of the rupture zone considering buoyancy.

Case (3)

Foundation failure in the rubble mound (plain crown wall) is described in the following limit state equation:

$$G_{c3} = -(F_H^p + F_{rubble})\omega_{1H} - (F_G - F_U)\omega_{1V} - W_1 + W_2 + W_3 \qquad (7.3)$$

Case (4)

Sliding failure of the crown wall with an extended leg on the seaward side is described in the following limit state equation:

$$G_{c4} = \frac{-F_H - F_{rubble}}{cos\theta} = (F_G - F_U + F_{G_1}) \cdot (\sin\theta + \frac{\sin\varphi_d}{\cos\varphi_d}\cos\theta) \qquad (7.4)$$

where F_{G_1} is the weight of the zone reduced for buoyancy above the slip line from the inner most edge of the foot to the heel of the crown wall.

Case (5)

Rupture failure of the rubble mound, when the crown wall has an extended leg on the seaward side. The limit state equation is described in the following:

$$G_{c5} = F_{G_{1,2}}\frac{\sin(\varphi_d - \theta)}{\cos\varphi_d} - (F_H^p + F_{rubble})\frac{\cos(\varphi_d - \theta)}{\cos\varphi_d}$$

$$+(F_G - F_U)\frac{\sin(\varphi_d - \theta)}{\cos\varphi_d} \qquad (7.5)$$

where $F_{G_{1,2}}$ is the weight of zone 1 and 2 reduced for buoyancy.

Case (6)

Rupture failure of the rubble mound, when the crown wall has an extended leg on the seaward side. The limit state equation is described in the following:

$$G_{c6} = -(F_H^p + F_{rubble})\omega_{1H} - (F_G - F_U)\omega_{1V} \qquad (7.6)$$

$$-W_1 - W_2 + W_3 + W_4$$

7.3 Application of reliability in crown wall design

A deterministic design is performed based on the three rupture failure modes identified in the plane crown wall case, and the three rupture failure cases where an extended leg is attached to the seaward side of the crown wall, see section 3.2. Thereafter the reliability index is calculated to give a qualitative evaluation.

7.3.1 Reliability analyses of the 12 crown wall designs

Characterization of the stochastic parameters are shown in Table 7.3 and explanation of the stochastic parameters used in the reliability evaluation is described in section 7.1. Results from the reliability evaluation of the 12 crown wall designs based on 2 real sea wave data, 3 overtopping levels and 6 kinematical rupture figures is given in the following Table 7.2.

Design No.	**Plane crown wall**					
	Sliding (1)		Rupture failure (2)		Rupture failure (3)	
	β	P_f	β	P_f	β	P_f
1	2.26	$1.1 \cdot 10^{-2}$	2.12	$1.7 \cdot 10^{-2}$	2.81	$2.5 \cdot 10^{-3}$
2	2.28	$1.1 \cdot 10^{-2}$	2.14	$1.6 \cdot 10^{-2}$	2.85	$2.2 \cdot 10^{-3}$
3	2.30	$1.1 \cdot 10^{-2}$	2.18	$1.5 \cdot 10^{-2}$	2.86	$2.1 \cdot 10^{-3}$
4	2.46	$7.0 \cdot 10^{-3}$	2.34	$9.6 \cdot 10^{-3}$	2.82	$2.4 \cdot 10^{-3}$
5	2.53	$5.7 \cdot 10^{-3}$	2.43	$7.5 \cdot 10^{-3}$	2.87	$2.1 \cdot 10^{-3}$
6	2.60	$4.7 \cdot 10^{-3}$	2.53	$5.7 \cdot 10^{-3}$	2.21	$1.8 \cdot 10^{-3}$
Design No.	**Crown wall with an extended leg**					
	Sliding (4)		Rupture failure (5)		Rupture failure (6)	
	β	P_f	β	P_f	β	P_f
1	4.02	$2.8 \cdot 10^{-3}$	2.60	$4.7 \cdot 10^{-3}$	4.43	$4.8 \cdot 10^{-4}$
2	4.04	$2.6 \cdot 10^{-3}$	2.63	$4.2 \cdot 10^{-3}$	4.47	$3.9 \cdot 10^{-4}$
3	4.06	$2.4 \cdot 10^{-3}$	2.67	$3.7 \cdot 10^{-3}$	4.51	$3.3 \cdot 10^{-4}$
4	3.77	$8.3 \cdot 10^{-3}$	2.72	$3.5 \cdot 10^{-3}$	3.61	$1.5 \cdot 10^{-2}$
5	3.80	$7.3 \cdot 10^{-3}$	2.80	$2.5 \cdot 10^{-3}$	3.65	$1.5 \cdot 10^{-2}$
6	3.83	$6.4 \cdot 10^{-3}$	2.88	$2.0 \cdot 10^{-3}$	3.70	$1.1 \cdot 10^{-2}$

Table 7.2: Probability of failure within a return period of 50 years for the 12 crown wall designs, 3 overtopping levels and 6 kinematical admissible rupture mechanisms

i	X_i	Definition	μ_{X_i}	σ_{X_i}	$\frac{\sigma_{X_i}}{\mu_{X_i}}$	Distribution	Reference
1	H_{so}	Deep water significant wave height (m)				Weibull	Burcharth (1992b)
2	k	Weibull parameter				normal	see Table 7.1
3	A	Weibull parameter				normal	see Table 7.1
4	b	Scale parameter for (R_u)	1	0.06	0.06	normal	van der Meer (1991)
5	R_u	Run-up				Weibull	van der Meer (1991)
6	U_{pu}	Uncertainty of the uplift pressure formula	1.00	0.30	0.30	normal	Pedersen (1996)
7	$U_{F_{H_1}}$	Uncertainty of the horizontal load factor	0.21	0.02	0.095	normal	Pedersen (1996)
8	$U_{F_{H_2}}$	Uncertainty of the horizontal load factor	1.60	0.10	0.06	normal	Pedersen (1996)
9	ρ_c	Average density of crown wall (KN/m^3)	2.3	0.115	0.05	normal	Burcharth (1992b)
10	ψ	Angle of dilation	0.29	0.035	0.10	normal	
11	φ'	Effective friction angle	0.73	0.09	0.12	log-normal	Nadin F. et al (1994)
12	Z	Uncertainty of rupture eq.	1	0.10	0.10	normal	Sørensen C.S. (1993)

Table 7.3: Characterization of the stochastic parameters for plane crown wall, and a crown wall with an extended leg

It is seen that the probability of failure is very low for plane crown walls and the crown walls with an extended leg on the seaward side, cf. Table 7.2. This is due to the conservative design of the crown walls based on $R_{u,0.1\%}$. In some countries e.g. the Netherlands it is accepted to used $R_{u,2\%}$, which would have given a smaller crown wall width. The probability of failure of the plane crown wall is dominant for the rupture failure mode (2). In the case of a crown wall with an extended leg on the seaward side the probability of failure of rupture failure mode (5) is dominant.

8

Reliability based design of the armour and toe berm interaction

In this chapter the reliability based design of the armour and toe berm interaction is presented. The stochastic parameters are presented and the limit state equations are formulated. An illustrative example is shown to describe the reliability based interaction in a mutiple system of failure.

8.1 Characterization of the stochastic parameters for the armour layer and toe berm

Typical parameters of importance are described in the following and should be used in the reliability evaluation of the armour layer and toe berm interaction. The parameters should at least be defined by a mean value and a standard deviation (normal distributed) if the actual distribution is unknown. Some of the parameters have very small variational coefficients and can be regarded as deterministic parameters. This holds for all the geometrical parameters applied in the forthcoming reliability evaluation.

8.1.1 Modelling uncertainty of the design equations

The *uncertainty of the derived toe berm stability equations* are assumed normal distributed, and reference is given to section 4 for the variation of coefficient of the equations.

The *uncertainty of the derived static stability of the armour layer* equations are assumed normal distributed, and reference is given to section 4 for the variation of coefficients.

8.1.2 Modelling uncertainty of the design wave parameters

Statistically variability of wave parameters i.e. significant wave height H_s and peak wave period T_p are the most significant parameters in breakwater design. For design purposes the 50 year return wave heights are used to design the breakwater. Modelling the wave height in deepwater is presented in subsection 6.1.3.

8.1.3 Modelling the uncertainty of the waterdepth at the structure

The waterlevel at sea in a design condition often include tidal elevation , and extreme conditions of wind setup resulting in storm surge. Reference is given to subsection 6.1.6.

8.1.4 Modelling the nominal diameter of the armoured stones

The *mean nominal size of the toe berm and armour layer rock* is assumed to follow a normal distribution with a coefficient of variation of 5%.

8.1.5 Modelling the average mass density of rock

The *average mass density of rock material* for the toe berm and armour layer is assumed normal distributed with mean value $\rho_s = 2.6\ t/m^3$ and a coefficient of variation of 3 - 5%, which is accepted by authors, Burcharth (1992) and van der Meer (1993).

8.1.6 Modelling the slope of the armour layer

The *slope* of the armour layer is assumed normal distributed with an expected value $\cot\alpha = 2$ and a coefficient of variation of 5%, which is accepted by authors Burcharth (1992) and van der Meer (1993).

8.2 Limit state equations for the main armour and toe berm interaction

The design equations have been formulated for the main armour and toe berm interaction including the uncertainty of the equations, reference is given to section 4 for further investigation. Only a simplified expression will be presented in the following to illustrate the limit state equations derived from the design equations for the main armour and toe berm interaction.

The following limit state equation for the toe berm is the same as Gerding's equation (4.1) before interaction takes place

$$G_1 = Z_{toe}(0.24 \cdot \frac{h_t}{D^t_{n50}} + 1.60) \cdot N_{od}^{0.15} - \frac{H_s}{\Delta D^t_{n50}} \tag{8.1}$$

where Z_{toe} is the uncertainty of the toe berm equation and is assumed to be normally distributed with an expected value equal to 0.96 and a variation of 0.1.

The limit state equation for the main armour *plunging waves* is expressed as:

$$G_2 = 6.2P^{0.18} \left(\frac{S}{\sqrt{N}}\right)^{0.2} \frac{1}{\sqrt{\xi_m}} - \frac{H_s}{\Delta D^a_{n50}} \tag{8.2}$$

where the equation (8.2) covers breaking and non breaking wave conditions, with the limits given by van der Meer (1988), the equation is the same as equation (4.4). The constant 6.2 in the equation is normally distributed with a coefficient of variation equal to 0.065.

The stabilizing effect on the toe berm from the rock material in the armour layer can be derived from Figure 4.5 and is modelled by equation (8.3)

$$G_3 = Z^1_{toe}(0.26 \cdot \frac{h_t}{D^t_{n50}} + 1.52) \cdot N_{od}^{0.15} - \frac{H_s}{\Delta D^t_{n50}} \tag{8.3}$$

where Z^1_{toe} is the uncertainty of the modified toe berm equation which is assumed to follow a normal distribution with a coefficient of variation equal to 18%.

The corresponding damage level of the armour at the intersection point is defined as S^*_A and modelled according to the following equation:

$$G_4 = 8.44P^{0.18} \left(\frac{S}{\sqrt{N}}\right)^{0.32} \frac{1}{\sqrt{\xi_m}} - \frac{H_s}{\Delta D^a_{n50}} \tag{8.4}$$

where the constant 8.44 is modelled as the uncertainty of the modified armour equation and assumed to follow a normal distribution with a coefficient of variation equal to 30%.

The stability of the toe is greatly reduced when the toe berm width is reduced, because the rest of the armour layer will fail, thus altering the static stability of the armour layer.

The limit state equation for the main armour after partial damage from the toe berm is expressed in following equation :

$$G_5 = 6.6P^{0.18}\left(\frac{S}{\sqrt{N}}\right)^{0.32}\frac{1}{\sqrt{\xi_m}} - \frac{H_s}{\Delta D^a_{n50}} \tag{8.5}$$

where the constant 6.6 is assumed to have a variation coefficient corresponding to 29%.

The negative effect is expected to commence when $N_{od} \geq D^*_T$ and is modelled by the following limit state equation:

$$G_6 = Z^2_{toe}\left(0.13 \cdot \frac{h_t}{D^t_{n50}} + 2.58\right) \cdot N^{0.15}_{od} - \frac{H_s}{\Delta D^t_{n50}} \tag{8.6}$$

where Z^2_{toe} is the uncertainty of the modified toe berm equation assumed to follow a normal distribution with a coefficient of variation equal to 26%.

8.3 Reliability evaluation of armour layer and toe berm stability

The limit state equations that have been formulated in section 8.2 consist of multiple possible failure modes. Therefore the probability of failure for the main armour and toe berm can be described in a series system consisting of the toe berm stability equation, Gerding (1993), static stability of the armour layer van der Meer (1988), parallel system of the modified toe berm stability equation considering partial damage of the armour layer and a parallel system where partial failure of the toe berm causes instability of the armour layer. The probability of failure for the series system of failure modes including two parallel systems is:

$$P_f = P(S_A \geq S^{cr}_A \vee D_T \geq D^{cr}_T$$

$$\vee(D_T \geq D^*_T \wedge S^1_A > S^{cr}_A) \vee (S_A \geq S^*_A \wedge D^1_T > D^{cr}_T)) \tag{8.7}$$

where P_f can be estimated by FORM.

In the following section an example of a rubble mound breakwater is designed according to existing design equations prior to the reliability evaluation. This is to illustrate the reliability of the main armour and toe berm interaction.

8.3.1 Deterministic design of a rubble mound breakwater - example

The toe berm is designed according to the Gerding eq. (1993), and the armour layer is designed according to van der Meer (1988) static stability equations for rock material. The figure below shows the important design parameters for a rubble mound breakwater.

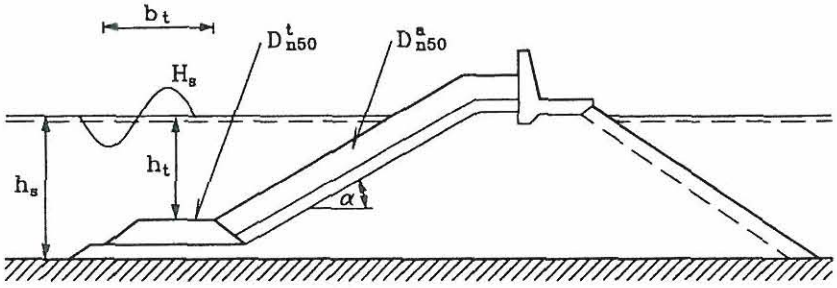

Figure 8.1: *Definition of the design parameters used in the armour layer and toe berm stability equations.*

The design wave height is based on a assumed Weibull distribution with the following coefficients $k = 2.00$, $A = 2.50$,$\lambda = 1$, and $B = 0.18$. The significant wave height according to a 50 year return wave period is $H_{so}^{50y} = 5.13\ m$.

Damage design level for the toe is taken as $N_{od} = 2$ and for the armour layer $S = 4$. These damage levels are taken as acceptable design criteria and used in the reliability evaluation. The toe berm width is equal to $b_t = 4D_{n50}^t$. The main parameters satisfying the design criteria see Figure 8.1.

$h_t = 6.5\ m$, $D_{n50}^t = 0.89\ m$, $D_{n50}^a = 1.78\ m$, $\Delta = 1.62$
,$s_m = 0.04$, $\cot\alpha = 2$, $N = 7500$, $P = 0.4$, $h_s = 10m$

8.3.2 Results of the reliability calculations

A reliability analysis is performed on the example in section 8.3.1. The stochastic parameters used in this calculation are presented in Table 8.2. The result of the reliability calculations are presented in Table 8.1 for the single failure modes including the α^2 sensitivity values.

	Armour layer	Toe berm	Negative effect armour layer		Positive effect toe berm	
	$S_A \geq S_A^{cr}$	$D_T \geq D_T^{cr}$	$S_A^1 > S_A^{cr}$	$D_T \geq D_T^*$	$D_T^1 > D_T^{cr}$	$S_A \geq S_A^*$
Reliability index β	−0.16	−0.19	−1.06	0.00	0.08	−0.49
Probability of failure P_f	0.56	0.57	0.87	0.50	0.47	0.69
$\alpha^2_{H_{s0}}$	0.41	0.37	0.17	0.17	0.25	0.43
α^2_k	0.10	0.09	0.03	0.04	0.06	0.10
α^2_A	0.24	0.22	0.11	0.09	0.14	0.28
$\alpha^2_{D^a_{n50}}$	0.07		0.03			0.07
$\alpha^2_{D^t_{n50}}$		0.01		0.01	0.01	
α^2_Δ	0.06	0.06	0.03	0.02	0.04	0.07
$\alpha^2_{\cot\alpha}$	0.02		0.01			0.02
$\alpha^2_{Z_{toe}}$		0.25				
$\alpha^2_{U_{armour}}$	0.10					
$\alpha^2_{Z^1_{toe}}$					0.50	
$\alpha^2_{U^1_{armour}}$			0.62			
$\alpha^2_{Z^2_{toe}}$				0.67		
$\alpha^2_{U^2_{armour}}$						0.03
$\sum$	1.00	1.00	1.00	1.00	1.00	1.00

Table 8.1: *Results from the reliability calculation.*

It is seen that with the current design, the interaction between the armour layer and toe berm (positive effect and negative effect) is important. In the following, the armour layer and the toe berm interaction will be modelled as a series system of parallel systems with the simple bounds, and the probability of failure is described as shown in section 5.4, based on the simple bounds.

i	X_i	Definition	μ_{X_i}	σ_{X_i}	$\frac{\sigma_{X_i}}{\mu_{X_i}}$	Distribution	Reference
1	H_{so}	Deep water significant wave height (m)				weibull	Burcharth (1992)
2	k	Weibull parameter	2.00	0.18	0.09	normal	Burcharth (1994)
3	A	Weibull parameter	2.50	0.25	0.10	normal	Burcharth (1994)
4	D^a_{n50}	Equivalent armour length (m)	0.89	0.045	0.05	normal	Burcharth (1992)
5	D^t_{n50}	Equivalent toe length (m)	1.78	0.089	0.05	normal	Burcharth (1992)
6	Δ	Reduced weight of rock material	1.62	0.08	0.05	normal	Burcharth (1992)
7	$\cot\alpha$	Slope of armour	2.0	0.1	0.05	normal	Burcharth (1992)
8	Z_{toe}	Model uncertainty of Gerdings eq. (8.1)	0.96	0.1	0.10	normal	
9	U_{armour}	Model uncertainty, armour eq. (8.2)	6.2	0.4	0.065	normal	van der Meer (1993)
10	Z^1_{toe}	Model uncertainty,toe berm eq. (8.3)	1.00	0.18	0.18	normal	
11	U^1_{armour}	Model uncertainty, armour i eq. (8.5)	1.00	0.29	0.29	normal	
12	Z^2_{toe}	Model uncertainty, toe berm eq. (8.6)	1.00	0.26	0.26	normal	
13	U^2_{armour}	Model uncertainty, armour i eq. (8.4)	1.00	0.30	0.30	normal	

Table 8.2: Characterization of the stochastic parameters for the main armour and toe berm interaction

The probability of failure for each limit state is denoted as P_{f_1} to P_{f_6} from left to right in Table 8.1. For the two parallel systems the upper and lower bounds are described as follows:

The positive effect on the toe berm

The upper bound probability of failure for the parallel system can be described as follows:

$$P_f^{Up} = \min_{i=5}^{6} (P_{f_5}, P_{f_6}) = 0.47 \tag{8.8}$$

The lower bound probability of failure for the parallel system can be described as follows:

$$P_f^{Lp} = P_{f_5} \cdot P_{f_6} = 0.32 \tag{8.9}$$

The simple bounds for the parallel system (positive effect) is described as:

$$0.32 \leq P_f \leq 0.47 \qquad \text{positive effect} \tag{8.10}$$

The negative effect on the toe berm

The upper bound probability of failure for the parallel system can be described as follows:

$$P_f^{Up} = \min_{i=3}^{4} (P_{f_3}, P_{f_4}) = 0.50 \tag{8.11}$$

The lower bound probability of failure for the parallel system can be described as follows:

$$P_f^{Lp} = P_{f_3} \cdot P_{f_4} = 0.44 \tag{8.12}$$

The simple bounds for the parallel system (negative effect) is described as:

$$0.44 \leq P_f \leq 0.50 \qquad \text{negative effect} \tag{8.13}$$

It should be noted that the individual β points were used to calculated the simple bounds. This is an allowable approximation as long as the failure surface is not too non linear in the case of the two parallel systems.

Simple bounds for the serie system of parallel systems can be now be calculated from the lower and upper bounds of a series system. In the case of a lower bound solution where the components of the system are fully correlated the probability of failure of the system can be written as:

$$P_f^{Ls} = \max\ P_{fi} = 0.57 \tag{8.14}$$

where P_{fi} corresponds to probability of failure for components $i = 1, 2, 4, 6$.

The upper bound solution corresponds to no correlation, and can written as follows:

$$P_f^{Us} = 1 - (1 - P_{f1})(1 - P_{f2})(1 - P_{f3} \cdot P_{f4})(1 - P_{f5} \cdot P_{f6}) = 0.93 \tag{8.15}$$

There is a high degree of probability of failure for the current design presented which primarily is based on the uncertainty of the Weibull distribution and the uncertainty of the stability equations denoted as U^1_{armour}, Z_{toe}, Z^1_{toe} and Z^2_{toe}. Assuming there is no correlation between the failure modes the probability of failure for the system will be on the safe side, while full correlation will give a probability of failure of the system on the unsafe side. An average of the two probability of failures will give a realistic value as the probability of failure is high. The probability of failure of the multiple system of failure modes is $P_f^s \approx 0.75$. To increase the accuracy of the simple upper and lower bounds the implementation of Ditlevsen (1979) narrow bounds can be determined based on the correlation matrix $\boldsymbol{\rho}$ and the reliability index.

9

Optimal Reliability based design of vertical breakwaters

The following chapter is devoted to optimal design of vertical breakwaters using the reliability approach.

9.1 Optimal reliability based design model

Realization of the design variables, describing the cost functions associated with initial cost design and the cost of failure during the expected design lifetime, to minimized the total costs. The preceeding chapters form a basis for performing optimal reliability based analysis. Application of optimal reliability analysis of a conventional vertical breakwater design will be studied to give a qualitative evaluation.

The optimal reliability based design model can be subdivided as shown in Figure 9.1

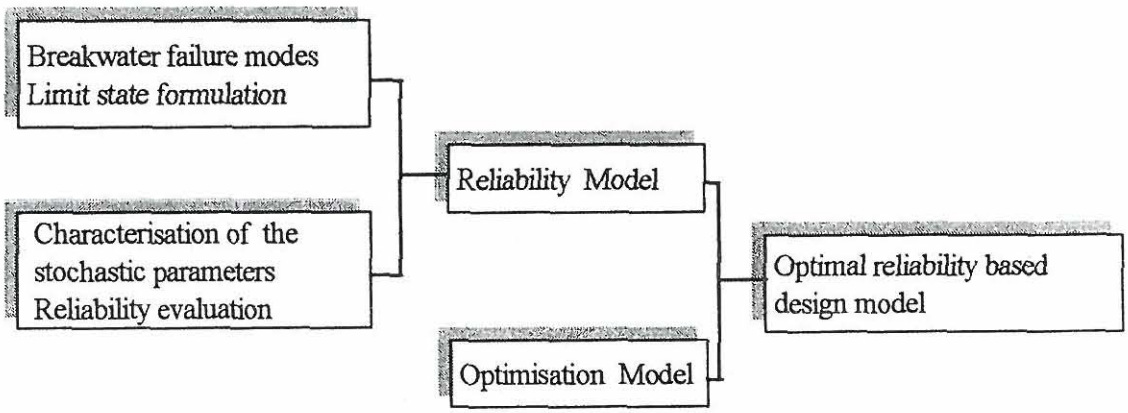

Figure 9.1: *Design flow diagram for optimal reliability based design*

In Figure 9.1 a optimal reliability based design model consists of a reliability model and optimization model which are linked together.

Breakwater failure modes and limit state formulation

The response of vertical breakwaters induced by the wave loads are modelled in a system consisting of main breakwater failure modes. In this chapter optimal system reliability of vertical breakwaters will be restricted to rupture failure of the foundation.

Reliability evaluation

Reliability evaluation of breakwater design will be estimated in a FORM analysis by identification of the failure modes, characterization of the stochastic variables, definition of the failure level and estimation of relevant sensitivity measures.

Reliability model

The reliability model is obtained by linking the limit state equations to the reliability formulation. The linking consist of calculating the safety index for a given set of design variables, i.e. geometrical parameters.

Optimization model

The optimization model consists of optimization variables, formulation of a objective function (cost related function) and the requirements for the reliability indices in the constraints.

Optimal reliability based design model

The reliability model and optimization model are linked to form a optimal reliability based design model where the sensitivities of the objective function and constraints with respect to the optimization variables are estimated.

Application of the mathematical optimal reliability model model is presented again to enhance the understanding:

The design (decision) variables are denoted $\mathbf{b} = (b_i, \ldots, b_N)$, for $i = 1..N$, i.e. the number of design variables N.

If the objective function is chosen as the total expected costs C_T of the structure during the lifetime, the optimal design can be found as the solution to the optimization problem

$$\min_{\mathbf{b}} \quad C_T(\mathbf{b}) = C_I(\mathbf{b}) + C_F P_f(\mathbf{b}) \tag{9.1}$$

$$B_i(\mathbf{b}) \geq 0 \qquad , i = 1, \ldots, M \tag{9.2}$$

$$b_i^l \leq b_i \leq b_i^u \qquad , \; i = 1, \ldots, N \tag{9.3}$$

where b_i^l and b_i^u are lower and upper bounds to b_i, B_i is the deterministic constraint associated with the design variables b_i , C_I is the initial/construction costs, C_F is the costs of failure, andP_f is the probability of failure during the expected lifetime of the breakwater.

Alternatively an element reliability-index based optimization problem can be formulated

$$\min_{\mathbf{b}} \quad C_I(\mathbf{b}) \tag{9.4}$$

$$s.t. \quad \beta_i(\mathbf{b}) \geq \beta_i^{min} \quad ,i = 1,\ldots,m \tag{9.5}$$

$$B_i(\mathbf{b}) \geq 0 \quad ,i = 1,\ldots,M \tag{9.6}$$

$$b_i^l \leq b_i \leq b_i^u \quad ,i = 1,\ldots,N \tag{9.7}$$

where β_i is the reliability index for failure mode i and β_i^{min} is the corresponding lower bound on the reliability index. Equivalent solutions from (9.1)-(9.3) and (9.4)-(9.5) can be obtained by suitable choices of β_i^{min} $i = 1,...m$ The above optimization problems are usually non-linear and non-convex. The optimization problems can be solved effectively using non-linear optimization algorithms and FORM.

The reliability indices in (9.5) are determined on the basis of limit state functions written as $g_i(\mathbf{x}(\mathbf{b}),\mathbf{b}) = 0$, $i = 1,...,m$. In a traditional deterministic design the design (optimization) problem the constraint (9.5) is exchanged by the deterministic constraint

$$B_i(\mathbf{b}) = g_i(\mathbf{x}^{\mathbf{D}}(\mathbf{b},\gamma),\mathbf{b}) \geq 0 \quad ,i = 1,\ldots,m \tag{9.8}$$

where $\mathbf{x}^{\mathbf{D}}$ are design values calculated using the statistical parameters for the stochastic variables $\mathbf{X}$ and γ are the partial safety factors.

9.2 Vertical breakwaters

Optimal design of a vertical breakwater for construction or rehabilitation is always of interest to the design engineer, so that the monetary aspects (initial costs plus repair) of the structure are kept at a minimum without compromising the project. Including a reliability formulation in an optimization problem will clearly identify the most sensitive design variables and give the desired probability of failure for the given design lifetime of the structure.

Optimal reliability based design can be evaluated from the extensive set of failure mechanism identified in Figure 1.4. The main failure modes sliding, rupture failure, overturning and bearing pressure will be applied as they are the most significant failure mechanisms. In principle the local failure mechanisms should be included as they may become critical in the design phase.

The geometrical parameters can be the design variables which are denoted as $\mathbf{b} = (b_i, \ldots, b_N)$, for $i = 1..N$, i.e. the number of design variables N see Figure 9.2.

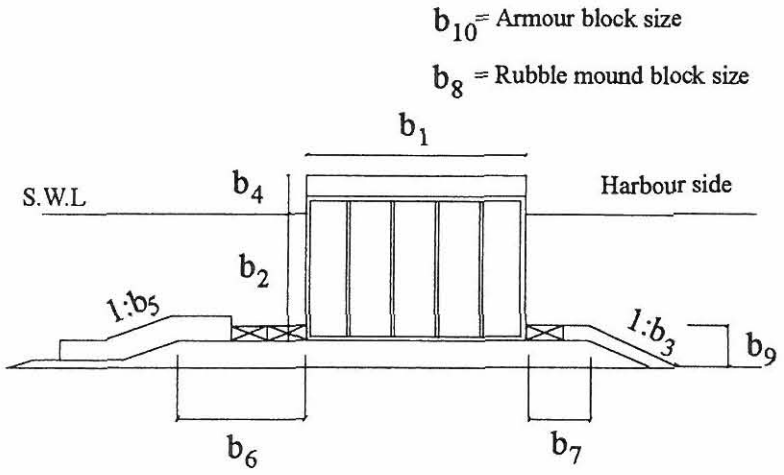

Figure 9.2: *Definition of the design variables for optimal reliability design.*

The combination of design variables (geometrical variables) will usually result in several sets of acceptable upper and lower bounds of the parameters. Restriction to the design variables cannot always be based on a cost benefit analyses i.e. a breakwater has to be aesthetic to the harbour authorities as well as the common public.

9.2.1 Modelling expected costs function

The cost function for a vertical breakwater is divided up into initial cost of the structure prior to operation, cost of failure during construction and when the breakwater is in use. Initial construction costs are usually fixed in the form of a tender which a contractor is expected to stay within, for the project. Cost of failure is more diverse as costs in terms of damage to the breakwater change dramatically within the expected lifetime of the structure. The cost of failure can be subdivided into a number of items

Cost of failure is divided into failure prior to the completion of the breakwater and failure after construction of the breakwater is completed.

Cost of failure C_{F_1} **during** construction

- Increase in initial costs to complete construction of the breakwater.
- Damage to other structures in the port i.e. wharves, buildings and vehicles.
- The number of days the port is suspended from normal operation.
- Shipping operations moving to other ports and change in landward transport operations.
- Claims from suspended shipping operations, industry etc.
- Loss of human lives
- Indirect economic loss i.e bad reputation

Cost of failure C_{F_2} **after** construction

- Damage to other structures in the port.
- The number of days the port is suspended from normal operation.
- Shipping operations moving to other ports and change in landward transport operations.
- Claims from suspended shipping operations, industry etc.
- Loss of human lives
- Indirect economic loss i.e bad reputation

Economic optimization of a vertical breakwater can be evaluated from the above considerations. The cost objective function in a optimal reliability analysis is chosen as the total expected costs C_T of the structure during the expected lifetime, equation (9.9)

$$\min_{\mathbf{b}} \quad C_T(\mathbf{b}) = C_I(\mathbf{b}) + C_{F_1} P_{f_1}(\mathbf{b}) + C_{F_2} P_{f_2}(\mathbf{b}) \tag{9.9}$$

$$b_i^l \leq b_i \leq b_i^u \quad , \; i = 1, \ldots, N \tag{9.10}$$

where b_i^l and b_i^u are lower and upper bounds to b_i. C_I is the initial construction cost of the caisson and rubble mound, C_{F_1} is the costs of failure during construction and the corresponding probability of failure P_{f_1}, and C_{F_2} is failure after construction of the breakwater and P_{f_2} is the corresponding probability of failure during the expected lifetime of the vertical breakwater.

It is necessary to quantify the individual probabilities of failure in terms of limit states and safety classes. This is traditionally done by defining serviceability limit state (SLS) and ultimate limit state (ULS) of breakwaters. The corresponding safety classes are defined as low, normal and high depending on the usage of the structure and the certifying authorities. Usually SLS have higher accepted probabilities of failure compared to ULS. This is at present being evaluated by members of PROVERBS (MAST III Marine Science and Technology 1996 -1999) sponsored by the European Union.

In terms of the cost function presented in eq. (9.9), P_{f_1} would lie in the bounds of ULS and P_{f_2} would lie in the bounds of SLS.

Inspection and maintenance cost should also be included in the cost of failure to ensure safety and stability of the breakwater during the expected lifetime. Inspection will usually identify local failure modes which can be repaired, thus reducing the possibility of a primary failure mode causing damage to the structure. In terms of a reliability evaluation inspection and maintenance will lie in the bounds of a serviceability limit state.

9.3 Optimal design of vertical breakwaters with sand or clay subsoil - example

The preliminary dimensions of the vertical breakwater including the stochastic parameters for the sand subsoil are given in section 6.5, where a high and low rubble mound was considered. The reliability based optimization will be performed with the vertical breakwater on a high rubble mound cf. Figure 6.8 b.

Reliability based optimization of the vertical breakwater will be based on the two design parameters, the width of the conventional breakwater (B) and the height of the rubble mound (h_{II}). The series system evaluation is based on the rupture failure modes for sand and clay subsoils, illustrated in section 6.2.

For simplicity the cost of failure is neglected and the initial costs can be written as:

$$C_I(B, h_{II}) = C_w \cdot W_{caisson}(B) + C_r \cdot W_{rubble}(h_{II}) \tag{9.11}$$

where $W_{caisson}$ is the weight of the caisson and W_{rubble} is the corresponding weight of the rubble. The difference in price per unit weight between the weight of the rubble and caisson is chosen as $\frac{C_r}{C_w} = 2$.

The cost of construction is minimized with Ditlevsens (1979) upper and lower bounds including Hohenbichler (1987) approximation on the probability of failure of the series system of failure modes. The optimal reliability based problem can be described by:

$$\min \quad C_I(B, h_{II}) \tag{9.12}$$

$$s.t. \quad P_f(B, h_{II}) \leq P_f^s \tag{9.13}$$

$$15 \leq B \leq 31 \tag{9.14}$$

$$0.5\ m\ \leq h_{II}\ m\ \leq 6 \tag{9.15}$$

$$\tag{9.16}$$

where P_f^s is the probability of failure of the system, and the reliability index.

Optimal designs for different levels of the acceptable probability of failure P_f^s (target probability of failure for the series system) within a return period of 50 years for the *sand subsoil*, see Table 9.1:

P_f^s	β^u	β^s	β^l	B (m)	h_{II} (m)	Critical failure mode
0.1	1.27	1.26	1.24	29.50	4.50	**2**
0.2	0.86	0.84	0.80	24.50	4.00	**5**
0.3	0.56	0.53	0.51	22.50	5.00	**2**

Table 9.1: Optimal design for different levels of acceptable probability within a 50 year return period (sand subsoil series system).

where β^u and β^l are upper and lower reliability Ditlevsens bounds. The results given in Table 9.1 are an example of combining the two geometrical parameters, the height of the rubble mound and the width of the caisson breakwater based on the target probability of failure for the given series system. Other combinations exist which could be more favourable for the client.

For the clay subsoil the expected value and the covariance function are modelled as:

$$E[c_u(x,z)] = 130 + 3z \tag{9.17}$$

$$Cov[c_u(x_1,z_1), c_u(x_2,z_2)] = \tag{9.18}$$

$$37.5^2 \exp\Big(-|\frac{z_1 - z_2}{3.0}|\Big) \exp\Big(-(\frac{x_1 - x_2}{30.0})^2\Big)$$

where c_u is in kPa and x, z are taken in meters at the change of a new soil layer (origo $(x,z) = (0,0)$ is at the point where the rupture slip line enters the clay subsoil), $\mu_{c_u} = 130$ is the expected value of the undrained shear strength, $\sigma_{c_u} = 37.5$ is the standard deviation of the undrained shear strength and 3 is a constant signifying the linear increase of the undrained shear strength of the clay subsoil.

All the stochastic parameters described in section 6.5 are applied in the following reliability based optimization except for the angle of dilation and effective friction angle in the sand subsoil.

Optimal designs for different levels of the acceptable probability of failure P_f within a return period of 50 years for the *clay subsoil*, see Table 9.2:

P_f^s	β^u	β^s	β^l	B (m)	h_{II} (m)	Critical failure mode
0.1	2.25	1.26	1.25	31.0	3.0	**3**, clay subsoil
0.2	0.86	0.84	0.77	25.0	3.0	**3**, clay subsoil
0.3	0.59	0.53	0.50	22.0	3.5	**3**, clay subsoil

Table 9.2: Optimal design for different levels of acceptable probability within a 50 year return period (clay subsoil series system).

where β^u and β^l are upper and lower reliability Ditlevsens bounds. The results given in Table 9.2 are an example of combining the two geometrical parameters, the height of the rubble mound and the width of the caisson breakwater based on the target probability of failure for the given series system. Other combinations exist which could be more favourable for the client.

10

Conclusion

10.1 Summary

Rubble mound breakwaters and vertical breakwaters are structures which are typically used to protect harbours. In this thesis the most important failure modes (failure mechanisms) of rubble mound breakwaters and conventional vertical breakwaters have been identified and described.

Reliability methods are introduced as a design tool for rubble mound breakwater and vertical breakwater design.

Available research results on vertical breakwater wave loading, existing foundation stability methods, including sliding and overturning is reviewed. A new reliability-based way of approaching foundation stability of vertical breakwaters on a rubble mound with sand or clay subsoil is presented. The existing failure modes used in traditional design are described. Kinematical admissible rupture mechanisms are formulated such that a reliability analyses can be performed. Stochastic models for uncertain parameters are described using the information from experimental tests and from the literature. Further, it is shown how the foundation failure modes can be modelled as components in a series system.

Application of reliability methods on existing Japanese vertical breakwaters (Mutsu -Ogawara v-section, West Breakwater at Niigata East Port (I2-section) and Second West Breakwater at Niigata West Port) has been presented. The main results show a high probability of failure for the vertical breakwaters compared to traditional engineering structures. But compared to observed failure rates the vertical breakwater reliability levels are realistic. In all three cases the sand subsoil is comparatively weak and resulting in rupture failure modes **5** and **6** being the most dominant. Sensitivity values from the reliability analysis show that the horizontal wave induced load, the reduced friction angle of the rubble mound, and the sand subsoil were dominating.

Reliability based optimization formulations for rational design of vertical wall breakwaters are derived. They are based on the cost of constructing the structure. Finally an illustrative example is presented of a conventional vertical breakwater on a high rubble mound with sand and clay subsoil.

Available research on crown wall wave loading based on run up, and overtopping is reviewed. Plane crown wall and crown wall with an extended leg are designed on the basis of foundation failure of the rubble mound only. Application of reliability methods on crown wall is presented, considering limited overtopping and similar real sea states (Bilbao and Fallornica). Characterization of the stochastic parameters, and reliability evaluation of the deterministic design are performed. It is found that the critical foundation failure mode is (2) plane crown wall and (5) for the crown wall with an extended leg.

The main armour and toe berm interaction reliability analyses presented in this thesis are based on the experimental data from Lamberti (1994) and has clearly shown a positive effect of the armour stones moving onto the toe berm, thus enhancing stability of the toe berm. It is also observed that the increased erosion of the toe berm will reduce the stability of the armour layer drastically at limited water depth above the toe berm.

The armour layer and toe berm stability equations are modelled by a series system of parallel systems which is applicable in a reliability analyses. Characterization of the stochastic parameters is performed prior to the reliability evaluation. An illustrative example is presented to show the effect of applying simple bounds to the probability of failure for the system.

10.2 Concluding remarks and recommendations for further research

Optimal reliability based assessment of the derived rupture failure mechanisms in the rubble mound and subsoil of conventional vertical breakwaters has been presented. The method is applicable to a wide range of vertical breakwaters, but evaluation of accepted probability of failure levels for different safety classes and limit states is important, before this tool can be fully accepted by the civil engineering community.

It was shortly mentioned that the total cost function for a vertical breakwater should include inspection and maintenance costs. Therefore identifying inspection and maintenance costs and the cost of failure of large breakwater structures is needed to be implemented in the optimal reliability based design of breakwaters. To correctly evaluate the lifetime of the structure.

The limit state function corresponding to rupture failure of the foundation of a conventional breakwater was evaluated by use of the upper bound solution. In order to evaluate the accuracy of theses limit states they have to be compared to other methods available e.g. finite element models or lower bound methods.

Little information was available in the prototype cases for the stochastic variability of relevant soil parameters e.g. effective friction angle φ', angle of dilation ψ and undrained shear strength of clay c_u to evaluate the uncertainty of the parameters. These parameters are very significant in the probabilistic analysis. Therefore more research in terms of the stochastic nature of the rubble/subsoil at the site is needed, and especially on the spatial variability of the soil parameters.

Three dimensional wave loads has been presented in short form and can in principle replace the long-crested wave loads in terms of the overall design, but the methods are still crude and need further verification in terms of experimental work. Especially the following two points are important:

a) The main wave direction, and the directional spreading are needed to give a wide range of application for wave loads in a short crested sea on vertical breakwaters.

b) The impulsive wave loads from plunging breakers close to vertical breakwaters, and the dynamic response of the foundation in short crested seas.

A way of quantifying a system of failure modes for vertical breakwaters has been presented. Using this system in a reliability analysis has clearly shown that it is applicable as a design tool, but not all vertical breakwater failure modes were included. So therefore further reliability analyses of the vertical breakwater failure mode system, including a wide range of failure modes as presented in Figure 1.4, should be evaluated in future work.

The rupture failure of the foundation of crown walls was evaluated by use of the upper bound solution, to determine the limit states. Theses limit states have to be compared to other methods available e.g. finite element models or lower bound methods.

Reliability evaluation of a multiple system of failure is presented for the armour layer and toe berm interaction based on laboratory investigation. Further experimentation is required to clarify the large uncertainty of the design equations derived from the laboratory data for the combined effect of armour and toe berm stability. The question of scale effects should also be investigated.

References

Ahrens, J.P., Heimbaugh, M.S. , (1986). *Irregular waves overtopping sea walls* proc. Conf. Oceans '86. IEEE, Washington, USA.

Aminiti,P., Franco, L. , (1988). *Wave overtopping on rubble mound breakwaters.* proc. 21t ICCE, Malaga.

Andersen, E.Y. & B.S. Andreasen & P. Ostenfeld-Rosenthat (1992). *Foundation reliability of anchor block for suspension bridge.* Proc. IFIP WG7.5, Lecture notes in Eng. Vol. 76, Springer Verlag, 1992 pp. 131-140.

Bagnold, R.A. , (1939). *Interim report on wave-pressure research*, J. Inst. Civil Engrs., Vol. 12, pp. 202 - 206

Battjes J.A. , (1982). *Effect of short-crestedness on wave loads on long structures* Report SR146, Hydraulics Research, Wallingford. Applied Ocean Research, 1982, Vol. 4, No 3 pp.165 - 172

Bradbury, A.P., Allsop, N.W.H., Stephens, R.V. , (1988a). *Hydraulic performance of breakwater crown walls.* Report SR146, Hydraulics Research, Wallingford.

Bradbury, A.P., Allsop, N.W.H. , (1988b). *Hydraulic effects of breakwater crown walls.* Proc. conf. Breakwaters '88,ICE Eastbourne.

Burcharth, H.F. (1991). *Introduction of partial coefficients in the design of rubble mound breakwaters.* Conf.- on Coastal Structures and Breakwaters, Inst. of Civil Engineering, London.

Burcharth, H.F. (1992a). *Development of a partial coefficient system for the design of rubble mound breakwaters.* PIANC PTC II Working Group 12, Subgroup F report.

Burcharth, H.F. (1992b). *Reliability evaluation of a structure at sea.* Proceedings of the Short Course on Design and Reliability of Coastal Structures. Venice, Scuola di S. Giovanni Evangelista, 1992. 23rd International Conference on Coastal Engineering.

Burcharth, H.F. , (1993). *The design of breakwaters* Chapter 28, Coastal, estuarial and harbour engineering reference book, E & FN SPOON, UK, 1993.

Burcharth, H.F. & J.D. Sørensen & E. Christiani (1994). *On the evaluation of failure probability of monolithic vertical wall breakwaters.* Proc. "Wave Barriers in Deepwater", Port and Harbour Research Institute, Yokosuka, Japan, 1994, pp. 458-46.

Burcharth H.F., J.D. Sørensen & E. Christiani (1995) *Application of reliability analysis for optimal design of monolithic vertical wall breakwaters*, Proc. COPEDEC 1995, Rio de Janeiro, Brazil.

Bruining, J.W. (1994). *Wave forces on vertical breakwaters. Reliability of design formula.* Delft Hydraulics Report H 1903, MAST II contract MAS2-CT92-0047.

Chen W.F. & Liu X.L. (1990). *Limit analysis in soil mechanics.*, Developments in geotechnical engineering vol. 52. Elsevier Science Publishers B.V., (1990).

Cherubini C. & Giasi C.I. (1993). *The coefficient of variations of some geotechnical parameters.* Probabilistic methods in geotechnical engineering, A.A Balkema (1993).

Christiani, E., Burcharth, H.F., Sørensen J.D. , (1994). *Reliability evaluation of a concrete crown wall on a rubble mound breakwater considering sliding failure, overturning and rupture failure of the foundation* Aalborg University, Hydraulics & Coastal Engineering laboratory Denmark.

Christiani E., Burcharth H.F. and Sørensen J.D. (1995) *Reliability evaluation of armour layer and toe berm interaction* presented at the 4 th. workshop meeting 1995, MAST II, Rubble Mound Breakwater failure modes MAS2-CT92-0042.

Christiani E., Burcharth H.F. and Sørensen J.D. (1995) *Geotechnical failure of a concrete crown wall on a rubble mound breakwater considering sliding failure and rupture failure of the foundation*, presented at the 5 th. workshop meeting 1995, MAST II, Rubble Mound Breakwater failure modes MAS2-CT92-0042.

Christiani E., Burcharth H.F. and Sørensen J.D. (1996) *Reliability based optimal design of vertical breakwaters modelled as a series system of failure*, 25 th International Conference on Coastal Engineering, ICCE 96 , Florida, USA.

Ditlevson, O. (1979). *Narrow reliability bounds for structural systems.* Journal of structural safety, Vol 3, pp. 195 - 229.

DS 415 (1984). *Code of practice for foundation engineering.* Danish society of engineers, NP-168 N.

Enevoldsen, I. & J.D. Sørensen (1994). *Reliability-based optimisation in structural engineering.* Structural Safety, Vol. 15, 1994, pp. 169-196.

Franco C. (1996) *Wave overtopping and loads on caisson breakwater under three dimensional sea states*, note from DIIAR Politecnico di Milano, P. Leonardo da Vinci 32, 20133, Milan Italy.

Gerding E. , (1993) *Toe stability of rubble mound breakwaters.* M.Sc. thesis, Delft Hydraulics

Gill, P.E., Murray, W. & Wright, M.H. , (1981) *Practical optimization.* Academic Press Inc., London.

Goda Y. , (1969). *Reanalyses of laboratory data on wave transmission over breakwaters.*, Rept. Port and Harbour Res. Inst., Vol. 8, No. 3, pp. 3 - 18

Goda, Y. and T. Fukumori (1972). *Laboratory investigation of wave pressures exerted upon vertical and composite walls.* Coastal Engineering in Japan, Vol. 15. pp 81-90, 1972.

Goda, Y. (1974). *A new method of wave pressure calculation for the design of composite breakwater.* Proc. 14th Int. Conf. Coastal Eng., Copenhagen, Denmark.

Goda, Y. (1975). *Irregular wave deformation in the surf zone* Coastal Engineering in Japan, JSCE, Vol.18 pp. 13-16.

Goda, Y. , (1985). *Random seas and design of maritime structures.* University of Tokyo Press.

Goda, Y. (1992). *The design of upright breakwaters.* Proceedings of the Short Course on Design and Reliability of Coastal Structures. Venice, Scuola di S. Giovanni Evangelista, 1992. 23rd International Conference on Coastal Engineering, pp 547 - 568, 1992.

Goda, Y. (1994a). *On the uncertainties of wave heights as the design load for maritime structures.* Wave Barriers in Deepwater, Vol. 15. pp 419-436, 1994.

Goda, Y. (1994b). *Dynamic response of upright breakwaters to impulsive breaking waves.* Coastal Engineering, 1994, Vol. 22. pp. 135 - 159

Hansen, B. (1979). *Definition and use of friction angles.* Proc. Int. Conf. VII ECSMFE, Brighton, UK, 1979.

Helm-Petersen, J. (1997). *Wave disturbance in harbours.* Ph.D. thesis, Aalborg University, Denmark (in print).

Hiroi, I. , (1919). *On a method of estimating the force of waves* ,Memoirs of Engg. Faculty, Imperial University of Tokyo, Vol. X, No.1., p. 19.

Hitachi, S. (1994). *Case study of breakwater damages - Mutsu -Ogawara Port -* Wave Barriers in Deepwater, Vol. 15. pp 308 - 331, 1994

Hohenbichler, M., Gollwitzer, S. & Kruse, W. and Rackwitz, R. (1987). *New light on first- order and second- order reliability methods.* Structural safety, Vol. 4, No. 4, pp. 267 - 284.

Keaveny, J.M., Nadim F. & S. Lacasse (1989). *Autocorrelation Function for Offshore Geotechnical Data.* Proc. ICOSSAR89, 1989, pp. 263-270.

Klammer P. & Oumeraci H. (1996). *Wave impact loading of vertical face structures for dynamic stability analysis - Prediction formulae.* 25 th International Conference on Coastal Engineering, ICCE 96, Florida, USA.

Kobayashi, M. & Terashi M. & Takahashi K. (1987). *Bearing capacity of a rubble mound supporting a gravity structure.* Report of Port and Harbour Research Institute Vol. 26, No. 5. Japan.

Lamberti A. , (1994) *Preliminary results on main-armour toe-berm interaction.* RMBFM 3rd Workshop -DH, De Voorst -15-16 November, 1994.

Lundgren, H. , (1969) *Wave shock forces: an analysis of deformations and forces in the wave and in the foundation.* Proc. Int. Symposion on Wave Action, Vol. 2, Delft, Netherlands.

Nadim, F. & S. Lacasse, and T.R. Cuttormsen (1994). *Probabilistic foundation stability analysis: Mobilised friction angle vs available shear strength approach.* Structural Safety & Reliability, 1994, Balkema, Rotterdam.

Nataf, A. , (1962) *Determination des distribution dont les marges sont données.* Comptes redus de l'Academie des Sciences, Vol. 225, 1962, pp. 42 - 43.

Madsen, H.O., S. Krenk & N.C. Lind (1986). *Methods of Structural Safety.* Prentice-Hall, 1986.

Mitsuyasu, H. et al. (1975). *Observations of the directional spectrum of ocean waves using a cloverleaf buoy.* Journal of Physical Oceanography, Vol. 1,pp. 750-760.

Nielsen S.R.K. and Burcharth H.F. (1983). *Stochastic design of rubble mound breakwaters.* Proc. 11 th IFIP Conference on system modelling and optimization, Copenhagen.

OCDI (1991). *Technical standards for port and harbour facilities in Japan* . Port and Harbour Research Institute, Ministry of Transport, 1991.

Oumeraci H. & Kortenhaus, A. (1994). *Analysis of the dynamic response of upright breakwaters to impulsive breaking wave forces.* Coastal Engineering, 1994, Vol. 22. pp. 159 - 183.

Pedersen J. , (1996). *Wave forces and overtopping on crown walls of rubble mound breakwaters - An experimental study.* Ph.D. thesis, Aalborg University, Denmark.

PIANC PTC II (1996). *Breakwaters with vertical and inclined concrete walls* Working Group 28, report of subgroup B, analyses of cases 1996.

Sainflou, G. , (1928). *Essai sur les dgues maritimes, verticales*, Annales Ponts et Chaussées, Vol. 98, No. 4.

Sand, S.E. (1979). *Three dimensional deterministic structure of ocean waves.* Ph.D. Thesis, Technical University of Denmark.

Schittkowski, K. (1985). *NLPQL: A FORTRAN Subroutine solving constrained non-linear programming problems.* Annals of operations research, Vol 5, pp. 485 - 500.

SPM , (1984). *Shore Protection Manual.* U.S. Army Corps of Engineers, Coastal Engineering Research Center, Vicksburg, U.S.A.

Sørensen, J.D. (1994a). *Structural reliability theory.* Probabilistic Approach to the Design of Reliable Coastal Structures, 29 nov. - 10 december 1994, Bologna, Italy.

Sørensen, J.D., H.F. Burcharth and E. Christiani (1994b). *Reliability analysis and optimal design at monolithic vertical wall breakwaters.* Proc. 6th IFIP WG7.5 Assissi, Italy. Chapman & Hall.

Sørensen, C.S., Clausen, C.J.F., Andersen, H. , (1993). *Bearing Capacity Analyses for the Great Belt East Bridge Anchor Blocks. Limit State Design in Geotechnical Engineering.* ISLAD 93, pp. 305-312

Takahashi, S., Tanimoto, K., and K. Shimosako (1994). *Dynamic response and sliding of breakwater caisson against impulsive breaking wave forces.* Rept. of Port and Harbour Research Inst. 1994.

Takayama, T. , (1992). *Estimation of sliding failure probability of present breakwaters for probabilistic design.* Report of Port and Harbour Research Inst., Vol. 31, No. 5, 1992.

Tanimoto , (1976). *Wave forces on a composite-type breakwater.* Proc 1976 Annual Res. Present. of Port and Harbour Res. Inst. (in Japanese).

Tanimoto, Takahashi, S., & Myose,K. , (1984). *Experimental study of random forces on upright sections of breakwaters.* Rept. Port and Harbour Res. Inst., Vol. 23, No. 3, pp. 47 - 99. (in Japanese).

Tanimoto, K. Takahashi, S. and Kimura, K. , (1987). *Structures and hydraulic characteristics of breakwaters - The state of the art of breakwater design in Japan.* Rept. Port and Harbour Res. Inst., Vol. 26, No. 5, pp. 11 - 15.

Toft-Christensen, P. and Baker, M.J. (1982). *Structural reliability theory and its applications.* Springer- Verlag, Berlin.

van der Meer J.W. , (1988) *Rock slopes and gravel beaches under wave attack.* Delft Hydraulics Communication No. 396, Netherlands.

van der Meer, J.W., Stam C.-J.M , (1991). *Wave runup on smooth and rock slopes.* Delft Hydraulics, publications number 454, Netherlands.

van der Meer J.W., Juhl,J. and van Driel,G. , (1992) *Probabilistic calculations of wave forces on vertical structures* . Proc. Final workshop, MAST G6-S Coastal Structures, Lisbon.

van der Meer J.W. , (1993) *Conceptual design of rubble mound breakwaters* . Delft Hydraulics Communication No. 483, Netherlands.

van der Meer J.W. d'Angremond K and Juhl J. , (1994) *Probabilistic calculations of wave forces on vertical structures.* 24 th International Conference on Coastal Engineering, Kobe, Japan, Vol. 2., pp. 1754 - 1767.

A

Conventional vertical breakwater foundation failure modes

List of symbols

B_r : Width of the caisson
B_z : Width of the initial rupture zone in the caisson or rubble mound
c_u : Undrained shear strength of clay
F_G : Weight of the construction, considering reduced buoyancy of the caisson
F_H : Goda's horizontal force acting on the caisson
F_H^p : Goda's horizontal force acting on the caisson
including horizontal pore pressure component along the rupture boundary
F_U : Goda's wave induced uplift force along the base of the
: vertical breakwater
F_R : Resultant force acting on the base of the vertical breakwater
SWL : Sea water level
W_E : External work done
W_I : Total internal energy dissipation in the foundation
W_n : The individual energy dissipation terms in the soil, n=1,2.... etc
δ : Unit increment movement along the line of fracture or rotational vector
ρ_c : Average density of caisson
γ_w : Specific density of water
γ_s : Specific density of the rubble mound
ψ : Angle of dilation
φ' : Effective friction angle
φ_{d_1} : Reduced effective friction angle of the rubble mound material
φ_{d_2} : Reduced effective friction angle of the subsoil
θ : Geometrical angle
ω : Displacement vector
σ : Stress component
ϵ : Strain component
p_u : Goda's uplift pressure along the base of the caisson

A.1 Introduction

In the design of the gravitational caisson, the construction and the underlying soil have to sustain the wave forces and weight of the caisson during the expected lifetime of the structure. A gravitational caisson can in principle be designed as shown in Figure 1.1a and 1.1b.

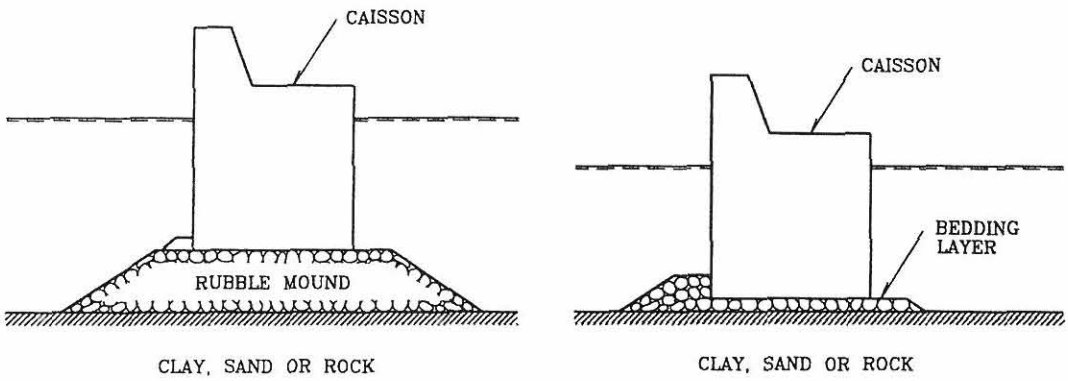

Figure A.1: *a,b Caisson breakwater on high rubble foundation and on bedding layer.*

Figure A.1 b is the caisson type which is placed directly on the seabed, when the waterdepths are relatively low, $5 < h_s < 10$ meters. Figure, A.1 a, is the caisson type placed on a large rubble mound in deep water, where $(h_s > 10m)$. This is primarily due to the expensive costs of placing a caisson directly on the seabed. The main forms of failure modes related to gravitational caissons in vicinity of the foundation are

- Sliding
- Rupture failure (depending on a variety of soil characteristics)
- Crushing at the heel of the caisson
- Overturning

Foundation failure modes for conventional vertical breakwaters, sliding and rupture failure are presented in the following. Kinematically correct slip surfaces and failure zones in undrained clay and friction based soil are derived by upper bound theory by equating the external work and internal energy dissipation in the foundation.

Wave loads are calculated by Goda's wave pressure formula , for a conventional vertical breakwater (Goda et al. 1972 and Goda 1974).

Failure modes involving foundation failures must be evaluated in any design. Excess settlement due to consolidation of soft soil is another important failure mode, which is not discussed in this report. Slip failure modes represent failure states and any related calculation can only give information related to the safety against failures, i.e no information related to in-service conditions can be extracted. The evaluation of safety against foundation slip failures is based on the force balance and the work balance equations and in this paper related to kinematically correct slip surface and failure zones (Rankine, Prandtl zones and slip fans). The ratio between stabilizing and driving forces/moments are taken as a measure of the safety level. For a given type of slip failure mode the minimum value of this ratio is found by an iterative procedure. All relevant types of slip failure modes must be investigated in this way in order to obtain the true minimum value of the stability ratio. Stability ratio calculations based on kinematically correct slip failures provide in principle results on the unsafe side, i.e. the ratio of stabilizing forces over driving forces is greater than or equal to the correct value. However, the method gives results very close to the true values. The method is applicable to static and quasi-static load conditions and it might be applied with some modifications to cover also dynamic loads where inertia forces are of importance. In this report only the conventional static load approach is discussed and exemplified.

A.2 Assumption of the soil characteristics applied in the derivation of the failure modes

A correct solution for the bearing capacity has to be statically and kinematical admissible. It is difficult to find solutions which fulfil both conditions. General solutions are kinematical admissible where the displacement field satisfies the boundary conditions for displacement and flow rule. Therefore restriction to the applied material parameters have to be considered, before applying the upper bound solution.

Following assumptions are done:

- The normality condition has to be full filled, so that the soils friction angle and the soils angle of dilation are the same (plasticity theory).
- The soil is homogeneous and isotrop.
- Rupture failure is considered. Investigations into consolidation of the foundation is not taken into consideration.

A.3 Upper bound theorem and plasticity of the soil

The upper bound theorem will be applied to the postulated kinematical admissible rupture figures in the following sections. The definition of the upper bound theorem is defined as follows:

If an estimate of the plastic collapse load is made by equating internal rate of dissipation of energy to the rate of which external forces do work in any postulated mechanism of deformation of the body, the estimate will either be high or correct.

The upper bound solution is based on equating the external work to the internal stresses during an increment movement of a kinematical admissible mechanism, and at the same time accepting that plastic flow must have occurred prior to rupture failure.

The upper bound solution can be formulated as follows for a given failure surface consisting of external forces per unit area T and body forces per unit volume of the body F.

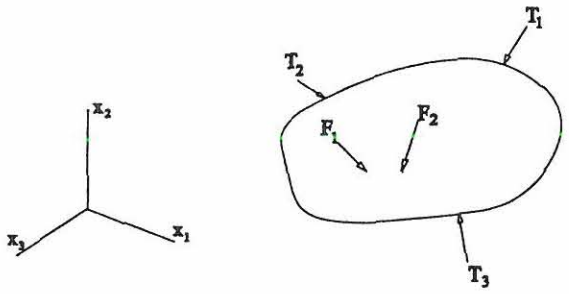

Figure A.2: *A body of rigid-plastic material acted on by external forces and body forces.*

From Figure A.2, the work equation can be expressed as the work done by the external forces and the body forces which is identical or greater than the work done by the internal stresses. Here the upper bound solution is based on a kinematical admissible velocity field, and if this is found then collapse must occur under the present velocity field. A kinematical velocity field, $\overline{v}$, must satisfy the boundary conditions of a compatible rupture figure for a given rigid-plastic material.

The work equation is as follows:

$$\int_A \overline{T}\overline{v}dA + \int_V \overline{F}\overline{v}dV \geq \int_V \overline{\sigma}\ \overline{\varepsilon}dV \tag{A.1}$$

where A is the area, V is the volume, $\overline{\sigma}$ is the internal stresses, and $\overline{\varepsilon}$ is the strains.

The yield surface in an ever changing plastic material can be written in the form of $f(\overline{\sigma})$, where $\overline{\sigma}$ is a six dimensional stress tensor $\overline{\sigma} = (\sigma_x, \sigma_y, \sigma_z, \tau_x, \tau_y, \tau_z)$, but for simplicity shown in two dimensions in Fig A.3.

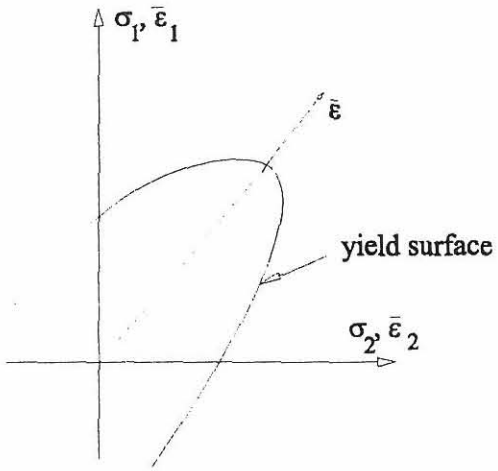

Figure A.3: *Two dimensional case of the stress and strain relationship in soils , including the yield surface*

The state of the material is descrribed by the yield function:

$$f(\overline{\sigma}) \begin{cases} < 0 & \text{no rupture} \\ = 0 & \text{rupture} \\ > & \text{rupture} \end{cases} \tag{A.2}$$

The material is rigid and plastic, if the material is stiff for $f(\overline{\sigma}) < 0$ and plastic for $f(\overline{\sigma}) = 0$

In this study the number of internal dissipation energy terms will differ for a postulated rupture figure and the type of material.This is shown in the following where clay and friction based soil are considered.

A.4 Effective friction angle

The effective friction angle φ' is the important parameter, determining the bearing capacity of friction based soil. It is the main parameter used in the upper bound theory. The effective friction angle used in the calculations is determined experimentally and in many cases can be bias, because the history of the chosen material is unknown. Hansen B. (1979) has shown a method to determine material deterioration and strength, which is applicable to determining the bearing capacity of a kinematical rupture figurer. This results in a reduction of the effective friction angle φ_d.

$$\tan \varphi_d = \frac{\sin \varphi' \cos \psi}{1 - \sin \varphi' \sin \psi} \tag{A.3}$$

where ψ is the angle of dilation of the material. The angle of dilation represent deformation of the considered material and is less than the effective friction angle.

A.5 Wave induced uplift pressure in the soil

The wave induced uplift pressure is calculated from the wave pressure formulae by Goda et al. (1972) and Goda (1974) for the case of a conventional vertical front where wave breaking on the wall is not enhanced by a steep sea bed or structural configuration. The formulae are based on model tests in head-on waves but were modified to cover also oblique waves on the basis of work by Tanimoto et al. (1976). The formulae include the effect of breaking waves to the extent of normal accidental (non-provoked) wave breaking. The formulae are currently used in the Japanese standards. Fig. A.4 shows the related definition sketch for the wave uplift pressure.

Although the wave induced uplift pressure at the front edge of the base plate is equal to p_3 it is suggested by Goda to use a somewhat reduced value

$$p_u = \frac{1}{2}(1 + cos\beta)\ \alpha_1\, \alpha_3\, \rho_w\, g\, H_{design} \tag{A.4}$$

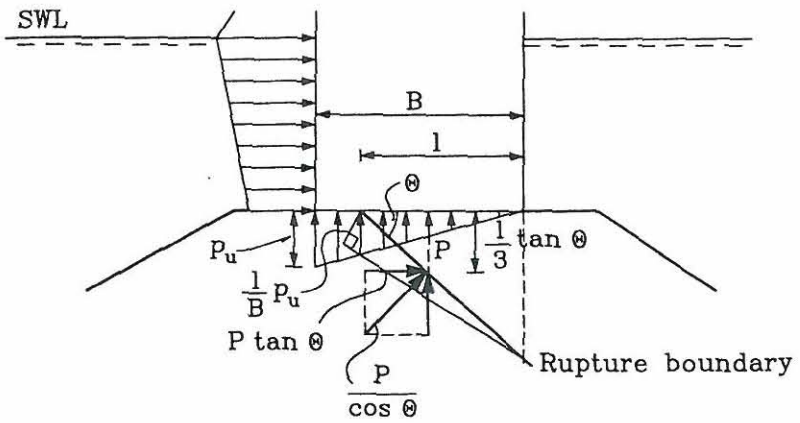

Figure A.4: *Definition sketch for the wave induced uplift pressure along the boundary of rupture*

This wave induced uplift pressure is calculated along the base plate of the vertical breakwater and only gives the vertical component of the pressure.

The pore pressure resultant along the rim of the rupture zone in soil is $P/\cos\theta$, where P is the vertical component along the length l. The horizontal component of the force is:

$$P\tan\theta = \frac{1}{2}\frac{l^2}{B}p_u\tan\theta \tag{A.5}$$

The horizontal wave induced pressure arises along the pore pressure build up in the rubble mound due to the impermeable concrete plane base. In the following derivation of the foundation failure modes an extra contribution is added on the horizontal load component along the rupture boundary. This increases the safety of a given design of a vertical breakwater.

A.6 Caisson breakwater foundation failure modes

Figure A.5 *a* and *b* present an overview of the various kinematically admissible foundation failure modes corresponding to static load cases. The following rupture figures will be derived by applying upper bound theorem to all ten cases.

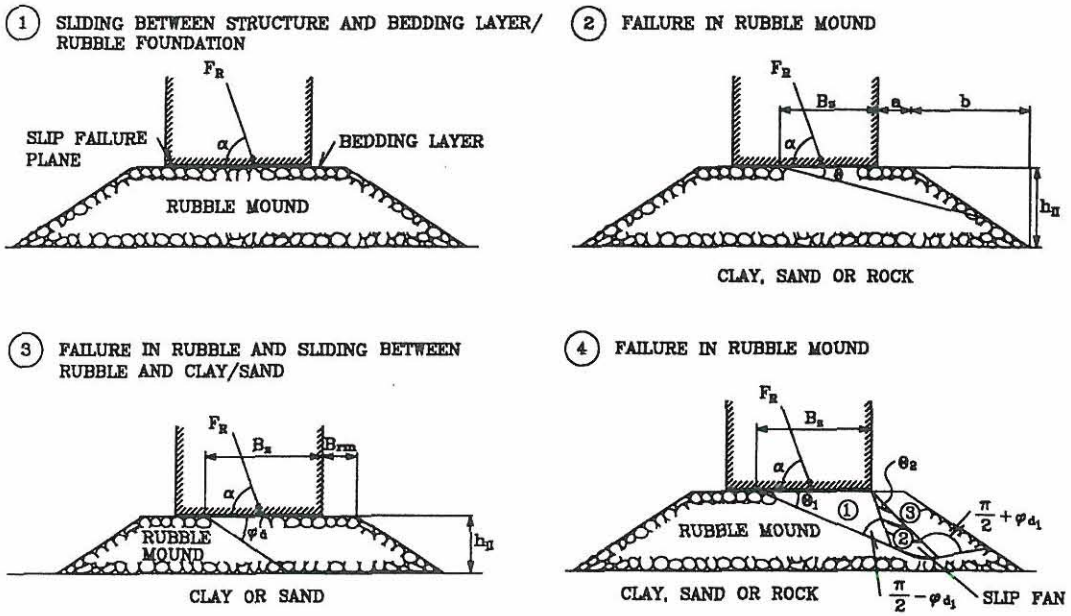

Figure A.5: *a Various kinematically admissible foundation failure modes*

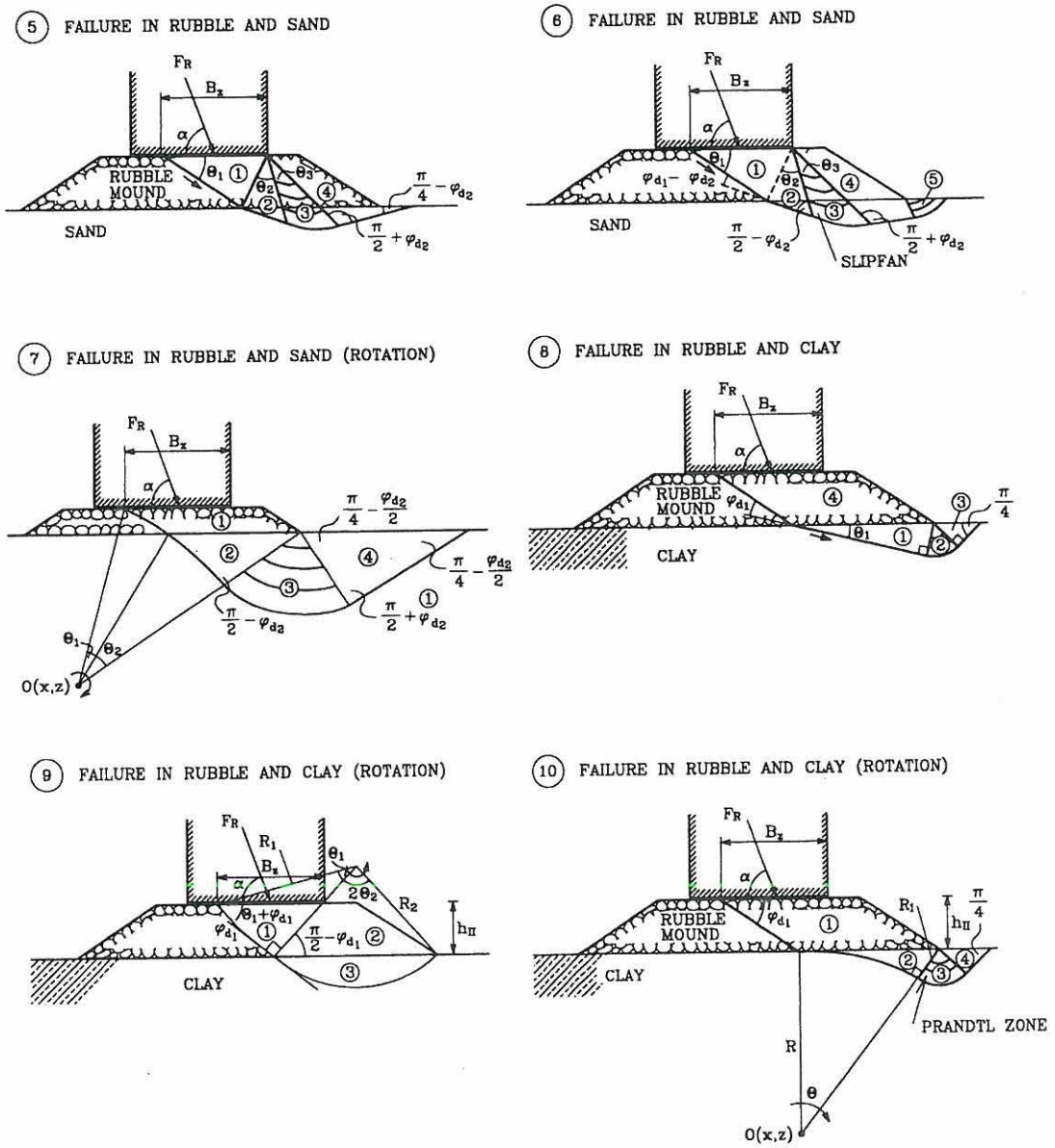

Figure A.5 b *Various kinematically admissible foundation failure modes*

A.6.1 Sliding between caisson and bedding layer /rubble foundation

Case 1. in Fig A.5a is considered

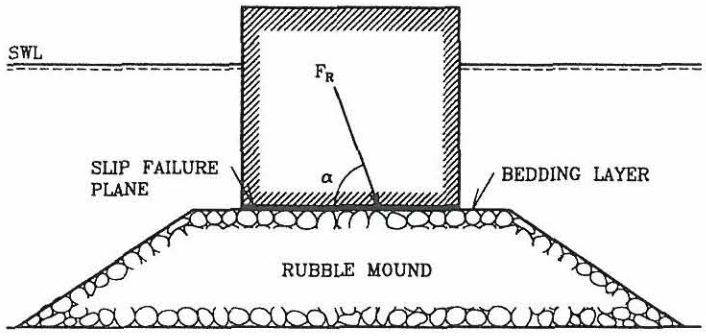

Figure A.6: *Sliding failure on bedding layer or rubble mound .*

Sliding, i.e. horizontal displacement of the caisson, can occur as a slip either at the interface between the caisson concrete base plate and the rubble material, or entirely in the rubble material.

Corresponding to the first mentioned case stability against sliding exists when the ratio of the resultant horizontal force, F_H, to the resultant vertical force is equal to or less than $\tan\mu$, i.e.

$$F_H \leq (F_G - F_U)\tan\mu \tag{A.6}$$

where F_G is the weight of the caisson reduced for buoyancy, F_U is the wave induced uplift force on the base plate and μ is the angle of friction between the concrete base plate and the rubble mound or the bedding layer. Reference is given to OCDI (1991) and Takayama (1992) for values of $\tan\mu$.

When sliding failure takes place entirely in the rubble mound, e.g. in the bedding layer, then μ must be substituted by the reduced effective angle of friction φ_{d_1} of the rubble mound material.

The figure below shows the displacement of sliding rupture in the rubble mound.

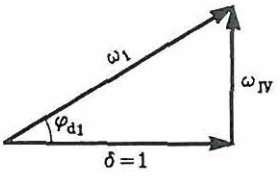

Figure A.7: *Displacement field for sliding along a rubble underlayer.*

where $\delta = 1$ is the displacement of the body a unit increment along the base of the vertical breakwater.

A.6.2 Failure in the rubble mound

Case 2 in Figure A.5 a. is considered.

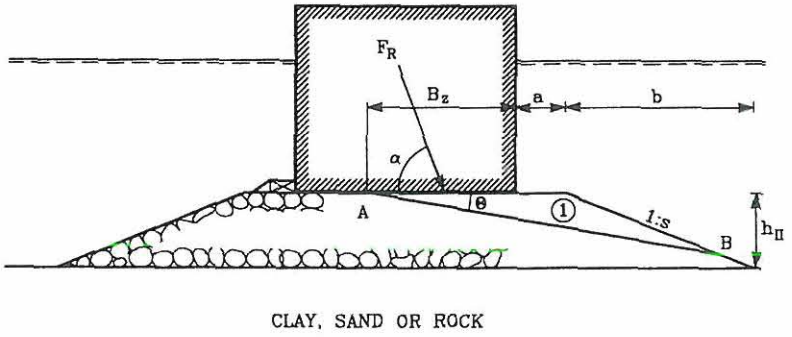

Figure A.8: *Rupture failure in the rubble mound.*

The kinematic admissible rupture figure is presented in Fig A.8. The rupture in the rubble mound takes place along the plane A to B. By equating the external work and internal work for an infinitesimal deformation ω_1, the following derivation of the limit state equation is possible:

The weight of zone 1 as a function of θ is

$$F_{G_1} = \frac{1}{2}(\gamma_s - \gamma_w)(B_z + a)^2 \frac{\tan\theta}{1 - 1.5\tan\theta} \tag{A.7}$$

The final work equation as a function of θ

$$0 = F_{G_1} \frac{\sin(\varphi_{d_1} - \theta)}{\cos\varphi_{d_1}} - F_H^p \frac{\cos(\varphi_{d_1} - \theta)}{\cos\varphi_{d_1}} + (F_G - F_U) \frac{\sin(\varphi_{d_1} - \theta)}{\cos\varphi_{d_1}} \tag{A.8}$$

where F_H^p is the horizontal force (derived from wave induced pressure and pore pressure along the rupture boundary in the rubble mound), $F_G - F_U$ is the weight of the caisson reduced for buoyancy minus the wave induced uplift, φ_{d_1} is the reduced friction angle of the rubble mound material, $(\gamma_s - \gamma_w)$ is the reduced specific weight of the rubble, B_z is the width of rupture zone underneath the caisson base plate, and ω_{1H} and ω_{1V} are horizontal and vertical components of ω_1, see Figure A.9.

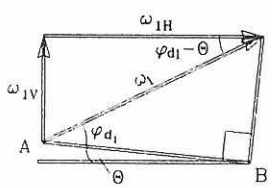

Figure A.9: *Displacement field for the stiff rupture zone.*

where ω_1, ω_{1H} and ω_{1V} are shown below:

$$\omega_{1H} = \frac{\cos(\varphi_{d_1} - \theta)}{\cos\varphi_{d_1}} \tag{A.9}$$

$$\omega_{1V} = \frac{\sin(\varphi_{d_1} - \theta)}{\cos\varphi_{d_1}} \tag{A.10}$$

where θ is the unknown angle to be determined by minimizing the ratio between the stabilizing work and driving work, equation (A.8).

A.6.3 Failure in rubble mound and sliding rubble and clay/sand

Case 3 in Fig A.5 a is considered.

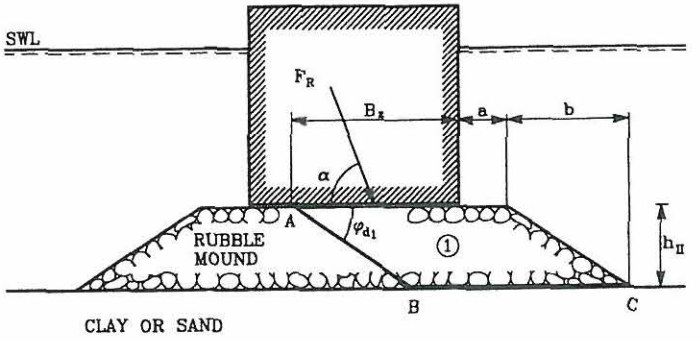

Figure A.10: *Failure in rubble and sliding between rubble and clay/sand.*

Rubble mound placed on clay

The bearing capacity of the clay can be devised from rupture along AB which contributes to sliding rupture along BC.

$$F_H = l_{BC} c_u = c_u (B_z + a + b - \frac{h_{II}}{\tan \varphi_{d_1}}) \tag{A.11}$$

where horizontal force F_H, $a+b$ is the berm width on the rear side of the caisson cf. Figure A.10, h_{II} is the height of the rubble mound, c_u is the undrained shear strength of the clay and B_z is the width of the first rupture zone below the caisson.

Rubble mound placed on sand

The bearing capacity of the sand subsoil can be devised from rupture along AB which contributes to sliding rupture between the rubble mound and subsoil along BC.

The weight of zone 1 is

$$F_{G_1} = (\gamma_s - \gamma_w) \left(\frac{1}{2} b h_{II} + \frac{1}{2} \frac{h_{II}^2}{\tan \varphi_{d_1}} + (B_z + a - \frac{h_{II}}{\tan \varphi_{d_1}}) h_{II} \right) \tag{A.12}$$

The work equation

$$0 = (F_G - F_U) \tan \varphi_{d_2} + F_{G_1} \tan \varphi_{d_2} - F_H^p \tag{A.13}$$

where F_H^p is the horizontal force (derived from wave induced pressure and pore pressure along the rupture boundary in the rubble mound), F_G is the weight of the vertical breakwater reduced for buoyancy, F_U is the wave induced uplift force and F_{G_1} is the weight of the zone 1 reduced for buoyancy cf. Figure A.10.

A.6.4 Foundation failure in the rubble mound, friction based soil

Case 4 in fig A.5 a is considered.

The soil is considered to be homogeneous and characterized as friction based soil. An upper bound solution to a kinematical admissible rupture figure in the foundation is applied. The figure below shows the rupture zones limited in the rubble mound.

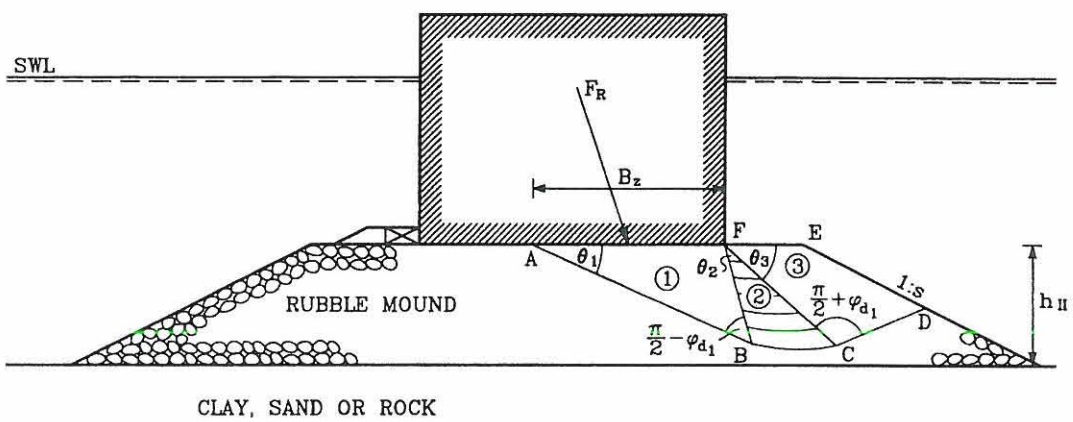

Figure A.11: *Failure in rubble mound in friction based soil.*

Considering that the soil exhibits plastic behaviour, the work equation can be formulated as shown in the following, when the foundation is forced to move a unit increment $\delta = 1$ along the first slip line AB.

The first zone is characterized as a stiff zone which exhibits no internal energy dissipation as is the case for zones 1 - 3 along the rim of the rupture boundary as the normality condition is fulfilled. This zone slides down the rupture line AB causing a instantaneous shift of zone 1. Zone 2 is a set of rotating logarithmic fans which exhibit displacement in the same direction as zone 1 until a resultant displacement reverses and causes the soil to exhibit a holding capacity. Zone 3 moves as a stiff zone holding part of zone 2, zone 1 and the external forces, when equilibrium is present.

The geometric lengths of rupture figures are presented as r (radius) and l (length) subscript. These geometrical lengths are used to determine the area of each individual rupture zone and the displacement of each rupture zone:

The initial radius of the rupture fan, close to the first stiff zone.

$$r_{BF} = B_z \frac{\sin\theta_1}{\sin(\frac{\pi}{2} - \varphi_{d_1})} \tag{A.14}$$

The radius of zone 2 along FC.

$$r_{FC} = r_{BF} e^{\theta_2 \tan\varphi_{d_1}} \tag{A.15}$$

The following length parameters are found to determine the area of the zone 3.

$$l_{FG} = \frac{r_{FC}\sin(\frac{\pi}{2} + \varphi_{d_1})}{\sin\theta_7} \tag{A.16}$$

$$l_{EG} = l_{FG} - l_{EF} \tag{A.17}$$

where l_{EF} is the berm width on the rear side of the caisson cf. Fig A.12.

$$l_{CG} = \frac{r_{FC}\sin\theta_3}{\sin\theta_7} \tag{A.18}$$

where $\theta_7 = \frac{\pi}{4} - \frac{\varphi_{d_1}}{2}$

$$l_{DG} = \frac{l_{EG}\sin(\frac{\pi}{2} - \arctan(s))}{\sin\theta_6} \tag{A.19}$$

where $\theta_6 = \varphi_{d_1} + \theta_3 + \arctan(s)$.

$$l_{CD} = l_{CG} - l_{DG} \tag{A.20}$$

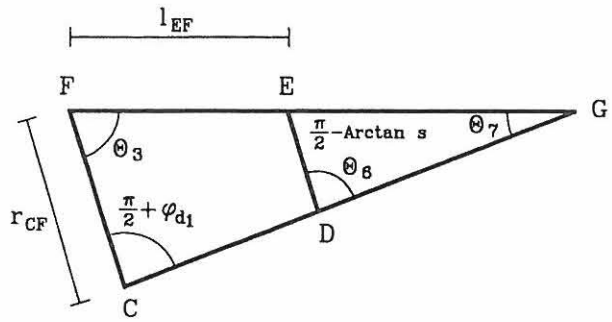

Figure A.12: *Geometrical figure of zone 3.*

Displacement field corresponding to the rupture figure

The displacement of the first rupture zone:

$$\omega_1 = \frac{1}{\cos\varphi_{d_1}} \tag{A.21}$$

$$\omega_{1H} = \omega_1 \cos(\theta_1 - \varphi_{d_1}) \tag{A.22}$$

$$\omega_{1V} = \omega_1 \sin(\theta_1 - \varphi_{d_1}) \tag{A.23}$$

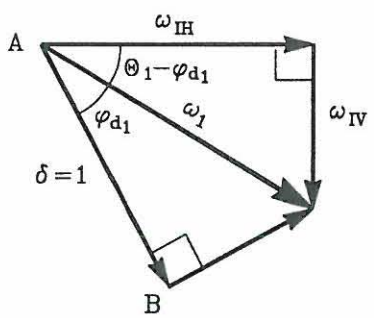

Figure A.13: *Displacement field of the first stiff zone .*

The vertical displacement vector ω_{2V} in zone 2 as a function of θ:

$$\omega_{2V}(\theta) = \omega_1 e^{\theta \tan \varphi_{d_1}} \sin(\varphi_{d_1} - \theta_1 + \theta);\ \theta \in [0; \theta_2] \tag{A.24}$$

where ω_1 is the displacement of the Prandtl zone along the fracture line BF.

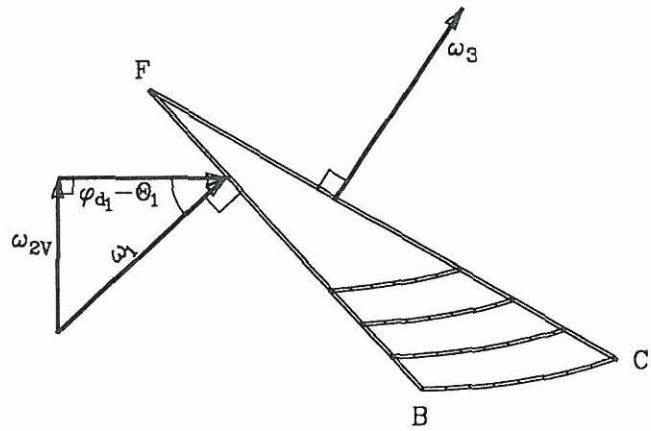

Figure A.14: *Displacement field of slip fans along BF.*

The displacement vector for zone 3 moves as a stiff zone, see Figure A.15.

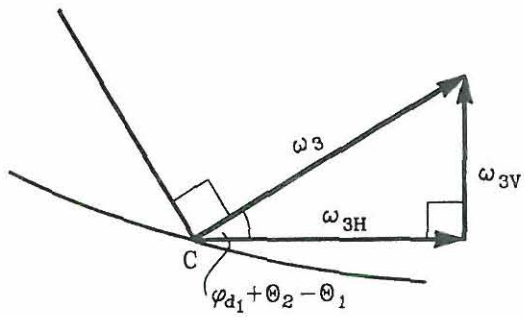

Figure A.15: *Displacement field of zone 3.*

$$\omega_3 = \omega_1 e^{\theta_2 \tan \varphi_{d_1}} \tag{A.25}$$

$$\omega_{3V} = \omega_3 \sin(\varphi_{d_1} + \theta_2 - \theta_1) \tag{A.26}$$

Self weight of the soil in the rupture zones 1 - 3

The work done by the self weight of the soil in zone 1, W_1.

$$W_1 = (\gamma_s - \gamma_w)\omega_{1V}\Omega_1 \tag{A.27}$$

where Ω_1 is the area of rupture zone 1

$$\Omega_1 = \frac{1}{2}B_z l_{AB}\sin\theta_1 \tag{A.28}$$

Work done by the self weight of the slip fan in zone 2, W_2.

$$W_2 = (\gamma_s - \gamma_w)\int_0^{r_{CF}}\int_0^{\theta_2} e^{\theta\tan\varphi_{d_1}}\sin(\varphi_{d_1} - \theta_1 + \theta)r\,dr\,d\theta \tag{A.29}$$

where the analytic solution of W_2 is

$$\begin{aligned} W_2 = {} & \frac{(\gamma_s - \gamma_w)r_{CF}^2}{2\tan^2\varphi_{d_1} + 2}\left[e^{\theta_2\tan\varphi_{d_1}}\left[\tan\varphi_{d_1}\sin(\varphi_{d_1} - \theta_1 + \theta_2)\right.\right. \\ & \left.\left. - \cos(\varphi_{d_1} - \theta_1 + \theta_2)\right] - \tan\varphi_{d_1}\sin(\varphi_{d_1} - \theta_1) - \cos(\varphi_{d_1} - \theta_1)\right] \end{aligned} \tag{A.30}$$

Work done by the self weight of the soil in zone 3, W_3.

$$W_3 = (\gamma_s - \gamma_w)\omega_{3V}\Omega_3 \tag{A.31}$$

where Ω_3 is the area of rupture zone 3.

$$\Omega_3 = \frac{1}{2}l_{FG}\sin\theta_7 l_{CG} - \frac{1}{2}l_{EG}\sin\theta_7 l_{DG} \tag{A.32}$$

To establish the work done in equilibrium where the work from the external forces and self weight in each individual zone are computed, gives the following bearing capacity of the friction based soil.

$$F_H^p \omega_{1H} + (F_G - F_U)\omega_{1V} = -W_1 + W_2 + W_3 \tag{A.33}$$

$$\begin{aligned} & F_H^p \frac{\cos(\theta_1 - \varphi_{d_1})}{\cos\varphi_{d_1}} + (F_G - F_U)\frac{\sin(\theta_1 - \varphi_{d_1})}{\cos\varphi_{d_1}} \qquad (A.34) \\ = \; & -(\gamma_s - \gamma_w)\left(\frac{1}{2} l_{AB} B_z \sin\theta_1 \frac{\sin(\theta_1 - \varphi_{d_1})}{\cos\varphi_{d_1}}\right. \\ & -\frac{(\gamma_s - \gamma_w) r_{CF}^2}{2\tan^2\varphi_{d_1} + 2}\left[e^{\theta_2 \tan\varphi_{d_1}}\left[\tan\varphi_{d_1}\sin(\varphi_{d_1} - \theta_1 + \theta_2)\right.\right. \\ & \left. - \cos(\varphi_{d_1} - \theta_1 + \theta_2)\right] - \tan\varphi_{d_1}\sin(\varphi_{d_1} - \theta_1) - \cos(\varphi_{d_1} - \theta_1)\Big] \\ & \left. -\frac{e^{\theta_2 \tan\varphi_{d_1}}}{\cos\varphi_{d_1}}\sin(\varphi_{d_1} + \theta_2 - \theta_1)\left(\frac{1}{2} l_{FG}\sin\theta_7 l_{CG} - \frac{1}{2} l_{EG}\sin\theta_7 l_{DG}\right)\right) \end{aligned}$$

where θ_1 is the unknown angle to be determined by minimizing the ratio between the stabilizing work and driving work.

A.6.5 Failure in rubble mound and friction based soil

Case 5 in Figure A.5 b. is considered.

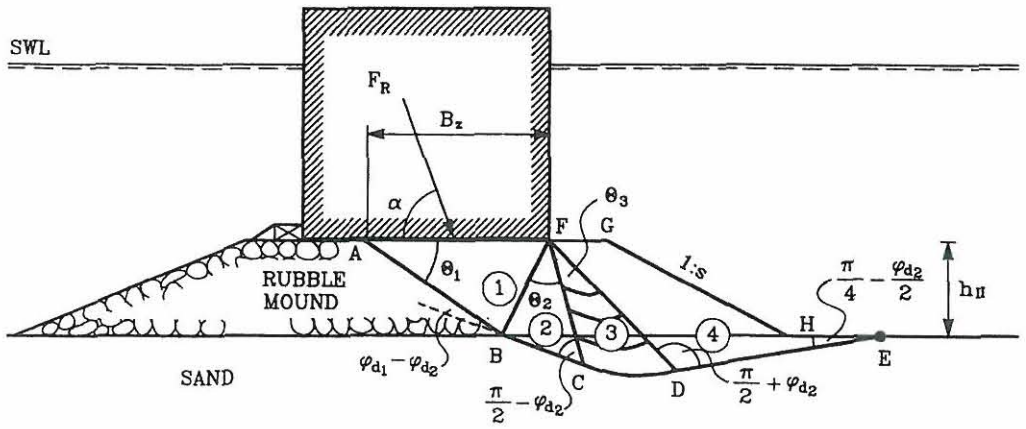

Figure A.16: *Fracture failure in rubble and sand .*

Considering that the soil exhibits plastic behaviour, the work equation can be formulated as shown in the following, when the foundation is forced to move a unit increment $\delta = 1$ along the first slip line AB.

The first zone is characterized as a stiff zone which exhibits no internal energy dissipation as is the case for zones 1 - 4 along the rim of the rupture boundary as the normality condition is full filled. This zone slides down the rupture line AB causing an instantaneous shift of zone 1 and an altered displacement of the second stiff zone due to an altered friction angle φ_{d_2}. Zone 3 is a set of rotating logarithmic fans which exhibit displacement in the same direction as zone 2 until a resultant displacement reverses and causes the soil to exhibit a holding capacity. Zone 4 moves as a stiff zone holding part of zone 3, zone 2, zone 1 and the external forces, when equilibrium is present.

The geometric lengths of rupture figures are presented as r (radius) and l (length) subscript. These geometrical lengths are used to find the area of each individual rupture zone and the displacement of each rupture zone:

The initial radius of the rupture zone, close to the first stiff zone.

The initial length of zone 2, close to the first stiff zone.

$$l_{BF} = \sqrt{B_z^2 + \left(\frac{H_{II}}{\sin\theta_1}\right)^2 - 2\left(\frac{H_{II}}{\sin\theta_1}\right) B_z \cos\theta_1} \tag{A.35}$$

The initial radius of the rupture fan, close to the second stiff zone.

$$r_{CF} = l_{BF} \frac{\sin\left(\pi - (\varphi_{d_1} - \varphi_{d_2} + \arcsin(\frac{B_z \sin\theta_1}{l_{BF}}))\right)}{\sin(\frac{\pi}{2} - \varphi_{d_2})} \tag{A.36}$$

The radius of the rupture fan, close to zone 4.

$$r_{DF} = r_{CF} e^{\theta_3 \tan\varphi_{d_1}} \tag{A.37}$$

The following length parameters are found to determine the area of the zone 4, given by the material parameters in the rubble mound.

$$l_{D'F} = h_{II} / \cos(\frac{\pi}{4} + \frac{\varphi_{d_2}}{2}) \tag{A.38}$$

$$l_{DD'} = r_{DF} - l_{D'F} \tag{A.39}$$

The length $l_{D'E}$ and L_{FH} in zone 4, close to zone 3 on the rear side of the caisson cf. Figure A.17.

$$l_{D'E} = l_{DD'} \frac{\sin(\frac{\pi}{2} + \varphi_{d_2})}{\sin(\frac{\pi}{4} - \frac{\varphi_{d_2}}{2})} \tag{A.40}$$

$$l_{FH} = \sqrt{(l_{FG} + sH_{II})^2 + H_{II}^2} \tag{A.41}$$

where s is the slope (1:s) of the rubble mound on the rear side.

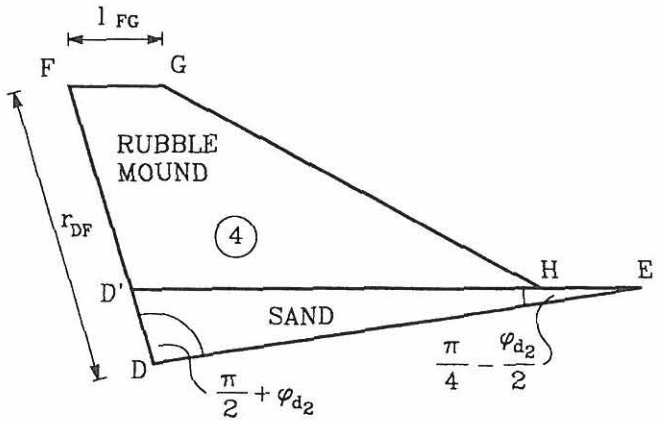

Figure A.17: *Geometrical figure of zone 4 .*

Displacement field corresponding to the rupture figure

The displacement vector in the horizontal and vertical direction for the first stiff zone is

$$\omega_{1H} = \omega_1 \cos(\theta_1 - \varphi_{d_1}) \tag{A.42}$$

$$\omega_{1V} = \omega_1 \sin(\theta_1 - \varphi_{d_1}) \tag{A.43}$$

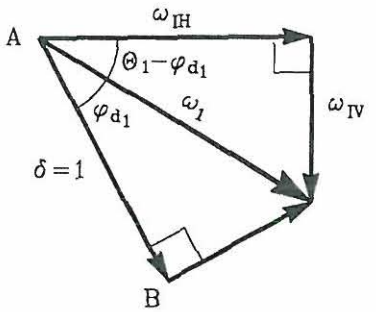

Figure A.18: *Displacement field of the first stiff zone.*

Displacement of zone 2 moves as a stiff zone. In reality the displacement should be described in terms of φ_{d_1} and φ_{d_2}. The displacement of the rupture zone 2 follows the first zone so no discontinuity is present.

$$\omega_{2V} = \omega_{1V} \tag{A.44}$$

The vertical displacement vector ω_{3V} of zone 3 can be formulated as a function of θ as:

$$\omega_{3V}(r,\theta) = \omega_1 e^{\theta \tan \varphi_{d_1}} \sin(\varphi_{d_1} - \theta_1 + \theta);\ \theta \in [0;\theta_3] \tag{A.45}$$

where ω_1 is the displacement of zone 3 along the fracture line CF.

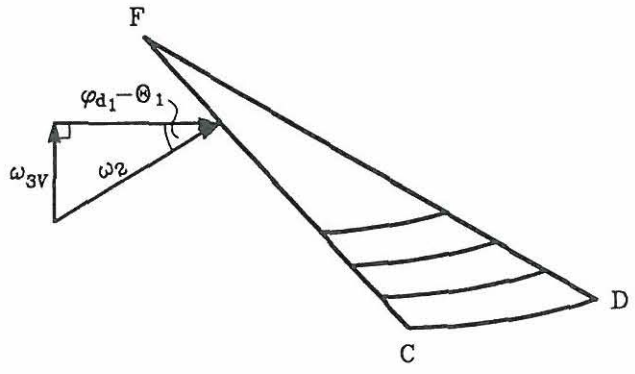

Figure A.19: *Displacement field of the slip fans in zone 3.*

Zone 4 moves as a stiff zone. The displacement field for zone 4 is shown below.

$$\omega_4 = \omega_1 e^{\theta_3 \tan \varphi_{d_2}} \tag{A.46}$$

$$\omega_{4V} = \omega_4 \sin(\varphi_{d_1} - \theta_1 + \theta_3) \tag{A.47}$$

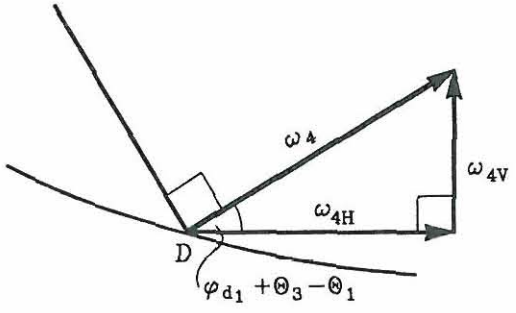

Figure A.20: *Displacement field of zone 4.*

Self weight of the soil in the rupture zones 1 - 4

Work done by the self weight of the soil in zone 1, W_1.

$$W_1 = (\gamma_s - \gamma_w)\omega_{1V}\Omega_1 \tag{A.48}$$

where Ω_1 is the area of rupture zone 1

$$\Omega_1 = \frac{1}{2}B_z H_{II} \tag{A.49}$$

work done by the self weight of the soil in zone 2, W_2.

$$W_2 = (\gamma_s - \gamma_w)\Omega_2\omega_{2V} \tag{A.50}$$

where Ω_2 is the area of rupture zone 2

$$\Omega_2 = \frac{1}{2}L_{BF}r_{CF}\sin\theta_2 \tag{A.51}$$

where $\theta_2 = \varphi_{d_1} + \arcsin(\frac{B_z \sin\theta_1}{l_{BF}}) - \frac{\pi}{2}$ as long as $\theta_2 \geq 0$

Work done by the self weight of the soil in zone 3, W_3.

$$W_3 = (\gamma_s - \gamma_w)\int_0^{r_{DF}}\int_0^{\theta_3}\omega_{3V}(\theta, r)r\,dr\,d\theta \tag{A.52}$$

where the analytic solution of W_3 is

$$\begin{aligned} W_3 = \frac{(\gamma_s - \gamma_w)r_{DF}^2}{2\tan^2\varphi_{d_1} + 2}\,[e^{\theta_3\tan\varphi_{d_1}}\,[\tan\varphi_{d_1}\sin(\varphi_{d_1} - \theta_1 + \theta_3) \\ - \cos(\varphi_{d_1} - \theta_1 + \theta_3)] - \tan\varphi_{d_1}\sin(\varphi_{d_1} - \theta_1) - \cos(\varphi_{d_1} - \theta_1)] \end{aligned} \tag{A.53}$$

Work done by the self weight of the soil in zone 4, W_4.

$$W_4 = (\gamma_s - \gamma_w)\omega_{4V}\Omega_4 \tag{A.54}$$

where Ω_4 is the area of rupture zone 4

$$\begin{aligned}\Omega_4 = & \frac{1}{2}l_{FH}l_{FG}\sin\left(\arctan\left(\frac{H_{II}}{l_{FG}+sH_{II}}\right)\right) \\ & +\frac{1}{2}l_{FH}(r_{DF}-l_{DD'})\sin\left(\frac{\pi}{4}-\frac{\varphi_{d_1}}{2}-\arctan\left(\frac{H_{II}}{l_{FG}+sH_{II}}\right)\right) \\ & +\frac{1}{2}l_{D'E}l_{DD'}\sin\left(\frac{\pi}{4}-\frac{\varphi_{d_2}}{2}\right)\end{aligned} \tag{A.55}$$

To establish the work done in equilibrium, where the external forces and self weight in each individual zone are computed, gives the following bearing capacity of the friction based soil.

$$F_H^p\omega_{1V} + (F_G - F_U)\omega_{1H} = -W_1 - W_2 + W_3 + W_4 \tag{A.56}$$

The angles θ_1 in the limit state equation is the unknown angle to be determined by minimizing the ratio between the stabilizing work and driving work.

A.6.6 Failure in rubble and sand

Case 6 in Fig A.5b.

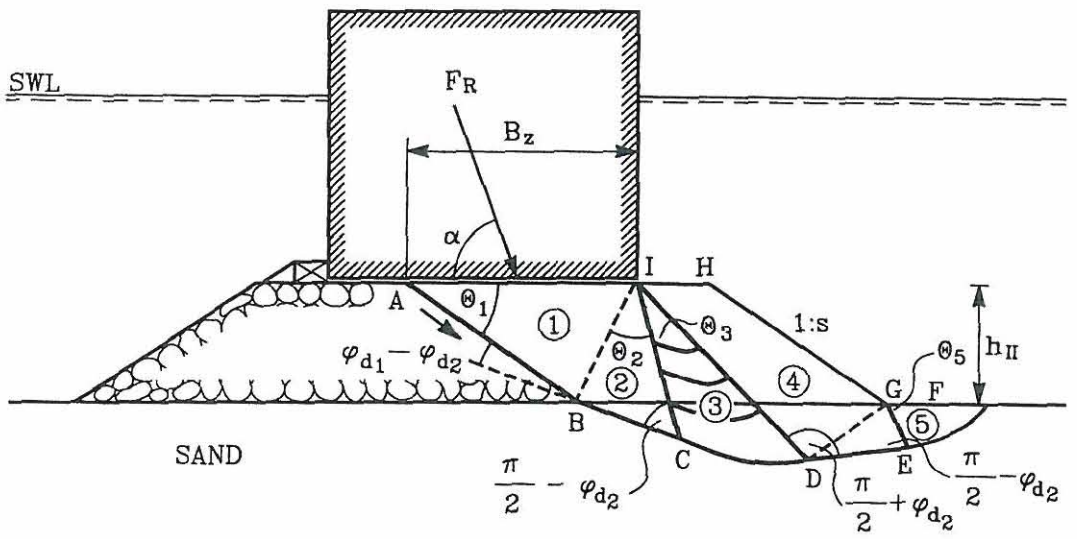

Figure A.21: *Rupture in rubble mound and sand subsoil.*

Considering that the soil exhibits plastic behaviour, the work equation can be formulated as shown in the following, when the foundation is forced to move a unit increment $\delta = 1$ along the first slip line AB.

The first zone is characterized as a stiff zone which exhibits no energy dissipation as is the case for zones 1 - 5 along the rim of the rupture boundary as the normality condition is full filled cf. section 1.2. This zone slides down the rupture line AB causing an instantaneous shift of zone 1 and a change of the second stiff zone due to an altered friction angle φ_{d_2}. Zone 3 is a set of rotating logarithmic elements which exhibit displacement in the same direction as zone 2 until a resultant displacement reverses and causes the soil to exhibit a holding capacity. Zone 4 moves as a stiff zone and causes rupture at the rear foot of the rubble mound, forming a rupture fan, zone 5. These two zones reduce the ability of zone 1 - 3 and the externals loads to cause rupture. .

The geometric lengths of rupture figures are presented as r (radius) and l (length) subscript. These geometrical lengths are used to find the area of each individual rupture zone and the displacement of each rupture zone:

The initial length of zone 2, close to the first stiff zone.

$$l_{BI} = \sqrt{B_z^2 + \left(\frac{H_{II}}{\sin\theta_1}\right)^2 - 2\left(\frac{H_{II}}{\sin\theta_1}\right) B_z \cos\theta_1} \tag{A.57}$$

The initial radius of the rupture fan, close to the second stiff zone.

$$r_{CI} = l_{BI} \frac{\sin\left(\pi - (\varphi_{d_1} - \varphi_{d_2} + \arcsin(\frac{B_z \sin\theta_1}{l_{BI}}))\right)}{\sin(\frac{\pi}{2} - \varphi_{d_2})} \tag{A.58}$$

The radius of the rupture fan, close to zone 4.

$$r_{DI} = r_{CI} e^{\theta_3 \tan\varphi_{d_1}} \tag{A.59}$$

The following length parameters are found to determine the area of the zone 4, given by the material parameters in the rubble mound.

$$l_{D'I} = h_{II} / \cos(\frac{\pi}{4} + \frac{\varphi_{d_2}}{2}) \tag{A.60}$$

$$l_{DD'} = r_{DI} - l_{D'I} \tag{A.61}$$

The length $l_{D'F'}$ and l_{IG} in zone 4, close to zone 3 on the rear side of the caisson cf. Figure A.22.

$$l_{D'F'} = l_{DD'} \frac{\sin(\frac{\pi}{2} + \varphi_{d_2})}{\sin(\frac{\pi}{4} - \frac{\varphi_{d_2}}{2})} \tag{A.62}$$

$$l_{GI} = \sqrt{(l_{IH} + sH_{II})^2 + H_{II}^2} \tag{A.63}$$

where s is the slope (1:s) of the rubble mound on the rear side.

The lengths $l_{D'G}$, $l_{GF'}$ and l_{GE} in zone 5, cf. Figure A.22.

$$l_{D'G} = l_{GI} \frac{\sin\left(\frac{\pi}{4} - \frac{\varphi_{d_2}}{2} - \arctan\left(\frac{H_{II}}{l_{IH} + sH_{II}}\right)\right)}{\sin\left(\frac{3\pi}{4} + \frac{\varphi_{d_2}}{2}\right)} \tag{A.64}$$

where $\theta_5 = \frac{\pi}{4} - \frac{\varphi_{d_2}}{2}$

$$l_{GF'} = l_{D'F'} - l_{D'G} \tag{A.65}$$

$$l_{GE} = l_{GF'} \frac{\sin(\frac{\pi}{4} - \frac{\varphi_{d_2}}{2})}{\sin(\frac{\pi}{2} + \frac{\varphi_{d_2}}{2})} \tag{A.66}$$

$$r_{GF} = l_{GE} e^{\theta_5 \tan \varphi_{d_2}} \tag{A.67}$$

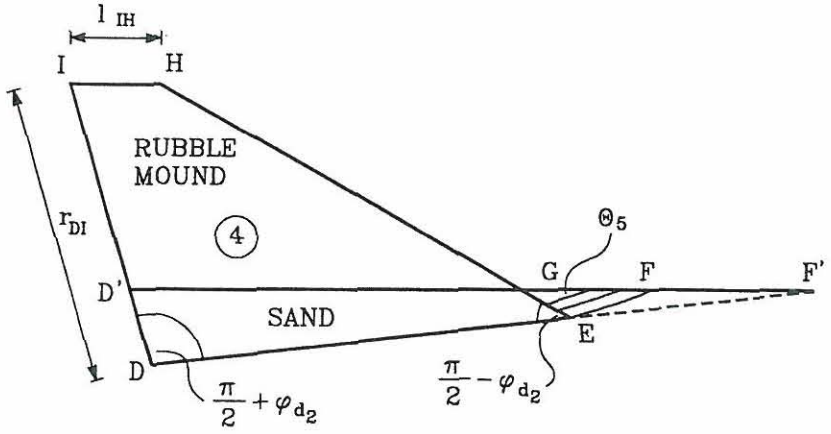

Figure A.22: *Geometrical figure of zone 4.*

Displacement field corresponding to the kinematical admissible rupture figure cf. A.21

The displacement vector for zone 1 is

$$\omega_1 = \frac{1}{\cos \varphi_{d_1}} \tag{A.68}$$

$$\omega_{1H} = \omega_1 \cos(\theta_1 - \varphi_{d_1}) \tag{A.69}$$

$$\omega_{1V} = \omega_1 \sin(\theta_1 - \varphi_{d_1}) \tag{A.70}$$

Displacement of zone 2 moves as a stiff zone. In reality the displacement should be described in terms of φ_{d_1} and φ_{d_2}. The displacement of the rupture zone 2

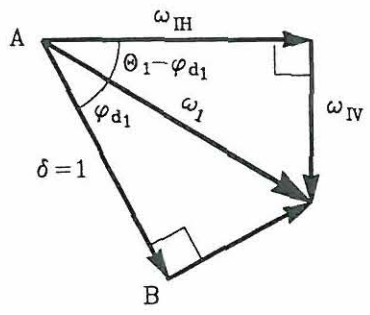

Figure A.23: *Displacement field of the first stiff zone .*

follows the first zone so no discontinuity is present.

$$\omega_{2V} = \omega_{1V} \tag{A.71}$$

The vertical displacement vector ω_{3V} in zone 3 can be formulated in polar coordinates as:

$$\omega_{3V}(r,\theta) = \omega_1 e^{\theta \tan \varphi_{d_1}} \sin(\varphi_{d_1} - \theta_1 + \theta);\ \theta \in [0;\theta_3]\, r \in [0; r_{DI}] \tag{A.72}$$

where ω_1 is the displacement of the slip fans in zone 3 along the fracture line CF see Figure A.24.

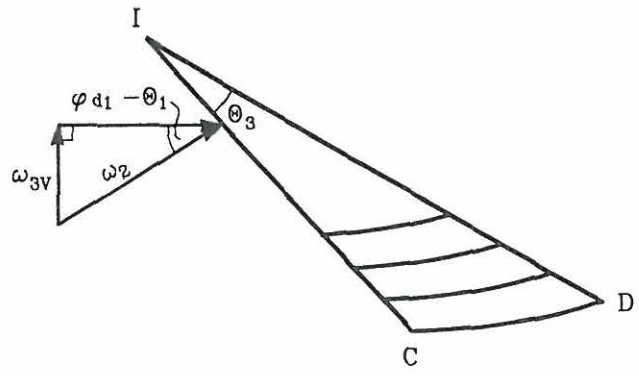

Figure A.24: *Displacement field of the slip fans in zone 3.*

The displacement of zone 4 moves as a stiff zone see Figure A.25.

$$\omega_4 = \omega_1 e^{\theta_3 \tan \varphi_{d_2}} \tag{A.73}$$

$$\omega_{4V} = \omega_4 \sin(\varphi_{d_1} + \theta_3 - \theta_1) \tag{A.74}$$

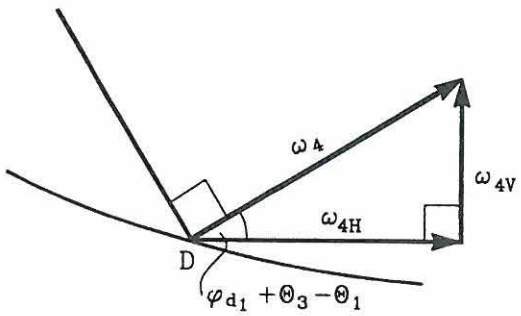

Figure A.25: *Displacement field of zone 4.*

The displacement vector for the slip fans in zone 5 see Figure A.26.

$$\omega_{5V} = \omega_4 e^{\theta \tan \varphi_{d_2}} \sin(\theta_3 + \varphi_{d_1} - \theta_1 + \theta);\ \theta \in [0; \theta_5] \tag{A.75}$$

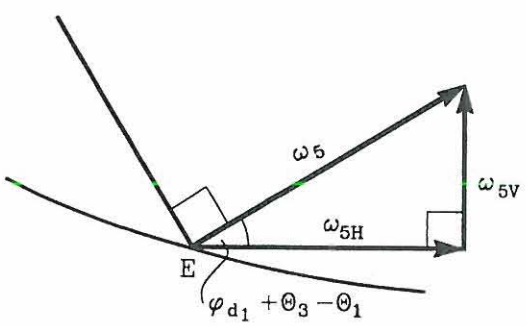

Figure A.26: *Displacement field of the slip fans in zone 5.*

Self weight of the soil in the rupture zones 1 - 5

Work done by the self weight of the soil in zone 1, W_1.

$$W_1 = (\gamma_s - \gamma_w)\omega_{1V}\Omega_1 \tag{A.76}$$

where Ω_1 is the area of rupture zone 1

$$\Omega_1 = \frac{1}{2} B_z H_{II} \tag{A.77}$$

work done by the self weight of the soil in zone 2, W_2.

$$W_2 = (\gamma_s - \gamma_w)\Omega_2\omega_{2V} \tag{A.78}$$

where Ω_2 is the area of rupture zone 2

$$\Omega_2 = \frac{1}{2}L_{BI}r_{CI}\sin\theta_2 \tag{A.79}$$

where $\theta_2 = \varphi_{d_1} - \arcsin(\frac{B_z \sin\theta_1}{l_{BI}}) - \frac{\pi}{2}$ as long as $\theta_2 \geq 0$

Work done by the self weight of the soil in zone 3, W_3.

$$W_3 = (\gamma_s - \gamma_w)\int_0^{r_{DI}}\int_0^{\theta_3}\omega_{3V}(\theta, r)r\,dr\,d\theta \tag{A.80}$$

where the analytic solution of W_3 is

$$\begin{aligned} W_3 = {} & \frac{(\gamma_s - \gamma_w)r_{DI}^2}{2\tan^2\varphi_{d_1} + 2}\left[e^{\theta_3\tan\varphi_{d_1}}\left[\tan\varphi_{d_1}\sin(\varphi_{d_1} - \theta_1 + \theta_3)\right.\right. \\ & \left.\left. - \cos(\varphi_{d_1} - \theta_1 + \theta_3)\right] - \tan\varphi_{d_1}\sin(\varphi_{d_1} - \theta_1) - \cos(\varphi_{d_1} - \theta_1)\right] \end{aligned} \tag{A.81}$$

Work done by the self weight of the soil in zone 4, W_4.

$$W_4 = (\gamma_s - \gamma_w)\omega_{4V}\Omega_4 \tag{A.82}$$

where Ω_4 is the area of rupture zone 4

$$\begin{aligned} \Omega_4 = {} & \frac{1}{2}l_{GI}l_{IH}\sin\left(\arctan\left(\frac{H_{II}}{l_{IH} + sH_{II}}\right)\right) \\ & + \frac{1}{2}l_{IH}(r_{DI} - l_{DD'})\sin\left(\frac{\pi}{4} - \frac{\varphi_{d_1}}{2} - \arctan\left(\frac{H_{II}}{l_{IH} + sH_{II}}\right)\right) \\ & + \frac{1}{2}L_{D'F'}L_{DD'}\sin\left(\frac{\pi}{4} - \frac{\varphi_{d_2}}{2}\right) \\ & - \frac{1}{2}l_{GF'}l_{GE}\sin\theta_5 \end{aligned} \tag{A.83}$$

Work done by the self weight of the soil in zone 5, W_5.

$$W_5 = (\gamma_s - \gamma_w) \int_0^{r_{GF}} \int_0^{\theta_5} \omega_{5V}(\theta) r dr d\theta \tag{A.84}$$

where the analytic solution of W_5 is

$$\begin{aligned} W_5 = \frac{(\gamma_s - \gamma_w) r_{GF}^2}{2\tan^2\varphi_{d_1} + 2} \Big[e^{\theta_5 \tan\varphi_{d_1}} \big[\tan\varphi_{d_1} \sin(\varphi_{d_1} - \theta_1 + \theta_3 + \theta_5) \\ - \cos(\varphi_{d_1} - \theta_1 + \theta_3 + \theta_5) \big] - \tan\varphi_{d_1} \sin(\varphi_{d_1} - \theta_1 + \theta_3) \\ - \cos(\varphi_{d_1} - \theta_1 + \theta_3) \Big] \end{aligned} \tag{A.85}$$

To establish the work done in equilibrium, where the external forces and self weight in each individual zone are computed, gives the following bearing capacity of the friction based soil.

$$F_H^p \omega_{1V} + (F_G - F_U)\omega_{1H} = -W_1 - W_2 + W_3 + W_4 + W_5 \tag{A.86}$$

The angles θ_1 in the limit state equation is the unknown angle to be determined by minimizing the ratio between the stabilizing work and driving work.

A.6.7 Failure in rubble and sand (rotation)

Case 7 in Fig A.5b is considered.

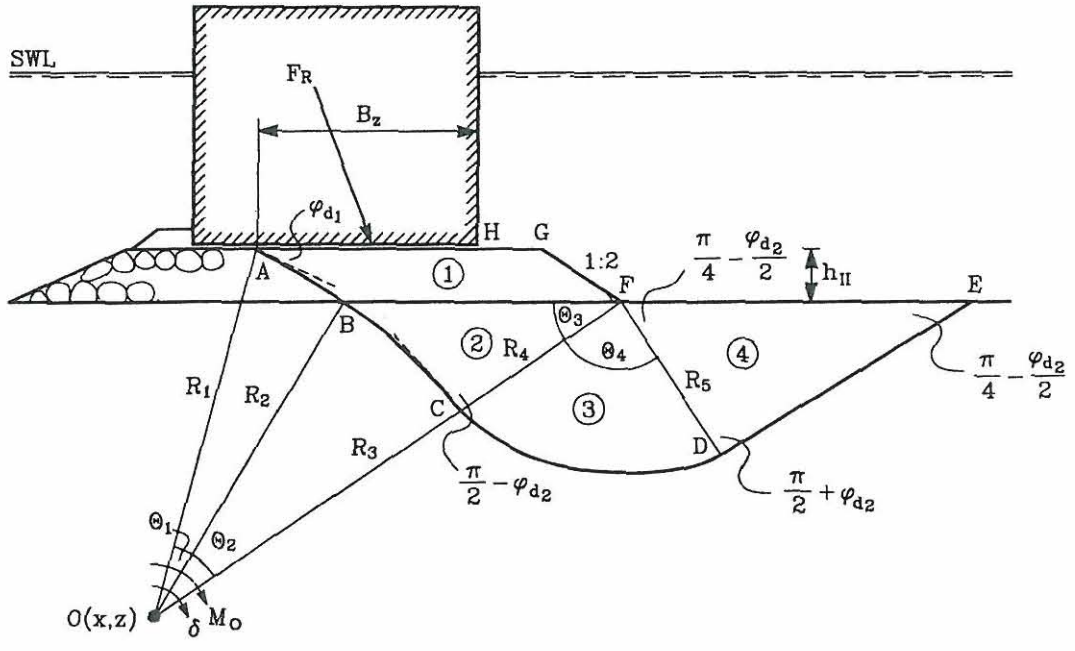

Figure A.27: *Rupture in the rubble mound and sand subsoil (rotation mechanism)*

Considering that the soil exhibits plastic behaviour, then the work equation can be formulated as shown below, when the foundation is forced to move a unit increment $\delta = 1$ about the point $O(x, z)$.

This is a postulated rotation mechanism which exhibits rupture failure along the first logarithmic spiral (friction based soil) AB, moving zone 1 cf. Figure A.27. Zone 2 rotates and moves in the same direction , but is configured to soil characteristics in the subsoil as $\varphi_{d_2} \neq \varphi_{d_1}$. Part of zone 3 moves in the direction of zone 1 and 2, and rests has a holding capacity. Zone 4 exhibits holding capacity thus holding the wave loads, weight of the structure and stiff rupture zones 1, 2 and part of 3.

The geometric lengths of rupture figures are represented as R (radius) and l (length) subscript. These geometrical lengths are used to determine the area of each individual rupture zone and the displacement of each rupture zone:

Radius R_1 is determined from the point of rotation $O(x, z)$.

The radius at the point of rupture along base of the vertical breakwater.

$$R_2 = R_1 e^{\theta_1 \tan \varphi_{d_1}} \tag{A.87}$$

The radius at the point of rupture along base of the rubble mound.

$$R_3 = R_2 e^{\theta_2 \tan \varphi_{d_2}} \tag{A.88}$$

where θ_2 always is positive.

Radius of the second stiff zone, R_4

$$R_4 = R_2 \frac{\sin(\pi - \theta_2 - \theta_3)}{\sin \theta_3} - R_3 \tag{A.89}$$

where R_4 always is positive.

External work

The external work is calculated as the moment around the center of rotation $O(x, z)$ multiplied by a unit increment of the angle δ.

$$W_E = \delta M_o \tag{A.90}$$

where M_o is the resultant force F_R acting on the base plate multiplied by the perpendicular length to the point $O(x, z)$.

Self weight of zone 1 - 4

There is no work along the rim of the rupture zones as the normality condition is assumed fulfilled. Therefore only the movement of the weight contributions are taken into consideration.

Work done by the self weight of the soil in zone 1, W_1.

$$W_1 = \delta(\gamma_s - \gamma_w) l_1 \Omega_1 \tag{A.91}$$

where Ω_1 is the area of rupture zone 1 and l_1 is the perpendicular length between the point of rotation and the center gravity of zone 1. l_1 is found numerically by dividing zone 1 into a number of triangles and calculating an average center of gravity relative to the center of rotation O(x,z).

Work done by the self weight of the soil in zone 2, W_2.

$$W_2 = \delta(\gamma_s - \gamma_w) l_2 \Omega_2 \tag{A.92}$$

where Ω_2 is the area of rupture zone 2 and l_2 is the perpendicular length between the point of rotation and the center gravity of zone 2. l_2 is found numerically by dividing zone 2 into a number of triangles and calculating an average center of gravity relative to the center of rotation O(x,z).

Work done by the self weight of the soil in zone 3, W_3.

$$W_3 = \delta(\gamma_s - \gamma_w) l_3 \Omega_3 \tag{A.93}$$

where Ω_3 is the area of rupture zone 3 and l_3 is the perpendicular length between the point of rotation and the center gravity of zone 3. l_3 is found numerically by dividing zone 3 into a number of triangles and calculating an average center of gravity relative to the center of rotation O(x,z). It should noted that zone 3 partly moves in the direction of the wave loads and has a bearing capacity.

Work done by the self weight of the soil in zone 4, W_4.

$$W_4 = \delta(\gamma_s - \gamma_w) l_4 \Omega_4 \tag{A.94}$$

where Ω_4 is the area of rupture zone 4 and l_4 is the perpendicular length between the point of rotation and the center gravity of zone 4. l_4 is found numerically by dividing zone 4 into a number of triangles and calculating an average center of gravity relative to the center of rotation O(x,z).

To establish the work done in equilibrium where the external forces and self weight in each individual zone are computed gives the following bearing capacity of the friction based soil.

$$0 = W_3 + W_4 - W_E - W_1 - W_2 \tag{A.95}$$

where (x, z) are the unknown coordinates to be determined by minimizing the ratio between the stabilizing and driving work.

A.6.8 Foundation failure, slip in the rubble mound and rupture failure in the clay subsoil

Case 8 in Fig A.5b is considered.

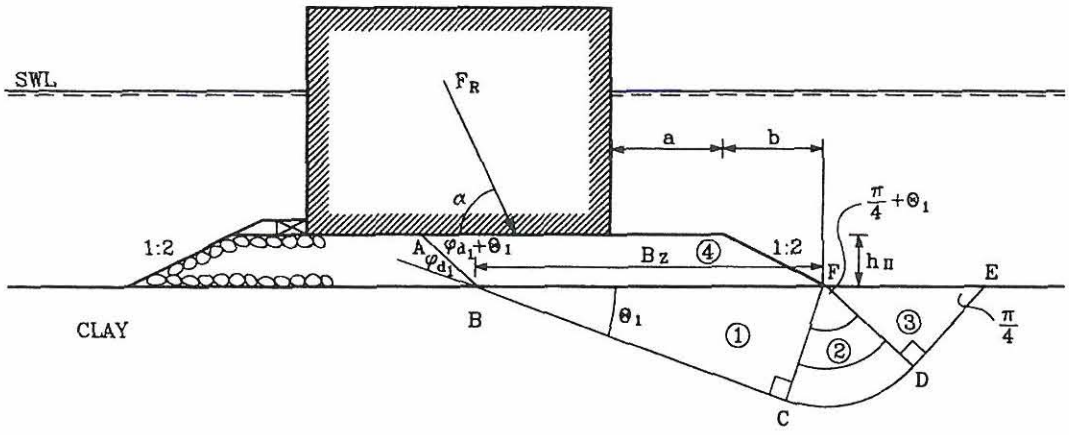

Figure A.28: *Failure in rubble mound and pure translation mechanism in clay.*

There is a resultant external Load F_R cf. Figure A.28 and the weight of zone 4 which causes a slip plane along AB due to the extent of the reduced effective angle of friction. No internal energy dissipation is calculated along AB, due to the assumption of the normality condition. The rupture slip line proceeds into clay causing instantaneous shift of zone 1 and producing internal energy dissipation along the rim of the rupture boundary BC. Zone 1 moves into the Prandtl zone which exhibits internal energy dissipation along the rim CD and up towards the point of rotation in a circular motion. The Prandtl zone causes the Rankine zone to rupture as a stiff element up towards the sea bed producing internal energy dissipation along DE.

The total internal work W_I in the rupture zone has to be greater than the external work W_e, to ensure stability of the foundation.

External work

The external work is calculated from the horizontal force F_H^p (derived from wave induced pressure and pore pressure along the rupture boundary line in the rubble mound) and from the buoyancy reduced weight of the caisson F_G, F_U wave induced uplift force and buoyancy reduced weight F_{G_4} of the rubble mound in zone 4.

By applying the work equation the external work can be expressed as follows.

$$W_E = \delta((F_G - F_U + F_{G_4}) \cdot \sin\theta_1 + F_H^p \cdot \cos\theta_1) \tag{A.96}$$

where θ_1 is defined in Figure A.28 and is the only unknown parameter and F_{G_4} is

$$F_{G_4} = (\gamma_s - \gamma_w)\left(\frac{1}{2}\frac{H_{II}}{\tan(\varphi_{d_1} + \theta_1)}H_{II} + (B_z - b)H_{II} + \frac{1}{2}bH_{II}\right) \tag{A.97}$$

Internal work

The internal work is the sum of the work produced along the rim of all fracture zones and work produced in the Prandtl zone. No work is produced along the fracture line AB, when rupture takes place, because friction based soils do not exhibit plastic behaviour, where strain in the soil proceeds independent of the stress, except for very large strain in the so called residual case, where the friction base soil is greatly weaken. Normally the weakening of the friction based soil is not included in the calculation. The internal work can be expressed as W_I:

$$W_I = W_1 + W_2 + W_3 + W_4 + W_5 + W_6 - W_7 \tag{A.98}$$

where W_1, W_2, W_3 is the work produced along the rims of the fracture zones BC, CD, DE

The fracture zones 1 and 3 are regarded as stiff zones. W_4 is the internal work in zone 2., W_5 self weight of zone 1., W_6 self weight in zone 2., W_7 self weight in zone 3.

The internal work can be formulated as shown below:

$$W_1 = \delta \int_0^{B_z \cdot \cos\theta_1} c_u(l)dl \tag{A.99}$$

$$W_2 = \delta \int_0^{B_z \cdot \sin\theta_1 (\frac{\pi}{4} + \theta_1)} c_u(a)da \tag{A.100}$$

$$W_3 = \delta \int_0^{B_z \cdot \sin\theta_1} c_u(a)da \tag{A.101}$$

where c_u is the undrained shear strength of clay and B_z is the width of the first stiff zone.

Internal work considering the Prandtl fracture zone.

Prandtl fracture:

$$W_4 = \delta R_1 \int_0^{R_1} \int_0^{(\frac{\pi}{4}+\theta_1)} c_u(a,\theta_1) d\theta_1 \; da \tag{A.102}$$

where δ is rotation of the top point in the Prandtl zone, a unit increment.

Self weight of zone 1 - 3

The weight of each zone in the soil considering uplift can have effect on the total weight as the first stiff zone is forced to moved down the rupture line BC. This might change the area of zone 1, zone 2 and zone 3 and the corresponding weights.

$$W_5 = (\gamma_s - \gamma_w)\delta \sin\theta_1 \int_{\Omega_1} d\Omega_1 \tag{A.103}$$

where Ω_1 is the area of rupture zone 1.

Work done by the self weight of the soil in zone 2, W_2.

$$W_6 = (\gamma_s - \gamma_w)\delta \sin\theta_1 \int_{\Omega_2} d\Omega_2 \tag{A.104}$$

where Ω_2 is the area of rupture zone 2.

Work done by the self weight of the soil in zone 3, W_3.

$$W_7 = (\gamma_s - \gamma_w)\delta \frac{\sqrt{2}}{2} \int_{\omega_3} d\Omega_3 \tag{A.105}$$

where Ω_3 is the area of rupture zone 3.

The internal work W_I and external work W_E have to be in equilibrium so therefore $W_I = W_E$. The dimensionless bearing capacity of the foundation can now be formulated, when c_u is constant.

$$0 = W_I - W_E \tag{A.106}$$

where θ_1 is determined by minimizing the ratio W_I/W_E

A.6.9 Foundation in rubble and clay, rotation mechanism

Case 9 in Figure A.5 is considered.

The slip line AB is theoretically a logarithmic spiral. The areas, 1 and 2 move as stiff zones and interact with the clay subsoil, where a circular rupture zone evolves. The kinematic admissible rupture figure is described by a rotation mechanism about point D.

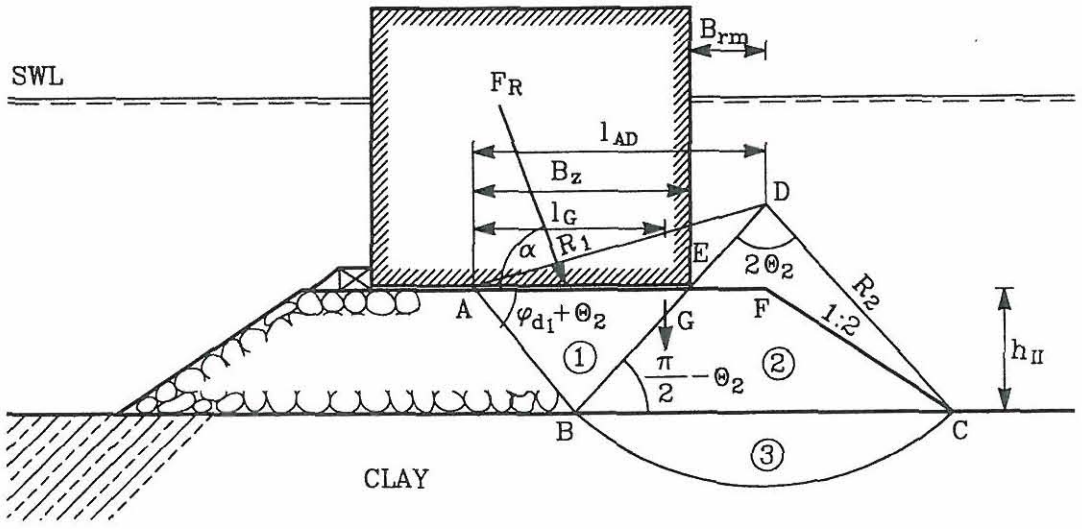

Figure A.29: *Rupture in the rubble mound and clay subsoil.*

The geometrical lengths and the radius for the kinematically admissible rupture figure are cf. Figure A.29.

$$l_{BC} = B_z + B_{rm} + 2h_{II} - \frac{h_{II}}{\tan(\varphi_{d_1} + \theta_2)} \tag{A.107}$$

As noted above, the slip line AB is approximated by a straight line. The radius R_2 then becomes

$$R_2 = \frac{1}{2} l_{BC} / \sin\theta_2 \tag{A.108}$$

Further l_{AD} becomes

$$l_{AD} = \frac{h_{II}}{\tan(\varphi_{d_1} + \theta_2)} + \frac{1}{2} l_{BC} \tag{A.109}$$

The center of gravity for zone 1 and 2 is defined by the length l_G, cf. Figure A.29

$$l_G = \frac{(l_{AD} - \frac{1}{2}l_{BC})(\frac{1}{3}l_{AD} + \frac{5}{6}l_{BC} - h_{II}) + \frac{1}{2}(l_{BC} - 2h_{II})l_{BC} + \frac{2}{3}h_{II}^2}{\frac{1}{2}l_{AD} + \frac{3}{4}l_{BC} - h_{II}} \tag{A.110}$$

External work done

The external work W_E done by the wave loads, the pore pressure along the rupture boundary line and the weight of the vertical breakwater is for an infinitesimal rotation δ around point D

$$W_E = \delta M_o \tag{A.111}$$

where M_o is the moment around D of the wave loads, the pore pressure and the weight of the caisson.

The work done due to the weight of zones 1 *and* 2 *is a rotation around* D

$$W_{1,2} = \delta(\gamma_s - \gamma_w)(l_{AD} - l_G)(\Omega_1 + \Omega_2) \tag{A.112}$$

where Ω_1 and Ω_2 are the areas of zone 1 and 2, and $l_{AD} - l_G$ is the perpendicular length between the point of rotation and the center of gravity for zone 1 and 2.

The work done by the weight of zone 3 is zero as the resultant displacement of the center of gravity is horizontal.

The internal work done in zone 3 *along the rim of the rupture boundary* BC *is*

$$W_3 = \delta R_2^2 \int_0^{2\theta_2} c_u(\theta) d\theta \tag{A.113}$$

where c_u is the undrained shear strength of the clay.

The limit state equation for the rupture mechanism in Figure A.29 is then:

$$W_3 - W_{1,2} - W_E = 0 \tag{A.114}$$

θ_2 is the unknown angle to be determined by minimizing the ratio between the stabilizing work and driving work.

A.6.10 Foundation failure involving the rotation mechanism

Case 10 in Figure A.5b is considered.

The failure mode is kinematically admissible and is determined from the position of the center of rotation $O(x, z)$. The plane failure mode is shown in Figure A.30. Note that it is assumed that tensile stresses cannot occur under the caisson base plate.

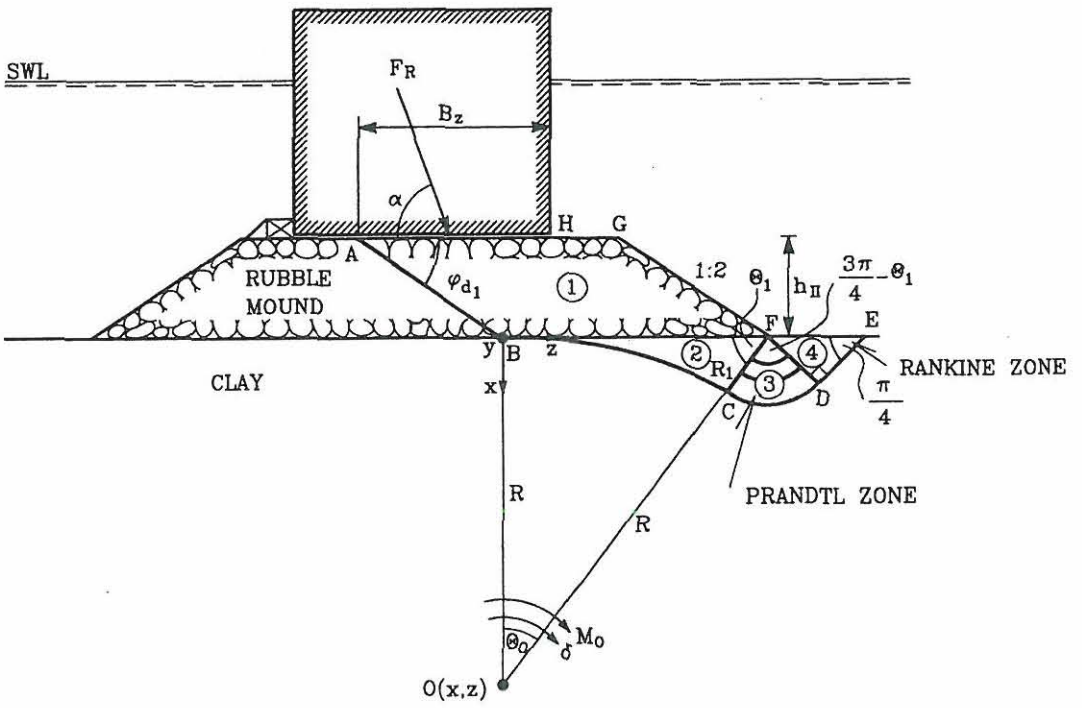

Figure A.30: *Rupture in the rubble mound and clay subsoil.*

The width of the rupture zone can be determined from case 3, page 9.

The total internal work W_I in the rupture zone has to be greater than the external work W_E, to ensure stability of the foundation.

External work

The external work is calculated as the moment around the center of rotation $O(x, z)$ multiplied by a unit increment of the angle δ.

$$W_E = \delta M_o \tag{A.115}$$

where M_o is the moment of the wave induced loads, weight of the caisson considering buoyancy, weight of the rubble mound in zone 1 and horizontal pore pressure relative to the point of rotation $O(x, z)$.

Internal work

The total internal work covers the rim of all fracture zones and the contribution from the Prandtl and Rankine fracture zone. The sum of the internal work can be expressed as W_I:

$$W_I = W_2 + W_3 + W_4 + W_5 + W_6 \tag{A.116}$$

where W_2, W_3, W_4 is the work along the rim of the fracture zones BC, CD, W_5, and DE internal work in the Prandtl zone, W_6 internal work in the Rankine zone

Internal work along the rim of the fracture zones can be calculated from the point of rotation $O(x, z)$:

$$W_2 = \delta R^2 \int_0^{\theta_o} c_u(\theta) d\theta \tag{A.117}$$

$$W_3 = \delta R R_1 \int_0^{\frac{3\pi}{4} - \theta_1} c_u(\theta) d\theta \tag{A.118}$$

$$W_4 = \delta R \int_0^{R_1} c_u(a) da \tag{A.119}$$

where c_u is the undrained shear strength of clay.

Internal work considering the Prandtl and Rankine ruptures zones zones.

Prandtl fracture:

$$W_5 = \delta R_1 \int_0^{R_1} \int_0^{\frac{3\pi}{4}-\theta_1} c_u(a,\theta) d\theta \; da \tag{A.120}$$

Rankine fracture:

$$W_6 = \delta \int_0^{R_1} \int_0^{R_1-a} c_u(a,l) dl \; da \tag{A.121}$$

The rotation point can be calculated as the point where the ratio between total internal work W_I and external work W_E is a minimum without failing.

References

Chen W.F. & Liu X.L. (1990). *Limit state analysis in soil mechanics.* Vol 52, Elsevier Science Publishers B.V..

Goda, Y. and T. Fukumori (1972). *Laboratory investigation of wave pressures exerted upon vertical and composite walls.* Coastal Engineering in Japan, Vol. 15. pp 81-90, 1972.

Goda, Y. (1974). *A new method of wave pressure calculation for the design of composite breakwater.* Proc. 14th Int. Conf. Coastal Eng., Copenhagen, Denmark.

Hansen, B. (1979). *Definition and use of friction angles.* Proc. Int. Conf. VII ECSMFE, Brighton, UK, 1979.

OCDI (1991). *Technical standards for port and harbour facilities in Japan* . Port and Harbour Research Institute, Ministry of Transport, 1991.

Takayama, T. , (1992). *Estimation of sliding failure probability of present breakwaters for probabilistic design.* Report of Port and Harbour Research Inst., Vol. 31, No. 5, 1992.

Tanimoto , (1976). *Wave forces on a composite-type breakwater.* Proc 1976 Annual Res. Present. of Port and Harbour Res. Inst. (in Japanese).